Final Report

BELLONA

AE3200 Design Synthesis

Group 22

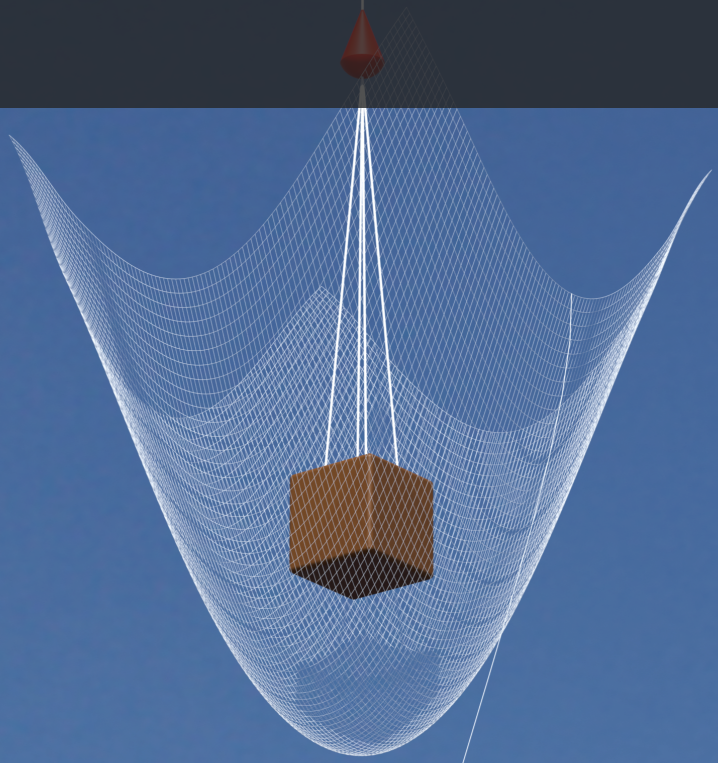

Delft University of Technology

TU Delft

This page is intentionally left blank.

Final Report

BELLONA

by

Group 22

Student Name	Student Number
Alex Dontu	5971063
Alexandru Minculescu	5983681
Andrei Potfalean	5935830
Andrei-Cristian Tabără	5985161
Daris Kariņš Bērziņš	5981956
Frederic Rahlfs	5917573
Giovanni Zattoni	5944422
Jan Wanatowicz	6016138
Marc Arnold Küster	5982596
Piotr Blanchard	5925509

Statement on the Use of Generative AI:

- Generative AI was used to support text structuring and idea generation.
- Generative AI was used to improve grammar, clarity, and writing style.
- Generative AI was used to assist with code development and LaTeX formatting.
- All outputs were critically reviewed, verified, and adapted by the authors.
- Full responsibility for the content and correctness of this report lies with the authors.

Version:	1.2
Tutor:	Theodoros Michelis
Backup Tutor:	Lourenco Tercio Lima Pereira
Coaches:	João Pechirra de Carvalho Borrego
	Jaap Jorritsma
Duration:	April 20, 2026 - June 26, 2026
Faculty:	Faculty of Aerospace Engineering, Delft
Cover:	Final Design Render

TU Delft

Executive Overview

Incursions of uncooperative balloons into controlled or secure airspace present a growing challenge for airports, border control, and critical infrastructure operators. This report outlines the detailed design of BELLONA, an advanced autonomous system designed to counter this threat by non-destructively intercepting and capturing a free-floating balloon at an altitude and range of up to 6 km each within 25 minutes.

The project responds to a documented and growing problem: uncontrolled meteorological and hybrid-use smuggling balloons drifting into airport or otherwise restricted airspace, forcing costly closures (up to €2M). Several limitations in existing solutions (kinetic interceptors, lasers, small-UAV net-guns, ground-based net guns, or manual helicopter intercept) have been identified:

- Poor safety: Kinetic, laser, and existing net-based interception generates uncontrolled, falling debris, while manual helicopter interception endangers the crew of the helicopter
- Slow response: Kinetic interception requires cumbersome communication with military forces, while all solutions require manual, physical intervention, which prevents a rapid response
- Target variability: The identified spectrum of balloon shapes and sizes prevents small-UAV net-guns from operating against all possible targets

Analysis of these gaps in the market led to the development of the BELLONA mission statement:

BELLONA aims to counter uncooperative balloons before they disrupt critical airspace or pose a safety hazard to those on the ground.

Several concepts are developed to match these requirements, with a trade-off conducted to select the final concept with an emphasis on interception performance, safety, and cost. This process results in the selection and further detailed design of concept BELLONA, consisting of a quadcopter tail-sitter UAS that flies beneath a target balloon's suspended payload, fires a net to capture it, and tows the combined system to a safe recovery zone under a fully autonomous mission profile.

Figure 1: Final BELLONA Aircraft Configuration

System Overview

The system is capable of launching the UAS from the ground station within three minutes of receiving a launch command from the operator. The UAS takes off vertically before transitioning to a spiraling climb profile up to the search volume as provided by the airport or other operator, taking less than ten minutes. Once the search volume is reached, the UAS locates the balloon using its onboard sensor suite (LiDAR, mmWave radar, and NIR/RGB cameras), and transitions to hover directly underneath the target. The UAS then launches a net vertically upwards to capture the payload hanging underneath the balloon, before using a tether attached to the net to both close the net about the payload and drag the payload down to a defined safe landing zone for recovery and reset.

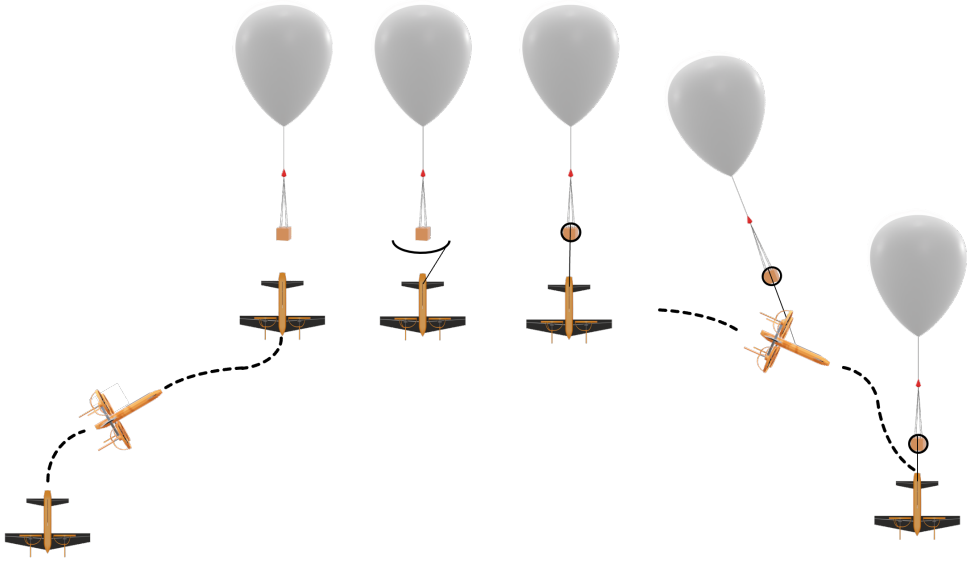

Figure 2: Diagram of Mission Design

This method avoids each of the technical challenges that exist in current solutions: the interaction is completely non-destructive and maximally avoids debris or other risks, can respond quickly and remove the target from the airspace within 25 minutes, and can account for many different balloon-payload configurations through the use of a flexible net.

Figure 3: Render of Net Capture

Table 1: Key BELLONA Parameters

Parameter	Value
UAS type	Tail-sitter eVTOL
Nominal flight speed	30 m/s
Horizontal range	6 km
Interception altitude	6 km
Total interception time	25 min
UAS mass	52 kg
Wingspan	4.2 m
Propeller count	4
Installed battery capacity	4.7 kWh
Intercepted balloon size	2-6 m diameter
Intercepted balloon payload	up to 50 kg

Detailed design of the propulsion system and aerodynamic surfaces can be found in Chapter 6, the electronic components in Chapter 7, the net-launcher and capture mechanisms in Chapter 8, the structural elements of the UAS in Chapter 9, and the ground system in Chapter 10.

Operations

Under EU UAS regulations, BELLONA falls into the Specific category, and includes all necessary hardware components for certification. Tests required for final certification are pending prototype manufacturing, while a preliminary risk assessment determines that the majority of remaining risks relate to the capture mechanism and balloon interaction. This will be mitigated through additional simulation in further design iterations and testing once prototypes are available. A preliminary life-cycle assessment is also performed, determining that dominant environmental damage stems from manufacturing, rather than operations. This identifies the key sustainability objective as maximization of mission count without replacement of parts.

Figure 4: BELLONA Taking Off

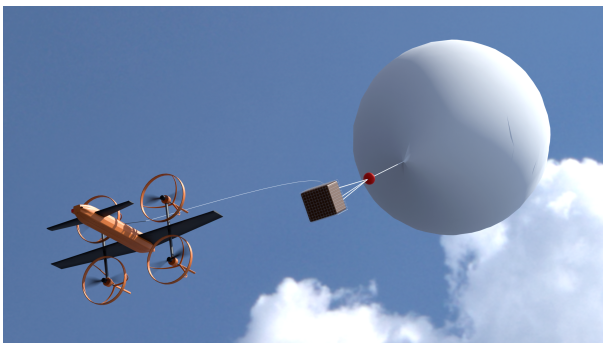

Figure 5: BELLONA Descending with a Balloon

Financial Model

The financial model assumes direct unit sales of one complete deployable BELLONA system, consisting of one UAS, one ground station, commissioning and customer handover, plus recurring annual maintenance/service revenue. The business model assumes the vast majority of profit comes from annual servicing revenue, while system sales are used to expand the base of deployed systems. The reference deployment is assumed to be three BELLONA systems distributed along an airport runway. The target year for profitability is year 6 from initial sales, with an estimated return on investment of 9%.

Table 2: Executive Financial Snapshot of the Updated BELLONA Model

Financial quantity	Updated value / interpretation
New-unit sales price	€121,000 per unit
One-time COGS	€99,622 per new unit
Annual service revenue	€11,999 per active unit per year
Recurring service COGS	€2,400 per active unit per year
Direct operator mission cost	€150 per mission
Total external funding before target year	€3.15M

Following this report, necessary steps before regular operation of BELLONA include prototype manufacturing and integration, ground testing, flight testing, capture-interaction validation, and pre-production release. The capture-load chain, including the net, tether, reel, hardpoint, and associated flight-control logic, is identified as the critical coupled dependency determining progress toward representative flight-capture trials, while propulsion refinement, sensor-fusion validation, and ground-station procedures can mature in parallel.

List of Acronyms

Acr.	Definition	Acr.	Definition	Acr.	Definition
FOC	Field-oriented control				
AC	Alternating current	**FoM**	Figure of merit	**PID**	Proportional-integral-derivative
ADS-B	Automatic Dependent Surveillance–Broadcast	**FoV**	Field of view	**PLC**	Programmable logic controller
AGL	Above ground level	**FSM**	Finite State Machine	**PPA**	Propulsion, Performance and Aerodynamics
ANSP	Air navigation service provider	**FTE**	Full-time equivalent employee	**PSF**	Pounds per square foot
AP	Aerial Platform	**GCS**	Ground Control Station	**PWM**	Pulse-width modulation
AR	Aspect ratio	**GFRP**	Glass fibre reinforced polymer	**QA**	Quality assurance
ARC	Air Risk Class	**GHG**	Greenhouse gas	**QI**	Quasi-isotropic
ATC	Air traffic control	**GMSL2**	Gigabit Multimedia Serial Link 2	**R&D**	Research and development
BI	Balloon Interaction	**GNSS**	Global Navigation Satellite System	**RAMS**	Reliability, Availability, Maintainability and Safety
BIG	Balloon Interaction Group	**GRC**	Ground Risk Class	**RCS**	Radar cross-section
BMS	Battery management system	**GS**	Ground system	**REQ**	Requirement
C2	Command and control	**GWP**	Global warming potential	**RF**	Radio frequency
CAA	Civil aviation authority	**HDPE**	High-density polyethylene	**RGB**	Red, green and blue
CAC	Customer acquisition cost	**HV**	High voltage	**ROI**	Return on investment
CAD	Computer-aided design	**I^2C**	Inter-Integrated Circuit	**RPM**	Revolutions per minute
CAGR	Compound annual growth rate	**ILT**	Inspectie Leefomgeving en Transport	**RSK**	Risk
CAN	Controller Area Network	**INDI**	Incremental Nonlinear Dynamic Inversion	**SAIL**	Safety Assurance and Integrity Level
CAPEX	Capital expenditure	**IR**	Infrared	**SCE**	Sensing, Control and Electronics
CBS	Cost Break-down Structure	**KF**	Kalman Filter	**SEN**	Sensing
CFD	Computational fluid dynamics	**KPI**	Key performance indicator	**SF**	Safety factor
CFRP	Carbon fibre reinforced polymer	**LC**	Load case	**SIL**	Software-in-the-loop
CG	Centre of gravity	**LCA**	Life-cycle assessment	**SMS**	Structures, Materials and Sustainability
COGS	Cost of goods sold	**LE**	Leading edge	**SNR**	Signal-to-noise ratio
COM	Communication	**LiDAR**	Light Detection and Ranging	**SORA**	Specific Operations Risk Assessment
ConOps	Concept of operations	**LiPo**	Lithium-polymer	**SPL**	Sound pressure level
CTR	Control	**LQR**	Linear-quadratic regulator	**SSD**	Solid-state drive
DAA	Detect-and-Avoid	**LS**	Life-Cycle Support	**ST**	Sensing and Tracking
DATCOM	Data Compendium	**LTE**	Long-Term Evolution	**STK**	Stakeholder
DC	Direct current	**LV**	Low voltage	**STR**	Structures
DOD	Depth of discharge	**LWIR**	Long-wave infrared	**SUS**	Sustainability
MAC	Mean aerodynamic chord	**SYS**	System		
EAS	Equivalent airspeed	**MIMO**	Multiple-input multiple-output	**TAS**	True airspeed
EASA	European Union Aviation Safety Agency	**MPC**	Model Predictive Control	**TMA**	Terminal Manoeuvring Area
EF	Emission factor	**MSN**	Mission	**TMPR**	Tactical Mitigation Performance Requirement
EIRP	Effective isotropic radiated power	**MTOW**	Maximum take-off mass	**TRA/TSA**	Temporary Reserved Airspace / Temporary Segregated Airspace
EKF	Extended Kalman Filter	**MVP**	Minimum viable product	**TSPR**	Total System Performance Requirement
EMI	Electromagnetic interference	**NIR**	Near-infrared	**UART**	Universal Asynchronous Receiver-Transmitter
EOL	End of life	**OE**	Operations and Environment	**UAS**	Unmanned aircraft system
EPDM	Ethylene propylene diene monomer	**OGS**	Operations and Ground Station	**UAV**	Unmanned aerial vehicle
ESC	Electronic speed controller	**OPEX**	Operating expenses	**UD**	Unidirectional
OSC	Operational Safety Case	**UHMWPE**	Ultra-high-molecular-weight polyethylene		
eVTOL	Electric vertical take-off and landing	**OSO**	Operational safety objective	**UI**	User interface
FBD	Functional Breakdown Diagram	**OTS**	Off-the-shelf	**UKF**	Unscented Kalman Filter
FBS	Functional Breakdown Structure	**OVC**	Overcast	**UPS**	Uninterruptible power supply
FC	Flight controller	**P&E**	Power and electronics	**UWB**	Ultra-wideband
FCS	Flight control system	**P&L**	Profit and loss	**V&V**	Verification and validation
FFD	Functional Flow Diagram	**PCB**	Printed circuit board		
FMCW	Frequency-modulated continuous-wave	**PDU**	Power distribution unit		
FMEA	Failure Modes and Effects Analysis				

Contents

Executive Overview i

List of Acronyms iv

1 Introduction & Project Objectives 1

2 Market Analysis 2
- 2.1 Problem Relevance and Operational Demand . . . 2
- 2.2 Stakeholder Analysis . . . 4
- 2.3 Competitive Positioning Summary 5

3 Key Stakeholder Requirements & Design Drivers 5
- 3.1 Requirement Derivation . . . 5

4 Functional Analysis 6
- 4.1 Functional Flow Diagram . . . 6
- 4.2 Functional Breakdown Structure . 8

5 Design Methodology 12
- 5.1 Conceptual Design . . . 12
- 5.2 Iterative Concurrent Sizing and Convergence . . . 13

6 Propulsion, Performance and Aerodynamics 13
- 6.1 PPA Sizing Problem and Mission Drivers . . . 14
- 6.2 Overall Sizing Workflow . . . 15
- 6.3 Key Assumptions and Design Constants . . . 15
- 6.4 Aerodynamic Model . . . 18
- 6.5 Drag Polar and Performance Model 19
- 6.6 Wing Loading and Stall-Speed Constraint . . . 19
- 6.7 Transition and Tail-Sitter Constraints 20
- 6.8 Propulsion Sizing Methodology . . 21
- 6.9 Mission and Flight Performance . . 22
- 6.10 Canard, Stability and Control Sizing 24
- 6.11 Optimisation Results and Interpretation . . . 26
- 6.12 Final PPA Design Values . . . 27
- 6.13 PPA Verification and Validation . . 28

7 Electrical System 29
- 7.1 Sensing . . . 31
- 7.2 Control . . . 35
- 7.3 Communication . . . 37
- 7.4 Power & Electronics . . . 39

8 Balloon Interaction Group 48
- 8.1 BIG Subsystem Requirements . . . 48
- 8.2 Mission Architecture . . . 49
- 8.3 Operational Sequence of Balloon Interaction . . . 50
- 8.4 Capture Net Design . . . 51
- 8.5 Blank Rifle Cartridge Launcher Design . . . 56
- 8.6 Reel, Tether, and Tether Guide Design 57
- 8.7 Emergency Breakaway and Parachute Design . . . 59
- 8.8 Airframe Integration . . . 60
- 8.9 Mass, Power, and Cost Budget . . . 61
- 8.10 Balloon Interaction Verification and Validation Plan . . . 61

9 Structures and Materials 62
- 9.1 Structural Design Scope and Requirements . . . 62
- 9.2 Loads Identification and Materials Selection . . . 63
- 9.3 Verification and Validation . . . 79

10 Ground System 83
- 10.1 Ground System Scope and Design Objective . . . 83
- 10.2 Operations and Ground Station Requirements . . . 83
- 10.3 Ground System Architecture . . . 84
- 10.4 Operational Sequence and Functional Flow . . . 85
- 10.5 Communication Architecture . . . 87
- 10.6 Ground Station Electrical Architecture . . . 90
- 10.7 Mechanical Systems Design . . . 93
- 10.8 Mechanical Load Cases . . . 96
- 10.9 Mechanical Sizing and Component Selection . . . 97
- 10.10 CAD Implementation and Design Iteration . . . 99
- 10.11 Ground System Verification and Validation . . . 100
- 10.12 Limitations and Future Work . . . 100

11 Final Design 101
- 11.1 Technical Budgets . . . 101
- 11.2 CAD Integration . . . 102
- 11.3 Regulatory Compliance and Certification Strategy . . . 103

12 Operations and Logistic Concept Description 104
- 12.1 Airport Deployment Concept . . . 105
- 12.2 Airspace Coordination and Launch Approval . . . 105
- 12.3 Operational Readiness and Station Standby . . . 106
- 12.4 Nominal Mission Flow . . . 106

12.5 Operational Roles and Interfaces . 107
12.6 Dynamic Recovery-Zone Selection 108
12.7 Off-Nominal and Abort Concept . 109
12.8 Payload Handover and Authority Recovery 109
12.9 Post-Mission Logistic Reset 109
12.10 Maintenance and Availability Concept 110
12.11 Operational Design Implications . 111

13 Reliability, Availability, Maintainability, and Safety Characteristics 112
13.1 RAMS Boundary and Assumptions 112
13.2 Safety-Critical Functions and Characteristics 112
13.3 RAMS Verification Approach . . . 114

14 Production Plan 114
14.1 Production Scope and Assumptions 114
14.2 Production Streams 115
14.3 Assembly and Integration Flow . . 115
14.4 Integration Gates 116
14.5 Release to Flight and Interaction Testing 117
14.6 Post-Mission Reset and Reuse . . . 117
14.7 Production Limitations and Future Work 118

15 Risk Assessment 118
15.1 Methodology Overview 118
15.2 Risk Maps 121
15.3 Changelog 122

16 Return on Investment, Cost Breakdown and Operational Profit 123
16.1 Financial Model Scope and Key Assumptions 123
16.2 Cost Break-down Structure 125
16.3 Unit Economics 126
16.4 Sales Ramp, Revenue and Profitability 126
16.5 Operating Expenses, Staffing and Assets 127
16.6 Funding Plan and ROI Interpretation 128

17 Sustainability Assessment 129
17.1 Goal, Scope and Boundary 129
17.2 Inventory and Emission Factors . . 130
17.3 Operational Energy 131
17.4 Noise 131
17.5 Manufacturing, Maintenance and Reuse 132
17.6 Off-Nominal Environmental Effects 133
17.7 KPIs and Design Recommendations 133

18 Compliance and Sensitivity 134
18.1 Compliance Matrix 134
18.2 Final Design Sensitivity Analysis . 135

19 Future Developments 135
19.1 Project Design and Development Logic 136
19.2 Critical Development Dependency 136
19.3 Relation to Schedule and Cost Breakdown 136

20 Conclusion and Recommendations 138

References 139

1 Introduction & Project Objectives

The proliferation of uncooperative, free-floating balloons in commercial airspace presents a growing security and operational challenge for aviation authorities. These airborne hazards manifest in a variety of complex shapes and payload configurations, as illustrated in Figure 1.1. Successfully managing these threats requires a novel, conformable capture approach to ensure zero harm to third parties on the ground, the surrounding airspace, or the payload itself.

(a) Spherical Balloon Envelope with a Double-Tether Setup

(b) Irregular Balloon Profile with a Single-Tether Setup

Figure 1.1: Diverse Target Balloon Profiles

The **BELLONA** project sets out to bridge the capability gap between high-cost military intervention and passive monitoring. Our mission is to design a civilian-tailored, unmanned aerial system (UAS) and ground system capable of locating, intercepting, and safely recovering these airborne hazards through a fully autonomous mission profile with human-in-the-loop override capabilities. By focusing on a low-risk recovery approach, the project prioritizes safety and cost-per-sortie as its dominant success factors, offering a scalable alternative to traditional counter-UAS methods.
As illustrated in Figure 11.3, the core operational concept utilizes a unique quadcopter tailsitter design. This platform is engineered to transition into a stable hover directly beneath the target balloon's payload. From this underslung position, the system deploys an upward-firing net gun, securely wrapping a tether around the payload to capture it from below and ensure a controlled descent.

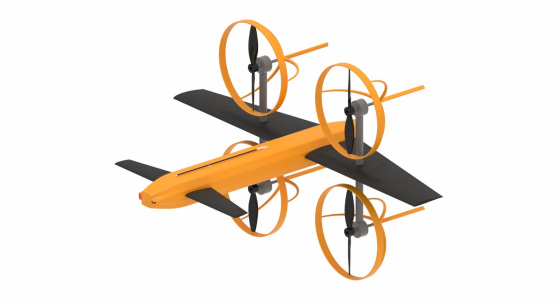

(a) Isometric View

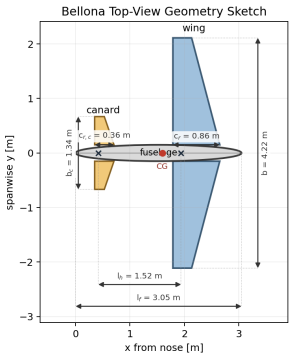

(b) Top View

Figure 1.2: Final Renders Showing the Isometric and Top Views of the Aircraft

A summary of the key geometric and mass properties for the Preliminary Performance Assessment (PPA) aircraft configuration is provided in Table 1.1.

Table 1.1: Selected Core Design and Sizing Metrics for the PPA Aircraft Configuration

Design Parameter	Value / Dimension
Maximum take-off mass (MTOW)	51.13 kg
Selected battery pack mass	11.40 kg
Wing area / span	2.55 m^2 / 4.22 m
Fuselage length	3.05 m
Canard area ratio / area	0.140 / 0.357 m^2

Strategic Goals

Beyond specific technical thresholds, the execution of the project is guided by three strategic pillars:

- **Safety-First Interception:** Moving away from destructive, kinetic solutions. The primary objective is to prove the feasibility of an upward net-capture and tethered-deflation approach that eliminates debris and minimizes risk to third parties on the ground.
- **Economic Accessibility:** Lowering the barrier of entry for airport authorities to manage their own airspace security. This involves optimizing the system for a low lifecycle cost, allowing for permanent, on-site deployment and immediate operational readiness.
- **Engineering Rigour and Synthesis:** The multidisciplinary design closes its mass-iteration loop at an MTOW of 51.13 kg. Driven by the high-altitude trajectory requirement, the 4.74 kWh pouch-cell battery provides sufficient energy to climb to the 6,000 m ceiling within 454.1 s, while preserving adequate margin against the mission energy budget.

Definition of Scope

To ensure a structured and manageable execution within the Design Synthesis Exercise (DSE) framework, the project boundaries are defined as follows:

- **System Focus:** The design effort encompasses the entire system architecture, specifically the tailsitter interceptor drone platform, the upward-firing net gun capture mechanism, and the integrating Ground Control Station (GCS).
- **Design Phase:** The project aims to achieve a high-fidelity conceptual design. Physical prototyping remains secondary to comprehensive analytical validation and performance simulation of the hover stability and net deployment dynamics.

2
Market Analysis

The economic viability of a new aerial system depends on the market it addresses and the cost at which it can be produced to compete within that market. This chapter analyses the balloon interception market to establish demand and identify the technology gap.

2.1. Problem Relevance and Operational Demand

Free-floating balloons create two distinct categories of airspace hazard that motivate a dedicated interception capability.

Meteorological balloon drift: Approximately 900 radiosondes are launched globally every day, ascending until burst at 20-35 km [1]. During ascent, these platforms may drift into controlled or restricted airspace near airports, creating an operational hazard for air traffic management. If the balloon enters a Terminal Manoeuvring Area (TMA), airport operations may need to be restricted or temporarily suspended until the hazard is removed. This creates a need for a rapid-response system capable of locating, intercepting, and safely removing uncontrolled balloons from airport-adjacent airspace. The economic relevance of this operational gap is significant. An active airspace threat can force immediate airspace restrictions, with single airline operational losses estimated at approximately $100 per minute for unplanned disruption events [2, 3]. This supports the business case for a reusable recovery system, while the detailed altitude and response-time requirements are formalized later in Chapter 3.

Hybrid-use and smuggling balloons: Since 2023, balloons repurposed for contraband delivery and hybrid airspace disruption have created an escalating security risk. Observed assets range between 2–6 m in diameter with payloads up to 50 kg. Recent incursions caused a major International Airport to close for more than 60 hours and cancel over 350 flights, affecting approximately 51,000 passengers [4] and causing an estimated €2 million in commercial losses [5]. A further incursion forced emergency airspace restrictions in Poland on Christmas Eve 2025. [6].

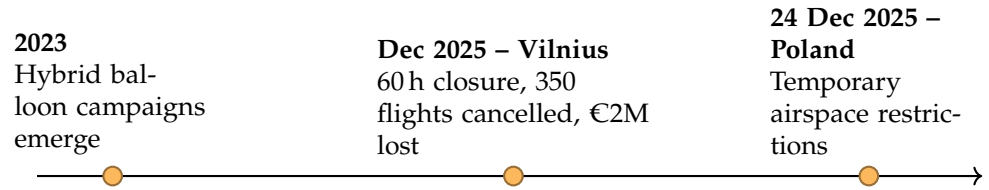

Figure 2.1: Timeline of Recent Hybrid Balloon Incursions and Observed Threat Characteristics

To remain commercially relevant against this cost and disruption profile, the system must be able to neutralize a target within roughly 15-25 minutes of detection, fast enough to prevent a drifting balloon from triggering a prolonged TMA closure. This response-time target, together with the observed envelope size and payload mass above, anchors the top-level requirements derived from the market in Chapter 3.

Both scenarios share a critical operational gap: no existing commercial system provides non-destructive, debris-free, UAS-based interception of large free-floating balloons in civilian airspace.

Existing Solutions and Technology Gap

Table 2.1 surveys the principal categories of existing counter-balloon and counter-UAS technology and their applicability to the present mission.

Table 2.1: Comparison of Existing Airspace Threat Mitigation Technologies Against the Requirements

Technology	Representative system	Cost per deployment	Gap vs. project requirements
Kinetic interceptor (missile)	Patriot / Iron Dome	$40k-$3M per shot [7]	Explosive; creates uncontrolled debris; prohibited in civilian airspace
Directed energy (laser)	Iron Beam (Rafael)	$0.10-$10 per shot [7]	Destroys envelope; uncontrolled descent; not certified for civilian use
Net-launching drone (anti-drone)	Fortem DroneHunter F700, ParaZero DefendAir, DroneCatcher	$1k-$3k per capture [7]	Designed for small rigid UAS (<1 m); net geometry unsuitable for 2-6 m elastic balloon envelopes; no buoyancy management post-capture
Ground-based net gun	UAVOS capture net	$5k-$50k system	Ground range <30 m; cannot reach 1-10 km altitude targets [8]
Manual helicopter interception	Ad hoc, case by case	$2k-$10k per sortie	Pilot safety risk; high cost; 30-60 min response time; not scalable

Small UAS interception has already been demonstrated, but no system addresses the very different problem of a large, buoyant target floating uncontrolled. This constitutes a clear and documented technology gap.

Market Context and Customer Segments

Counter-drone market valuations range from $1.8-3.2 billion in 2024-2025, with CAGR projections of 22-27% through 2030-2033 [9, 10]. UAS-based interception is the fastest-growing sub-segment, projected at 26% CAGR [11], reflecting demand for flexible, range-independent tools that ground-fixed systems cannot provide.

Three macro-level drivers shape the system's target market:

- **Hybrid airspace disruptions:** State-tolerated balloon campaigns disrupt civilian aviation at

low cost. Fielded solutions are lacking; Lithuania notably announced a €1 million prize for interception concepts in December 2025 [12].

- **Airport airspace protection:** While detection solutions account for 55% of market revenue [11], operators increasingly demand paired, non-destructive neutralization capability to protect approach cones [13, 14].
- **Non-destructive civilian compliance:** EASA regulations restrict explosive or kinetic countermeasures in civilian airspace, disqualifying dominant military solutions and creating a protected niche for BELLONA.

Five primary customer segments share these operational constraints: national meteorological services (recovering escaped radiosondes), airport operators (mitigating approach path risks), border security agencies (countering hybrid incursions), critical infrastructure operators (perimeter security), and scientific balloon operators (payload recovery).

2.2. Stakeholder Analysis

Beyond direct customers, several institutional and regulatory stakeholders dictate the project's approval, market access, and operational viability. Figure 2.2 maps both customer segments and broader interest groups by their institutional power and interest level.

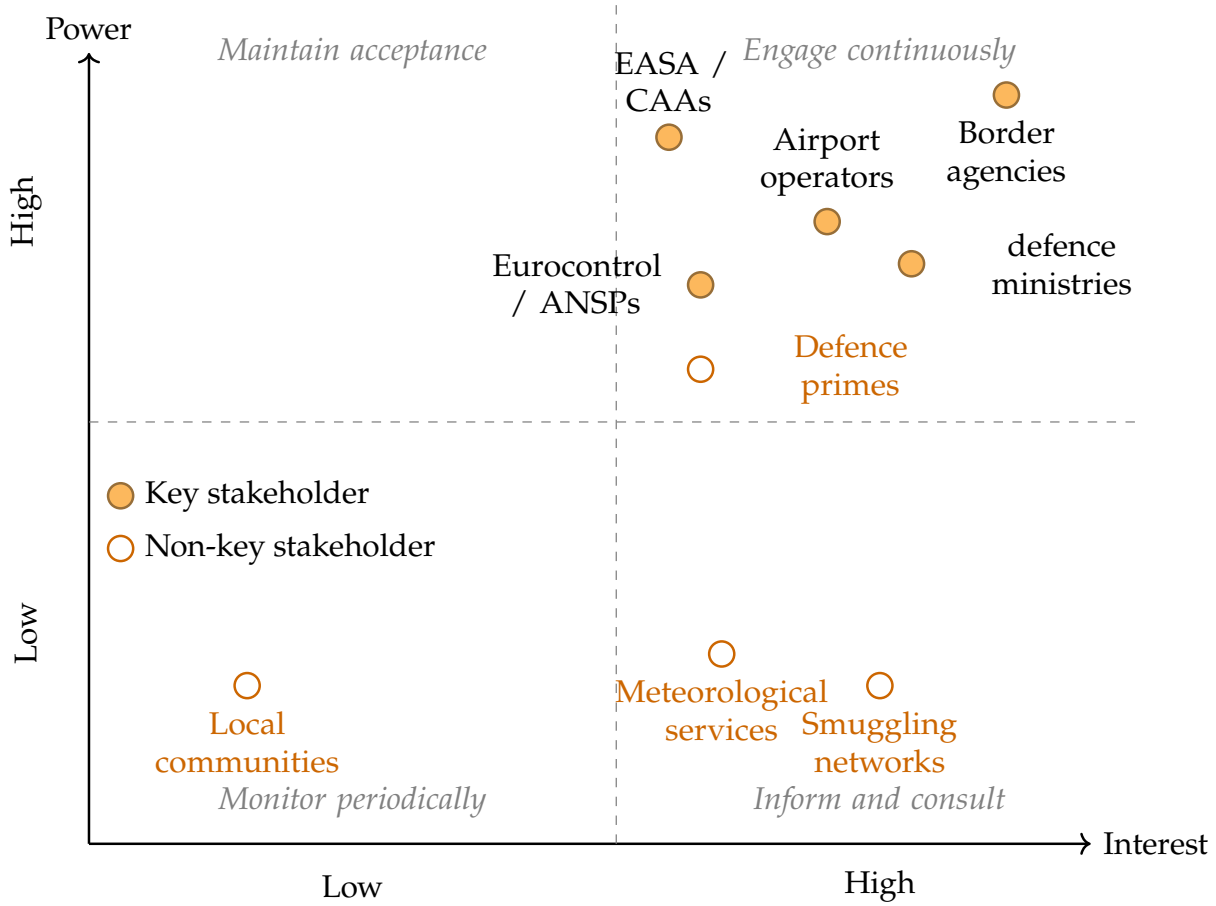

Figure 2.2: Power-Interest Map of Project Stakeholders. Stakeholders in the High-Power and High-Interest Quadrant Require Continuous Engagement, while Other Stakeholders Require Targeted Communication Depending on Their Influence and Interest

The concerns and priorities are translated directly into the stakeholder requirements listed in Chapter 3.

2.3. Competitive Positioning Summary

The project occupies a unique position at the intersection of three underserved requirements: civilian airspace legal compliance, non-destructive balloon-specific interception, and low cost. No commercial product currently satisfies all three simultaneously; the closest analogues, net-launching anti-drone interceptors, target objects about 100× smaller in cross-section and provide no buoyancy management. The total addressable market combines the growing counter-UAS sector with the hybrid balloon threat, for which states are actively funding technical solutions.

3 Key Stakeholder Requirements & Design Drivers

This chapter summarizes the key stakeholder and market requirements driving the design of BELLONA. These requirements follow from the operational problem and market analysis in Chapter 2, where free-floating balloons were identified as a safety, security, and economic risk to controlled airspace.

3.1. Requirement Derivation

The requirements are based on the main needs identified in the market analysis. Airport operators need a way to remove airspace hazards quickly, because prolonged airspace closures can be highly disruptive and costly. National security and border agencies need a response capability for hybrid-use or smuggling balloons. Meteorological and scientific operators benefit from non-destructive payload recovery, while aviation authorities and local communities require a solution that avoids uncontrolled debris and reduces risk to people and infrastructure on the ground.

Cost is also a key driver. Existing military or manually operated solutions are either too destructive, too expensive, or too slow for routine civilian use. BELLONA therefore has to be not only technically feasible, but also affordable enough to be relevant for airport operators and other civil users.

The resulting key stakeholder and market requirements are listed in Table 3.1. Only user-level requirements are included here. More detailed technical requirements are introduced in the relevant design chapters.

Table 3.1: Key Stakeholder and Market Requirements

ID	Requirement	Classification
REQ-STK-01	The system shall remove offending balloons from its covered airspace.	Key
REQ-STK-02	The system shall detect and track a balloon (2 m to 6 m diameter) up to 6000 m AGL.	Key
REQ-STK-03	The system shall intercept the uncooperative balloon within 10 min of acquisition.	Key
REQ-STK-10.2	The total system acquisition cost shall be less than €25000, excluding the ground station, inflation adjusted for 01.01.2026.	Key
REQ-STK-11	The operational cost per mission shall be less than €500 inflation-adjusted for 01.01.2026.	Key

These top-level requirements then flowed down according to Figure 3.1, established the boundary conditions for the system budgets, CAD layout, verification plan, and production logic, ensuring a common design baseline across all disciplines.

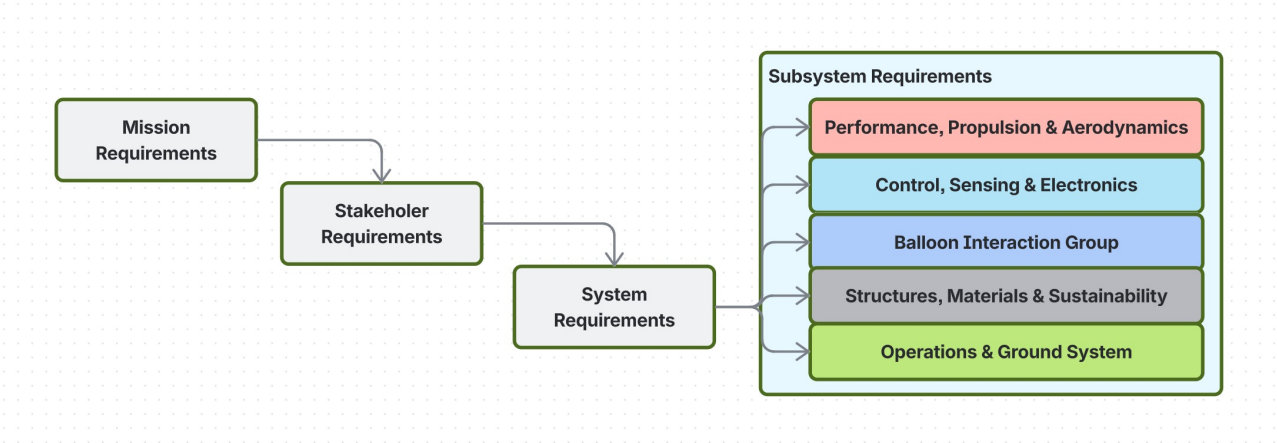

Figure 3.1: Requirement Flowdown for Subsystem Constraint Generation

4 Functional Analysis

4.1. Functional Flow Diagram

The Functional Flow Diagram (FFD), shown in Figure 4.1, translates the mission architecture into a time-ordered sequence of system functions. It shows how the UAS progresses from production and mission preparation to target acquisition, interception, recovery, and lifecycle closure. The updated diagram reflects the increased maturity of the detailed design by including the main functions of the selected sensing, communication, control, balloon-interaction, recovery, and lifecycle-support subsystems. Decision gates and feedback loops are included where the mission may be delayed, repeated, aborted, or redirected.

The FFD is organised into seven main phases: production of a mission-ready UAS, mission preparation, target acquisition, situational awareness, target interception, return to the landing area, and lifecycle closure. Continuous sensing, telemetry, and state-monitoring functions are represented as parallel support functions because they remain active throughout several mission phases. Safety-related functions are shown as feedback paths because they can interrupt or redirect the nominal sequence.

Producing a mission-ready UAS. The first phase covers the functions required to convert the frozen detailed design into an operational UAS. It starts with freezing the design for production, releasing the production baseline, and finalising the drawings and bill of materials. The required components are then procured as off-the-shelf parts or manufactured as custom structural parts, interfaces, and mounts. After inspection and acceptance, subsystem modules are built and assembled into the complete UAS. The integration step connects hardware, wiring, and software, verifies power and signal interfaces, checks subsystem inter-operability, and completes calibration. Ground and flight acceptance tests then confirm flight readiness and mission compliance before the final configuration is documented and the system is stored in a mission-ready state.

Preparing the mission. The preparation phase contains the first operational decision gates. After receiving the mission trigger, the system assesses mission feasibility using weather suitability, airspace and operating-area constraints, and battery or range margin. A feasible mission proceeds to pre-flight checks, while failed checks enter an issue-resolution loop before being repeated. Once all checks have passed, the mission parameters are configured. These include the geofence, no-fly zone, recovery zone, abort thresholds, and failsafe thresholds. Launch is authorised only after these conditions have been satisfied.

Acquiring the target. After launch authorisation, the UAS is dispatched, performs vertical take-off, transitions to wingborne climb, and may use a spiral climb to absorb excess ground track while gaining altitude. In parallel, the search area is defined and updated using ground cues received through the communication system. Once the UAS reaches the search volume and the target is within

the expected sensor engagement range, onboard searching starts. Candidate targets are detected using the forward-facing FMCW radar, LiDAR, and NIR camera. The radar provides range and velocity information, the LiDAR supports close-range three-dimensional profiling, and the NIR camera supports visual tracking under low-light conditions. Candidate detections are fused, filtered, and compared with the expected balloon characteristics. The flow progresses to interception only after the target has been confidently identified.

Maintaining situational awareness. Situational awareness is modelled as a continuous support flow. The UAS monitors its position, velocity, attitude, altitude, battery state, link status, and fault state through the flight controller and onboard telemetry. The flight controller provides low-latency UAS state estimation, while the companion computer processes the higher-bandwidth perception data from the radar, LiDAR, and camera sensors. The target-tracking pipeline estimates the balloon state and can propagate the state during short sensor dropouts, with increasing uncertainty. The resulting target and environment estimates support the onboard mapping, trajectory-generation, and guidance functions. Airspace awareness is maintained through ADS-B IN, while the Remote ID module broadcasts the UAS identity and state. Mission telemetry, video, and command data are handled through the LTE link, RF backup, DJI O3 video link, and emergency takeover channel. These functions support navigation, search, interception, landing, operator awareness, and contingency handling.

Intercepting the target. The interception phase is the most safety-critical part of the mission because the UAS transitions from target pursuit to physical interaction with the suspended payload. The UAS tracks the balloon-payload system, predicts its motion, and transitions from wingborne climb to terminal hover below the target. In hover, the launcher axis is aligned with the suspended payload and the capture geometry is checked against the allowable hover-position error, relative payload-UAS velocity, and launcher angular accuracy. If the geometry is outside the capture envelope, the UAS continues alignment or enters the repositioning loop.
Once the geometry is acceptable, the balloon-interaction system moves from the safe state to the armed state and performs a final launch-clearance check. If the check passes, the upward-launched net is fired toward the suspended payload. The corner weights open the pouch-shaped net above the UAS, allowing the payload to enter through the top opening. The system then checks whether the net deployed correctly. A successful deployment is followed by payload enclosure, closure-line tensioning, and capture confirmation. After confirmation, the tether and reel establish the mechanical load path between the UAS and the captured payload-balloon system.
During post-capture handling, the reel manages tether tension through retraction, controlled payout, and drag limiting, while reporting deployed tether length and reel state to the flight computer. If the tether load remains acceptable, the UAS proceeds to the return and controlled-descent phase with the captured system attached. If the load becomes unacceptable, the reel payout is adjusted and the load is reassessed. If the reel reaches the end-stop, the captured system becomes unsafe to tow, or an emergency command is issued, the breakaway sequence releases the UAS-side connection. The parachute remains attached to the payload-side tether, and the UAS performs an escape manoeuvre while the separated payload-net system descends under parachute.

Returning to the landing area and closing the mission. After the post-contact outcome has been secured, the UAS navigates to the recovery zone, descends, and lands. During descent, the control system manages thrust and attitude and can adjust thrust to correct lateral velocity. The rear-mounted RGB camera supports visual awareness during autonomous landing, while the flight controller and communication system maintain state monitoring and operator oversight. After landing, the recovery process secures the balloon and payload, retrieves deployed recovery equipment, and inspects the area for debris. A post-flight check is then performed and mission data are recorded for maintenance, validation, and future design improvement.

Closing the UAS lifecycle. The lifecycle-closure phase is entered when the UAS reaches its retirement criteria. It includes a final system health audit, structural inspection, propulsion and avionics static testing, extraction and archiving of lifetime telemetry, and synchronisation of the lifecycle logbook. Reusable subsystems are removed, tested, recertified where possible, and logged in the salvaged inventory. Hazardous materials are safely disposed of, recoverable materials are recycled, and the

UAS is formally deregistered with the relevant aviation authorities. The end-of-life outcome is then recorded through remote-ID deallocation, liability and insurance sign-off, and feedback of lessons learned into future design iterations.

4.2. Functional Breakdown Structure

The Functional Breakdown Structure (FBS), shown in Figure 4.2, reorganises the mission functions from the Functional Flow Diagram into functional groups. This view is used to assign functions to subsystem responsibilities and to keep the detailed design traceable to the mission-level flow. The table below defines the function identifiers used in the FBS and gives the role of each function in the system.

Table 4.1: Functional Breakdown

Category	Function Identifier & Name	Functional Definition
Life-Cycle Support (LS)	*0.1 Freeze design for production*	Establishes the final design baseline used for procurement, manufacturing, and assembly.
	0.2 Procure off-the-shelf parts	Obtains all selected commercial components required for the UAS.
	0.3 Manufacture custom parts	Produces the custom structural components, interfaces, and mounts required by the design.
	0.4 Inspect and accept parts	Verifies that procured and manufactured parts meet the required specifications before assembly.
	0.5 Build subsystem modules	Assembles components into functional subsystem modules before full-system integration.
	0.6 Assemble full UAS	Combines the subsystem modules into the complete aircraft configuration.
	0.7 Integrate hardware, wiring and software	Connects the electrical, mechanical, and software interfaces required for system operation.
	0.8 Verify interfaces and calibrate system	Confirms correct interface behaviour and calibrates the integrated UAS.
	0.9 Perform ground and flight acceptance tests	Demonstrates system readiness through ground and flight acceptance testing.
	0.10 Document configuration and store system	Records the accepted configuration and stores the UAS in a mission-ready state.
	7.1 Perform final system health audit	Assesses the condition of the UAS before retirement or lifecycle closure.
	7.2 Extract and archive all lifetime telemetry	Saves lifetime operational data for traceability, maintenance records, and future design use.
	7.3 Remove reusable subsystems	Removes components that can be tested, recertified, or reused.
	7.4 Safe disposal of hazardous materials	Disposes of batteries and other hazardous materials through controlled procedures.
	7.5 Recycle recoverable materials	Sends recoverable materials into appropriate recycling streams.
	7.6 Formal deregistration with aviation authorities	Completes the administrative closure of the retired UAS.
	7.7 Record end-of-life outcome	Records the final status of the vehicle, its registration, and remaining liabilities.
	7.8 Feed learned lessons into future design	Transfers operational and retirement findings into later design iterations.
Operations and Environment (OE)	*1.1 Receive mission trigger*	Receives and validates the external alert or activation command for the mission.
	1.2 Assess mission feasibility	Checks whether weather, airspace, operating-area, and energy conditions allow the mission.
	1.3 Perform pre-flight checks	Verifies readiness of the power, propulsion, sensing, communication, failsafe, and interaction systems.
	1.4 Configure mission parameters	Sets geofences, recovery zones, and abort or failsafe thresholds.
	1.5 Authorize launch	Confirms the final go/no-go decision, airspace clearance, and launch command.
	5.4 Recover payload and debris	Supports recovery of the payload, balloon material, deployed equipment, and debris.
	5.5 Post-flight check	Inspects the airframe, propulsion system, sensors, communication hardware, and interaction mechanism after landing.

Category	Function Identifier & Name	Functional Definition
	5.6 Record mission data	Stores flight telemetry, sensor data, and tracking information for later analysis.
Sensing and Tracking (ST)	*2.2 Search for target via ground cues*	Defines and updates the search area using external target-location cues.
	2.5 Start searching search volume	Begins onboard target search after the UAS reaches the assigned search volume.
	2.6 Detect via onboard sensors	Detects candidate balloon targets using the onboard sensor suite.
	2.7 Identify and confirm balloon target	Confirms the balloon by comparing candidate detections with expected balloon characteristics.
	3.1 Monitor own position and attitude	Estimates the UAS state using onboard navigation sensors and telemetry.
	3.2 Detect obstacles	Maintains obstacle and altitude awareness during flight.
	3.3 Monitor airspace status	Maintains awareness of surrounding airspace traffic and separation.
	4.1 Track target	Maintains the relative target estimate during approach and interception.
	4.2 Predict target motion	Estimates and propagates the balloon state to support intercept guidance.
Aerial Platform (AP)	*2.1 Dispatch UAS*	Launches the vehicle and transitions it from the ground state to controlled flight.
	2.3 Direct climb	Commands the climb segment toward the target search volume.
	2.4 Reach search volume	Arrives at the designated search volume where onboard search can begin.
	4.3 Approach target	Generates and follows an intercept trajectory toward the balloon-payload system.
	4.4 Transition to hover below target	Performs the pitch-up transition and establishes hover below the target.
	4.5 Align for interaction	Positions and orients the UAS so that the launcher is aligned with the suspended payload.
	5.1 Navigate to the landing area	Guides the UAS and captured system toward the selected recovery zone.
	5.2 Descend	Performs controlled descent using thrust and attitude control.
	5.3 Land	Selects the final landing point, executes final approach, and touches down safely.
Balloon Interaction (BI)	*4.6 Attempt payload capture with net*	Launches the net, encloses the payload, and closes the pouch after capture.
	4.7 Secure post-contact outcome	Tensions the tether, manages reel payout, and triggers breakaway parachute separation if required.

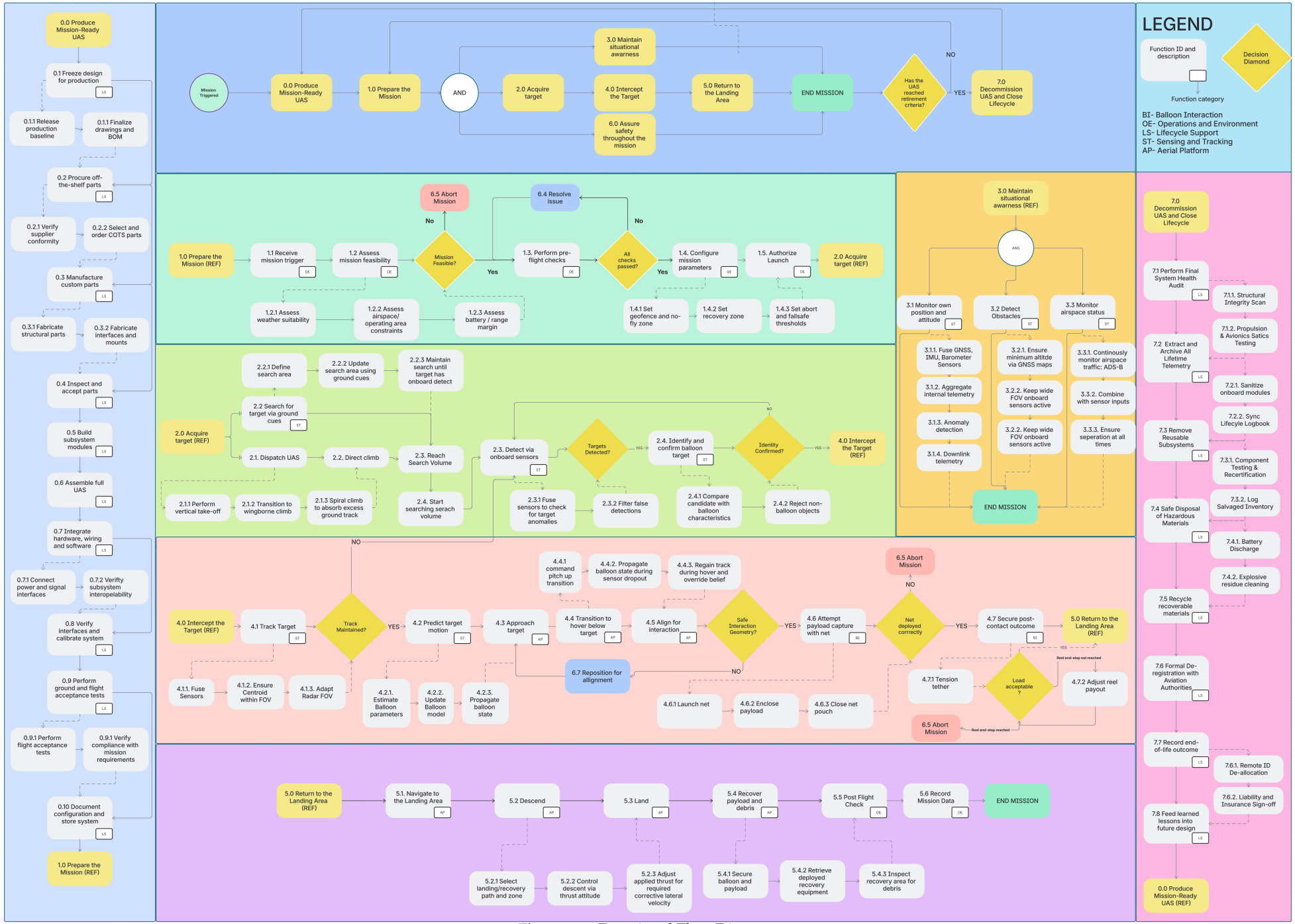

Figure 4.1: Functional Flow Diagram

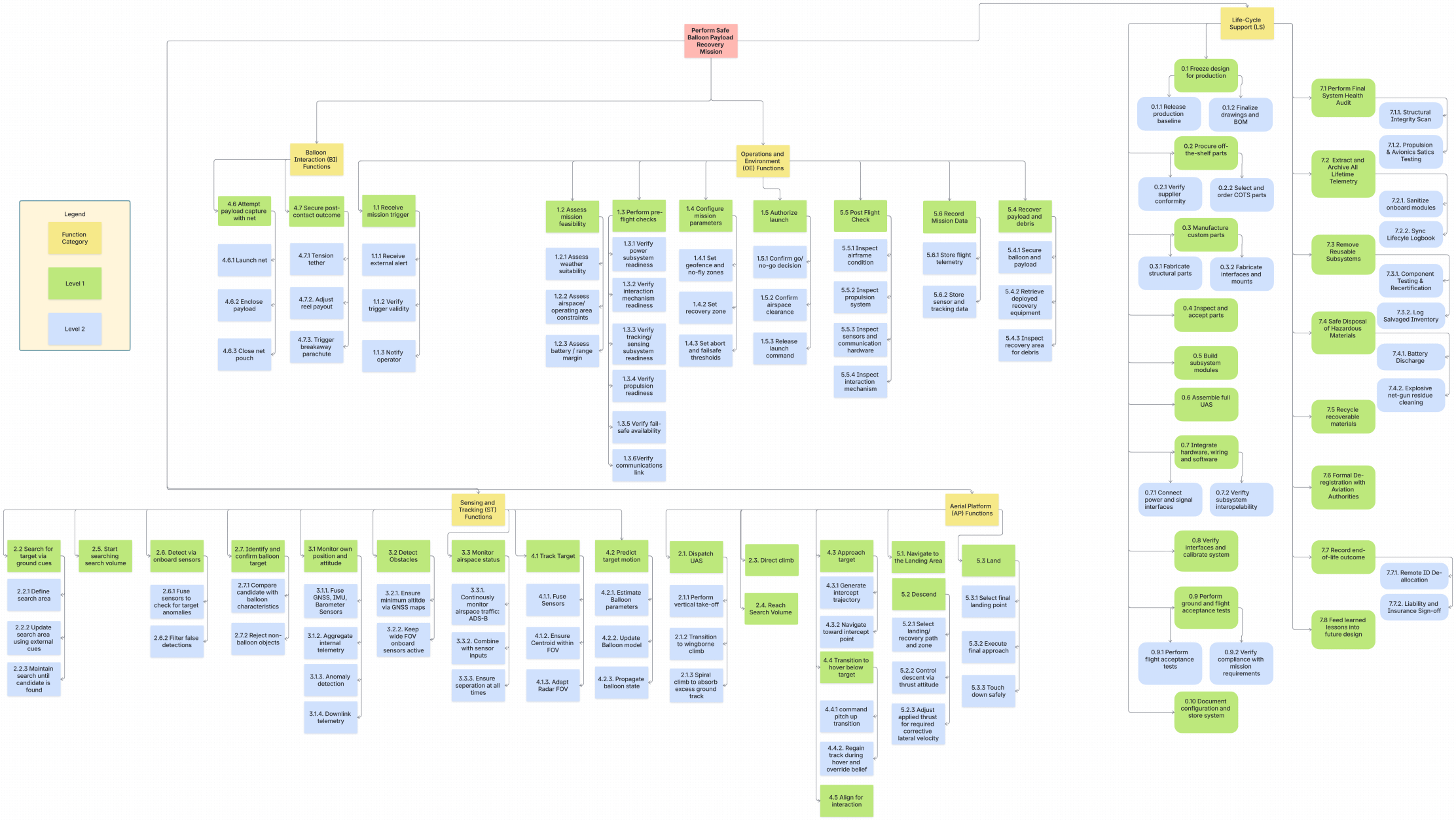

Figure 4.2: Functional Breakdown Structure Diagram

5
Design Methodology

The final design was developed using a constraint-driven concurrent engineering process. Instead of utilizing a single master optimizer, the methodology focused on optimizing individual subsystems in parallel, using a central iteration loop to drive the overall system toward convergence. The primary design drivers were the mission requirements (Chapter 3), the functional flow (Figure 4.1), the selected baseline concept, and the dynamically evolving mass, power, geometrical, and interface budgets.

5.1. Conceptual Design

With the requirements formalized, initial concepts were generated using Design option trees, where a balloon interaction mechanism was chosen per concept. Table 5.1 provides the overview used as the starting point for the concept descriptions and trade-off.

Table 5.1: Overview of the Five Concepts Entering the Trade-Off

ID	Concept	Core architecture	Recovery principle
A	Vertical Net Launch	Tail-sitter VTOL captures the suspended payload from below using an upward-launched net.	UAS weight and thrust pull the coupled system down, with parachute backup.
B	Pick and Drop	Carrier eVTOL deploys cooperative net drones and an intervention drone around the balloon-payload system.	Two-stage net containment, controlled deflation and guided parafoil descent.
C	Mechanical Clamping	Lift-and-cruise eVTOL secures the payload or attachment using deployable clamping beams.	UAS mass and directed thrust guide the coupled system to the recovery zone.
D	Cooperative Payload Net	Three multirotors suspend and close a shared net around the payload or lower flight train.	Added ballast and net hardware overcome free lift while the UAS team steers descent.
E	Kinetic Bolas	Hybrid UAS launches a weighted bolas line around the suspension line.	Tether reel-out, UAS weight and thrust guide the balloon-payload system downward.

These were then compared via a formal trade-off as shown in Table 5.2 in order to choose the best design for the subsequent preliminary and detailed design phases.

Table 5.2: Concept Trade-Off Matrix with Brief Score Justifications

Criteria	Concept A	Concept B	Concept C	Concept D	Concept E
Safety (0.25)	**4.1** No rupture; controlled tow	**2.3** Many stages; release risk	**3.0** Direct clamp; payload risk	**2.3** Ballast / formation risk	**4.1** Standoff; safe transit
Reliability (0.25)	**3.2** Simple net; transition risk	**2.8** Complex staging	**3.0** Shape-sensitive	**2.8** Multi-UAS coupling	**2.8** Bolas; line risk
Performance (0.25)	**3.8** Efficient transit; hover	**3.3** Adaptable; descent limits	**3.5** Strong lift; clamp limits	**2.5** Weak direct; hi-altitude	**3.5** Efficient; precise aim
Cost (0.15)	**4.2** Single UAS; simple gear	**2.0** Carrier + 4 drones	**4.4** Low-cost hardware	**1.4** 3 heavy UAS	**4.6** Lowest estimate
Sustainability (0.10)	**3.1** Reusable; high energy	**2.8** Contained; high reset	**2.9** Reusable; damage risk	**3.3** No envelope damage	**2.8** Simple; weak contain
Final Score	**3.72**	**2.69**	**3.33**	**2.45**	**3.57**
Ranking	**1**	**4**	**3**	**5**	**2**

5: Excellent	4: Good	3: Fair	2: Poor	1: Unacceptable

While this trade-off showed A as the winner, a comprehensive sensitivity study was carried out in order to ensure that this was due to technical superiority and not due to procedural issues. The normalized scores are shown in Table 5.3.

Table 5.3: Normalized Architectural Option Scoring and Ranking: Sensitivity Analysis

Concept	Concept A	Concept E	Concept C	Concept B	Concept D
Normalized Score (σ)	1.15	0.30	0.26	-0.71	-0.96

Concept A winning with a considerable margin in the normalized scores, underpins A as the legitimate winner. This was further supported by the finding that the cost criteria had a disproportionately large

impact due to having the largest standard deviation among all criteria. This allowed concept A to be chosen with confidence in its technical competitiveness and carried forward into the detailed design.

5.2. Iterative Concurrent Sizing and Convergence

The aircraft cannot be sized as independent subsystem blocks, because changes in one discipline directly affect the others. A central iteration loop was therefore used to manage shared system-level quantities: maximum take-off mass, centre-of-gravity range, battery capacity, installed propulsion power, structural loads, and major mechanical and electrical interfaces (Figure 5.1).

To maintain configuration control, each subsystem's analytical models were constructed modularly to interface with a centralized, integrated mass budget. Local subsystem calculations served as preliminary design evidence but were immediately superseded whenever the integrated system budget updated, ensuring all disciplines operated on an identical aircraft definition.

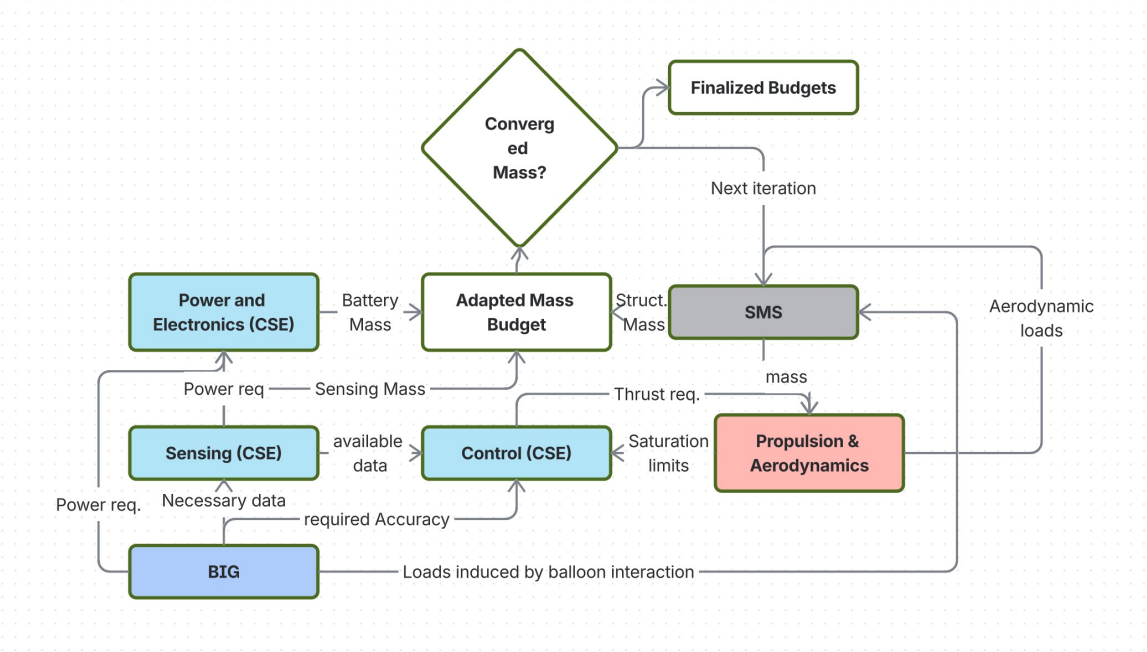

Figure 5.1: Iterative Design Loop Showing Subsystem Interaction and Convergence

The sizing loop progressed through the following iterative phases:

1. **Aerodynamic & Propulsion Baseline:** The performance, propulsion and aerodynamics models used the altitude, range, hover, and transition constraints to define the initial aircraft geometry, thrust requirement, and battery-energy target.
2. **Parallel Subsystem Sizing:** Electronics, balloon interaction, structures, ground operations, and production planning sized their components and interfaces against the current aircraft baseline.
3. **Structural Integration & Load Consolidation:** The structural discipline consolidated subsystem masses, mounting interfaces, aerodynamic loads, propulsion loads, landing loads, and payload-capture loads into common structural load cases.

Convergence was achieved through continuous, repeated budget checks of resource values (mass, power, volume, and energy demand). This disciplined feedback loop ensured that detailed subsystem work could proceed independently while forcing the final aircraft to close as a single, fully traceable, and coherent preliminary design configuration.

6
Propulsion, Performance and Aerodynamics

The propulsion, performance and aerodynamics design translates the selected tail-sitter concept into a flight vehicle that can take-off vertically, transition to wing-borne flight, climb to the balloon intercept point, hover below the suspended payload, and retain enough control authority for post-capture recovery.

This chapter presents the detailed PPA sizing methodology and the resulting selected design point. The purpose is to show how the governing assumptions, aerodynamic methods, propulsion constraints and performance calculations lead to the selected values.

6.1. PPA Sizing Problem and Mission Drivers

The PPA design is driven by the need to reach a balloon at an altitude of 6000 m and a horizontal ground range of 6000 m, while retaining the hover authority required for capture. The outbound flight is limited to 600 s. A terminal hover allowance of 300 s is included so that the aircraft can stabilise below the payload, perform the capture sequence, and absorb short operational delays. The post-capture recovery phase is represented at first order by the towing-descent footprint model in Subsection 6.9.3. The sizing includes a moderate 60 N towing force over a 900 s descent in the 13 m/s design wind, giving enough of a corrective lateral velocity to redirect the balloon to a safe landing location. Together, these mission constraints make aerodynamic efficiency, vertical thrust margin, and low-speed control authority the central sizing drivers, since the aircraft must minimise energy use during the long outbound segment while still retaining sufficient power and control authority for hover capture and recovery.

The tail-sitter architecture makes the PPA problem require special attention to the flight-transition requirements when switching between wingborne flight and rotor-powered VTOL and hover. Decreasing wing loading helps the aircraft accelerate from hover into wing-borne flight without stalling, but it also increases wing mass and drag. A higher thrust-to-weight ratio improves vertical-flight authority and transition control, but it increases motor, propeller, structural and battery demands. The selected design must therefore satisfy hover, transition, climb, aerodynamic trim and centre-of-gravity constraints simultaneously.

The PPA subsystem requirements are listed in Table 6.1. These requirements define the aircraft-level sizing checks for the intercept envelope, outbound trajectory, hover, transition, thrust, energy, trim, propulsion layout, and recovery authority.

Table 6.1: PPA Subsystem Requirements and Classifications

ID	Requirement	Classification
REQ-STK-03-MSN-04-SYS-08-PPA-01	The PPA subsystem shall complete the outbound intercept sequence within 600 s.	Key
REQ-STK-03-MSN-04-SYS-07-PPA-02	The PPA subsystem shall provide 300 s of terminal hover below the payload.	Key
REQ-STK-03-MSN-04-SYS-08-PPA-03	The PPA subsystem shall provide a wing stall equivalent airspeed that allows smooth transition between wingborne flight and VTOL/hover.	Key
REQ-STK-03-MSN-04-SYS-08-PPA-04	The PPA subsystem shall provide enough vertical-flight thrust margin with four rotors for gust rejection and precise aiming of the net gun.	Key
REQ-STK-01-MSN-01-SYS-01-PPA-05	The PPA subsystem shall ensure that the energy demand for the mission is exceeded by the battery capacity with necessary contingency corrections.	Driving
REQ-STK-03-MSN-04-SYS-08-PPA-06	The PPA subsystem shall maintain aerodynamic trim and a usable operational centre-of-gravity band in wing-borne flight.	Key
REQ-STK-01-MSN-01-SYS-45-PPA-07	The PPA subsystem shall fit the selected propeller disk area inside the aircraft layout without invalidating capture clearance or structural interfaces.	Non-driving
REQ-STK-03-MSN-04-SYS-08-PPA-08	The PPA subsystem shall size the aircraft for interception at an altitude of 6000 m.	Driving
REQ-STK-03-MSN-04-SYS-44-PPA-09	The PPA subsystem shall size the outbound trajectory for a horizontal ground range of 6000 m.	Driving
REQ-STK-01-MSN-01-SYS-01-PPA-10	The PPA subsystem shall provide a mission timing budget for outbound flight, terminal hover and first-order recovery allowance compatible with the 25 min restricted-airspace removal objective.	Driving
REQ-STK-05-MSN-06-SYS-11-PPA-11	The PPA subsystem shall retain propulsion and control-authority margin for interaction with a captured payload-balloon system with payload mass up to 50 kg.	Driving
REQ-STK-07-MSN-09-SYS-46-PPA-12	The PPA subsystem shall assess hover, transition and recovery authority in sustained winds up to 13 m/s.	Driving
REQ-STK-03-MSN-04-SYS-08-PPA-13	The PPA subsystem shall maintain sufficient climb lift margin such that the mission climb lift coefficient remains below the selected stall-margin limit.	Key
REQ-STK-03-MSN-04-SYS-08-PPA-14	The PPA subsystem shall close the aircraft design through an iterative mass, geometry and energy sizing loop that ensures compatibility with other subsystem designs.	Driving

6.2. Overall Sizing Workflow

The aircraft-level problem solved by the workflow is a constrained preliminary optimisation over main-wing area, canard area ratio, wing station and battery location. The objective is to minimise closed maximum take-off mass while satisfying the stall, time, climb, power, scissor and mass-closure constraints:

$$\underset{S_w,\, S_c/S_w,\, x_w,\, x_b}{\text{optimal}} \quad \text{resulting in} \quad \min_{\text{MTOW}} \quad \text{subject to} \quad \begin{cases} V_{S,\text{EAS}} \le V_{S,\text{EAS,max}} \\ t_{\text{outbound}} \le 600\,\text{s} \\ C_{L,\text{climb}} \le C_{L,\text{max},w}/n_{\text{stall}}^2 \\ P_{\text{peak}} \le P_{\text{available}} \\ x_{\text{CG,op}} \subseteq x_{\text{CG,scissor}} \\ |m_{i+1} - m_i| \le \varepsilon_m \end{cases} \tag{6.1}$$

Figure 6.1 shows the nested sizing logic used to converge the PPA design. The process starts at the top of Loop 1 with the initial aerodynamic assumptions, which are developed in Section 6.3 and Section 6.4. Loop 1 calls the wing-area sweep through marker 1, then updates the airfoil and finite-wing aerodynamic inputs after the sweep returns through marker 2. If the aerodynamic coefficients change, the sweep is repeated with the updated values. This makes the selected geometry consistent with the Reynolds-number, lift-curve and stall-speed assumptions used in the wing-loading and transition checks of Section 6.6 and Section 6.7.

Loop 2 evaluates all candidate wing areas following the workflow described above. For each wing area, marker 3 calls Loop 3, where the aircraft mass, rotor geometry, mission energy and component masses are closed for that candidate using the propulsion and mission-performance methods in Section 6.8 and Section 6.9. The mass closure uses geometry-dependent structural mass estimates from the Structures department, including terms linked to wing area, canard area and fuselage length, so that PPA geometry changes remain consistent with the structural mass budget. Inside Loop 3, markers 5 and 6 call the canard and wing-station sub-solve described in Section 6.10, which selects the lightest canard layout that satisfies centre-of-gravity, scissor and stall constraints. When the mass change is small enough, Loop 3 returns to Loop 2 through marker 4. Loop 2 then checks feasibility and, after all wing areas have been tested, selects the lightest candidate that satisfies the transition stall limit, climb-time limit, trim constraints, power limit and mass-closure requirement. The selected point is interpreted in Section 6.11 and summarised in Section 6.12.

6.3. Key Assumptions and Design Constants

Table 6.2 summarises the assumptions that most strongly govern the sizing result. They span four coupled areas: the mission envelope and mass closure, which set the energy and thrust requirements; the battery and propulsion models, which translate those requirements into component masses; the aerodynamic models, which determine wing area and stall margins. The PPA result is only as reliable as these inputs.

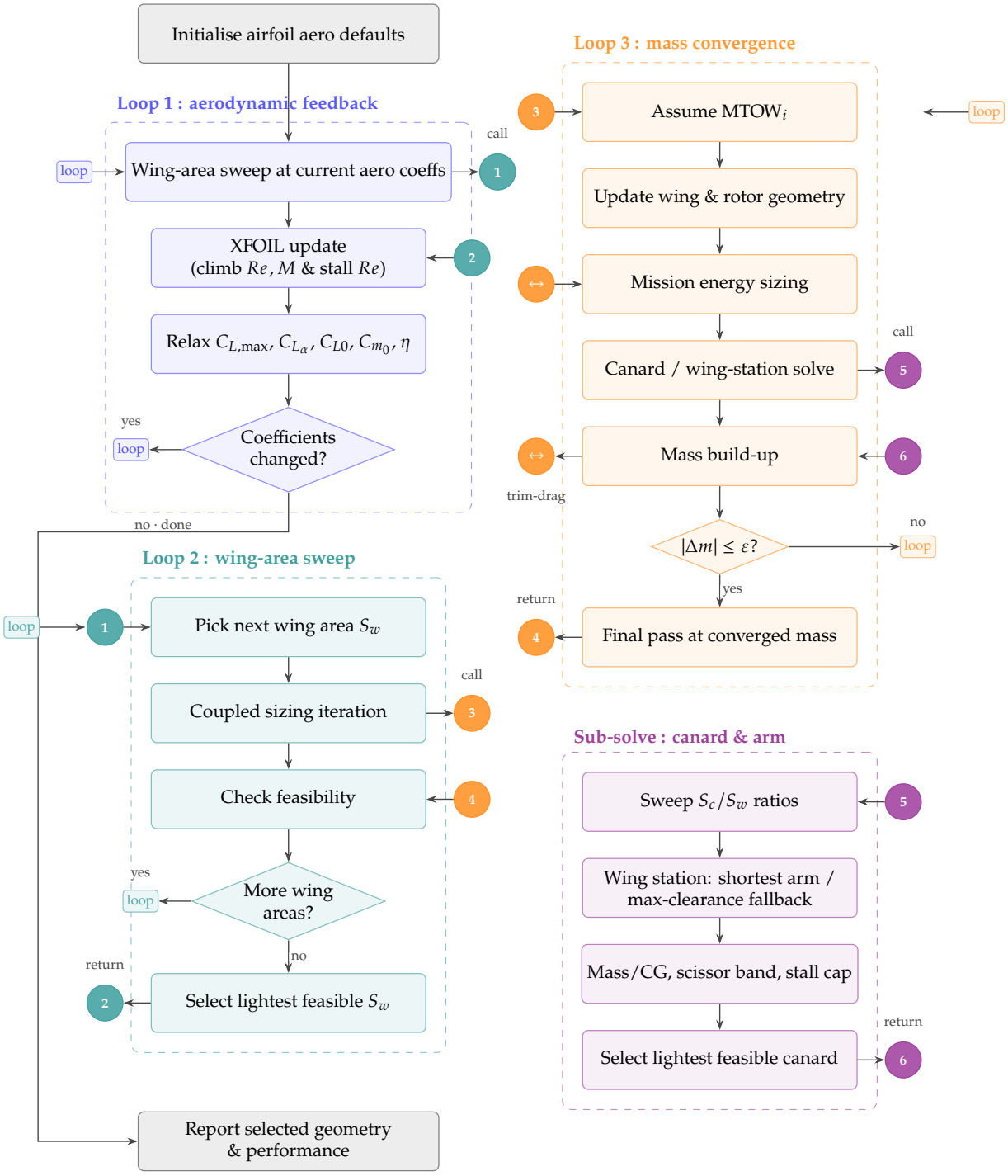

Figure 6.1: Python Code Iteration Layout of the Aircraft Sizing Procedure

Table 6.2: Main Assumptions and Modeling Choices Used for PPA Sizing

Assumption / modelling choice	Value / Model	Sizing Impact & Status
Mission envelope	6000m alt, 6000m range, 600s climb, 300s hover	Drives climb profile, energy budget, and battery mass. (Requirement-driven)
Initial seed MTOW	52.78 kg (iterated to closure)	Sizing loop initialization, taken from preliminary design mass estimation.
Battery sizing model	400 Wh/kg pack-level specific energy [15, 16]	NASA projections place nominal 2030 pack-level specific energy near 391 Wh/kg and aggressive 2030 pack-level specific energy near 525 Wh/kg, while the selected candidate cell family is checked separately against supplier cell data above 460 Wh/kg
Battery sizing factors	$\eta_{bat} = 0.95$, $DOD_{nom} = 0.80$, $k_{cont} = 1.15$	The battery efficiency and usable-depth assumption account for discharge losses and the decision to retain at least 20 % state of charge. The contingency factor is an internal mission margin applied after propulsion and non-propulsive energy are combined [17, 15].
Rotors & Thrust	4 rotors, $T/W = 1.30$	Design value above Stone and Clarke's $T/W \geq 1.15$ tail-sitter transition lower-bound check [18].
Disk loading	170 N/m^2 at max thrust	Chosen as a deliberately low disk-loading target to reduce hover induced power at the cost of larger propeller diameter. [19].
Hover efficiency chain	FoM = 0.70, $\eta_{motor} = 0.90$, $\eta_{ESC} = 0.95$	Converts ideal actuator-disk hover power into electrical hover power. The figure of merit is within the typical rotorcraft/eVTOL preliminary-design range of 0.5–0.8, while the motor and power-electronics values are conservative relative to NASA electric-machine and converter assumptions used in electrified-aircraft studies [19, 20].
Forward-flight efficiency	$\eta_{prop} = 0.75$, $\eta_{motor} = 0.90$, $\eta_{ESC} = 0.95$	Preliminary propulsive-efficiency chain used to convert electrical climb power into useful propulsive power. The propeller term is representative of small-UAS propeller performance in early sizing and must be replaced by supplier or test maps during detailed propulsion matching [21, 20, 22].
Wing geometry	AR 7.0, taper 0.40, 0° LE sweep, SD7037 airfoil	The wing uses a moderate aspect ratio to balance induced drag, stall angle and the bending-driven wing-weight increase associated with larger span. A taper ratio of 0.40 is selected as a practical unswept-wing value giving an almost elliptical lift distribution with a very small induced-drag penalty. Sweep is set to zero because the aircraft operates at low Mach number, so the critical-Mach benefit of sweep is unnecessary, while sweep would reduce maximum lift and increase structural and stall-behaviour penalties [23, 24].
Canard geometry	AR 5.0, taper 0.4, sweep 0° NACA 0012	The canard aspect ratio is kept moderate to balance lifting efficiency while limiting span, structural mass and integration complexity. The NACA 0012 section is selected as a symmetric preliminary control-surface airfoil with well-documented aerodynamic properties. [23, 24].
Max lift model	Low-Reynolds-number 2D polar data with finite-wing correction	Fixes stall speed and therefore the minimum feasible wing area. Low-Reynolds-number airfoil data are taken from the UIUC/Selig data set, while finite-wing lift-curve and maximum-lift corrections follow DATCOM-style preliminary methods [25, 26]. Higher-fidelity aerodynamic check pending.
Drag model	Component $C_{D,0}$ build-up plus induced drag	Sets climb power, energy consumption and the selected wing area. The component build-up uses skin-friction, form-factor, interference-factor and wetted-area terms, while induced drag is treated through aspect ratio and Oswald/span-efficiency assumptions[27, 28].

6.4. Aerodynamic Model

The aerodynamic model is introduced before the sizing calculations because it provides the calculated $C_{L,\max}$, lift-curve slopes, Reynolds-number conditions, trim lift split and drag coefficients used throughout the chapter. The selected airfoils and planform geometry are design inputs; the remaining aerodynamic entries in Table 6.3 are derived from low-Reynolds-number airfoil data, finite-wing corrections, component drag build-up, two-surface induced drag and a steady longitudinal trim calculation.

For each lifting surface, the selected area S, aspect ratio A and taper ratio λ first define the planform dimensions:

$$b = \sqrt{AS}, \qquad c_{\text{ref}} = \frac{S}{b}, \qquad c_r = \frac{2S}{b(1+\lambda)}, \qquad c_t = \lambda c_r. \tag{6.2}$$

These dimensions set the Reynolds-number range for the airfoil polar data. Using the reference chord as the characteristic length, the Reynolds number is evaluated as

$$Re = \frac{\rho V c_{\text{ref}}}{\mu}. \tag{6.3}$$

At the high-altitude climb reference condition, $V = 40.5\,\text{m s}^{-1}$, $\rho = 0.660\,\text{kg m}^{-3}$, and $\mu = 1.58{\times}10^{-5}\,\text{Pa s}$. This gives $Re_w = 1 \times 10^6$ for the wing and $Re_c = 4.5 \times 10^5$ for the canard. At the stall condition the corresponding values are 6.7×10^5 and 3×10^5, so the airfoil polar data are evaluated in the Reynolds-number range relevant to the selected geometry.

The XFOIL two-dimensional section polar provides c_{ℓ_α} and $c_{\ell,\max}$. The isolated finite-wing lift-curve slope of each lifting surface is then calculated using the DATCOM subsonic correction [25]:

$$C_{L_\alpha} = \frac{2\pi A}{2 + \sqrt{4 + \left(\frac{A\beta}{\eta_D}\right)^2 \left(1 + \frac{\tan^2 \Lambda_{1/2}}{\beta^2}\right)}}, \qquad \beta = \sqrt{1 - M^2}. \tag{6.4}$$

Here η_D is the DATCOM section-efficiency factor derived from the section lift slope, and $\Lambda_{1/2}$ is the half-chord sweep. The finite-wing maximum lift coefficient is obtained from the high-aspect-ratio Raymer [29] /DATCOM correction [25]:

$$C_{L,\max} = K_{\max}(\Delta y, \Lambda_{LE})\, c_{\ell,\max} + \Delta C_{L,\max}(M), \qquad \tan \Lambda_{LE} = \tan \Lambda_{c/4} + \frac{1-\lambda}{A(1+\lambda)}. \tag{6.5}$$

The factor $K_{\max}$ accounts for leading-edge sharpness and leading-edge sweep; at the low stall Mach numbers used here, the Mach correction is zero.

The trim lift split is then obtained from vertical-force and pitching-moment equilibrium:

$$q(S_w C_{L,w} + S_c C_{L,c}) = W, \qquad C_{m,\text{cg}}(C_{L,w}, C_{L,c}, C_{m_{ac}}) = 0, \qquad q = \frac{1}{2}\rho V^2. \tag{6.6}$$

Applying these relations gives finite-wing maximum lift coefficients of $C_{L,\max,w} = 1.2$ and $C_{L,\max,c} = 1.033$. The corresponding isolated finite-wing lift-curve slopes are $4.78\,\text{rad}^{-1}$ for the wing and $4.32\,\text{rad}^{-1}$ for the canard. The aircraft does not fly a separate level-cruise segment in the selected mission, so the quoted trim state is the high-altitude wing-borne climb reference condition. At $V_{\text{TAS}} = 40.5\,\text{m/s}$, $V_{\text{EAS}} = 29.8\,\text{m/s}$, and $q = 542\,\text{Pa}$, the longitudinal trim calculation gives $C_L = 0.363$, split into $C_{L,w} = 0.251$ and $C_{L,c} = 0.794$. The high canard coefficient is expected because the canard is both a lifting surface and the main longitudinal trim surface.

Table 6.3: Aerodynamic Inputs, Calculated Coefficients and Reference Flow Quantities

Quantity	Value
Wing / canard airfoil	SD7037 / NACA 0012
Wing / canard $C_{L,\max}$	1.2 / 1.0
Wing / canard isolated lift-curve slope	$4.8\,\text{rad}^{-1}$ / $4.3\,\text{rad}^{-1}$
Trim reference V_{TAS}, V_{EAS}, q	40.5 m/s, 29.8 m/s, 542 Pa
Wing / canard Reynolds number at climb	1.01×10^6 / 4.48×10^5
Wing / canard Reynolds number at stall	6.71×10^5 / 2.97×10^5
Aircraft, wing and canard trim C_L at $V_{\text{TAS}} = 40.5\,\text{m/s}$	0.4 / 0.3 / 0.8

6.5. Drag Polar and Performance Model

The climb calculation uses a geometry-dependent drag polar rather than a fixed drag coefficient. The drag coefficient is represented as

$$C_D = C_{D,0} + C_{D,i,w} + C_{D,i,c} + C_{D,i,\text{int}}, \tag{6.7}$$

where $C_{D,0}$ is built up from component skin-friction, form-factor, interference-factor and wetted-area terms estimated with the help of the methodology described in [29, 23]:

$$C_{D,0} = \sum_i \frac{C_{f,i} FF_i IF_i S_{\text{wet},i}}{S_w} + C_{D,\text{misc}}. \tag{6.8}$$

The two lifting surfaces are treated separately for induced drag, with $e_w = 0.78$ and $e_c = 0.70$ as the Oswald efficiency factors for the wing and canard, respectively. The additional $C_{D,i,\text{int}}$ term is kept separate from these e-values and represents the tandem-surface induced-interference contribution because both surfaces carry positive lift.

The resulting component zero-lift drag is $C_{D,0} = 0.01307$, and the trimmed wing-borne climb drag coefficient is $C_D = 0.03121$. At the selected trim point, $L/D = 11.61$, close to the maximum evaluated value of 11.65 at $C_L = 0.325$. This is the drag state used in the mission-performance calculation.

Table 6.4: Selected Drag Build-Up and Induced-Drag Parameters

Quantity	Value
Trimmed C_D, L/D	0.03, 11.6
UAS zero-lift drag $C_{D,0}$	0.013
Wing / canard / fuselage $C_{D,0}$ contributions	0.0073 / 0.001 / 0.0033
Hardware plus miscellaneous $C_{D,0}$	0.0015
Wing / canard Oswald efficiency factors	0.78 / 0.70
Maximum L/D in evaluated range	11.7 at $C_L = 0.33$

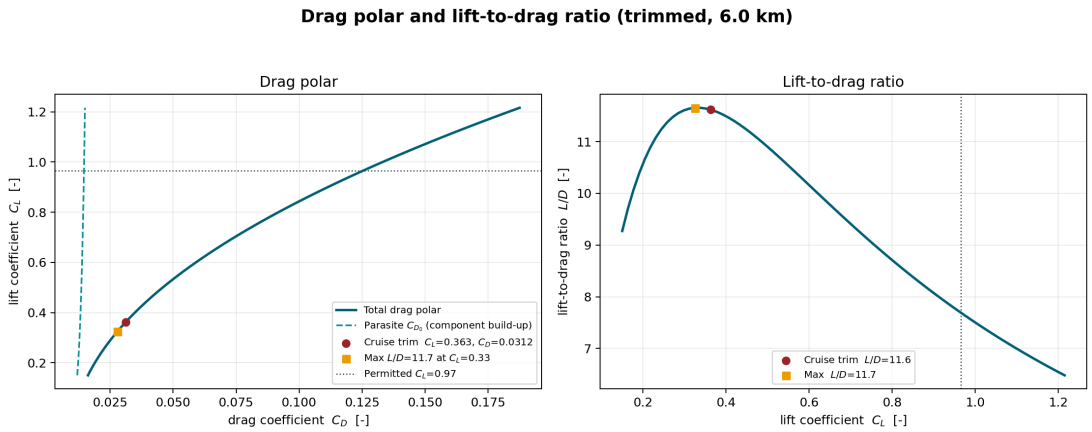

Figure 6.2: Selected Aircraft Drag Polar and Lift-to-Drag Ratio for the Converged Geometry. The Marked Trim Point Corresponds to the High-Altitude Wing-Borne Climb Condition Used in the Mission Energy Model

6.6. Wing Loading and Stall-Speed Constraint

Wing loading sets the fixed-wing side of the sizing problem. For the closed mass $W = 501.4\,\text{N}$ and selected wing area $S_w = 2.55\,\text{m}^2$,

$$\frac{W}{S_w} = 196.6\,\text{N/m}^2 \quad \left(20.05\,\text{kg/m}^2\right). \tag{6.9}$$

Using $C_{L,\max,w} = 1.2$, the equivalent-airspeed stall speed is

$$V_{S,\text{EAS}} = \sqrt{\frac{2W}{\rho_0 S_w C_{L,\max,w}}} = 16.25\,\text{m/s}. \tag{6.10}$$

The binding back-transition cap is 16.54 m/s, leaving a stall-speed margin of 0.29 m/s. This small margin is the reason the selected wing area is the first feasible point in the sweep; smaller wings save

mass but violate the transition stall corridor. The cap exists because if the wing stalls too rapidly during back-transition, the resulting pitch-up moment exceeds rotor control authority before the transition is complete.

6.7. Transition and Tail-Sitter Constraints

The transition assessment converts the stall-speed result from Section 6.6 into a tail-sitter manoeuvre compatibility check. The sizing question is the largest wing stall EAS that still allows the aircraft to complete both forward transition, from hover to wing-borne climb-out, and back-transition, from wing-borne flight to hover before capture. This limiting stall speed becomes the transition-derived cap used in the wing-area selection.

Both transition legs are evaluated with a reduced-order point-mass model in the vertical plane, following the tail-sitter transition approach of Stone and Clarke [18]. The model integrates horizontal and vertical motion, while the pitch attitude is imposed through a fixed pitch-rate schedule. At this preliminary sizing stage, the prescribed schedule represents the available differential-thrust rotation authority and the total thrust resultant acts along the body axis. Individual rotor thrusts and moments are left for the later six-degree-of-freedom simulation.

The instantaneous speed, flight-path angle and angle of attack follow from the velocity components,

$$V = \sqrt{u^2 + w^2}, \qquad \gamma = \operatorname{atan2}(w, u), \qquad \alpha = \theta - \gamma. \tag{6.11}$$

where u, w are the horizontal and vertical velocity components, x, h are downrange distance and altitude, θ is the aircraft pitch attitude and γ is the flight-path angle. Resolving thrust, lift, drag and weight into the earth-fixed axes gives

$$\begin{aligned} m\dot{u} &= T\cos\theta - D\cos\gamma - L\sin\gamma, \\ m\dot{w} &= T\sin\theta - D\sin\gamma + L\cos\gamma - W, \\ \dot{x} &= u, \qquad \dot{h} = w, \end{aligned} \tag{6.12}$$

with $W = mg$. The aerodynamic forces are referenced to the main-wing area and use aircraft-level coefficients built from the wing and canard contributions:

$$L = qS_wC_L, \quad D = qS_wC_D, \quad C_L = C_{L,w}(\alpha) + \tfrac{S_c}{S_w}C_{L,c}(\alpha), \quad C_D = C_{D,w}(\alpha) + \tfrac{S_c}{S_w}C_{D,c}(\alpha). \tag{6.13}$$

Below stall, the surface coefficients use the linear finite-wing lift slope and induced drag. During back-transition the wing is deliberately pitched beyond stall, so the simulation switches to a Viterna–Corrigan flat-plate extrapolation above the stall angle. This gives continuous lift and drag through the high-angle-of-attack part of the pitch-up without requiring a full unsteady aerodynamic model.

The thrust level is set by a simple vertical-rate controller and clipped by the available T/W. On the forward leg, the commanded vertical speed blends from the initial VTOL climb rate to the wing-borne climb target. On the back leg, it blends toward zero vertical speed for hover capture. This keeps the reduced-order model tied to the intended handover task without adding a detailed flight controller.

The model can generate a stall-speed cap without being rerun for every wing-area candidate. After dividing Equation 6.12 by mass, the thrust acceleration depends on T/W, while the aerodynamic terms depend on S_w/m. The stall-speed definition fixes that ratio for a trial V_S:

$$\frac{S_w}{m} = \frac{2g}{\rho_0 V_S^2 C_{L,\max}}, \qquad \frac{L}{m} = g\frac{\rho}{\rho_0}\frac{V^2}{V_S^2}\frac{C_L}{C_{L,\max}}, \qquad \frac{D}{m} = g\frac{\rho}{\rho_0}\frac{V^2}{V_S^2}\frac{C_D}{C_{L,\max}}. \tag{6.14}$$

For fixed T/W, $C_{L,\max}$, drag model, altitude and canard area ratio, the transition path is therefore a function of the trial stall speed. The trial V_S is swept for each leg, and the largest value that still satisfies the handover criteria in Table 6.5 is taken as that leg's cap. This size-independence is a preliminary-design approximation because $C_{L,\max}$ and $C_{D,0}$ still vary weakly with Reynolds number.

Table 6.5: Entry Conditions and Handover Criteria for the Two Simulated Transition Legs

Quantity	Forward (hover → wing)	Back (wing → hover)
Leg altitude / density	sea level	6000 m
Entry attitude θ_0	90° (vertical)	α_{trim} (level)
Entry velocity (u, w)	$(0,\ 2\,\text{m/s})$	$(1.30\,V_{S,\text{TAS}},\ 0)$
Entry height h_0	20 m	reference 0
Target attitude θ_f	$\gamma_c + \alpha_{\text{hand}} = 19°$	110°
Pitch rate $\dot{\theta}$	12 °/s	12 °/s
Altitude-hold gain k_h	$1.5\,\text{s}^{-1}$	$1.5\,\text{s}^{-1}$
Handover condition	$V \geq 1.25\,V_{S,\text{TAS}}$, wing attached	$V \leq 0.25$ m/s
Maximum angle of attack	wing stall α_s	120°
Height band	ground clearance $h \geq 0$	±10 m
Time / distance limit	25 s / 250 m	10 s

The back-transition timing criterion is driven by sensing and estimation. During the pitch-up into hover, the balloon-payload relative state may have to be propagated through a degraded line-of-sight interval. The sensing verification in Figure 7.7 shows less than 5 m position divergence over a 10 s dropout, so the PPA sizing uses approximately 10 s as the allowable back-transition blackout window. Matching this timing criterion gives a back-transition stall cap of 16.54 m/s EAS.

The forward-transition check is less restrictive. The selected design accelerates from the final velocity reached in the 20 m vertical climb to the wing-borne climb-out speed, reaching approximately 20.2 m/s over about 250 m. The resulting forward-transition stall cap is 45.0 m/s EAS. The binding cap is therefore the back-transition value. Since the selected aircraft has $V_{S,\text{EAS}} = 16.25$ m/s, the transition margin is 0.29 m/s. These results support preliminary wing-area selection; detailed transition validation still requires a six-degree-of-freedom simulation with the final controller.

6.8. Propulsion Sizing Methodology

The propulsion system is sized for vertical flight authority and then checked against wing-borne climb power. Steady hover requires $T = W$, while the installed system is sized for $T_{\max} = 1.30W$. The additional thrust is held as control-authority margin for differential-thrust commands during gust rejection, target alignment, nose attitude control in wind, and transient tether disturbances during capture. With $T/W = 1.30$, the installed thrust is $T_{\max} = 651.8$ N, or 163.0 N per rotor for four rotors. The pure-hover thrust per rotor is 125.3 N, so the nominal thrust margin is 30% before control-allocation and installation losses.

The preliminary maximum-thrust disk-loading target is 170 N/m^2. This gives an equivalent minimum disk area of 0.959 m^2 per rotor and an equivalent propeller diameter of 1.10 m. At MTOW pure hover, the effective disk loading for this notional disk is 130.8 N/m^2. These values define the PPA propulsion interface; they are not a final catalogue propeller selection.

Actuator-disk theory gives the ideal induced hover power $P_i = T\sqrt{T/(2\rho A)}$ [19]. At 6000 m, the ideal induced power for pure weight support is 5 kW. The sizing hover power is calculated at the installed thrust condition $T_{\max} = 1.30W$, using $n_r = 4$ rotors, $T_r = 163.0$ N per rotor, $A_r = 0.959$ m^2 per rotor and $\rho = 0.660$ kg/m^3. With FoM = 0.70, $\eta_{\text{motor}} = 0.90$ and $\eta_{\text{ESC}} = 0.95$, the base electrical hover power before the station-keeping reserve is

$$P_{\text{hover},e,0} = \frac{n_r T_r \sqrt{T_r/(2\rho A_r)}}{\text{FoM}\,\eta_{\text{motor}}\,\eta_{\text{ESC}}} = \frac{7.40\,\text{kW}}{0.70 \cdot 0.90 \cdot 0.95} = 12.36\,\text{kW}, \qquad T_r = \frac{T_{\max}}{n_r}. \tag{6.15}$$

The energy model then retains a conservative hover-power allowance to cover persistent station-keeping control effort and gust rejection during the capture window. Applying the hover reserve factor $k_h = 1.22$ gives

$$P_{\text{hover},e} = k_h P_{\text{hover},e,0} = 1.22 \cdot 12.36\,\text{kW} \approx 15.1\,\text{kW}. \tag{6.16}$$

The reserve factor $k_h = 1.22$ [30] accounts for installation losses, control-allocation overhead and altitude density uncertainty. The peak electrical draw in the sizing mission is 15.85 kW, as illustrated by the electrical power curve from Figure 6.5, compared with the selected 16.0 kW climb-power sizing point.

6.9. Mission and Flight Performance

6.9.1. Take-off and Transition

The mission begins with a 20 m vertical take-off at 2 m/s, giving a 10 s take-off time and 0.042 kWh at the conservative hover-power allowance. The transition allowance accelerates from the final VTOL speed to approximately $1.2V_S = 19.5\,\mathrm{m/s}$ at $1.0\,\mathrm{m/s^2}$, using half of that allowance and approximately 0.041 kWh. These energy terms are small, but the transition speed requirement drives the wing-area constraint.

6.9.2. Climb and Intercept Trajectory

Wing-borne climb is evaluated with the constant-equivalent-airspeed method described in [31]. For each candidate climb EAS, the local density converts EAS to true airspeed, the drag polar gives the required propulsive power, and the excess-power relation gives the steady rate of climb:

$$V_{\mathrm{TAS}} = V_{\mathrm{EAS}}\sqrt{\frac{\rho_0}{\rho}}, \qquad P_r = DV_{\mathrm{TAS}}, \qquad P_a = \eta_{\mathrm{ff}}P_{e,\mathrm{avail}}, \qquad RC_s = \frac{P_a - P_r}{W}. \tag{6.17}$$

Because the climb is flown at constant EAS, the true airspeed increases with altitude. The integrated climb rate therefore includes the standard acceleration correction

$$RC = \frac{RC_s}{1 + \frac{V_{\mathrm{TAS}}}{g}\frac{\mathrm{d}V_{\mathrm{TAS}}}{\mathrm{d}h}}. \tag{6.18}$$

The available propulsive power is obtained from electrical input power using the forward-flight efficiency chain

$$\eta_{\mathrm{ff}} = \eta_{\mathrm{prop}}\eta_{\mathrm{motor}}\eta_{\mathrm{ESC}} = 0.75 \cdot 0.90 \cdot 0.95 = 0.641. \tag{6.19}$$

The code evaluates this formulation over a two-dimensional grid of available electrical power and candidate EAS. The selected climb uses $P_{e,\mathrm{avail}} = 16.0\,\mathrm{kW}$ and $V_{\mathrm{EAS}} = 29.8\,\mathrm{m/s}$, giving the lowest-energy candidate that satisfies the 600 s outbound time budget and the climb lift-coefficient limit.
At this selected condition, $V_{\mathrm{TAS}} = 40.5\,\mathrm{m/s}$ near 6000 m, dynamic pressure $q = 542\,\mathrm{Pa}$, and $C_L = 0.363$. The climb lift limit is $C_{L,\mathrm{max},w}/1.25^2 = 0.778$, while the maximum mission value is 0.403, so the selected climb is power-limited.
Figure 6.3 shows the selected trajectory produced by this stepwise integration. A straight climb would overshoot the 6000 m range before reaching altitude, so the aircraft spirals over the launch region with a 250 m radius until 3.22 km altitude, then uses the remaining ground track for straight climb-out to the target. During the spiral steps, the coordinated-turn load factor is included in the lift coefficient and induced-drag calculation. The spiral adds 7.23 km of arc length, with maximum load factor 1.12 and maximum bank angle 26.4°.

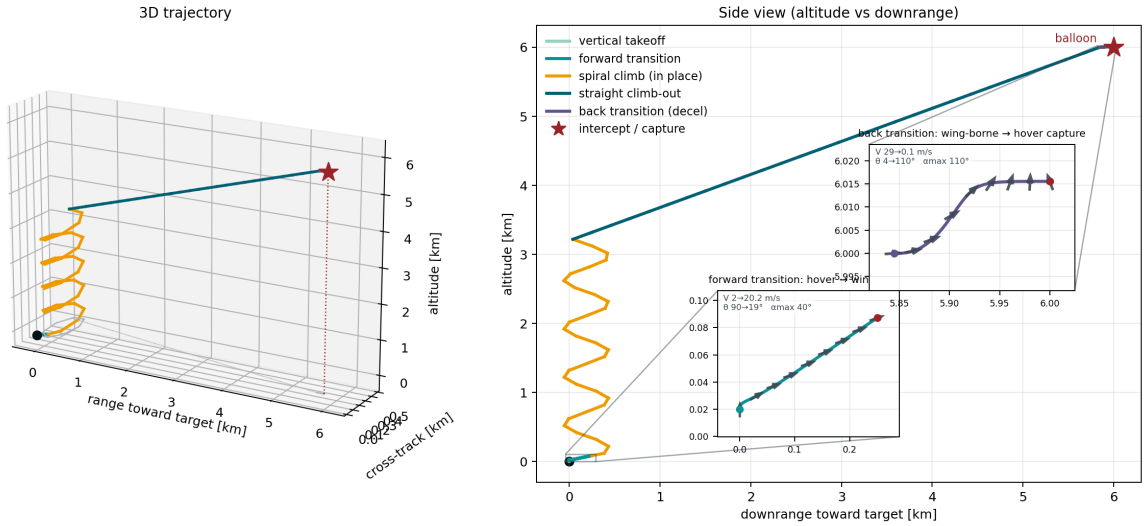

Figure 6.3: Selected Mission Trajectory to the Balloon Intercept Point. The Initial Spiral Prevents Downrange Overshoot Before the Aircraft Reaches the Altitude Needed for the Final Climb-Out

The wing-borne climb takes 424.6 s. Including vertical take-off and transition, the outbound sequence is 454.1 s, leaving 145.9 s against the 600 s outbound budget. The maximum climb angle is 24.3°.

6.9.3. Cruise and Recovery

The selected trajectory has zero level-cruise distance, because the spiral and final climb-out reach the 6000 m altitude and 6000 m ground range together. If a future trajectory introduces a level-cruise segment, the added energy should be evaluated from the same drag polar as the climb model,

$$E_{\text{cruise}} = \frac{DVt}{\eta_{\text{ff}}}, \qquad D = qS_w C_D, \tag{6.20}$$

with C_D taken from Section 6.5.

Post-capture recovery is treated with a first-order towing-descent footprint model. The captured balloon system is assumed to experience a station-keeping drag of $D_{\text{hold}} = 894.4\,\text{N}$ in the 13 m/s design wind. The current reel and towing interface uses $F_{\text{tow}} = 60\,\text{N}$, giving the towing-authority fraction

$$\alpha = \frac{F_{\text{tow}}}{D_{\text{hold}}} = \frac{60}{894.4} = 0.067. \tag{6.21}$$

Because the balloon drag scales with V^2, a force fraction α gives a velocity fraction $\sqrt{\alpha}$. The available lateral correction speed is therefore

$$V_{\text{corr}} = \sqrt{\alpha} V_{\text{wind}} = \sqrt{0.067} \cdot 13\,\text{m/s} = 3.37\,\text{m/s}. \tag{6.22}$$

The towing-power allowance is based on the useful lateral work rate needed to create this correction velocity, converted to electrical input power with the same forward-flight efficiency chain used in Equation 6.19:

$$P_{\text{tow},e} = \frac{F_{\text{tow}} V_{\text{corr}}}{\eta_{\text{ff}}} = \frac{60 \cdot 3.37}{0.75 \cdot 0.90 \cdot 0.95} = 0.315\,\text{kW}. \tag{6.23}$$

Over the representative 15 min descent, this gives a recovery-energy allowance of 0.079 kWh before battery-level contingency and depth-of-discharge corrections.

For the same 15 min descent, the uncontrolled wind drift is $V_{\text{wind}} t_{\text{des}} = 11.7\,\text{km}$. The design towing force gives a reachable correction radius of

$$R_{\text{corr}} = V_{\text{corr}} t_{\text{des}} = 3.03\,\text{km}, \qquad A_{\text{corr}} = \pi R_{\text{corr}}^2 = 28.9\,\text{km}^2. \tag{6.24}$$

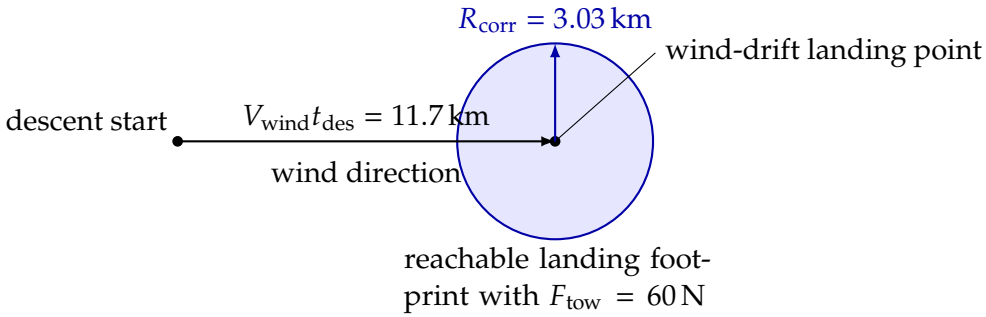

Figure 6.4: Illustrative Towing-Descent Landing Footprint for the Selected Recovery Design Force. The Footprint Is Centered on the Wind-Drift Landing Point and Has a Radius Set by the Available Correction Speed

6.9.4. Mission Energy and Battery Closure

Figure 6.5 shows the mission profile and the recovery-inclusive segment energy budget. The outbound and terminal-hover propulsion load is 2.93 kWh, dominated by wing-borne climb at about 1.59 kWh and terminal hover at 1.26 kWh. Vertical take-off and transition together add about 0.08 kWh. The post-capture towing descent from Subsection 6.9.3 adds 0.079 kWh, giving a total propulsion load of 3.01 kWh. No level cruise segment is required because the spiral and final climb-out reach the required altitude and range together.

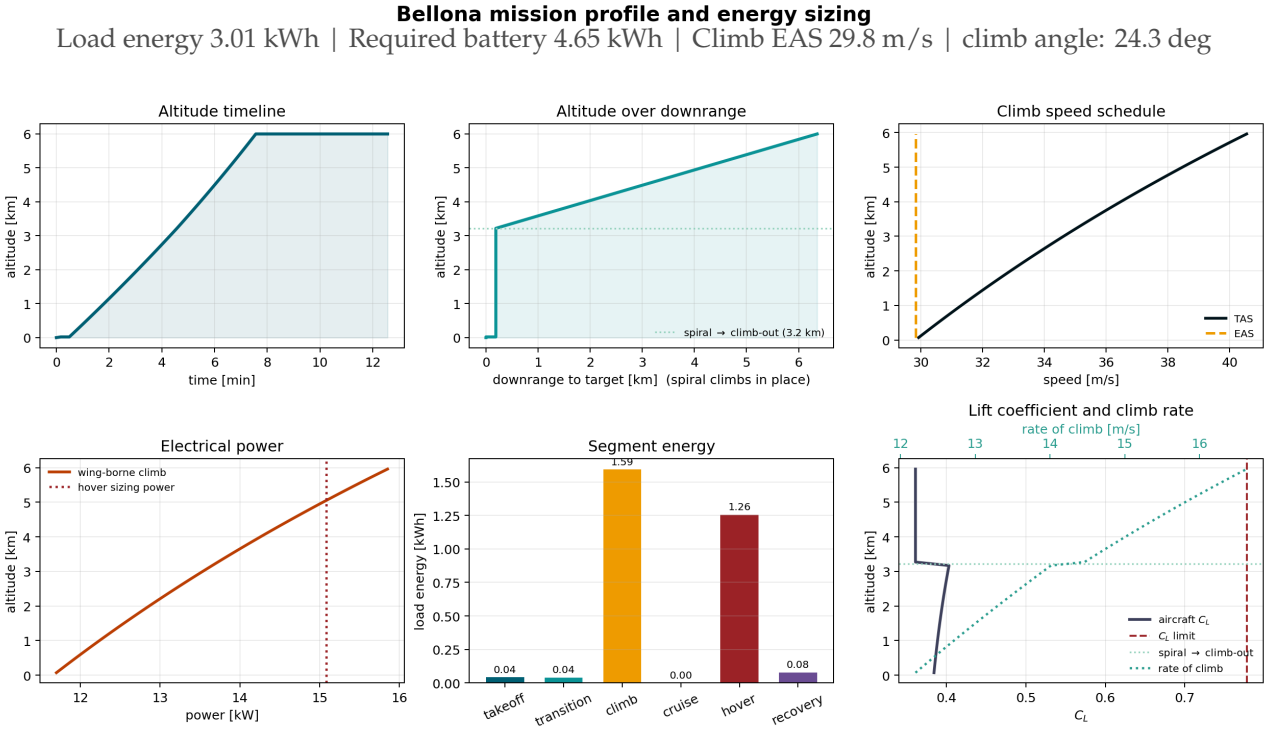

Figure 6.5: Mission Altitude, Speed, Power, Lift Coefficient and Segment Energy Profile. Climb and Terminal Hover Dominate the Energy Budget, While the Towing Descent Is Included as a Smaller Post-Capture Allowance

The required installed battery energy corrects the propulsion load, non-propulsive energy, battery efficiency, nominal depth of discharge and mission contingency. The non-propulsive energy is taken from Subsection 7.4.3:

$$E_{\text{bat}} = k_{\text{cont}} \frac{E_{\text{out+hover}} + E_{\text{tow},e} + E_{\text{nonprop}}}{\eta_{\text{bat}} DOD_{\text{nom}}} = 1.15 \frac{2.93\,\text{kWh} + 0.079\,\text{kWh} + 0.063\,\text{kWh}}{0.95 \cdot 0.80} = 4.65\,\text{kWh}. \tag{6.25}$$

For continuous aircraft sizing, the battery is represented by a pack-level specific energy of 400 Wh/kg. The required installed energy in Equation 6.25 therefore gives a preliminary battery mass target of

$$m_{\text{bat,est}} = \frac{E_{\text{bat}}}{e_{\text{bat,pack}}} = \frac{4.65\,\text{kWh}}{0.400\,\text{kWh/kg}} = 11.63\,\text{kg}. \tag{6.26}$$

Electrical component selection subsequently identified a discrete battery pack with 11.40 kg mass and 4.74 kWh installed energy. The selected pack provides about 0.09 kWh, or roughly 2%, more installed energy than the recovery-inclusive requirement.

6.10. Canard, Stability and Control Sizing

The canard and wing station are sized by a scissor-plot method. The forward centre-of-gravity limit is driven by controllability, and the aft limit is driven by static stability. The canard area ratio S_c/S_w and wing station x_w are solved simultaneously because moving the wing changes both the aerodynamic centre location and the canard moment arm. The selected canard area ratio is $S_c/S_w = 0.140$, giving $S_c = 0.357\,\text{m}^2$ and a canard-to-wing arm of 1.44 m. This point is selected as the lightest feasible canard and wing-station combination that keeps the operational centre of gravity inside the scissor band. The selected centre of gravity is $x_{\text{CG}}/\bar{c} = -0.323$, inside the feasible band from -0.393 to -0.248.

The stability side of the scissor plot uses the lift-curve slope of the canardless aircraft, because the canard contribution is added separately through the canard volume and lift-slope terms. Since the canard is upstream of the main wing, the slope used in the stability line is corrected for the canard wake over the immersed part of the wing. The canard is assumed to see freestream dynamic pressure, while the inboard wing area inside the canard wake sees both reduced effective angle of attack and

reduced dynamic pressure:

$$C_{L_\alpha,A-h,\text{eff}} = C_{L_\alpha,A-h}\left[(1-k_w)+k_w\left(1-\frac{\partial\epsilon}{\partial\alpha}\right)\left(\frac{V_w}{V}\right)^2\right]. \tag{6.27}$$

Here $C_{L_\alpha,A-h}$ is the canardless aircraft lift-curve slope before wake correction, k_w is the fraction of wing area immersed in the canard wake, $\partial\epsilon/\partial\alpha$ is the canard-induced downwash gradient at the wing, and $(V_w/V)^2$ is the wake dynamic-pressure ratio. For the selected geometry, $k_w = 0.409$, $\partial\epsilon/\partial\alpha = 0.563$, and $(V_w/V)^2 = 0.85$, giving $C_{L_\alpha,A-h,\text{eff}} = 3.72\,\text{rad}^{-1}$ from the isolated canardless aircraft value of $5.00\,\text{rad}^{-1}$.

The longitudinal moment model gives $C_{m,\text{cg},0} = 0.0451$ and $\mathrm{d}C_m/\mathrm{d}C_L = -0.124$, corresponding to an achieved static margin of $0.124\bar{c}$. The static margin was not imposed as a hard constraint; it emerges from the scissor solution at the selected wing station. At trim, the wing carries 347.8 N and the canard carries 153.6 N, so the canard provides 30.6% of the total lift while balancing the wing-body nose-down moment. The canard operates at $C_{L,c} = 0.8$, below $C_{L,\max,c} = 1.0$.

The controllability curve in the scissor plot is evaluated at the maximum lift coefficient reached in the optimised wing-borne mission profile, with a 1.15 margin factor. This gives $C_{L,A-h,\text{control}} = 1.15 \cdot 0.403 = 0.464$, capped by the permitted lift limit, while the wing maximum lift coefficient is $C_{L,\max,w} = 1.2$. The selected scissor point is therefore representative of the flown mission profile, but the highly loaded canard leaves only a small residual stall margin at the trim point. Using the isolated canard lift-curve slope, the difference between $C_{L,c} = 0.794$ and $C_{L,\max,c} = 1.033$ corresponds to roughly 3° of angle-of-attack margin. Future design iterations should check a more conservative controllability case based on the maximum lift achievable by the wing, or increase the canard area, arm or incidence authority, to reduce the risk that an off-nominal higher-angle-of-attack wing-borne state cannot be trimmed by the canard.

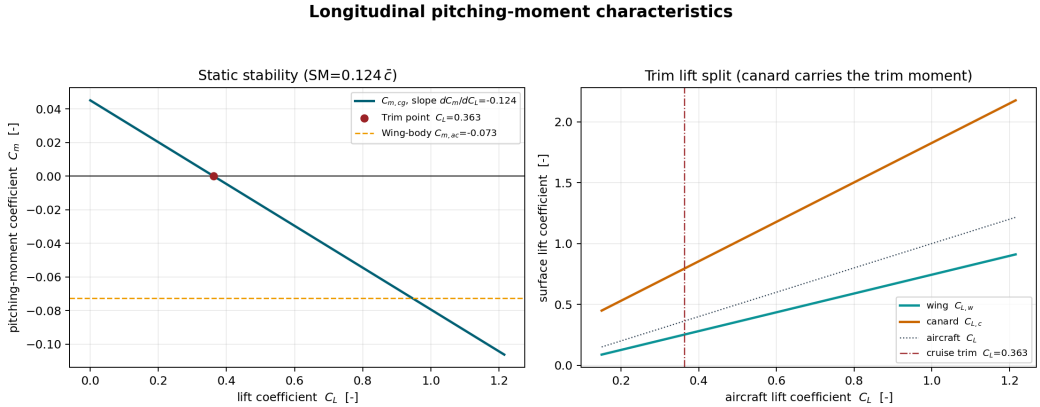

Figure 6.6: Pitching-Moment Curve for the Selected Longitudinal Trim Model. The Trim Point Occurs Where the Net Pitching Moment About the Centre of Gravity Is Zero

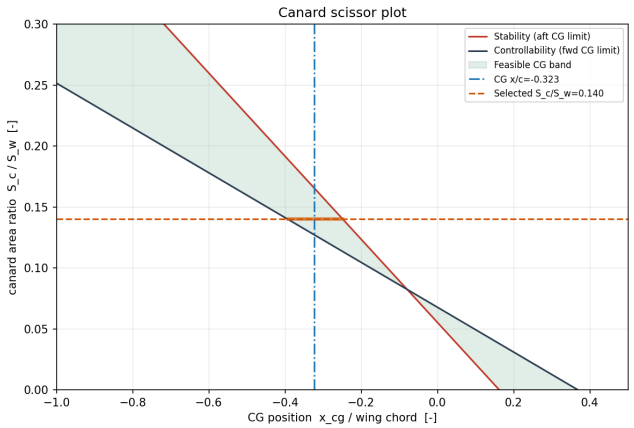

Figure 6.7: Canard Scissor Plot Showing the Selected Canard Area Ratio and Centre-of-Gravity Location. The x-Axis Is Referenced to the Leading Edge of the Mean Aerodynamic Chord, so $x_{CG}/\bar{c} = 0$ Denotes the MAC Leading Edge. The Selected Canard Is Near the Minimum Feasible Area Ratio

The scissor result should be read as a combined canard-area and centre-of-gravity check. The acceptable region is the overlap between the controllability and static-stability limits after applying the operational centre-of-gravity envelope. The selected point therefore leaves a usable CG band while avoiding unnecessary canard area, mass and trim drag; the same CG location is shown in the top-view geometry at the end of the chapter (Figure 6.10).

6.11. Optimisation Results and Interpretation

The selected point is $S_w = 2.55\,\mathrm{m}^2$, where the aircraft closes at 51.1 kg. The point is selected because it is the lightest feasible design under the current fixed assumptions.

Figure 6.8 shows the sweep. It is an optimisation trade, not a formal sensitivity analysis, because the battery model, aerodynamic coefficients, propulsion efficiencies, wind assumptions and recovery model are not varied independently. The faded infeasible markers are diagnostic closed sizing points: accepted wing areas use the lightest scissor- and stall-feasible candidate, while rejected closed points report the largest-clearance near miss. They should not be read as a smooth continuation of the feasible trend.

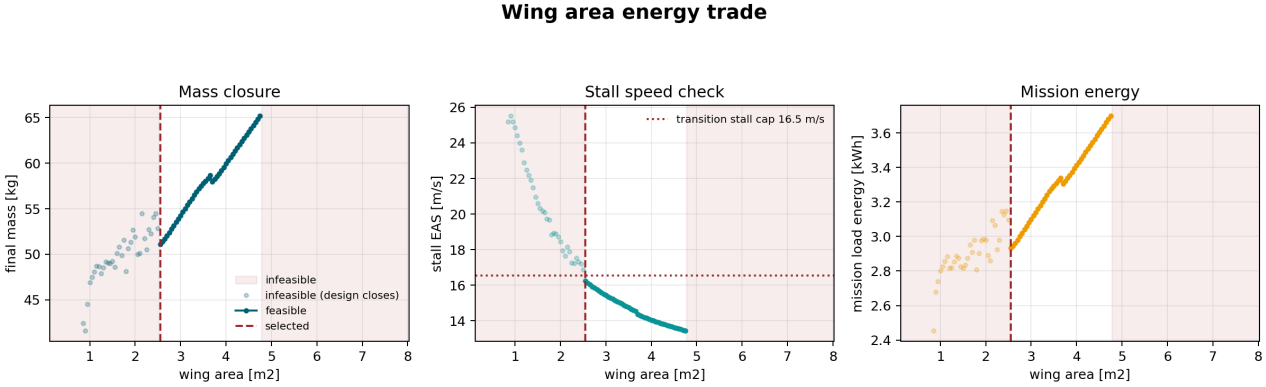

Figure 6.8: Wing-Area Sweep Used to Select the Minimum Feasible PPA Design Point Under the Current Fixed Assumptions

The canard sizing is nested inside the wing-area selection, so $S_c/S_w = 0.140$ is an active constraint. Battery, reel, capture-hardware and propulsion mass-property changes can move the centre of gravity toward the scissor limits.

6.11.1. Sensitivity Analysis

A sensitivity study was performed to identify which assumptions most strongly affect the closed aircraft mass and the residual transition stall margin. Each input was perturbed individually while the coupled mass, wing-area, mission-energy and canard-sizing loop was rerun. The airfoil coefficients were held at the converged values from the selected design, so the study isolates the selected sizing assumptions without repeating the full Reynolds-feedback loop. The frozen-airfoil baseline closes at 50.86 kg, which is within 1% of the final selected PPA mass, so the results are interpreted as relative sensitivities around the selected design point.

Table 6.6: One-at-a-Time Perturbations Used in the PPA Sensitivity Study

Perturbed assumption	Change	Reason for inclusion
Transition stall cap, battery specific energy, wing $C_{L,\max}$, thrust-to-weight ratio, hover figure of merit, hover reserve factor, forward-flight efficiency, wing Oswald factor, terminal hover time and intercept altitude	±10%	Main aerodynamic, propulsion, energy-storage and mission-envelope assumptions.
Disk loading	±15%	Rotor disk loading was given a wider band because it remains a preliminary propeller-sizing interface.
Excrescence drag fraction	±50%	The drag increment is a small uncertain allowance, so a wider relative perturbation is more informative.

Figure 6.9 shows that the maximum take-off mass is governed by assumptions that affect wing loading, battery mass and climb power. The transition stall cap is the strongest driver. A tighter cap forces a larger wing to keep the equivalent-airspeed stall speed inside the back-transition corridor, increasing

the closed mass by about 14% for the evaluated perturbation. Relaxing the cap reduces the required wing area and lowers mass, although the reduction is smaller because the optimiser then meets other mass and trim constraints.

Battery specific energy is the second major mass driver. Reducing the pack-level specific energy increases the battery mass, which then raises wing loading, hover power and the structural mass required to close the aircraft. The coupling is visible in the asymmetric response: a lower specific energy raises MTOW by roughly 12%, while the corresponding favourable perturbation reduces MTOW by about 5%. Intercept altitude and forward-flight efficiency have similarly high leverage because they set the climb power, climb duration and energy required to reach the balloon. The aerodynamic induced-drag assumptions, represented by the wing Oswald factor, also rank highly because they change the energy-optimal climb state and the selected wing area.

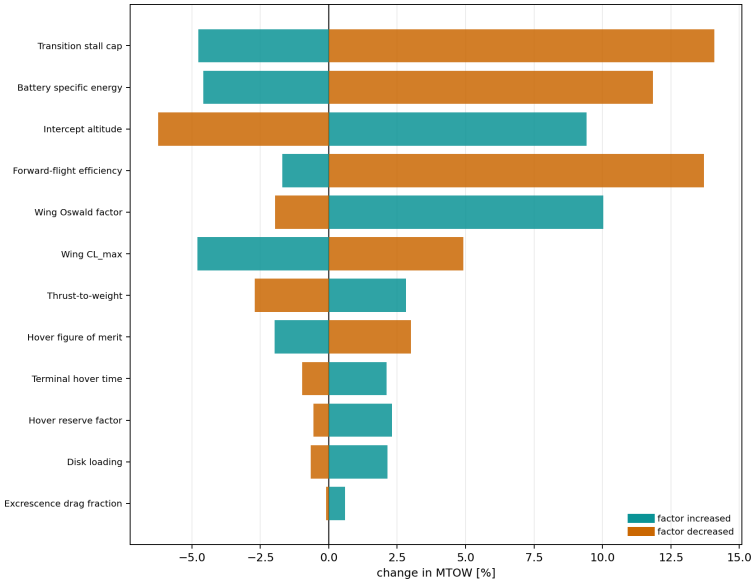

Figure 6.9: Sensitivity of Closed Maximum Take-Off Mass to the Main PPA Sizing Assumptions. The Bars Show the Mass Change After the Coupled Sizing Loop Is Rerun for Each Individual Perturbation.

The lower-ranking MTOW sensitivities are still useful for design prioritisation. A 10% change in thrust-to-weight ratio, hover figure of merit, hover reserve factor or disk loading changes MTOW by only a few percent in the screening run. These inputs remain important for hardware selection and thermal margins, but they do not dominate the aircraft-level mass closure. The excrescence-drag fraction has the smallest effect even under a wide perturbation, indicating that the preliminary sizing is driven more by induced drag, transition compatibility and energy storage than by small external-drag allowances.

The sensitivity results set the verification priority for the next PPA loop. The transition model and maximum-lift estimate should be checked first, because the current design is close to the back-transition stall boundary. Battery pack performance and forward-flight propulsive efficiency are the next highest-impact assumptions, since they drive both mass and energy closure. Aerodynamic validation should focus on induced drag and finite-wing maximum lift before detailed refinement of small external-drag increments.

6.12. Final PPA Design Values

Figure 6.10 shows the selected top-view geometry. The main wing has area 2.55 m^2, span 4.22 m, root chord 0.86 m and tip chord 0.34 m. The canard has area 0.357 m^2 and span 1.34 m. The fuselage length is 3.05 m.

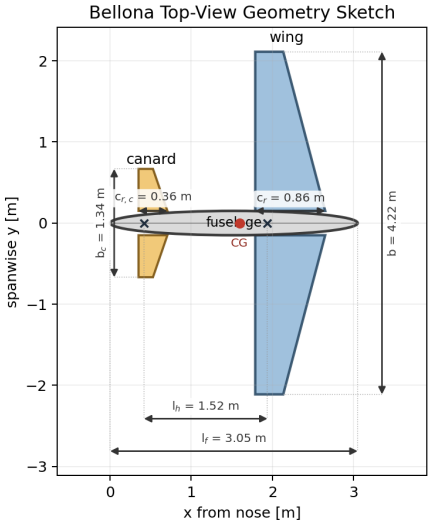

Figure 6.10: Top-View Geometry of the Selected Wing, Canard, Fuselage and Centre-of-Gravity Layout

Table 6.7: Mass Breakdown Used in the Selected PPA Sizing Point

Component group	Mass [kg]
Wing	7.91
Canard	1.27
Fuselage	10.30
Propulsion system	11.46
Battery	11.40
Sensing, avionics, control and communication	2.26
Capture hardware, reel and parachute	3.60
Wiring and harness	0.43
Mass margin	2.50
Total	**51.1**

The component allocation in Table 6.7 reconciles the PPA design point with the subsystem mass budgets while preserving the closed maximum take-off mass used for the aerodynamic, performance and control-margin calculations. The mass margin covers residual integration items, local fittings, fasteners, harness growth and small subsystem changes that are not yet fixed in detail.

Table 6.8: Final Selected PPA Design Values

Quantity	Selected value
Maximum take-off mass / weight	51.1 kg / 501.4 N
Wing area / span / wing loading	2.55 m^2 / 4.22 m / 196.6 N/m^2
Canard area ratio / area	0.140 / 0.357 m^2
Fuselage length / static margin	3.05 m / 0.124$\bar{c}$
Stall EAS / transition margin	16.25 m/s / 0.29 m/s
Trimmed L/D / C_D	11.61 / 0.03121
Installed thrust / equivalent minimum disk diameter	652 N / 1.10 m
Conservative hover allowance / peak electrical power	15.08 kW / 15.85 kW
Mission load / required installed battery energy	3.01 kWh / 4.65 kWh
Selected battery pack mass / energy	11.40 kg / 4.74 kWh
Outbound / outbound plus hover time	454.1 s / 754.1 s

6.13. PPA Verification and Validation

This section presents the verification and validation (V&V) status of the Propulsion, Performance and Aerodynamics (PPA) subsystem. Each requirement is linked either to completed verification evidence: sizing, design analysis, trajectory simulation, or a budget check; or to a planned verification activity such as dynamic simulation, supplier data, aerodynamic analysis at increasing fidelity, wind-tunnel testing, or integrated subsystem demonstration. The aerodynamic follow-up can include lifting-line, vortex-lattice and panel methods before CFD or test-based validation is used for the highest-risk effects. In Table 6.9, a checkmark (✓) indicates that the requirement is currently supported by available evidence, while a cross (×) indicates that further verification or validation is still required. At present the outbound mission is closed at aircraft level, whereas transition, propulsion, trim and recovery still

require dynamic or supplier-data verification.

Table 6.9: Propulsion, Performance and Aerodynamics Verification and Validation Plan

Req. ID	Verification and Validation Steps	Met
REQ-STK-03-MSN-04-SYS-08-PPA-01	The outbound sequence has been closed at 454.1 s against the 600 s budget using the climb-trajectory model, leaving 145.9 s margin.	✓
REQ-STK-03-MSN-04-SYS-07-PPA-02	The 300 s terminal hover has been included in the energy budget using the conservative station-keeping allowance of 15.08 kW. A coupled hover-control demonstration will be performed. The result will set the required hover-power reserve and may change battery capacity, rotor thrust margin or terminal-hover controller sizing.	×
REQ-STK-03-MSN-04-SYS-08-PPA-03	The stall EAS of 16.25 m/s has been checked against the 16.54 m/s back-transition cap. Verification of $C_{L,\max}$, the lift-curve slopes including canard-wing interference, and the drag polar should combine lifting-line, vortex-lattice or panel methods for lift distribution and interference checks with CFD or wind-tunnel testing for stall and drag confirmation. Six-degree-of-freedom transition simulation will also be performed. The result will fix the transition margin and may drive wing area, canard loading or transition-control authority.	×
REQ-STK-03-MSN-04-SYS-08-PPA-04	The installed thrust of 652 N and per-rotor hover demand of 125 N have been checked against the $T/W = 1.30$ sizing point.	✓
REQ-STK-01-MSN-01-SYS-01-PPA-05	The recovery-inclusive mission load energy of 3.01 kWh and required installed battery energy of 4.65 kWh have been computed using the contingency, depth-of-discharge and efficiency corrections. The selected 11.40 kg, 4.74 kWh pack exceeds the required installed energy by about 0.09 kWh.	✓
REQ-STK-03-MSN-04-SYS-08-PPA-06	The centre of gravity has been placed inside the scissor band with $\mathrm{d}C_m/\mathrm{d}C_L = -0.124$, using the canard-wake lift-slope correction in the stability line. Dynamic stability and control derivatives will be verified with controls. The result will define the final operational CG envelope and may require moving mass items, changing canard incidence or revising control allocation.	×
REQ-STK-01-MSN-01-SYS-45-PPA-07	The equivalent 1.10 m actuator-disk diameter has been included as the minimum propulsion-layout interface. Candidate hardware clearance is checked with the electrical-system propulsion selection.	✓
REQ-STK-03-MSN-04-SYS-08-PPA-08	The selected mission trajectory reaches the 6000 m intercept altitude, as shown in Figure 6.3.	✓
REQ-STK-03-MSN-04-SYS-44-PPA-09	The selected trajectory reaches the required 6000 m horizontal ground range while avoiding downrange overshoot through the initial spiral climb.	✓
REQ-STK-01-MSN-01-SYS-01-PPA-10	The timing budget closes the 454.1 s outbound sequence and 300 s terminal hover allowance. Full compatibility with the 25 min restricted-airspace removal objective still depends on coupled recovery timing and descent-path verification. The result will determine the recovery time margin and may change reserve energy, towing force or descent strategy.	×
REQ-STK-05-MSN-06-SYS-11-PPA-11	The sizing includes a $T/W = 1.30$ thrust margin and a first-order post-capture towing allowance. Coupled payload, tether and aircraft dynamics with a captured 50 kg payload remain to be verified. The result will set the post-capture control margin and may change propulsion sizing, tether-interface loads or the recovery operating mode.	×
REQ-STK-07-MSN-09-SYS-46-PPA-12	The recovery allowance uses the 13 m/s sustained-wind design case and the hover power model includes station-keeping margin. Transition and coupled recovery authority in sustained wind still require dynamic verification. The result will define the wind operating envelope and may change hover reserve, transition limits or recovery operating limits.	×
REQ-STK-03-MSN-04-SYS-08-PPA-13	The maximum mission climb lift coefficient is 0.403, below the selected climb lift limit of $C_{L,\max,w}/1.25^2 = 0.778$.	✓
REQ-STK-03-MSN-04-SYS-08-PPA-14	The coupled sizing loop closes the aircraft mass from an initial 52.78 kg to 51.1 kg, with a final mass-closure error of −0.002 kg. The loop uses geometry-dependent structural mass estimates and retains subsystem-compatible battery, propulsion and layout interfaces.	✓

7 Electrical System

The electrical system architecture provides the foundational power distribution, signal routing, and safety mechanisms required to sustain autonomous flight and manage payload operations. The architecture is split into a high-voltage propulsion rail and multiple regulated low-voltage avionics rails, mitigating electromagnetic interference between heavy inductive motor loads and sensitive sensing electronics.
The system architecture overview is visually mapped in Figure 7.1.

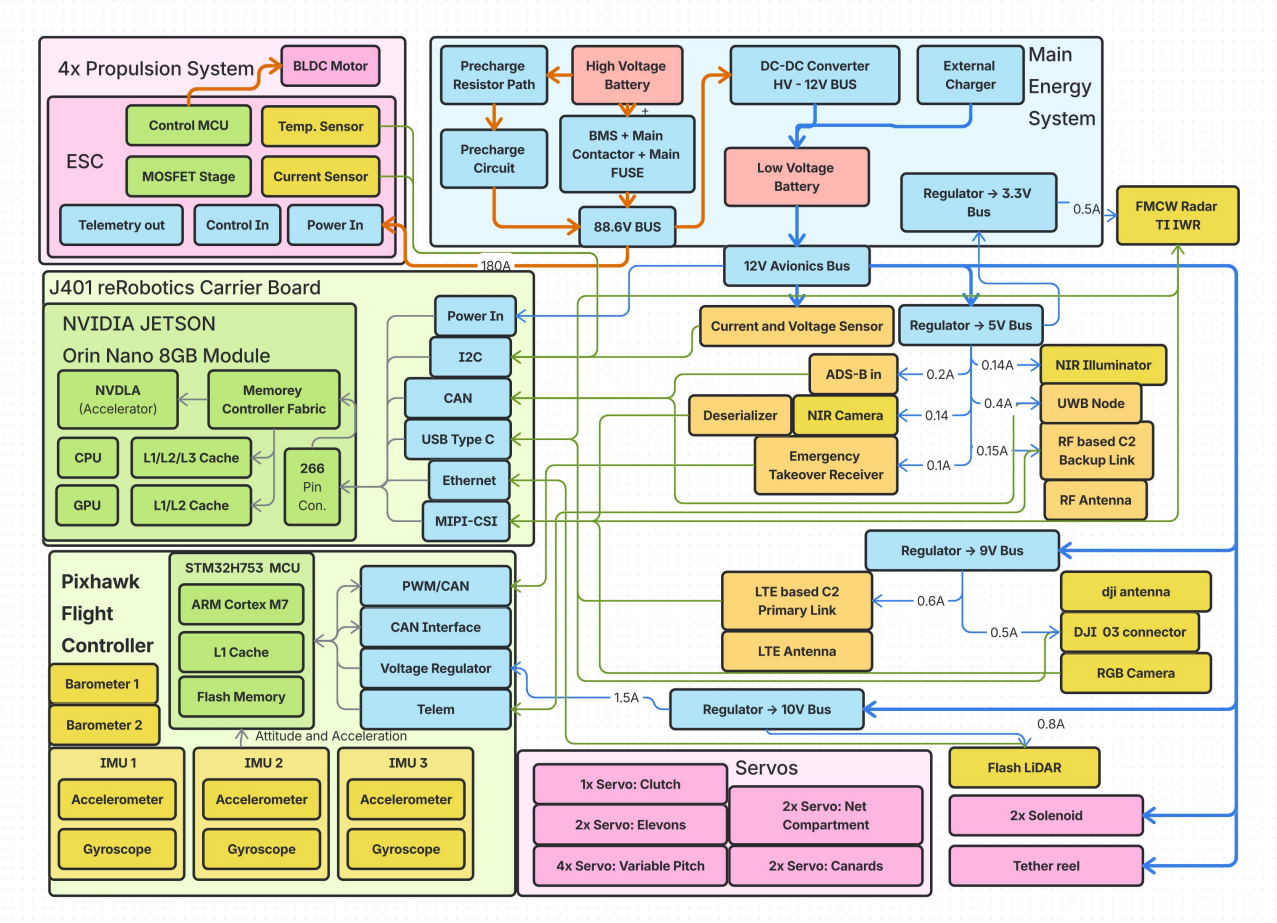

Figure 7.1: High-Level Electrical System Architecture Mapping Power Distribution and Data Lines

All components must adhere to the following requirements:

Table 7.1: System Consolidated Requirements and Classifications

ID	Requirement	Classification
Sensing Subsystem Requirements		
REQ-STK-02-MSN-02-SYS-02-SEN-01	The sensing subsystem shall detect targets at a distance of ≥ 300 m.	Driving
REQ-STK-02-MSN-02-SYS-03-SEN-02	The sensing subsystem shall estimate target range, heading, and altitude within 2% accuracy.	Driving
REQ-STK-02-MSN-02-SYS-02-SEN-03	The sensing subsystem shall sample the target at least once per second.	Non-driving
REQ-STK-02-MSN-02-SYS-02-SEN-04	The sensing module shall handle sensor dropouts with a locational divergence of less than 5 m over 10 s.	Key
REQ-STK-07-MSN-09-SYS-19-CTR-05	The core sensing capabilities shall be unaffected by external conditions.	Key
REQ-STK-12-MSN-14-SYS-26-SEN-06	The sensing subsystem shall provide position, altitude, attitude, velocity, battery, fault, and relative state data during manual override.	Key

ID	Requirement	Classification
REQ-STK-13-MSN-16-SYS-28-SEN-07	The sensing subsystem shall compare redundant positioning estimates.	Key
REQ-STK-13-MSN-16-SYS-29-SEN-08	The sensing subsystem shall detect redundant attitude estimate discrepancies exceeding 2% accuracy.	Key
REQ-STK-13-MSN-17-SYS-33-SEN-09	The sensing subsystem shall flag lost tracking, unsafe closing rates, or unsafe geometry as abort triggers before interception.	Key
Control Subsystem Requirements		
REQ-STK-03-MSN-04-SYS-07-CTR-01	The control subsystem shall execute the full mission autonomously.	Driving
REQ-STK-02-MSN-02-SYS-07-CTR-02	The control subsystem shall maintain hover within 0.5 m absolute position error and 0.5 m/s relative velocity.	Driving
REQ-STK-07-MSN-09-SYS-19-CTR-03	The control subsystem shall maintain stable flight and control authority in maximum wind gusts.	Driving
REQ-STK-12-MSN-14-SYS-26-CTR-04	The high-frequency control system shall allow immediate manual takeover and operator-controlled flight without autopilot assistance.	Key
REQ-STK-13-MSN-16-SYS-30-CTR-05	The control subsystem shall tolerate a single control surface/actuator failure.	Driving
REQ-STK-13-MSN-16-SYS-30-CTR-06	The control subsystem shall detect loss of thrust or abnormal motor response and trigger a safe mode via an FSM.	Key
REQ-STK-13-MSN-16-SYS-30-CTR-07	The control subsystem shall maintain stable flight, abort, return-to-home, or execute a controlled descent/landing after a single motor failure.	Driving
Communication Subsystem Requirements		
REQ-STK-02-MSN-02-SYS-02-COM-01	The communication subsystem shall receive Ground-Radar cues at a distance of $\geq$ 7.2 km.	Driving
REQ-STK-12-MSN-14-SYS-26-COM-01	The communication subsystem shall provide a command uplink for manual override during all mission phases.	Key
REQ-STK-12-MSN-15-SYS-27-COM-01	The communication subsystem shall broadcast UAS identity, position, altitude, velocity, and status via a transponder per airspace regulations.	Key
REQ-STK-13-MSN-16-SYS-31-COM-01	The communication subsystem shall transmit safe-mode state, disturbance type, telemetry, and link status at $\geq$ 2 Hz during safe mode.	Key
REQ-STK-13-MSN-16-SYS-32-COM-01	The communication subsystem shall trigger lost-link safe mode if the C2 link is lost for $>$ 2 s during flight.	Key
Power and Electronics Subsystem Requirements		
REQ-STK-01-MSN-01-SYS-01-P&E-01	The P&E subsystem shall provide at least 4.53 kWh of nominal installed battery energy.	Driving
REQ-STK-01-MSN-01-SYS-01-P&E-02	The P&E subsystem shall provide a nominal high-voltage bus above 90 V.	Driving
REQ-STK-03-MSN-04-SYS-08-P&E-01	The P&E subsystem shall support a continuous high-voltage pack current of at least 215.4 A.	Driving
REQ-STK-13-MSN-16-SYS-31-P&E-01	The P&E subsystem shall maintain safety-critical low-voltage rails within ±5% of nominal voltage.	Key
REQ-STK-13-MSN-16-SYS-30-P&E-01	The BMS shall monitor cell voltage, pack current, and pack temperature during operation and charging.	Key
REQ-STK-13-MSN-16-SYS-30-P&E-02	The P&E subsystem shall protect the main battery output and each ESC branch against overcurrent and short-circuit faults.	Key
REQ-STK-13-MSN-16-SYS-32-P&E-01	The P&E subsystem shall disconnect the high-voltage bus or command safe mode after a critical electrical fault.	Driving

7.1. Sensing

The primary objective of the sensing subsystem is to provide continuous, high-fidelity spatial awareness of both the UAS and the target balloon. The autonomous intercept requires accurate and high-frequency data to ensure controller operation.

7.1.1. Sensor Selection

To successfully intercept or interact with an airborne target, the multi-modal sensor suite must balance range, resolution, and update frequency. The tradeoff for both the initial tracking stage and the terminal navigation stage is given in Table 7.2. Advanced options such as Pulse-Doppler Radar and LWIR Camera are compared to more off-the-shelf components like LiDARs, and NIR or RGB Cameras.

Table 7.2: Sensor Trade-Off Matrix with Multi-Stage Weightings and Feasibility Filtering

Criteria / Sensors	Pulse-Doppler Radar	FMCW Radar (77 GHz)	NIR Camera (+ Illum.)	LWIR Camera (Thermal)	Flash LiDAR
Cost W: [S_1=0.1, S_2=0.1]	**2** High cost ($10k–$40k)	**5** Ultra low cost ($50–$500)	**5** Low cost ($50–$200)	**1** Prohibitive ($40k–$70k)	**3** Moderate cost (≈$1k)
Detect. Range W: [S_1=0.2, S_2=0.0]	**4** Long range (1–3 km)	**2** Short range (10–300 m)	**2** Short range (10–300 m)	**3** Mid range (400–800 m)	**1** Critical limit (<50 m)
Pose Accuracy W: [S_1=0.2, S_2=0.5]	**1** Poor resolution at close range	**4** High range/vel accuracy	**4** Excellent spatial resolution	**3** Moderate; prone to thermal blur	**5** Millimeter-level 3D point cloud
Env. Robustness W: [S_1=0.2, S_2=0.2]	**5** All-weather; immune to rain	**5** High robustness; penetrates fog	**2** Light dependent; blocked by fog	**2** Blinded by thick cloud/fog	**1** High aerosol scattering loss
Ang. Wideness W: [S_1=0.2, S_2=0.1]	**3** Mechanical scan (±60°)	**5** Wide electronic FOV (140°)	**4** Wide optical FOV (60–110°)	**3** Narrow FOV; requires gimbal	**2** Very narrow FOV (10–20°)
Weight W: [S_1=0.1, S_2=0.1]	**2** Heavy payload (0.8–15 kg)	**5** Ultra-lightweight (≈12 g)	**5** Miniature SWaP (15–50 g)	**1** Heavy cooling systems (0.8–4 kg)	**3** Moderate weight (≈250 g)
Feasibility Gate	S1: × S2: ×	S1: ✓ S2: ✓	S1: ✓ S2: ✓	S1: × S2: ×	S1: × S2: ✓
Final Score (S_1)	**0.00**	**4.20**	**3.40**	**0.00**	**0.00**
Final Score (S_2)	**0.00**	**4.50**	**3.80**	**0.00**	**3.50**

While range is the driving factor, cost was also a severe constraint. This led to the choice of sensor suite as illustrated in Figure 7.2. The FMCW radar provides reliable velocity data and distance tracking regardless of lighting conditions. The Livox LiDAR establishes high-density 3D point clouds for target profiling at medium to close ranges. The GMSL2 NIR Camera delivers high-frame-rate tracking in poorly lit conditions, complemented by the DJI O3 RGB camera for real-time visual verification. To enable the use of cameras even in blackout conditions, a NIR illuminator is included [1]. Detailed Budgets for cost, power, and mass can be found in Table 7.10.

(a) Radar: IWR6843ISK (Link) **(b)** NIR Camera: Axo2 (Link) **(c)** LiDAR: Livox MID-70 (Link) **(d)** RGB Camera: DJI O3 (Link)

Figure 7.2: Overview of All Integrated Vehicle Sensors

The ranges and FoV of these sensors complement each other as shown in Figure 7.3

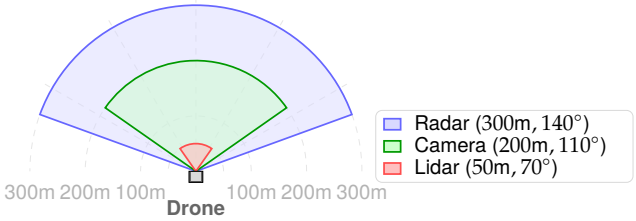

Figure 7.3: Illustration of the Main Sensors Range and FoV

The radar, the lidar and the NIR camera will be placed in the nose of the drone, pointing in the direction of flight. The RGB Camera will be placed on the bottom rear of the drone to enable safe autonomous landing.
Estimating and predicting the balloon motion using this overlapping sensor suite introduces challenges in fusing the modalities. To account for drift and gust-driven unpredictable motion, the tracking pipeline must continuously infer the target's center and velocity vector.

[1] WULF FIIR LED 850NM/940NM IR 50mm Illuminator, accessed: 16.06.2026: https://a1decoy.co.uk/products/wulf-fiir-led-850nm-940nm-ir-50mm-illuminator

A simulation was set up, incorporating the exact specs of the chosen products, in order to confirm and verify the capabilities of the proposed sensor suite. The simulation results indicate that the proposed sensor suite can provide state estimates with sufficient accuracy over the operational engagement range, as shown in Figure 7.4a and quantified in Figure 7.4b. It is also apparent that at very close ranges, there is a residual uncertainty in the estimation, which has to be accounted for in the design of the other subsystems.

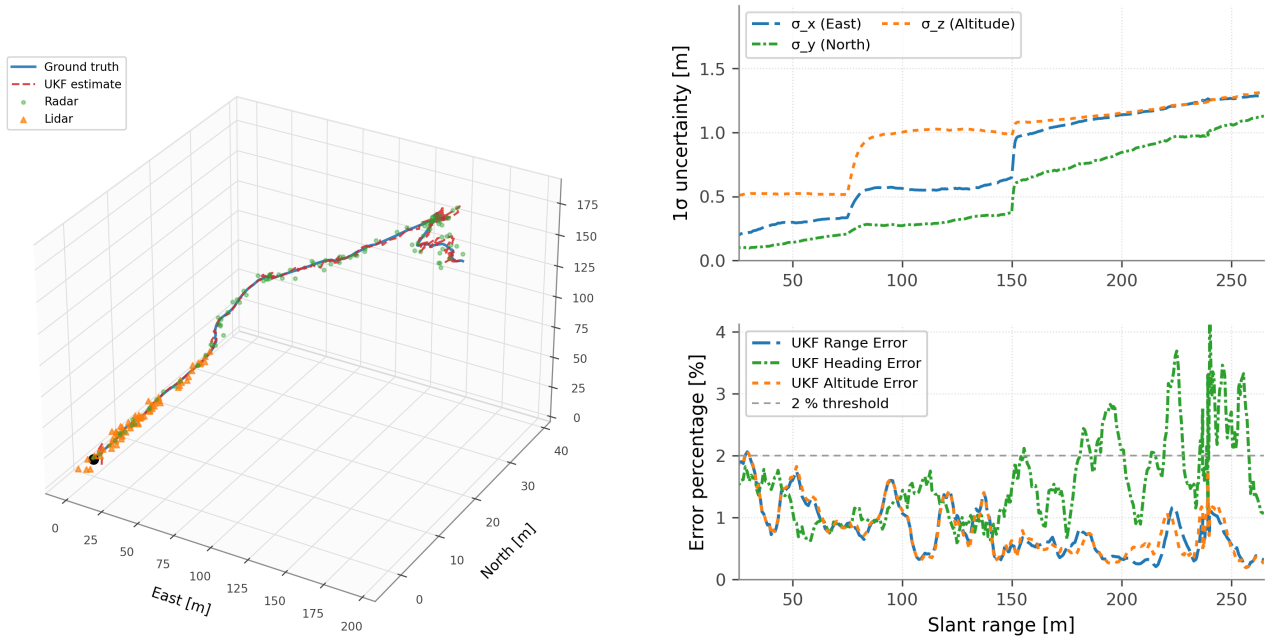

(a) Estimated Target Trajectory Relative to Vehicle Reference Frame

(b) State Estimation Error Bounds as a Function of Range

Figure 7.4: Sensor State Estimation Accuracy and Variance Profile Under Simulation Parameters

7.1.2. State Estimation

State estimation is required to fuse noisy measurements from multiple sensors into a consistent estimate of the balloon and drone states. Kalman-filter-based estimators are the de facto standard for recursive state estimation in robotics and autonomous systems [32]. Accordingly, three variants of the Kalman filter family are evaluated: the standard Kalman Filter (KF), the Extended Kalman Filter (EKF), and the Unscented Kalman Filter (UKF). Their suitability is assessed using tracking accuracy and computational latency for the balloon-tracking and drone dead-reckoning tasks.

The primary design question is therefore not whether Kalman filtering should be used, but which member of the Kalman filter family provides the best trade-off between estimation accuracy and computational cost for each subsystem [33].

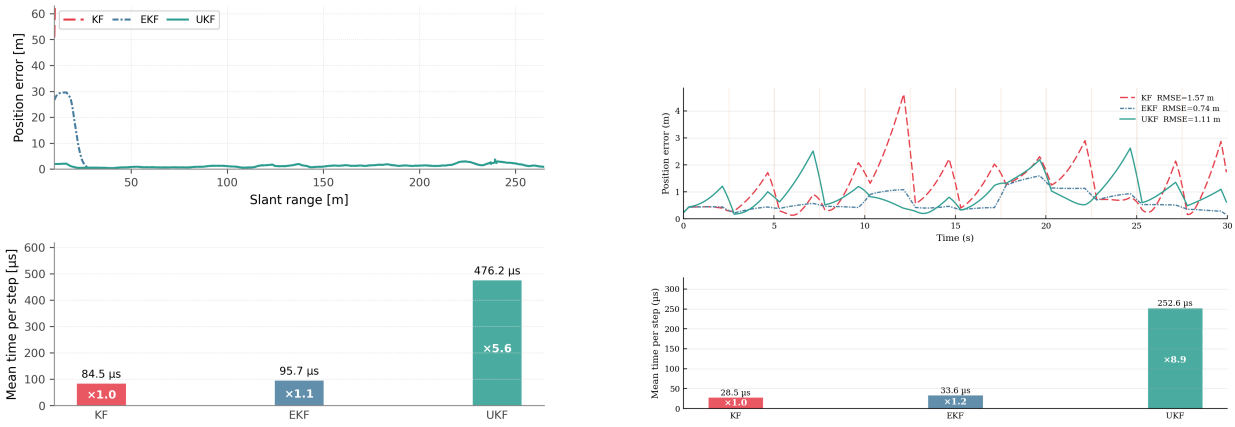

(a) Balloon Tracking Performance and Computational Latency Across KF, EKF, and UKF

(b) Drone Dead Reckoning Performance and Computational Latency Across KF, EKF, and UKF

Figure 7.5: Performance and Computational Benchmarks for the Evaluated Kalman Filter Architectures

The architectural requirements for the two estimation tasks differ significantly:

- **Balloon Estimation:** The relative balloon-tracking problem exhibits strongly nonlinear measurement dynamics. As shown in Figure 7.5a, both the KF and EKF experienced increased tracking error and occasional divergence, whereas the UKF maintained robust estimation performance. The additional computational cost is acceptable because the estimator executes on the Nvidia Jetson companion computer.
- **Drone Dead Reckoning:** The onboard navigation problem exhibits only moderate nonlinearities and operates under strict real-time constraints. As shown in Figure 7.5b, the EKF achieves an appropriate balance between estimation accuracy and computational efficiency, making it suitable for execution on the flight controller. This choice is consistent with PX4, which employs the EKF2 estimator for onboard state estimation.

The complete state estimation and navigation pipeline is illustrated in Figure 7.6.

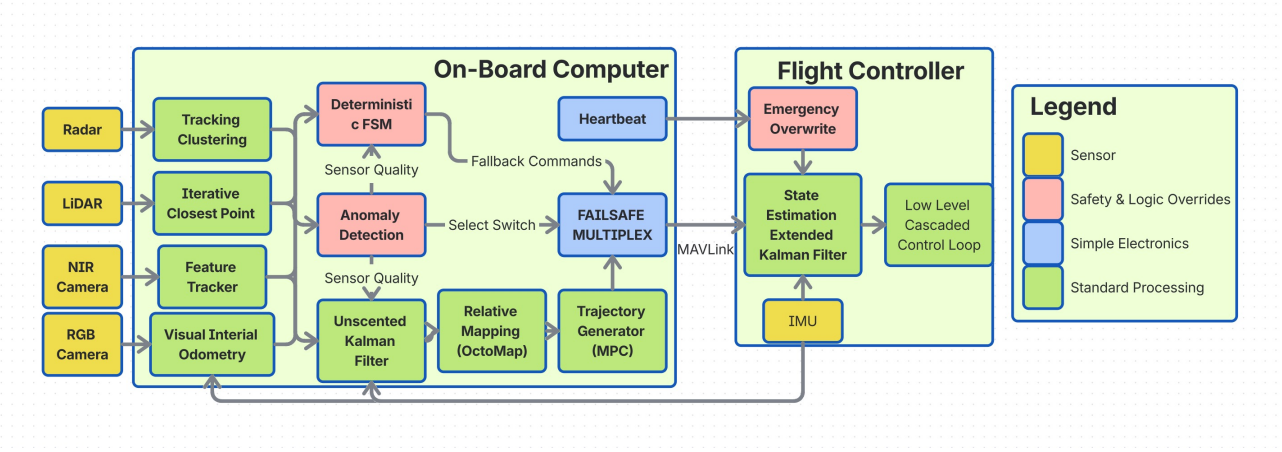

Figure 7.6: Complete Navigation, Mapping, and Control Pipeline Architecture

The UKF state estimate provides the balloons' relative pose used to register sensor measurements within OctoMap [34], which provides a spatially and computationally efficient 3D mapping framework. By utilizing a hierarchical octree structure, OctoMap compresses uniform volumes and dynamically allocates memory only where obstacles exist to prevent RAM saturation within the 3D search space. Based on this map, a Model Predictive Control (MPC) framework [35] generates optimal trajectories for all flight conditions. MPC is selected according to the trade-off shown in Table 7.3. Although MPC incurs a higher computational cost than PID and LQR approaches, the availability of a high-performance companion computer makes this penalty acceptable in exchange for direct constraint handling and multivariable optimization capabilities.

Table 7.3: Navigation Controller and Trajectory Generation Trade-Off Matrix

Controller	Constraint Handling	Multi-variable	Computation	Final Score
PID	1 (Poor)	1 (Poor)	3 (Excellent)	**5 / 9**
LQR	2 (Moderate)	2 (Good)	3 (Excellent)	**7 / 9**
MPC	3 (Excellent)	3 (Excellent)	2 (Moderate)	**8 / 9**

To ensure operational safety, a deterministic Finite State Machine (FSM) can override the main pipeline via a failsafe multiplexer, triggered by an anomaly detection module. Additionally, a heartbeat signal enables a hard overwrite by the FC in the event of a companion computer failure. Finally, the FC fuses the telemetry data using an EKF before passing the corrected state to the low-level control loop.
During temporary sensor dropouts, the filter can continue propagating the estimated state using the process model, although the estimation uncertainty grows with dropout duration as shown in Figure 7.7. This is a general state estimation framework independent of specific flight regimes. The accuracy depends on the gust model employed, which, due to insufficient data, is modelled as an Ornstein-Uhlenbeck process [36]. This process was selected because it produces temporally correlated disturbances with finite correlation times, unlike white noise, which changes instantaneously and unrealistically.
While this conservative model provides a baseline for testing, the synthetic trajectory data generated here is ultimately an approximation of real-world physics. Consequently, this data should be used

with caution.

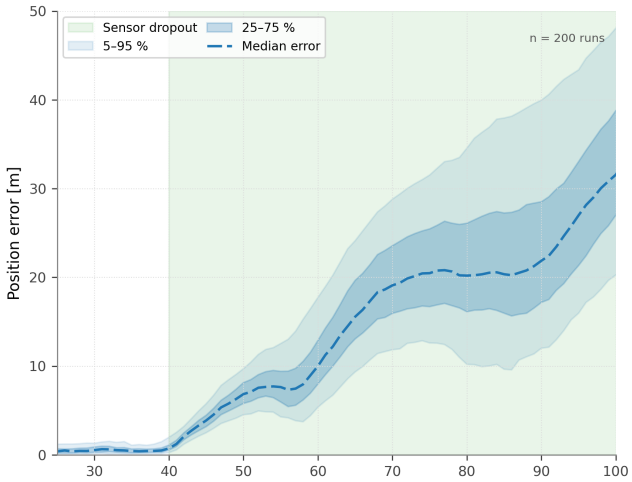

Figure 7.7: Kalman Filter Trajectory Estimation Performance During a Total Sensor Dropout Scenario

7.1.3. Sensor V&V

Table 7.4: Sensing Subsystem Verification and Validation Plan

Req. ID	Verification and Validation Steps	Met
REQ-STK-02-MSN-02-SYS-02-SEN-01	Validated via trajectory modelling using empirical sensor data, demonstrating satisfactory tracking up to a 300m range as shown in Figure 7.4a.	✓
REQ-STK-02-MSN-02-SYS-03-SEN-02	Sensor modelling with empirical data assessed compliance for Range and Altitude errors. Radar-only tracking exceeds the Heading error threshold, as shown in Figure 7.4b. This is acceptable as the error, for the long range, is still minimal.	~
REQ-STK-02-MSN-02-SYS-02-SEN-03	Verified software pipeline execution latency, confirming a processing cycle comfortably below 1.0 second as shown in Figure 7.5b.	✓
REQ-STK-02-MSN-02-SYS-02-SEN-04	The sensing module was validated under sensor dropout, showing locational divergence in Figure 7.7 of less than 5m in 10 seconds.	✓
REQ-STK-07-MSN-09-SYS-19-CTR-05	Validated radar-centric core capabilities to ensure robust environmental perception across all target operating conditions.	✓
REQ-STK-12-MSN-14-SYS-26-SEN-06	Verified that the core sensor stack integrates all modalities necessary to provide the required state information.	✓
REQ-STK-13-MSN-16-SYS-28-SEN-07	Verified that overlapping sensor modalities provide sufficient FoV coverage and data redundancy.	✓
REQ-STK-13-MSN-16-SYS-29-SEN-08	Validated via the redundant state estimation pipeline (Figure 7.6), which successfully isolates faulty data using anomaly detection.	✓
REQ-STK-13-MSN-17-SYS-33-SEN-09	Verified that the redundant state estimation pipeline (Figure 7.6) enables emergency overrides across multiple hardware stages.	✓

7.2. Control

While aerodynamic control was the driving factor in selecting a canard configuration, the finalized design remains inherently statically stable, as shown in Figure 7.8. However, because the mission profile demands extensive high-angle-of-attack (AoA) maneuvers—where conventional aerodynamic control surfaces risk stalling and losing effectiveness—the aircraft utilizes an active flight control system (FCS). This system blends aerodynamic control from the canards with propulsion-based control to maintain stability and maneuverability across all phases of flight.

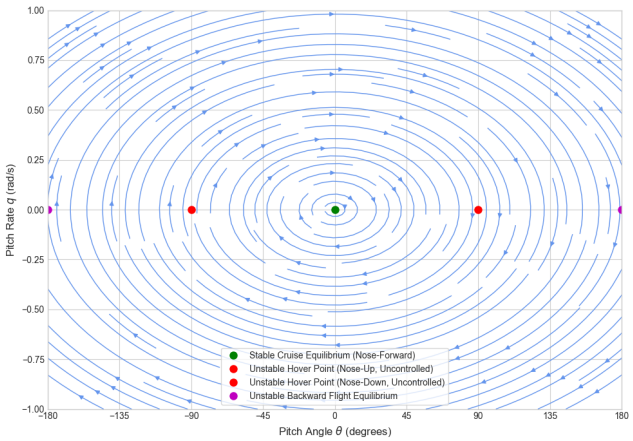

Figure 7.8: Open-Loop Pitch Axis Phase Portrait Tracking Angular Divergence Boundaries

7.2.1. Control Algorithm selection & Assessment

This controllability and stability must be guaranteed by means of active control, requiring advanced autopilot systems capable of high-frequency stabilization.

Next, the low-level control and guidance laws must be chosen. Two primary candidates were evaluated for execution: conventional PID control and advanced Incremental Nonlinear Dynamic Inversion (INDI) [37]. The operational difference in gust-rejection performance is evident in Figure 7.9a, where the UAS model was subjected to gust disturbances, and the responses under both control laws were recorded. Here, the PID was tuned via exhaustive search using the best gust rejection as a candidate. In the simulated gust-rejection scenarios, INDI outperformed the PID controller, reducing peak error by approximately 10%. This performance motivated its selection for the inner control loop of the UAS, as detailed in the system architecture shown in Figure 7.9b. In this arrangement, a high-level mission state machine selects the active flight mode from Hover, Transition, and Fixed-Wing regimes, each of which deploys tailored guidance laws.

A hybrid control topology pairing inner-loop INDI with outer-loop PI architectures is ultimately employed. The outer-loop PI structure is utilized because INDI performance can deteriorate when control effectiveness is poorly estimated or changes rapidly. For instance, airspeed control via throttle is better managed as a traditional PI loop. The throttle dynamics and aerodynamic drag are difficult to model accurately in transient conditions, making a conventional PI controller more practical for airspeed regulation.

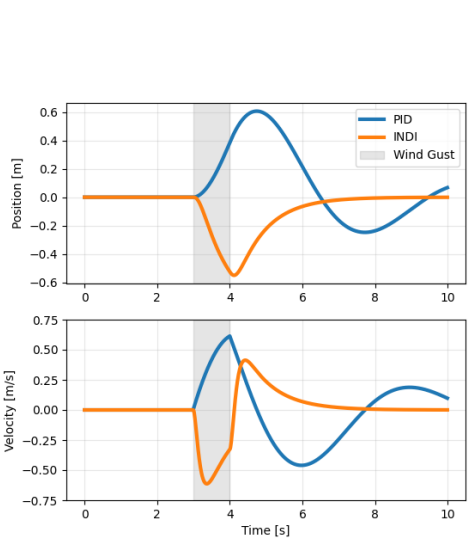

(a) Transient Tracking Error Responses Under Standard Gust Profiles

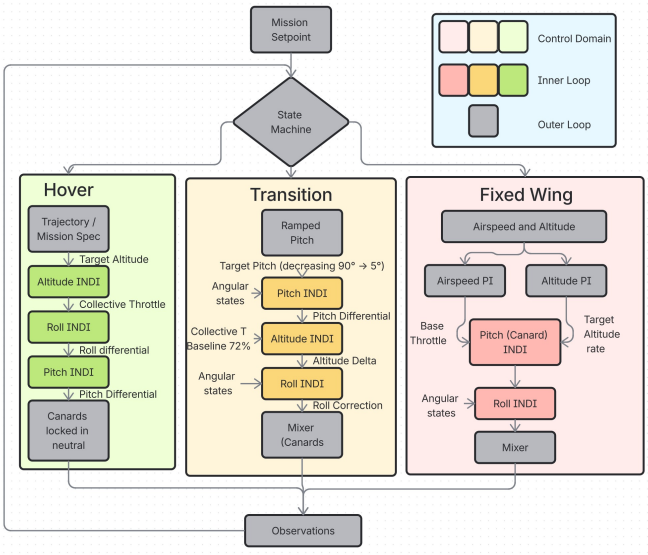

(b) Cascade Control Topology Block Scheme Hierarchy

Figure 7.9: Closed-Loop Control Performance Benchmarking and Signal Routing Block Layout

7.2.2. Control V&V

Table 7.5: Control Subsystem Verification and Validation Plan

Req. ID	Verification and Validation Steps	Met
REQ-STK-03-MSN-04-SYS-07-CTR-01	Validated via full-mission profile simulation, confirming autonomous execution across all sequential flight phases; full environmental validation remains pending real-world flight testing.	~
REQ-STK-02-MSN-02-SYS-07-CTR-02	Verified via closed-loop hover simulations, maintaining position within 0.5 m absolute error and relative velocity within 0.5 m/s as shown in Figure 7.9a.	✓
REQ-STK-07-MSN-09-SYS-19-CTR-03	Verified via gust-injection simulation, demonstrating robust hover stability under maximum environmental wind limits as shown in Figure 7.9a.	✓
REQ-STK-12-MSN-14-SYS-26-CTR-04	Verified via phase-portrait stability analysis (Figure 7.8), confirming open-loop natural stability suffices for immediate, unassisted manual operator takeover.	✓
REQ-STK-13-MSN-16-SYS-30-CTR-05	Validated via single-actuator failure simulation, confirming single-point-failure-tolerant flight using the integrated aerofoil and adaptive INDI control allocation [38].	✓
REQ-STK-13-MSN-16-SYS-30-CTR-06	Validated via thrust-loss simulation; the FDIR logic successfully processed tracking errors and telemetry to trigger the fail-safe FSM within milliseconds.	✓
REQ-STK-13-MSN-16-SYS-30-CTR-07	Validated via asymmetric thrust-loss injection, confirming that high-bandwidth INDI dynamic control reallocation maintains stability for abort and return-to-home recovery profiles.	✓

7.3. Communication

To ensure strict regulatory compliance and robust operational safety under Specific Operations Risk Assessment (SORA) guidelines, the external wireless infrastructure is structured into two separate domains: Active Mission Data Links and Air Traffic Coordination Systems.

7.3.1. External Communication Selection

The aircraft maintains four independent, isolated data streams to handle command, control, video telemetry, and emergency manual interception, illustrated in Figure 7.10.

- **Primary C2 LTE Link:** Managed via an onboard Teltonika RUT240 LTE modem, this cellular link serves as the primary data highway for long-range telemetry, mission updates, and real-time path corrections from the ground control station (GCS).
- **Backup C2 RF Link:** Running as a secondary redundant path, a Holybro SiK Telemetry Radio operating on the 433 MHz band establishes a direct point-to-point connection, automatically seizing control traffic if cellular data signals drop out.
- **High-Bandwidth Video Stream:** Broadcast by the DJI O3 Air Unit, this link routes high-definition visual feeds to the ground station, ensuring the operator can visually verify target acquisition.
- **Emergency Takeover Channel:** A low-latency, independent RC receiver link configured to directly override the companion computer, allowing a safety pilot to seize low-level manual flight control on the flight controller (FC) in an emergency.

(a) LTE Modem (Link) **(b)** RF Radio (Link) **(c)** DJI Video Stream (Link) **(d)** Receiver (Link)

Figure 7.10: Additional Communication Components

The choice of a primary LTE connection and a backup RF link comes down to their complementary nature, which is illustrated in Figure 7.6.

Further, for the RF-based components, it must be checked that their range is sufficient for the mission profile of a maximum distance of 8.4 km. This is done by using the Specs and checking if free space losses are prohibitive. For this, the free space loss over distance is illustrated in Figure 7.11. All receivers have sufficient link margin even at the maximum distance of 8.4km.

Table 7.6: Wireless Link Characteristics Comparison

Parameter	LTE	SiK 433 MHz
Range	Very high	Moderate
Bandwidth	High	Low
Infrastructure	Requires cell coverage	Independent
Latency	Moderate	Low
Failure mode	Network outage	LOS limitations

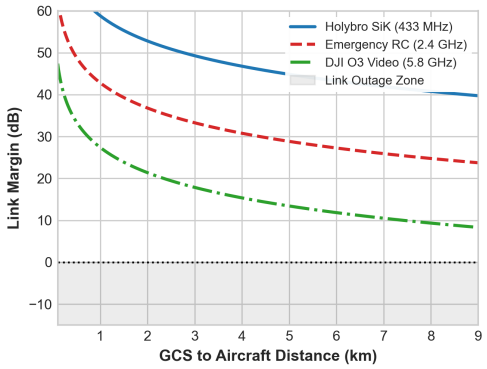

Figure 7.11: Link Budget of the Three RF-Based Communication Channels

Operating independently of the interactive command streams, two dedicated transponder systems provide airspace visibility and ensure collision avoidance:

- **ADS-B IN System:** A uAvionix pingRX Pro receiver provides cooperative traffic awareness and can support detect-and-avoid functionality when integrated with other safety measures.
- **Remote ID Module:** A self-contained, battery-powered beacon that broadcasts the UAS's position, altitude, and unique registration identity, satisfying civil aviation safety mandates without impacting the low-voltage power rail.

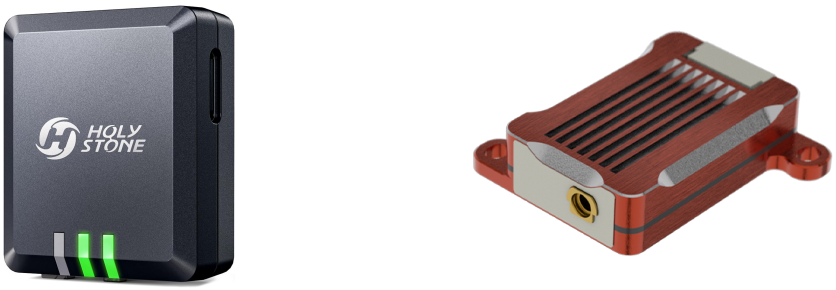

(a) Remote ID (Link) **(b)** ADS-B (Link)

Figure 7.12: Remote ID and ADS-B Systems

7.3.2. Internal Communication Architecture

The internal communication system is structured as a decentralized, topic-based publish-subscribe network. Hardware responsibilities are split based on bandwidth and criticality: high-level perception tasks are managed by the Onboard computer, while time-critical flight control loops are isolated on the flight controller. Inter-processor communication is established via dedicated I2C and UART bridges. As illustrated in Figure 7.13, data distribution is highly asymmetric:

- **High-Bandwidth Perception Bus:** The Jetson Orin Nano handles a collective peak data throughput of approximately 9.1 Gbit/s. This is dominated by the multi-modal sensor suite, including the RGB camera (5 Gbit/s) and the NIR camera (2.1 Gbit/s).
- **Low-Latency Flight Control Bus:** The Pixhawk 6X manages actuator and critical telemetry loops with an internal data rate of 10 Mbit/s via deterministic CAN and I2C protocols.

The maximum aggregated throughput on both buses remains safely below the theoretical bandwidth ceilings of the respective physical interfaces.

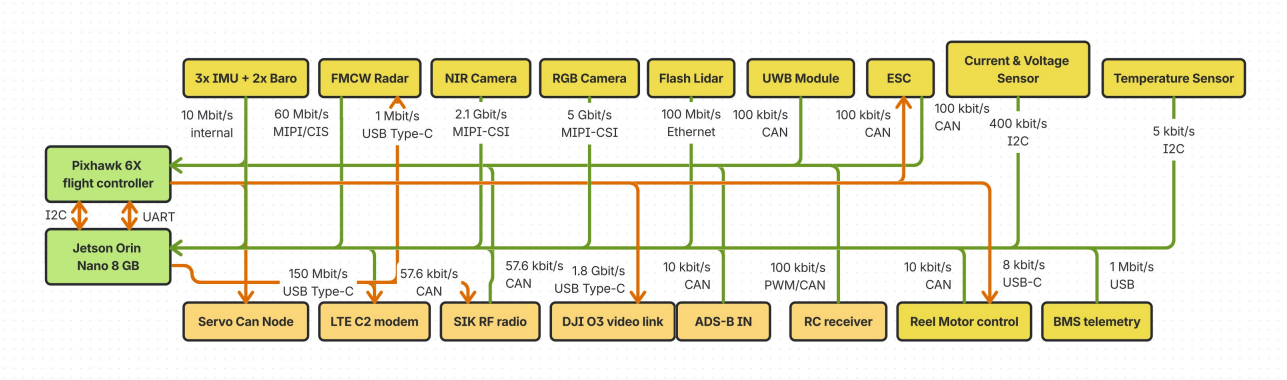

Figure 7.13: Internal Communication Diagram Showing Split Architecture

7.3.3. Communications V&V

Table 7.7: Communication Subsystem Verification and Validation Plan

Req. ID	Verification and Validation Steps	Met
REQ-STK-02-MSN-02-SYS-02-COM-01	The use of LTE-based C2 enables very high range sending and receiving as long as cell towers are available.	✓
REQ-STK-12-MSN-14-SYS-26-COM-02	Incorporation of an RC receiver, hardwired into the FC (Figure 7.13), allowing complete and exceptional emergency takeover.	✓
REQ-STK-12-MSN-15-SYS-27-COM-03	The UAS incorporates a remote ID system Figure 7.12a.	✓
REQ-STK-13-MSN-16-SYS-31-COM-04	The main communication channel and its backups provide more than sufficient bandwidth to transmit the necessary data at a frequency of up to 50Hz	✓
REQ-STK-13-MSN-16-SYS-32-COM-05	The incorporation of a heartbeat between the Onboard computer and the FC enables immediate safe mode in the case of communication dropout.	✓

7.4. Power & Electronics

7.4.1. Candidate Propulsion Unit

The PPA chapter defines the propulsion requirement as an interface: four propulsors, a required installed thrust of 163.0 N per propulsor, and an equivalent minimum actuator-disk diameter of 1.10 m from the preliminary disk-loading target. The electrical design uses this interface to identify a plausible motor, ESC and propeller set. The check in this section is a catalogue-level compatibility check; detailed propeller maps, motor thermal limits, ESC current limits and battery voltage sag still have to be verified.

The required total thrust follows from the PPA thrust-to-weight sizing point:

$$T_{\text{req,total}} = \left(\frac{T}{W}\right)_{\text{req}} m_{\text{TO}} g \tag{7.1}$$

Using $m_{\text{TO}} = 51.13\,\text{kg}$ and $T/W = 1.30$,

$$T_{\text{req,total}} = 1.30 \cdot 51.13 \cdot 9.81 = 652.1\,\text{N}. \tag{7.2}$$

For four propulsion units, this gives

$$T_{\text{req,motor}} = \frac{652.1}{4} = 163.0\,\text{N} = 16.6\,\text{kgf}. \tag{7.3}$$

At the maximum mission altitude, the lower air density changes the propeller operating point. For a fixed propeller diameter and rotational speed, static thrust can be calculated:

$$T = C_T \rho n^2 D^4, \tag{7.4}$$

where C_T is the thrust coefficient, ρ is the air density, n is the rotational speed, and D is the propeller diameter. If C_T, n, and D are held constant, thrust scales with density:

$$\frac{T_{6000}}{T_0} \approx \frac{\rho_{6000}}{\rho_0} = \sigma_{6000} = 0.539. \tag{7.5}$$

Producing 16.6 kgf at 6000 m would therefore correspond to a fixed-RPM sea-level thrust severity of

$$T_{SL,eq} = \frac{16.6}{0.539} = 30.8 \text{ kgf}. \tag{7.6}$$

This value is used only as a severity indicator for the high-altitude operating point. It is not a direct catalogue thrust requirement, because an electric propulsion system can shift rotational speed and power level.

The T-Motor A12XL-24S propulsion system is retained as a candidate implementation. It consists of the A12XL-24S motor, a 24S FOC 120 A ESC, and an MF4918P folding propeller (Link). The supplier-matched motor, ESC and propeller reduce integration uncertainty for a first detailed-design pass. The manufacturer lists a rated thrust range of 20–25 kgf and a maximum thrust of 45 kgf. The nominal PPA requirement of 16.6 kgf per motor lies below the rated range, while the high-altitude severity indicator of 30.8 kgf remains below the listed maximum thrust.

The MF4918P propeller diameter is 1.245 m, which is larger than the 1.10 m equivalent minimum diameter from PPA sizing. The corresponding disk area is about 1.22 m^2 per rotor. With the PPA installed thrust requirement, this gives an installed disk loading of approximately 134 N/m^2, above the preliminary 130.8 N/m^2 sizing target.

Table 7.8: Candidate Propulsion-Unit Characteristics Checked Against the PPA Interface

Parameter	Candidate value
Propulsion unit	T-Motor A12XL-24S propulsion system
Motor	A12XL-24S, KV48
ESC	24S FOC 120 A
Propeller	MF4918P folding propeller
Propeller diameter	49 in, equivalent to 1.245 m
Rated thrust	20–25 kgf
Maximum thrust	45 kgf
Mass per propulsion unit	2.865 kg, including wires and propeller
Number of units	4
Total propulsion-unit mass	11.46 kg

The selected propulsion candidate is checked against the required per-motor thrust using manufacturer performance data. The tabulated thrust, current and rotational speed are used to compute the corresponding thrust coefficient, allowing the propeller performance to be extrapolated to the lower air density at the 6000 m sizing condition. The values for C_T are calculated with the available manufacturer data, presented in Table 7.9.

Table 7.9: Manufacturer performance data for the selected A12XL-24S propulsion unit and corresponding thrust coefficient values

Throttle (%)	Current (A)	Thrust (g)	Torque (N m)	RPM (-)	Motor Efficiency (%)	Overall Efficiency (gf/W)	C_T (-)
30	5.45	6896	3.92	1074	87.60	13.70	0.0718
35	8.31	9434	5.27	1254	90.00	12.30	0.0721
40	12.03	12289	6.81	1413	91.20	11.10	0.0739
45	16.38	15290	8.43	1575	92.70	10.20	0.0740
50	21.72	18404	10.14	1699	91.00	9.30	0.0766
55	27.56	21572	11.89	1860	92.20	8.60	0.0749
60	33.85	24533	13.54	1980	91.10	8.00	0.0752
65	40.43	27415	15.17	2130	92.20	7.50	0.0726
70	48.30	30745	16.93	2250	91.10	7.00	0.0729
75	56.02	33744	18.56	2340	89.70	6.70	0.0740
80	65.37	37272	20.42	2433	87.60	6.30	0.0756
85	73.25	39767	21.76	2523	86.20	6.00	0.0750
90	79.92	41616	22.87	2580	84.60	5.70	0.0751
95	86.29	43493	23.85	2640	83.10	5.50	0.0750
100	92.88	45198	24.87	2700	81.50	5.20	0.0745

The selected thrust coefficient is $C_T = 0.073$, taken as the local average of the 65 % to 75 % throttle data

because this range corresponds to the expected high-altitude operating point. The rotational speed required at the 6000 m sizing condition is calculated from the propeller thrust relation:

$$n = \sqrt{\frac{T}{C_T \rho D^4}} = \sqrt{\frac{163}{0.073 \cdot 0.6602 \cdot 1.2446^4}} = 37.52\,\text{rev/s} \tag{7.7}$$

Converting to revolutions per minute,

$$RPM = 60 \cdot 37.52 = 2251 \tag{7.8}$$

This value lies within the manufacturer-tested range of the A12XL-24S propulsion unit and corresponds closely to the 70 % throttle data point. Using the specified KV of 48, the required voltage for achieving the required RPM, under no loads, would be around $46.9V$, lower than the specified $92V$ in the performance data.

7.4.2. Electrical Power Budget

The electrical power budget is used as the starting point for the battery and power-distribution design. The sensing, control, communication, propulsion, and balloon-interaction subsystems define the electrical loads that must be supplied by the battery.

The budget is split into sensing, avionics, control, communication, and balloon-interaction loads. The propulsion loads are added separately in the mission-energy calculation because they dominate the total energy requirement and vary strongly between climb, cruise, hover, and descent.

Sensing Loads

Table 7.10: Sensing Subsystem Electrical Load, Mass, and Cost Budget

Component	Qty.	Mass [kg]	Power [W]	Cost [€]
FMCW radar (TI IWR6843ISK)	1	0.200	1.75	200
NIR camera + illumination (Axo2 GMSL2 Sony IMX662)	1	0.200	0.70	350
Flash LiDAR (Livox Mid-70)	1	0.580	8.00	1000
DJI O3 RGB camera (DJI O3 Air Unit)	1	0.0364	–	–
Subtotal	–	1.0164	10.45	1550

The RGB camera is part of the DJI O3 Air Unit. Its mass is shown in the sensing budget because it is physically a camera module, while its power and cost are included with the DJI O3 video-downlink system in the communication budget to avoid double-counting.

Avionics Loads

Table 7.11: Avionics Electrical Load, Mass, and Cost Budget

Component	Qty.	Mass [kg]	Power [W]	Cost [€]
Pixhawk 6X (Link)	1	0.0902	3.0	275
Jetson Orin Nano 8GB (Link)	1	0.280	15.0	360
Seeed J401 carrier (Link)	1	0.200	5.0	160
PWM/CAN node (Link)	1	0.005	1.0	50
Subtotal	–	0.5752	24.0	845

The Jetson Orin Nano is budgeted at 15 W for nominal operation. The power-distribution system shall include an additional margin because the module can operate at higher power modes. The carrier-board power is treated as an allowance for board overhead, interface electronics, and cooling auxiliaries. The command interface node converts flight-controller commands to PWM/CAN-compatible actuator or ESC signals and is counted as part of the avionics power budget.

Control Loads

Table 7.12: Control-Actuation Electrical Load, Mass, and Cost Budget

Component	Qty.	Mass [kg]	Power [W]	Cost [€]
Canard servos (Link)	2	0.120	31.08	74
Subtotal	2	0.120	31.08	74

The control-actuation budget uses only 2 goBILDA 2000 Series dual-mode servos to actuate the canard surfaces. The power estimate is based on 70% of the 3.0 A stall current at 7.4 V, giving 15.54 W per servo. This is conservative for electrical sizing because the servos are not expected to operate continuously near stall during nominal flight, but the value gives margin for short-duration actuator loads.

Communication Loads

Table 7.13: Communication Subsystem Electrical Load, Mass, and Cost Budget

Component	Qty.	Mass [kg]	Power [W]	Cost [€]
ADS-B IN	1	0.020	0.75	400
Remote ID	1	0.016	0.00	40
Primary C2 LTE link	1	0.125	5.00	140
Backup C2 RF link	1	0.0235	0.50	60
Emergency receiver	1	0.0012	0.30	60
DJI O3 video downlink	1	0.031	15.00	200
Subtotal	–	0.2167	21.55	900

The Remote ID module is treated as a battery-powered self-contained unit and therefore does not add a continuous load to the onboard low-voltage power system. The DJI O3 mass is split between the transmitter module and antenna in the communication budget, while the camera module is included in the sensing budget. The emergency takeover receiver value is kept as a preliminary allowance and shall be updated once the final onboard receiver is selected.

Balloon-Interaction Electronics Loads

Table 7.14: Balloon-Interaction Electronics Electrical Load, Mass, and Cost Budget

Component	Qty.	Mass [kg]	Power [W]	Cost [€]
Trap-door servos (Link)	3	0.180	46.62	111
Guide servo (Link)	1	0.060	15.54	37
Net-gun solenoid, Adafruit 413 (Link)	1	0.091	3.00	15
Guide/reel solenoid, Adafruit 412 (Link)	1	0.039	3.60	8
Electric reel, Daiwa Seaborg 300J (Link)	1	0.560	240	500
Subtotal	–	0.930	308.76	671

The balloon-interaction electronics include five servos, two solenoids, and one electric reel. Two servos open the parachute trap-door, two servos open the net-gun trap-door, and one servo actuates the guide mechanism. The servo power is estimated using the same method as the control-actuation budget, taking 70% of the 3.0 A stall current at 7.4 V, which gives 15.54 W per servo. The solenoids are used as short-duration trigger actuators and are therefore treated as intermittent loads. The Adafruit 413 solenoid is allocated to the net-gun trigger, while the Adafruit 412 solenoid is allocated to the guide or reel trigger. The Daiwa Seaborg 300J electric reel is budgeted at 12 V and 7 A for rated high-current operation, corresponding to 84 W. The reel can draw up to approximately 20 A in the maximum-power case, so the interaction-mechanism power rail shall be checked against a possible short-duration peak of approximately 240 W.

Non-Propulsive Electrical Components Summary

Table 7.15: Non-Propulsive Electrical Load, Mass, and Cost Summary

Category	Mass [kg]	Power [W]	Cost [€]
Sensing	0.992	10.45	1550
Avionics	0.575	24.00	845
Control actuation	0.120	31.08	74
Communication	0.217	21.55	900
Balloon interaction electronics	0.930	308.76	601
Subtotal	**2.834**	**397**	**4198**

The non-propulsive electrical components require approximately 400W of installed operating power before margin. This value is conservative because the control servos, solenoids, and electric reel are intermittent loads and are not expected to operate continuously at their listed power during the full mission. The value is therefore used mainly for low-voltage power distribution and converter sizing, while the mission-energy calculation should account for the actual operating duration of each intermittent load.

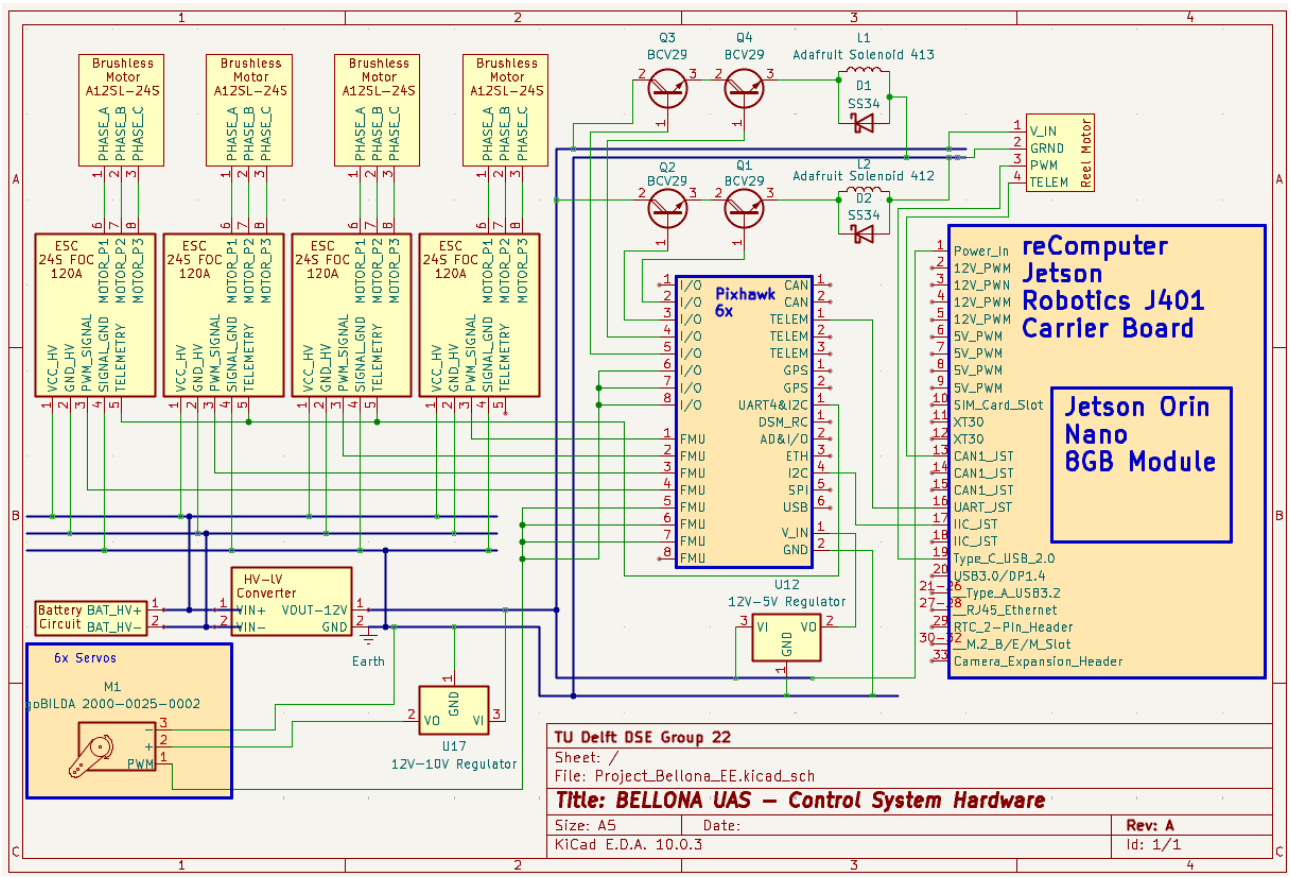

Figure 7.14: System Hardware Schematic Showing the Main Power, Signal, and Actuation Interfaces

Figure 7.14 shows the hardware implementation used to connect the electrical loads listed in the power and energy budgets. The high-voltage battery bus supplies the four propulsion ESCs and the HV–LV converter, while the low-voltage rails provide power to the Pixhawk flight controller, reComputer J401 carrier board, Jetson Orin Nano module, servos, and solenoid drivers. The Pixhawk acts as the primary real-time flight-control unit and sends command signals to the ESCs and actuator interfaces. The Jetson Orin Nano provides higher-level processing through the J401 carrier board, supporting mission logic and computationally heavier functions.

The schematic also separates the propulsion, control-actuation, and balloon-interaction electronics into identifiable branches. This supports traceability between the component-level power budget and the actual electrical architecture: each load category in the budget corresponds to a physical connection path in the system schematic. The 12 V and 5 V regulation stages are included to supply components with different voltage requirements, while the shared ground and signal routing ensure that command and feedback signals remain referenced to the same electrical system. This architecture, therefore, links the energy budget to the practical hardware implementation and provides a basis for wiring, protection, and integration checks.

7.4.3. Mission Energy Budget

Table 7.16: Mission Energy Budget

Energy term	Energy [Wh]
Take-off energy	~40
Transition energy	~40
Climb energy	~1590
Cruise energy	0
Hover energy	~1260
Total energy	2930

Table 7.17: Non-Propulsive Electrical Mission Energy Estimate

Category	Power [W]	Duration [h]	Energy [Wh]
Sensing	11.75	0.417	5
Avionics	24.00	0.417	10
Control actuation	31.08	0.417	13
Communication	21.55	0.417	9
Balloon interaction	308.00	0.083	26
Total non-prop.	**–**	**–**	**~63**

The energy values in Table 7.16 include only the propulsion energy required by the motors during the mission phases. The remaining onboard electrical loads are added separately using the non-propulsive electrical power budget. The total mission duration is taken as 25 min, corresponding to 0.417 h. The sensing, avionics, control, and communication loads are assumed to be available throughout the full

mission. The balloon-interaction electronics are assumed to operate during the capture phase only, which is taken as 5 min, corresponding to 0.083 h. The electrical energy (E) is calculated from power (P) and duration (t) as $E = Pt$
The total mission energy before contingency is therefore:

$$E_{\text{mission}} = E_{\text{prop}} + E_{\text{nonprop}} = 2930 + 63 = 2993 \text{ Wh} \tag{7.9}$$

A 15% mission contingency is applied to account for modelling uncertainty, wind variation, off-nominal manoeuvres, additional control effort, and possible extension of the capture or hover phase.

$$E_{\text{cont}} = 1.15 \cdot E_{\text{mission}} = 1.15 \cdot 2993 = 3441.9 \text{ Wh} \tag{7.10}$$

The usable energy requirement is then converted into a nominal installed battery energy requirement using the selected nominal depth-of-discharge limit. An 80% depth of discharge is used for nominal operation so that the mission is not sized around complete battery depletion. The remaining battery capacity provides reserve for voltage sag, cell imbalance, abort cases, controlled landing, and safe-mode operation.

$$E_{\text{nom,req}} = \frac{E_{\text{usable,req}}}{DOD_{\text{nom}}} = \frac{3441.9}{0.80} = 4302 \text{ Wh} \tag{7.11}$$

For the preliminary mission energy budget, a battery discharge efficiency of $\eta_{\text{batt}} = 0.95$ is assumed. This value accounts for internal resistance losses during discharge and represents a conservative estimate of the useful electrical energy delivered by the battery. Reported lithium-based Battery energy efficiencies are typically above this value at moderate discharge rates, with efficiency decreasing as discharge current increases [39]. Since the selected pouch cell is operated below its maximum continuous discharge rating, a 95% discharge efficiency is considered appropriate for preliminary sizing. Including this discharge efficiency, the required nominal installed battery energy becomes:

$$E_{\text{nom,req,final}} = \frac{E_{\text{usable,req}}}{\eta_{\text{batt}}} = \frac{4302}{0.95} = 4528 \text{ Wh} \tag{7.12}$$

The battery design process, therefore, starts from a nominal installed energy requirement of approximately 4.53 kWh. This requirement is used as the input for the battery trade-off, together with the voltage, current, mass, integration, and safety requirements of the propulsion and avionics systems.

Table 7.18: Battery Design Requirements Derived from the Mission Energy Budget

Battery design parameter	Requirement
Propulsion mission energy	2930 Wh
Non-propulsive electrical energy	63 Wh
Total mission energy	2993 Wh
Mission contingency	15%
Electrical System efficiency	95%
Nominal depth-of-discharge limit	80%
Required nominal battery energy	**4.53 kWh**

The battery pack shall provide a nominal high-voltage bus of approximately 90–92 V, compatible with the selected 20–24S propulsion system, while keeping the fully charged pack voltage below the ESC maximum voltage of 100 V. Including the 15.7 kW hover propulsion requirement and the 460 W auxiliary electrical load, the required continuous battery power is 16.16 kW. At a preliminary bus voltage of 90 V, this corresponds to a continuous pack current of 179.5 A. Applying a 20% sizing margin gives a design current requirement of 215.4 A.

7.4.4. Battery Design Trade-Off

Four battery concepts are considered in the trade-off: a custom RC LiPo pack assembly, a commercial high-voltage UAS battery module, a custom cylindrical-cell pack, and a custom pouch-cell pack. These options are retained because they are realistic candidates for achieving the required energy, discharge current, and aircraft packaging constraints. The trade-off is kept at the battery-concept level; the detailed cell chemistry and exact cell model are selected after the preferred battery concept is identified. This avoids selecting a specific cell before the most suitable pack architecture has been justified.

The trade-off criteria and their weights are given in Table 7.19. The highest weights are assigned to energy and mass efficiency, discharge-current capability, and packaging flexibility because these criteria directly determine whether the battery can meet the mission energy and power requirements within the aircraft mass and volume constraints. Safety and handling are included to account for operational risk during installation, charging, and use. Manufacturability and procurement are included to ensure that the selected concept remains feasible within the project schedule and production process.

Table 7.19: Battery Design Trade-Off Criteria and Weights

Criterion	Weight [%]	Reason
Energy and mass efficiency	30	The battery is one of the dominant mass contributors and must provide the required mission energy within the aircraft mass budget.
Discharge-current capability	25	The pack must support high propulsion current during climb and hover without excessive voltage sag or thermal loading.
Packaging flexibility	20	The aircraft layout requires a compact pack that can be integrated structurally and positioned near the desired centre of gravity.
Safety and handling	15	The battery concept must allow safe mechanical restraint, thermal monitoring, insulation, and operational handling.
Manufacturability and procurement	10	The design should remain feasible within the project schedule and component availability constraints.

Each option is scored from 1 to 5 for every criterion, and the weighted trade-off is shown in Table 7.20.

Table 7.20: Battery Design Trade-Off

Criteria / Battery options	Custom RC LiPo pack	Commercial HV UAS module	Custom pouch-cell pack	Custom cylindrical-cell pack
Energy and mass efficiency W: 30%	**4** Good specific energy, but module casing and wiring add to the mass	**4** Integrated design, but supplier layout limits mass optimisation	**5** Highest energy fit for required capacity and aircraft mass budget	**4** Competitive cells, but many holders and interconnects add to the mass
Discharge-current capability W: 25%	**5** High C-rate cells directly suited to peak propulsion loads	**4** Supplier-rated output, but current limit is fixed by module design	**5** Large-format cells support high current with few parallel paths	**4** High current possible, but load sharing across many cells is critical
Packaging flexibility W: 20%	**3** Several packs must be combined, reducing layout and CG freedom	**3** Fixed enclosure, voltage, and capacity constrain integration	**5** Flat cells can be stacked around the fuselage and CG needs	**4** Modular arrangement, but cylindrical gaps reduce volume efficiency
Safety and handling W: 15%	**2** Requires aircraft-level containment, sensing, and charge protection	**4** Supplied as a managed product with defined handling procedures	**4** Safe if enclosure, compression, insulation, and sensing are included	**3** Many individual cells increase inspection, balancing, and fault points
Manufacturability and procurement W: 10%	**4** Easy to source and assemble from available RC battery hardware	**5** Supplier-built pack minimizes custom assembly and sourcing risk	**3** Requires custom busbars, compression, sensing, and enclosure	**3** Many welds, holders, sense wires, and cell-level connections
Final weighted score	**3.75 / 5**	**3.80 / 5**	**4.65 / 5**	**3.90 / 5**

The custom pouch-cell pack is selected as the preferred battery concept for the detailed design. This option gives the strongest aircraft-level match because it combines high installed energy, high discharge capability, and strong packaging flexibility. The flat cell format allows the battery volume to be shaped around the fuselage layout and centre-of-gravity constraints, while the large cell capacity keeps the number of electrical interconnects low compared with an equivalent cylindrical-cell pack.

7.4.5. Battery pack design

Given the requirements for energy, current, and voltage, as well as the recommended battery configuration of 20–24 cells in series, the cell property ranges in Table 7.21 were derived. The cell voltage must allow a pack voltage close to the required 90–92 V high-voltage bus, the cell capacity must provide the required nominal installed energy without excessive parallelization, and the cell discharge rating must support the design current requirement of 215.4 A.

Table 7.21: Derived Cell-Level Requirements Before Cell Selection

Cell property	Required range/value	Reason
Nominal voltage	≈ 3.75–3.85 V	Allows a 24S pack near 90–92 V
Capacity	≥ 46.6 Ah for 24S1P	Provides at least 4.19 kWh nominal energy
Continuous discharge current	≥ 215.4 A	Supports design current with 20% margin
Continuous discharge rate	≥ 4.6C for a ∼ 47 Ah cell	Avoids exceeding cell current rating
Specific energy	≥ 400 Wh/kg	Keep consistency with PPA sizing

The selected cell is the ATOMFAIR high-energy anode-free pouch cell. The largest available variant has a nominal voltage of 3.8 V, a capacity of 52 Ah, and a maximum continuous discharge rating of 5*C* (Link). These values satisfy the derived cell-level requirements. A 24S1P configuration gives a nominal pack voltage of

$$V_{\text{pack,nom}} = N_s V_{\text{cell,nom}} = 24 \cdot 3.8 = 91.2 \text{ V}, \tag{7.13}$$

which lies within the required high-voltage bus range. The nominal installed pack energy is

$$E_{\text{pack,nom}} = N_s Q_{\text{cell}} V_{\text{cell,nom}} = 24 \cdot 52 \cdot 3.8 = 4742.4 \text{ Wh} \approx 4.74 \text{ kWh}. \tag{7.14}$$

This is higher than the required nominal installed energy of 4.53 kWh. The continuous current capability of the selected cell is

$$I_{\text{cell,max}} = C_{\text{max}} Q_{\text{cell}} = 5 \cdot 52 = 260 \text{ A}. \tag{7.15}$$

Since the pack is configured as 24S1P cells, the pack's current capability is equal to the cell current capability. The selected cell, therefore,e exceeds the required design current of 215.4 A, giving a current margin of

$$\text{Current margin} = \frac{260 - 215.4}{215.4} = 20.7\%. \tag{7.16}$$

The resulting battery pack is therefore selected as a 24S1P pack using 24 ATOMFAIR 52 Ah pouch cells. This configuration provides a nominal voltage of 91.2 V, a nominal installed energy of 4.74 kWh, and a maximum continuous current capability of 260 A.

Battery and Power Distribution Architecture

Based on the cell selection and pack sizing performed in the previous section, the electrical architecture is built around a 24S1P high-voltage battery pack using 24 ATOMFAIR 52 Ah pouch cells. This pack provides a nominal voltage of 91.2 V, a nominal installed energy of approximately 4.74 kWh, and a maximum continuous current capability of 260 A. These values satisfy the required installed energy of 4.53 kWh and the design current requirement of 215.4 A. The purpose of the power distribution architecture is therefore to connect this pack to the propulsion and auxiliary loads in a controlled, protected, and monitorable way.

The complete battery and power distribution schematic is shown in Figure 7.15. The architecture is divided into five functional regions: battery monitoring, main high-voltage protection, controlled bus connection, high-voltage power distribution, and charging. This structure ensures that the battery pack can supply the required propulsion power while still allowing the system to isolate faults, prevent uncontrolled inrush current, and monitor cell-level health during operation.

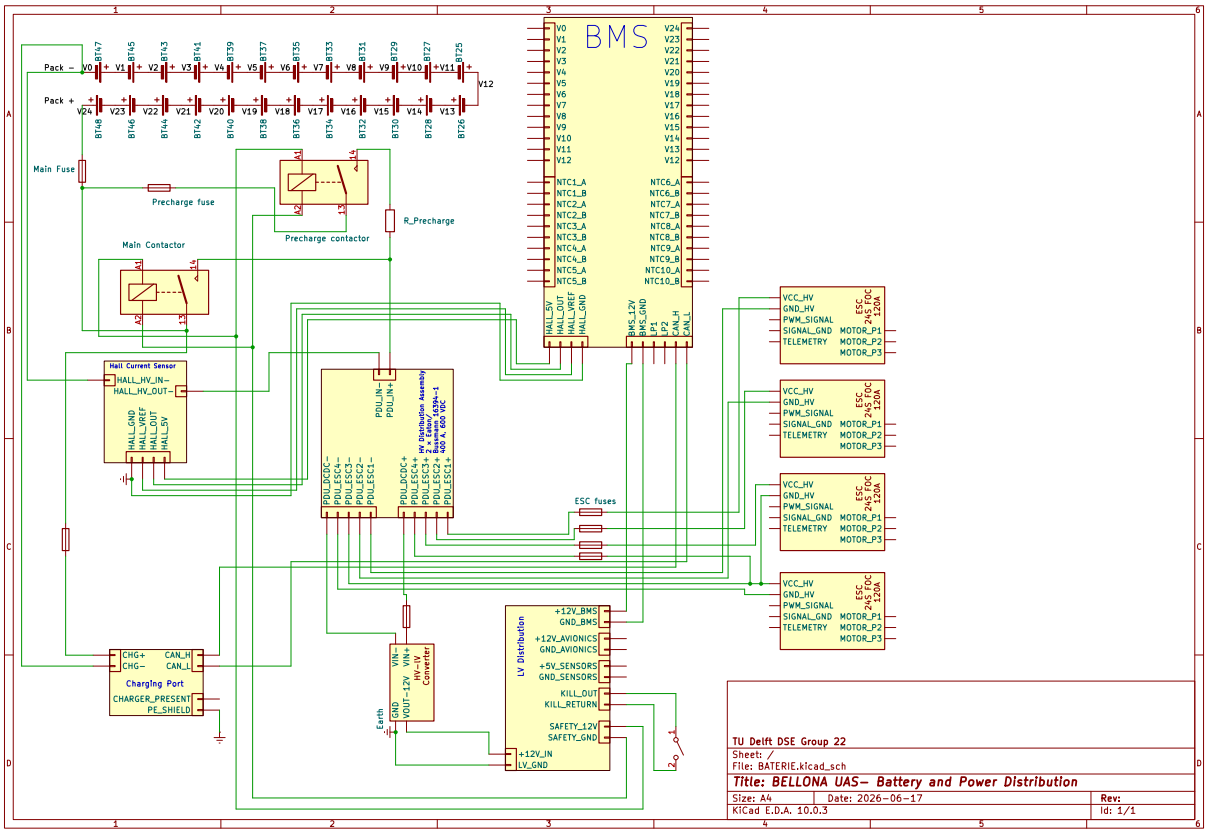

Figure 7.15: Battery and Power Distribution Schematic

The 24-cell battery pack is monitored by a Thunderstruck BMS controller (Link), which measures individual cell voltages, pack temperatures using Thunderstruck BMS thermistors (Link), and pack current through a Thunderstruck Hall-effect current sensor (Link). These measurements allow the system to detect over-voltage, under-voltage, over-temperature, imbalance, and abnormal current conditions. The BMS also controls the contactor-enable logic, so the high-voltage bus can be disconnected if a critical fault or kill-switch command is detected.

The main high-voltage output is protected by a 400 A Mersen A15QS400-4 fuse (Link). This rating is above both the 215.4 A design current and the 260 A maximum continuous pack current, so the fuse does not limit nominal operation. It is included for short-circuit and severe-fault protection, while continuous operational limits are supervised by the BMS and current sensor.

The high-voltage bus is switched by a normally-open TE Connectivity Kilovac EV200AAANA main contactor (Link). A pre-charge branch, consisting of a Gigavac P105BDA contactor (Link) and a 100 Ω HS100-100R-F resistor (Link), is placed in parallel with the main contactor. At start-up, the pre-charge branch charges the ESC and converter input capacitances gradually before the main contactor closes. This prevents high inrush current and reduces stress on the contactor, fuses, and downstream electronics.

After the contactor stage, the high-voltage bus enters an Eaton Bussmann 16394-1 power distribution unit (Link). The PDU distributes power to the four ESC branches and to the HV–LV converter. Each ESC branch is protected by an individual 100 A Mersen A15QS100-4 fuse (Link), so a severe fault in one propulsion branch can be isolated before propagating to the full high-voltage bus.

The HV–LV converter supplies the low-voltage avionics, sensors, BMS control electronics, contactor coils, and safety loop. The kill switch is implemented in the low-voltage contactor-control path. Activating it removes the contactor-enable signal and opens the main contactor, isolating the battery from the aircraft without requiring a manual switch rated for the full propulsion current.

Charging is performed through a dedicated Anderson 6801G3 charge port (Link) and protected charge

path. During charging, the BMS continues to supervise cell voltages and temperatures, allowing the charger to be disabled if any cell approaches its allowable limits. The resulting architecture provides controlled start-up, protected propulsion distribution, low-voltage supply, fault isolation, and supervised charging for the selected high-voltage battery pack.

7.4.6. Power and Electronics V&V

Table 7.22: Power and Electronics Subsystem Verification and Validation Plan

Req. ID	Verification and Validation Steps	Met
REQ-STK-01-MSN-01-SYS-01-P&E-01	The selected 24S1P battery pack provides 4.74 kWh of nominal installed energy, exceeding the required 4.53 kWh.	✓
REQ-STK-01-MSN-01-SYS-01-P&E-02	The selected 24S pack gives a nominal bus voltage of 91.2 V, which lies within the required 90–92 V range.	✓
REQ-STK-03-MSN-04-SYS-08-P&E-01	The selected cell discharge capability gives a maximum continuous pack current of 260 A, exceeding the required 215.4 A.	✓
REQ-STK-13-MSN-16-SYS-31-P&E-01	The HV–LV converter and low-voltage distribution block supply separate avionics, sensor, BMS, and safety-loop rails, as shown in Figure 7.15.	✓
REQ-STK-13-MSN-16-SYS-30-P&E-01	The schematic includes BMS cell-voltage taps, thermistor inputs, and a Hall-effect current sensor, allowing cell voltage, pack temperature, and pack current monitoring.	✓
REQ-STK-13-MSN-16-SYS-30-P&E-02	The schematic includes a 400 A main fuse and individual 100 A ESC branch fuses, protecting the main battery output and propulsion branches.	✓
REQ-STK-13-MSN-16-SYS-32-P&E-01	The BMS and kill-switch loop control the contactor-enable signal, allowing the high-voltage bus to be disconnected after a critical electrical fault.	✓

8 Balloon Interaction Group

The Balloon Interaction Group (BIG) is responsible for physically securing the target after interception. It captures the suspended payload below the balloon using an upward-launched net, establishes a tethered connection to the UAS, and provides emergency separation with backup parachute descent if the coupled system becomes unsafe to tow. This chapter defines the subsystem requirements, architecture, component sizing, airframe integration, budgets, and verification/validation plan for this subsystem.

8.1. BIG Subsystem Requirements

The BIG requirements in Table 8.1 are derived from the system-level mission requirements and define the capture, tethering, recovery-support, emergency-release, and reset functions of the subsystem. They are used as sizing drivers for the net opening, launcher accuracy and velocity, tether and reel capacity, emergency parachute, airframe clearances, and subsystem mass budget. Each requirement is assigned an identifier linking it to its parent requirements, together with a classification indicating its importance for the subsystem design.

Table 8.1: Balloon Interaction Subsystem Requirements

ID	Requirement	Classification
REQ-STK-05-MSN-06-SYS-11-BIG-01	The balloon interaction subsystem shall capture a suspended payload with a mass not exceeding 50 kg.	Key
REQ-STK-05-MSN-06-SYS-11-BIG-02	The balloon interaction subsystem shall be capable of capturing payloads contained within a 0.7 m radius bounding sphere, with principal dimensions of at least 0.1 m.	Key
REQ-STK-03-MSN-04-SYS-07-BIG-03	The balloon interaction subsystem shall accommodate lateral and vertical UAS hover-position errors of 0.25 m during capture.	Driving
REQ-STK-03-MSN-04-SYS-07-BIG-04	The balloon interaction subsystem shall accommodate a relative payload-UAS velocity of up to 0.25 m/s during capture.	Key

Table 8.1: Balloon Interaction Subsystem Requirements (continued)

ID	Requirement	Classification
REQ-STK-03-MSN-04-SYS-07-BIG-05	The balloon interaction subsystem shall launch the net assembly with an angular accuracy of 2.5 degrees relative to the nominal launch direction.	Driving
REQ-STK-05-MSN-06-SYS-11-BIG-06	The balloon interaction subsystem shall establish a tethered connection between the UAS and the captured payload-balloon assembly after capture.	Driving
REQ-STK-05-MSN-06-SYS-11-BIG-07	The balloon interaction subsystem shall have a net-UAS tether with a breaking load of at least 4 kN.	Non-driving
REQ-STK-05-MSN-06-SYS-11-BIG-08	The balloon interaction subsystem shall have a net-UAS tether with a total length of at least 25 m.	Driving
REQ-STK-05-MSN-06-SYS-11-BIG-09	The balloon interaction subsystem shall have a reel drum large enough to store the tether.	Driving
REQ-STK-05-MSN-06-SYS-13-BIG-10	The balloon interaction subsystem shall have a powered reel allowing at least 1 m/s retraction speed under 60 N tether load.	Driving
REQ-STK-05-MSN-06-SYS-12-BIG-11	The balloon interaction subsystem shall have a powered reel with an encoder capable of determining the current length of the tether deployed from the reel.	Driving
REQ-STK-05-MSN-06-SYS-12-BIG-12	The balloon interaction subsystem shall provide the tether state to the flight computer at a frequency of at least 5 Hz.	Non-driving
REQ-STK-05-MSN-06-SYS-13-BIG-13	The balloon interaction subsystem shall support controlled delivery of the captured payload-balloon assembly to the selected safe landing zone.	Driving
REQ-STK-13-MSN-17-SYS-31-BIG-14	The balloon interaction subsystem shall separate the tether from the UAS when the emergency separation mechanism is triggered.	Key
REQ-STK-13-MSN-17-SYS-31-BIG-15	The balloon interaction subsystem shall trigger the emergency separation mechanism when the tether reaches the end of the reel, or when it is triggered by the flight computer or manual intervention.	Key
REQ-STK-06-MSN-08-SYS-17-BIG-16	The balloon interaction subsystem shall have a parachute to reduce the descent speed of the separated payload-net system to at most 7 m/s at ground level after emergency separation.	Driving
REQ-STK-05-MSN-06-SYS-11-BIG-17	The balloon interaction subsystem shall not interfere with the propellers of the UAS.	Driving
REQ-STK-13-MSN-17-SYS-33-BIG-18	The balloon interaction subsystem shall have distinct safe and armed states for the net launcher.	Non-driving
REQ-STK-19-MSN-24-SYS-41-BIG-19	The balloon interaction subsystem shall have a mass less than 3.7 kg.	Driving
REQ-STK-11-MSN-13-SYS-25-BIG-20	The balloon interaction subsystem shall be fully resettable and reusable after at least 100 nominal missions, except for the consumable rifle cartridges.	Key
REQ-STK-11-MSN-13-SYS-25-BIG-21	The balloon interaction subsystem shall be resettable after a nominal mission in less than 10 min.	Non-driving

8.2. Mission Architecture

The balloon interaction subsystem is divided into four main functional assemblies: the capture net, the launcher, the tether/reel, and the emergency parachute. Together, these capture the suspended payload, establish a controlled tethered connection, allow recovery, and provide a safe abort mode. This section describes the function of each assembly. A sketch is shown in Figure 8.1.

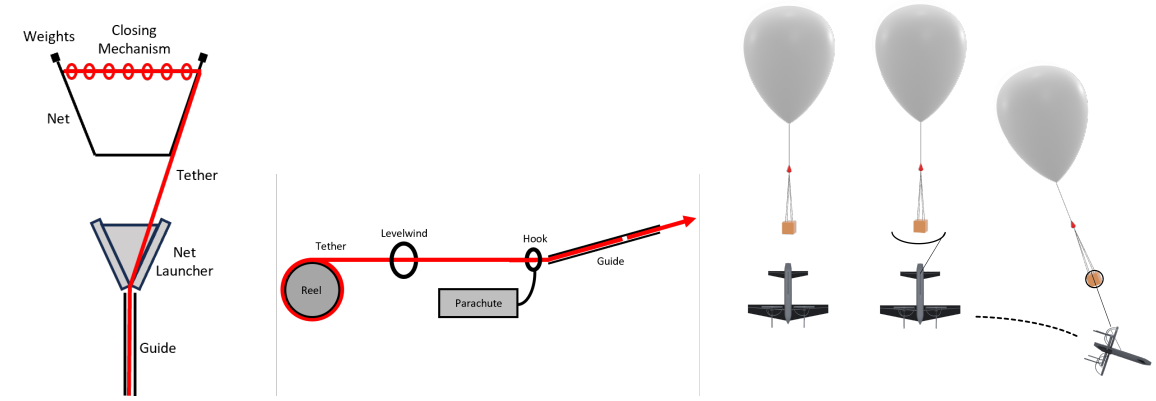

(a) Launch Configuration **(b)** Recovery Configuration **(c)** Interaction with Balloon

Figure 8.1: Sketch of Balloon Interaction Mission Architecture

The recovery and containment mechanisms are divided into four core structural and mechanical assemblies, each designed to manage specific stages of the interception, capture, and emergency mitigation sequence:

- **Capture Net Assembly:** The capture net assembly physically encloses the suspended payload. It consists of the pouch-shaped net, perimeter line, closure line, corner weights, and tether attachment. The net is launched upward and opens above the UAS. After the payload enters the pouch, the closure line actively tightens the upper perimeter of the net, ensuring the payload remains contained.
- **Launcher Assembly:** The launcher assembly is mounted along the UAS launch direction during terminal hover. It contains the packed net, corner weights, launch tubes, blank-cartridge actuation system, safety and arming mechanism, and structural attachments. Its function is to accelerate the corner weights so that the net reaches the required opening height and geometry before payload contact.
- **Tether/Reel Assembly:** The tether and reel assembly establishes the mechanical connection between the captured payload-balloon system and the UAS. The tether is connected to the net before launch and stored on a powered reel. During deployment, the reel allows low-resistance payout so that the net can open freely. After capture, the reel manages tether tension through retraction, controlled payout, and drag limiting, while also reporting deployed tether length and reel state to the flight computer.
- **Emergency Parachute Assembly:** The emergency separation and parachute assembly provides a controlled failure mode when continued towing would endanger the UAS, for example, due to sudden balloon rupture. If triggered, the UAS-side connection is released so that the aircraft can escape from the tethered load. The parachute remains attached to the payload-side tether and deploys with the separated net-payload system to reduce its descent speed.

8.3. Operational Sequence of Balloon Interaction

The operational sequence of the balloon interaction subsystem is shown in Figure 8.2. The sequence is divided into four phases: pre-launch, net deployment- recovery, and post-recovery. Decision gates are included throughout the sequence to ensure safe operation. Should conditions necessitate it, an abort sequence can be triggered.

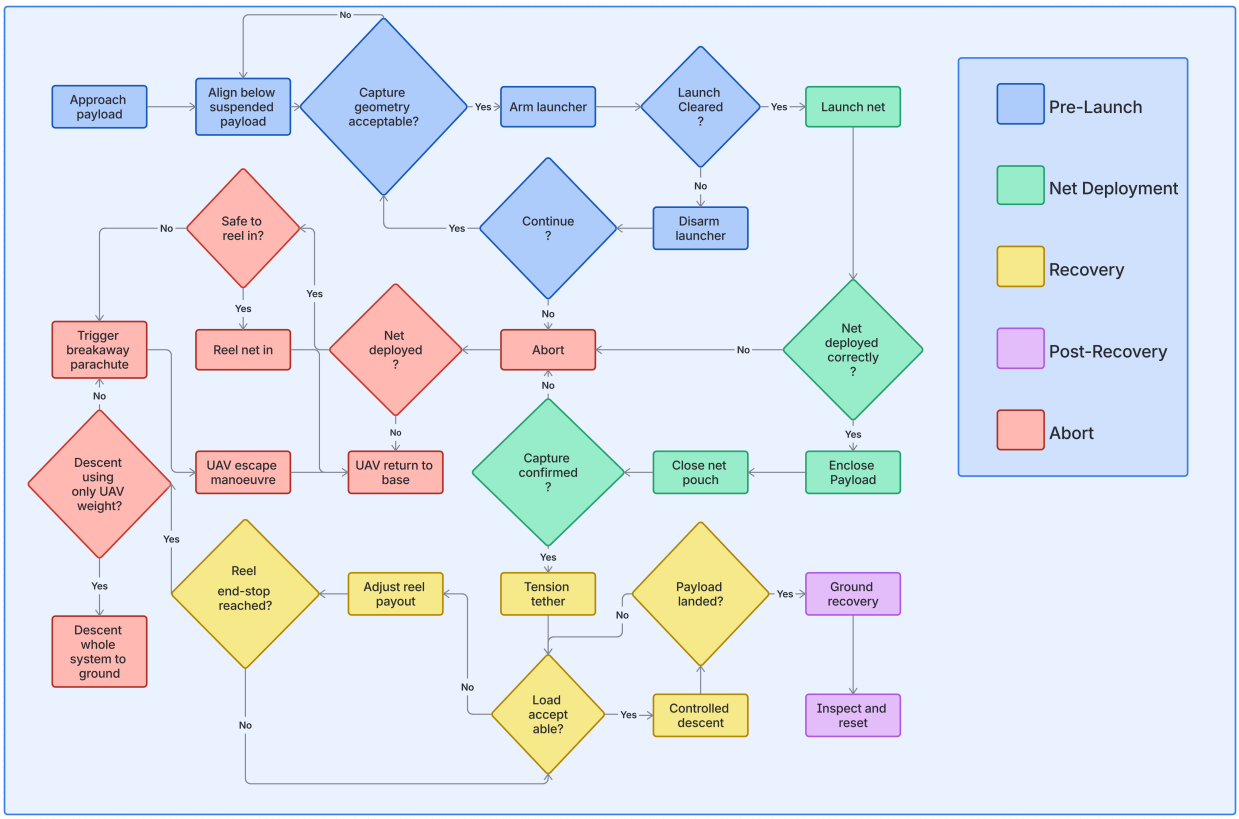

Figure 8.2: Balloon Interaction Operational Sequence

During the pre-launch phase, the UAS approaches the payload and aligns below the suspended payload. The capture geometry is then evaluated. If the UAS is not within the required capture envelope, it continues alignment. If the geometry is acceptable, the launcher is armed, and a final launch clearance check is performed. If this check fails, the launcher is disarmed, and the system either retries the capture alignment or aborts.

During the launch phase, the net is launched toward the payload. The system then checks whether the net is deployed correctly. If deployment fails, the mission enters the abort branch. If deployment is successful, the payload is enclosed, and the net pouch is closed. Capture is then confirmed before any significant tether load is applied.

During the recovery phase, the tether is tensione,d and the reel is used to manage the load. If the load is acceptable, the UAS performs a controlled descent of the captured payload-balloon system. If the load is not acceptable, reel payout is adjusted until the load returns within limits. If the reel end-stop is reached or the system becomes unsafe, the breakaway parachute is triggered, and the UAS performs an escape manoeuvre.

During abort handling, the system determines whether the net can be safely reeled in. If retraction is safe, the reel retrieves the net and the UAS returns to base. If retraction is unsafe but the coupled system remains stable, the UAS can reduce thrust and act as a passive load to help pull the balloon-payload system downward. If the load or aircraft state becomes unsafe, the breakaway parachute is triggere,d and the UAS separates from the net-tether-payload system. After payload landing, ground recovery is performed, and the subsystem is inspected, reset, and prepared for the next mission.

8.4. Capture Net Design

The capture net is the main mechanical interface used to capture the suspended payload after the UAS has positioned itself below the balloon. The selected design is a pouch-shaped net that is launched upward from the UAS. Four corner weights pull the top perimeter open during deployment, while the lower part of the net forms a receiving pouch for the payload.

The net is designed around three main functions. First, it must open wide enough to tolerate payload size, UAS positioning error, payload motion, and launch aiming error. Second, it must prevent the payload from passing through the mesh after impact. Third, it must close after the payload has entered

so that the payload cannot escape. The resulting design is a trapezoidal pouch with a large square top opening, a smaller square bottom grid, diamond side walls, four corner weights, and an actively tensioned closure line. Figure 8.3 shows the resulting net geometry and main dimensions.

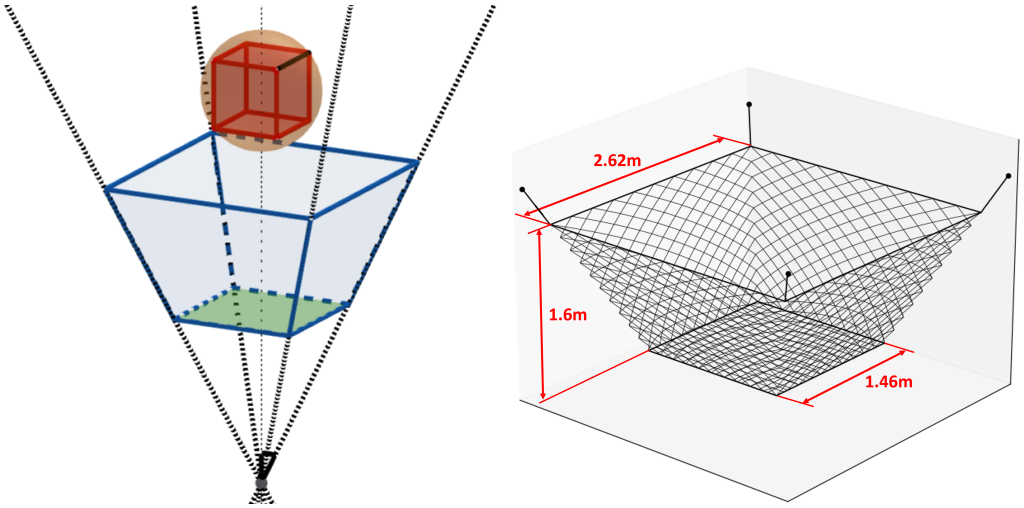

(a) Pouch-Shaped Capture Net **(b)** Final Net Dimensions

Figure 8.3: Capture Net Geometry and Sizing

8.4.1. Main Net Dimensions

The top opening is sized from the worst-case lateral space that must be available for the payload to enter the net, as imposed by Table 8.1. The payload is represented by a bounding sphere with radius 0.70 m. This radius is combined with the main lateral uncertainties: UAS hover-position uncertainty, relative payload motion during capture, and launch aiming uncertainty. These margins are included on each side of the payload because the payload may not be centered relative to the opening at the moment of capture. This results in a required width of 2.62 m, as shown in Figure 8.4a.

The net depth is set to 1.60 m. This value is chosen because the maximum payload height is 1.40 m, leaving an additional 0.20 m vertical margin. A shallower net would reduce mass, but would also increase the risk of the payload rebounding out of the opening before closure. A deeper net would improve containment, but would increase the launched mass and make deployment more difficult. The 1.60 m depth is therefore selected as a compromise between containment and launchability.

The bottom panel is made smaller than the top opening so that the net forms a pouch. The side-wall angle is selected as 20°, giving a bottom square side length of 1.46 m, as shown in Figure 8.4b. This angle was chosen to provide a sufficiently large vertical velocity component during deployment while also ensuring that the net opens effectively. This maintains sufficient area at the bottom to receive the payload while reducing unnecessary net area and mass. The final geometry is therefore a 2.62 m square top opening, a 1.46 m square bottom panel, and a 1.60 m net depth, as shown in Figure 8.3.

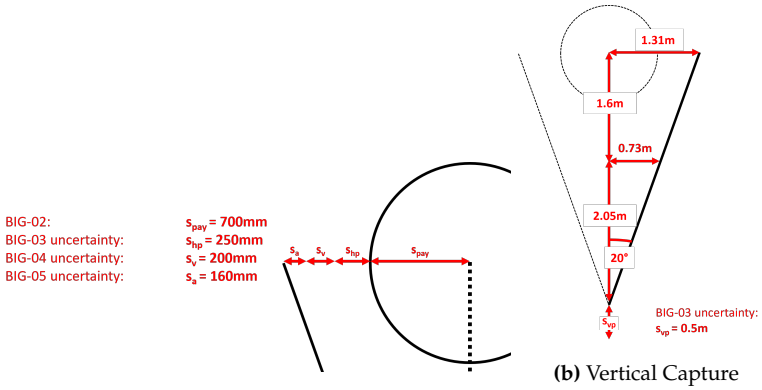

(a) Horizontal Capture Envelope **(b)** Vertical Capture Envelope

Figure 8.4: Capture Envelope Sizing

8.4.2. Mesh Spacing

The mesh spacing is selected based on the requirement that the payload principal dimensions are at least 100 mm. The bottom panel is the primary stopping surface when the payload enters the pouch,

so it uses the smallest mesh spacing. A square grid spacing of approximately 97 mm is selected for the bottom panel, preventing the smallest expected payload feature from passing through the bottom grid. The side walls use a diamond mesh with larger openings. This is justified because the side walls mainly guide and wrap around the payload rather than acting as the primary impact surface. Larger side-wall openings reduce line length and thus mass, while still providing enough structure for containment after closure. The side-wall spacing varies with the taper of the net, from approximately 146 mm near the lower perimeter to approximately 262 mm near the top opening. The resulting mesh layout is shown in Figure 8.5a. Excluding the tethers connecting the weights, this leads to a net rope length of about 277 m. With a 0.75 mm UHMWPE line mass of approximately 0.4 g/m, the corresponding mass is approximately 112 g.

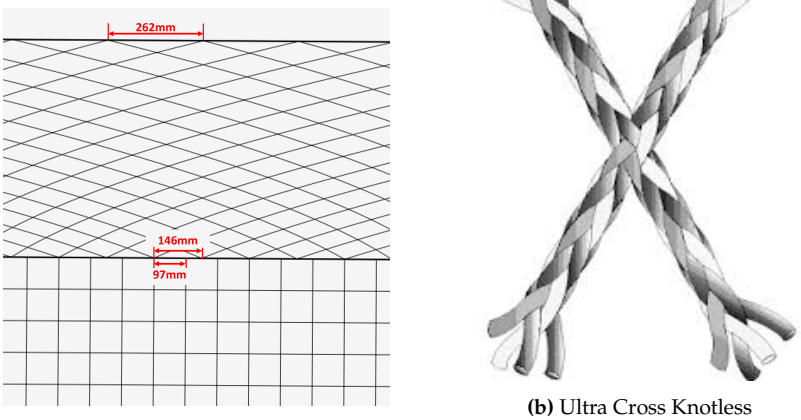

(a) Mesh Spacing Layout

(b) Ultra Cross Knotless Connection [40]

Figure 8.5: Capture Net Mesh Layout

The mesh intersections are selected as ultra-cross knotless connections. In this connection, the two UHMWPE strands are interwoven through the crossing rather than tied into a conventional knot, as shown in Figure 8.5b. This was selected because UHMWPE has low surface friction, and conventional knots can cause significant strength loss through tight bending radii and stress concentrations. The ultra cross connection fixes the mesh geometry while retaining more of the straight-line fiber strength. It also creates a smaller and smoother crossing than a bulky knot, reducing drag and packing volume [40]. The mass is estimated by allocating approximately 45 mm of additional line per crossing. For the approximately 1080 required intersections and attachments, this is about 49 m of additional line, corresponding to an additional mass of approximately 21 g.
To reinforce the net, a top and bottom perimeter line of 1 mm diameter is added. This leads to about 16.3 m of additional rope, or 12 g of extra mass.

8.4.3. Net Deployment

The deployment sequence is shown in Figure 8.6. The net is initially packed inside the launcher. At launch, the four corner weights are accelerated upward and outward. The launch direction of 27° follows from the 20° side-wall geometry of the deployed net. Launching the corner weights outward at this angle balances rapid opening of the top perimeter while maintaining a sufficiently large vertical velocity component to reach the payload height.
As there is no literature regarding the packing density of nets in net launchers, the estimate was based on published parachute packing data. Manually packed parachutes achieve packed densities of approximately 40–50% of their solid material density [41]. For the net used in this mission, a lower packing efficiency of 25% is assumed to avoid excessive compression and support reliable deployment. With a solid UHMWPE net volume of approximately 140 cm^3, this gives a packed net volume of approximately 560 cm^3. A launcher storage volume of 0.6 L is therefore used for the net mesh.
During the first part of deployment, the corner weights pull the top perimeter outward while the mesh unfolds underneath. The top opening reaches its full 2.62 m side length at approximately 3.65 m above the UAS. The net then continues upward until the top perimeter reaches a peak height of up to 6.05 m. The payload enters through the top opening and is intercepted by the lower grid and side

walls. This sequence is sketched in Figure 8.6.

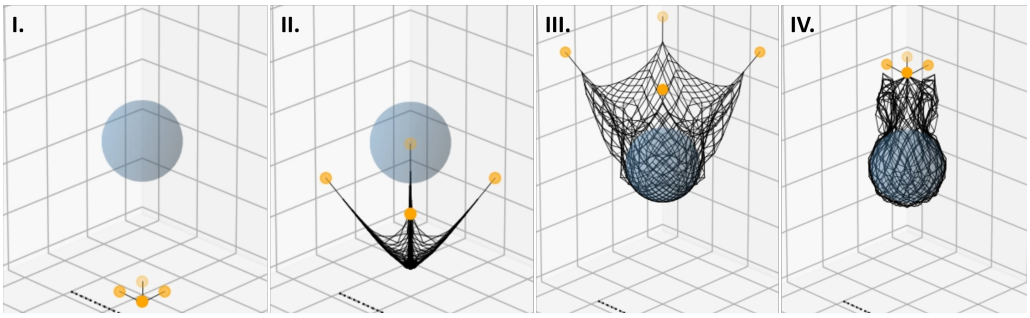

Figure 8.6: Net Deployment Sequence

The required launch velocity is estimated from an energy balance including both gravitational potential energy and aerodynamic drag. The drag force is modeled as

$$D = \frac{1}{2}\rho C_D A v^2 \tag{8.1}$$

where ρ is the air density, C_D is the drag coefficient, A is the projected drag area, and v is the vertical velocity of the launched net assembly.
The energy required to raise a launched mass M to height h_f, while accounting for quadratic drag, is then written as

$$E_{\text{required}} = \frac{M^2 g}{2\frac{1}{2}\rho C_D A}\left(e^{\frac{2\frac{1}{2}\rho C_D A h_f}{M}} - 1\right). \tag{8.2}$$

The corresponding launch velocity is obtained from rearranging the kinetic energy equation to

$$v_0 = \sqrt{\frac{2 \cdot E_{\text{required}}}{M}}. \tag{8.3}$$

Inserting the values from Table 8.2, gives a required initial energy of 263.12 J. This corresponds to an initial launch velocity of the entire net assembly of approximately 30.4 m/s. It can be seen in Figure 8.7 that this is mainly driven by the energy lost to drag.

Table 8.2: Input Parameters for the Net Deployment Energy Estimate

Symbol	Value	Origin
M	0.57 kg	Estimated launched net assembly mass
h_f	6.05 m	Required net peak height above launcher
ρ	1.225 kg/m^3	ISA sea-level air density
C_D	1.2	Conservative drag coefficient for deployed net geometry
A	0.21 m^2	Estimated projected drag area of deployed net assembly
g	9.81 m/s^2	Gravitational acceleration

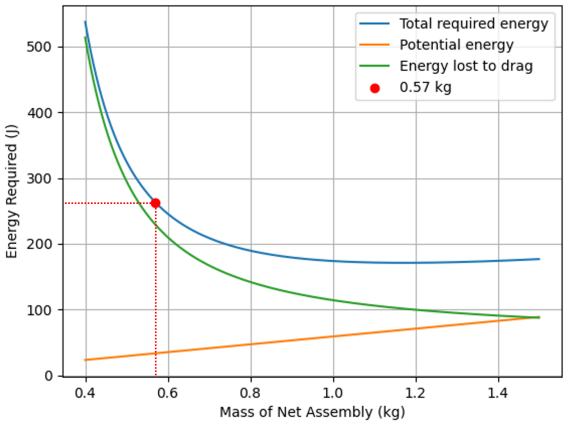

Figure 8.7: Net Deployment Energy Breakdown

8.4.4. Sizing of Weights

The four corner weights are required to open the top perimeter during launch. Without corner weights, the net would tend to rise as a compact bundle and would not reliably create the required capture opening before reaching the payload. The weights provide outward inertia, pulling the top corners apart while the rest of the mesh unfolds below.

Each corner weight is selected as 75 g, giving a total corner-weight mass of 300 g. This value is large enough to give the top perimeter opening authority, but still small enough to keep the launched assembly mass within the allowable range. Increasing the corner weights would improve opening reliability, but would also increase the required launch energy and launcher impulse. Reducing the corner weights would reduce launch energy, but would increase the risk of incomplete opening.

Based on the weight, the dimensions were derived, the result can be seen in Figure 8.8.

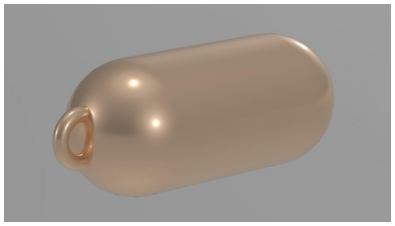

(a) Corner Weight CAD Model

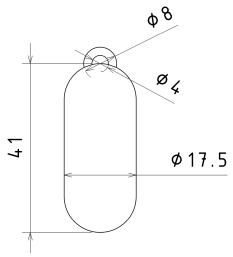

(b) Corner Weight Dimensions

Figure 8.8: Corner Weight Design

Since the launcher acts directly on the corner weights, these weights must transfer sufficient kinetic energy to the rest of the net during opening. A first estimate is obtained by assuming that the kinetic energy initially given to the four corner weights is redistributed to the complete launched net assembly. Losses due to line tensioning, folding, aerodynamic drag during opening, and internal deformation are accounted for with a safety factor but not directly calculated.

The minimum required corner-weight launch velocity can therefore be estimated by equating the kinetic energy of the corner weights to the kinetic energy required by the full launched assembly, giving.

$$v_1 = \sqrt{\frac{m_2}{m_1}} v_2. \tag{8.4}$$

where m_1 is the total mass of the four corner weights, m_2 is the total launched net assembly mass, v_1 is the required initial corner-weight velocity, and v_2 is the required velocity of the launched net assembly. Using the selected corner-weight mass and launched assembly mass gives a minimum corner-weight velocity of 41.9 m/s.

In reality, part of the energy is lost while the packed net unfolds, the lines become taut, the top perimeter opens, and the mesh deforms. To account for these losses, a conservative velocity safety factor of 1.3 is applied. Since kinetic energy scales with (v^2), this corresponds to approximately 70% additional kinetic energy. The resulting required corner-weight launch velocity is therefore 54.5 m/s.

8.4.5. Closure Line Design

The closure line is required because an open pouch alone does not guarantee retention after payload entry. The weights could rebound after potentially hitting the balloon, or the net could start to fall back after the payload. To prevent this, the top perimeter is closed after the payload has entered the net.

The closure system works like a drawstring bag, a similar technique to that described by H. Shin et al. to capture space debris [42]. A continuous 2 mm UHMWPE closure line is routed through loops around the top perimeter, as illustrated in Figure 8.9. The closure line is not tightened during initial deployment because early closure would reduce the capture opening and increase the risk of missing the payload. Instead, the closure line is actively tensioned by the reel after payload entry.

This active closure approach is selected because it separates the opening and retention functions. During launch, the corner weights maximize the opening. After capture, the reel tensions the closure line to reduce the opening and create a secure tethered connection. The closure line is also connected

to the main tether load path, so that after closure, the capture load can be transferred from the net into the tether and reel system.

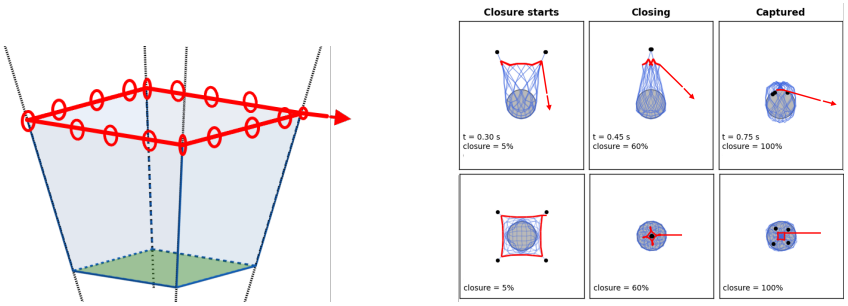

(a) Drawstring Closure Concept **(b)** Closure Sequence after Capture

Figure 8.9: Closure Line Mechanism

Only the tether portion pulled from the reel during launch is included in the launched assembly mass. This deployed portion is estimated at 20 g. The 100 g closing mechanism allocation includes the drawstring routing loops, attachment ring, local reinforcements, and splices required to transfer load from the net perimeter into the main tether.

8.4.6. Launched Net Assembly Mass

The total launched net assembly mass is 565 g. This includes all components accelerated upward during deployment, as listed in Table 8.3. This is slightly below the 570 g value used in the deployment and launcher sizing calculations, so the sizing remains conservative.

Table 8.3: Estimated Launched Net Assembly Mass

Component	Estimated mass [g]
Net mesh (including ultra cross connections)	133
Perimeter lines	12
Corner weights	$75 \times 4 = 300$
Closing mechanism	100
Launched tether portion	20
Total launched net assembly	**565**

8.5. Blank Rifle Cartridge Launcher Design

As outlined in Section 8.4, the corner weights must be launched with a velocity of 54.5m/s. To reliably achieve this launch velocity, a blank rifle cartridge-based launcher is used, for its combination of high energy density and reliability. A 7.62x51mm NATO blank cartridge is used, as it provides sufficient gas pressure to accelerate the projectiles to a suitable velocity while remaining lightweight at only 13 grams per cartridge.

Sizing of the launcher is done using an interior ballistics solver called PIBS [43], which solves the various differential equations governing the combustion of the smokeless powder in the cartridge and the propulsion of the projectile down the barrel. Some parameters used in the software are shown in Figure 8.10a, and the output of the software is shown in Figure 8.10b.

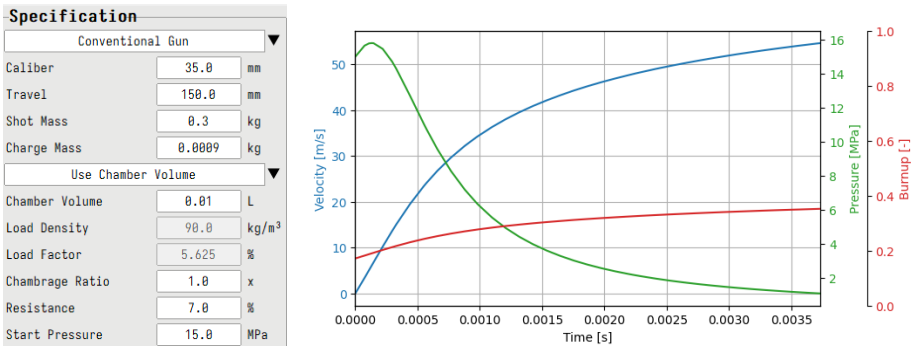

(a) Solver Input Parameters **(b)** Predicted Pressure and Velocity

Figure 8.10: PIBS Interior Ballistics Model for the Launcher

The final velocity of the projectiles is predicted to be 54.6 m/s by the software, meeting the requirements. The net launcher itself is designed to match the specifications provided to the software, with a $10cm^3$

manifold splitting the gas flow between four barrels, each of 17.5 mm diameter. the launcher is made of AISI 4130 steel, which allows for good resistance to pressure and heat, and is a common alloy used in similar applications.
A critical design parameter is the minimum wall thickness of the barrel and other pressure-retaining elements. The maximum pressure in the barrel predicted by the solver is 15.8 MPa. The minimum barrel wall thickness is estimated using the thin-walled hoop-stress relation,

$$t = \frac{PD}{2\sigma_y}, \tag{8.5}$$

where P is the internal pressure, D is the barrel diameter, and σ_y is the yield stress of AISI 4130 steel. Using a conservative yield stress of 435 MPa, the required wall thickness is 0.3 mm. A 1 mm wall thickness is selected to allow for easy manufacturing and to account for discrepancies in the internal ballistics software, giving a safety factor of approximately 3.
The blank cartridge is detonated by a small solenoidal actuator, which strikes the firing pin of the cartridge. The solenoid is attached via adhesive to a breechbloc,k which uses an interrupted screw to ensure easy reloading after use while retaining a strong pressure seal.
The resulting launcher geometry is shown in Figure 8.11.

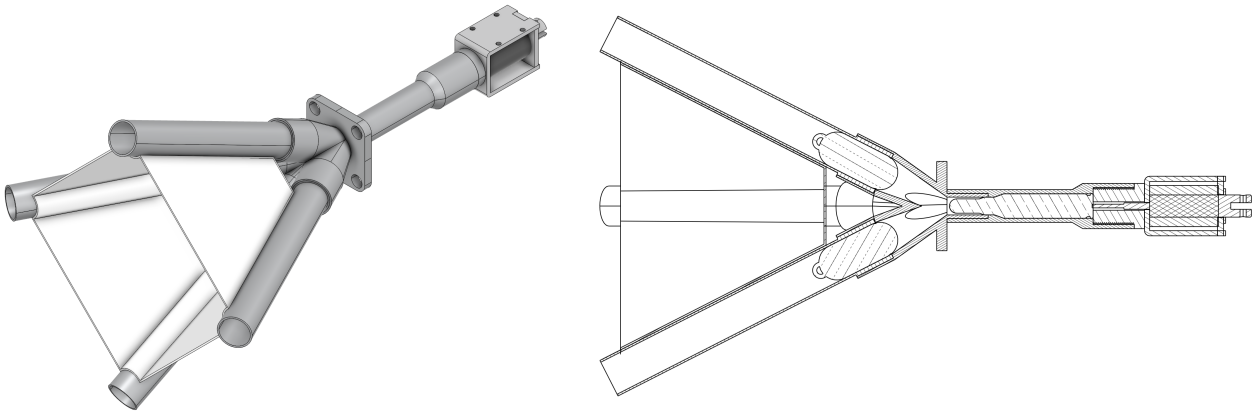

(a) Net Launcher CAD Model **(b)** Net Launcher Section View

Figure 8.11: Blank-Cartridge Launcher Geometry

The launcher assembly mass is summarized in Table 8.4. The steel launcher body is the dominant contribution, while the cartridge, solenoid and firing pin provide smaller contributions.

Table 8.4: Estimated Launcher Assembly Mass

Component	Estimated mass [g]
Barrels	$73 \times 4 = 292$
Net holder	33
Manifold and mounting hardware	492
Chamber	83
Breech block	46
Solenoid and firing pin	174
Blank rifle cartridge	13
Total launcher assembly	**1133**

8.6. Reel, Tether, and Tether Guide Design

The reel and tether connect the capture net to the UAS after payload capture and enable controlled recovery. During descent, the captured balloon-payload system is not pulled directly against the wind. Instead, it descends while drifting approximately with the wind, while the UAS applies a lateral towing force to guide it toward the selected recovery area, as described in Subsection 6.9.3. This reduces the required continuous tether load.

8.6.1. Reel Design

The required towing force is estimated with the descent-correction model shown in Figure 8.12a. For a 15 min descent in 13 m/s wind, a 3 km correction radius requires approximately 60 N of towing force. This value is used as the nominal reel load for guided recovery.

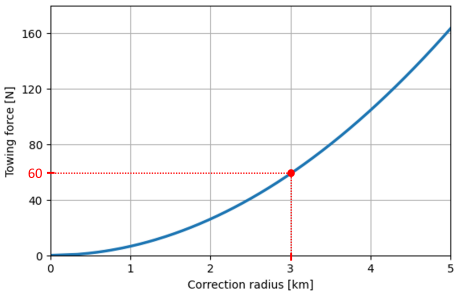

(a) Recovery Towing Force Estimate

(b) Daiwa 21 Seaborg 300J Reel [44]

Figure 8.12: Reel Design

A modified off-the-shelf Daiwa 21 Seaborg 300J electric reel, shown in Figure 8.12b is selected. The reel has a nominal mass of 560 g and a specified maximum winding force of 59 kg [44], corresponding to approximately 579 N. The reel is placed close to the UAS center of gravity to reduce moments and to introduce tether loads into the reinforced central fuselage structure.
The reel is modified for integration into the UAS. The original outer casing is removed because the reel is installed inside the fuselage and does not require its standalone protective housing. The handle and jog power lever are also removed, since manual operation is not required in flight. Instead, the reel computer receives commands through a datalink from the flight computer, while an actuated clutch controls payout and engagement. The reel is connected to the UAS electrical system and mounted through a custom structural adapter that transfers tether loads into the reinforced fuselage structure. The drag setting is adjusted before flight, because the recovery concept only requires a fixed maximum line tension rather than continuously variable drag. The existing levelwind mechanism is retained, but modified to accommodate the 2 mm UHMWPE tether, and the built-in encoder is used to determine deployed tether length.

8.6.2. Tether Design

The tether is a 2 mm diameter UHMWPE line. Its breaking load of approximately 410 kg is significantly larger than the nominal recovery load of 60 N, providing margin for gusts and unexpected payload motion. The total tether length is selected to be 30 m, of which approximately 20 m is deployed during nominal recovery. The remaining length provides reel-out margin during load spikes or unexpected relative motion.
The tether is already connected to the net before launch, but is routed so that it does not tension the net during deployment. After the payload enters the net, the same line acts as both the closure line and the main UAS-payload tether. Retraction closes the pouch and establishes the post-capture load path.

8.6.3. Tether Guide Design

The tether guide is used to prevent contact with the propellers and control surfaces during recovery. It is not intended to carry the main tether load. Instead, the primary tether load is transferred through the reel and its structural mounting into the fuselage. The guide only constrains the tether path and keeps the line inside clearance envelope.
The guide consists of a pultruded carbon-fibre reinforced polymer tube, a launch-retention hook (Figure 8.13c), a hinge, and a release mechanism (Figure 8.13b). The tether is routed internally through the tube, which prevents it from whipping or moving laterally into the propeller disk. A carbon-fibre tube is selected because it provides high bending stiffness at low mass, while the circular internal passage gives a simple and low-friction routing path for the tether. The complete guide assembly, including the tube, hinge, hook, release actuator, brackets, and fasteners, has a mass of 0.210 kg.

(a) Complete Tether Guide Assembly

(b) Guide Hinge and Release Mechanism

(c) Guide Launch Retention Hook

Figure 8.13: Tether Guide Assembly

During cruise to the balloon and launch, the guide is held in a stowed position by a retention hook, as

illustrated in Figure 8.14a. This prevents the guide from interfering with the net launcher and keeps the tether path compact while the UAS approaches the payload and deploys the net. After capture, tether tension passively rotates the guide about the hinge into the recovery configuration, shown in Figure 8.14b.

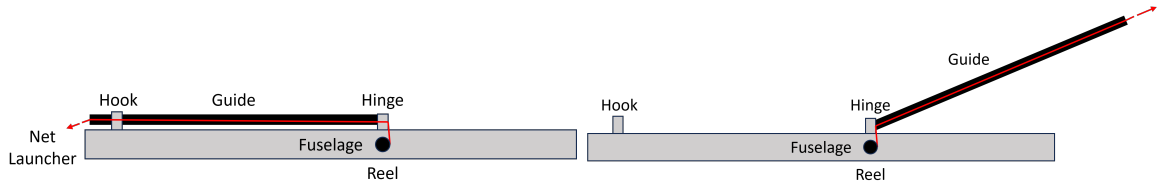

(a) Stowed Cruise and Launch Configuration **(b)** Deployed Recovery Configuration

Figure 8.14: Tether Guide Launch and Recovery Configurations

In the recovery configuration, the guide maintains a clean tether exit path. The tether remains free to slide axially through the guide so that the reel can control payout and retraction. At the same time, the tether cannot leave the guide laterally during nominal operation, ensuring that the line remains constrained even during payload motion or changes in tether angle.
The emergency separation function is integrated at the guide base. When separation is commanded by the flight computer or operator, the release actuator pulls the retaining pin, allowing the guide to separate from the UAS.

8.6.4. Reel, Tether, and Tether Guide Mass

The reel, tether, and guide assembly mass is summarised in Table 8.5. The modified reel and electronics contribute 520 g, the 30 m UHMWPE tether contributes 90 g, and the guide assembly contributes 210 g, giving a total of 820 g.

Table 8.5: Estimated Reel, Tether, and Guide Assembly Mass

Component	Estimated mass [g]
Modified Daiwa Seaborg 300J Reel and Electronics	520
UHMWPE tether	90
Guide assembly	210
Total	**820**

8.7. Emergency Breakaway and Parachute Design

The emergency breakaway and parachute system provides a controlled failure mode if the captured balloon-payload system becomes unsafe to tow. The main design case is a sudden loss of balloon lift, for example after balloon rupture, which could cause the payload-net system to fall and impose excessive loads on the UAS. In this case, the UAS must separate from the falling payload while ensuring that the payload system descends at an acceptable speed.
The parachute is stored in a dedicated compartment inside the UAS and is connected to the payload-side tether, as shown in Figure 8.15a. During nominal recovery, the parachute remains packed and does not affect the tether load path. If the breakaway sequence is triggered, the ground station is notified, the reel clutch is released, and the tether is allowed to free-spool under the high external load. At approximately the same time, the parachute compartment door is opened. Once the reel reaches the end of the tether, an end-of-line stop pulls the parachute out of its compartment. This deploys the parachute without requiring a separate ejection mechanism. The retaining pin at the guide base is also released, detaching the guide from the UAS while leaving it attached to the tether, net, and parachute assembly. This separates the UAS from the tether, net, parachute, guide, and captured payload. The UAS can then perform an escape manoeuvre, while the parachute remains attached to the separated payload-net system and reduces its descent speed. A small GPS transponder attached to the parachute broadcasts the position of the separated system, allowing the ground crew to track the descent location and respond accordingly.

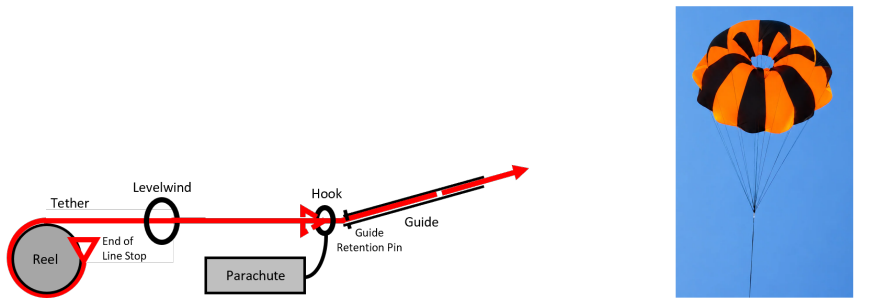

(a) Parachute Extraction Schematic

(b) Rocketman High-Performance CD 2.2 Parachute [45]

Figure 8.15: Emergency Breakaway and Parachute System

The parachute is sized for the worst-case 50 kg payload, including attached net and tether hardware. The selected 120" Rocketman High Performance CD 2.2 parachute is specified for a supported mass of up to 58.3 kg [45], providing margin relative to the design payload mass. It has a mass of 709 g and is packed into a cylindrical compartment with an internal diameter of 110 mm and a length of 300 mm. The compartment includes an actuated door that opens during emergency breakaway.
The emergency parachute assembly mass is summarized in Table 8.6.

Table 8.6: Estimated Emergency Parachute Assembly Mass

Component	Estimated mass [g]
Rocketman High Performance CD 2.2 parachute	709
Parachute container and actuated door	321
GPS transponder and release electronics	50
Total	**1080**

8.8. Airframe Integration

The subsystem is integrated inside the fuselage to effectively transfer capture loads into the main fuselage, while remaining lightweight. The main integration features are shown in Figure 8.16.

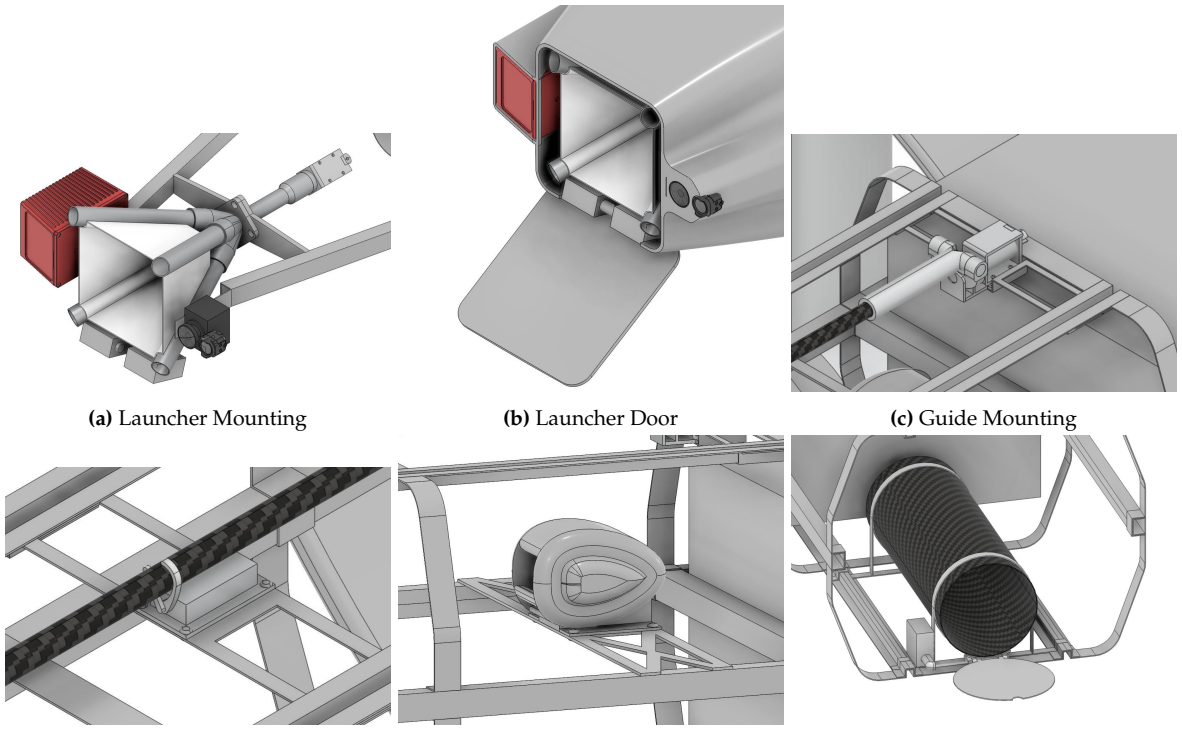

(a) Launcher Mounting **(b)** Launcher Door **(c)** Guide Mounting

(d) Retention Hook Mounting **(e)** Reel Installation **(f)** Parachute Compartment

Figure 8.16: BIG Airframe Integration

The launcher is attached to the reinforced central frame so that the firing loads are introduced directly into the primary structure. The reel is mounted close to the center of gravity to reduce moments during tethered recovery. The tether path runs from the reel through the fuselage and into the guide, which constrains the line away from the propellers and control surfaces while still allowing axial payout and retraction.

During nominal recovery, the guide constrains the tether path while the reel carries the primary tether load. If separation is commanded, the guide is released from the UAS and the parachute remains connected to the payload-side tether. The parachute compartment is placed towards the back of the fuselage bay and opens during breakaway so that the tether can extract the parachute as the reel reaches the end-stop.

8.9. Mass, Power, and Cost Budget

The mass, power, and cost budget of the Balloon Interaction Group is summarized in Table 8.7. The budget is divided into the main functional assemblies described in the previous sections: the launched net assembly, launcher, reel/tether/guide assembly, and emergency parachute assembly. Electrical power is only assigned to components requiring actuation or continuous operation. The resulting total subsystem mass is 3598 g, which remains below the 3.7 kg BIG mass requirement.

Table 8.7: Balloon Interaction Group Mass, Power, and Cost Budget

Component	Mass [g]	Power [W]	Cost [€]
Net mesh, including ultra-cross connections	133	0	300
Perimeter lines	12	0	5
Corner weights	300	0	10
Closing mechanism	100	0	15
Launched tether portion	20	0	5
Subtotal launched net assembly	**565**	**0**	**335**
Barrels	$73 \times 4 = 292$	0	120
Net holder	33	0	10
Manifold and mounting hardware	492	0	300
Chamber	83	0	50
Breech block	46	0	50
Solenoid and firing pin	174	3	20
Blank rifle cartridge	13	0	1
Subtotal launcher assembly	**1133**	**3**	**551**
Modified Daiwa Seaborg 300J reel and electronics	520	240	500
UHMWPE tether	90	0	10
Guide assembly	210	3	65
Subtotal reel, tether, and guide assembly	**820**	**243**	**575**
Rocketman High Performance CD 2.2 parachute	709	0	300
Parachute container and actuated door	321	3	35
GPS transponder	50	0	110
Subtotal emergency parachute assembly	**1080**	**3**	**445**
Total BIG subsystem	**3598**	**249**	**1906**

8.10. Balloon Interaction Verification and Validation Plan

This section describes the verification and validation plan for the Balloon Interaction Group subsystem requirements. Each requirement is linked to completed design evidence or to a planned verification activity. A checkmark (✓) indicates that the requirement is currently supported by sizing, design analysis, CAD integration, supplier data, or budget checks. A cross (×) indicates that further verification or validation is required through testing, simulation, or integrated subsystem demonstration.

Table 8.8: Balloon Interaction Group Verification and Validation Plan

Req. ID	Verification and Validation Steps	Met
REQ-STK-05-MSN-06-SYS-11-BIG-01	A representative suspended dummy-payload capture test will be performed, including checks of the net, tether, reel, and fuselage load path.	×
REQ-STK-05-MSN-06-SYS-11-BIG-02	The payload size envelope has been checked against the selected net depth, bottom grid spacing, and side-wall mesh geometry.	✓
REQ-STK-03-MSN-04-SYS-07-BIG-03	The lateral and vertical hover-position error has been included in the net opening and depth sizing.	✓
REQ-STK-03-MSN-04-SYS-07-BIG-04	A representative dynamic capture test will be performed for the specified relative payload-UAS velocity.	×
REQ-STK-03-MSN-04-SYS-07-BIG-05	Ground firing tests will be performed to measure launch direction and verify the angular accuracy.	×
REQ-STK-05-MSN-06-SYS-11-BIG-06	The net, closure line, tether, and reel routing have been designed to establish a continuous tethered load path after capture.	✓

Table 8.8: Balloon Interaction Group Verification and Validation Plan (continued)

Req. ID	Verification and Validation Steps	Met
REQ-STK-05-MSN-06-SYS-11-BIG-07	The 2 mm UHMWPE tether has been selected using supplier strength data.	✓
REQ-STK-05-MSN-06-SYS-11-BIG-08	The selected tether length is 30 m, which exceeds the required minimum tether length of 25 m.	✓
REQ-STK-05-MSN-06-SYS-11-BIG-09	A winding, payout, and rewind test will be performed to verify that the full tether length can be stored on the reel.	×
REQ-STK-05-MSN-06-SYS-13-BIG-10	A reel bench test will be performed to measure retraction speed under a 60 N tether load.	×
REQ-STK-05-MSN-06-SYS-12-BIG-11	The selected reel includes an encoder for deployed-line measurement.	✓
REQ-STK-05-MSN-06-SYS-12-BIG-12	A data-interface test will be performed to verify that tether-state data are sent to the flight computer at 5 Hz or higher.	×
REQ-STK-05-MSN-06-SYS-13-BIG-13	The recovery concept has been supported by a towing-force estimate. Recovery simulation or representative-load testing will be performed.	×
REQ-STK-13-MSN-17-SYS-31-BIG-14	A ground emergency-separation test will be performed to verify clean UAS-side release from the tether system.	×
REQ-STK-13-MSN-17-SYS-31-BIG-15	Functional tests will be performed for the end-of-reel trigger, flight-computer command, and manual command paths.	×
REQ-STK-06-MSN-08-SYS-17-BIG-16	The parachute has been selected for the worst-case payload mass. Data provided by the manufacturer gives 6.8 m/s for 50.5 kg.	✓
REQ-STK-05-MSN-06-SYS-11-BIG-17	The guide geometry and recovery configuration have been designed to keep the tether away from the propellers.	✓
REQ-STK-13-MSN-17-SYS-33-BIG-18	Functional tests will be performed to verify the launcher safe, armed, and fired states.	×
REQ-STK-19-MSN-24-SYS-41-BIG-19	The BIG mass budget gives a total subsystem mass of 3598 g, which is below the 3.7 kg mass requirement.	✓
REQ-STK-11-MSN-13-SYS-25-BIG-20	Repeated nominal reset and inspection cycles will be performed for the net, launcher, tether, reel, guide, and closure system.	×
REQ-STK-11-MSN-13-SYS-25-BIG-21	The nominal reset procedure will be timed, including rewinding, repacking, reloading, and inspection.	×

The many crosses in Table 8.8 indicate verification activities that are still pending, not requirements that have failed. Most concern dynamic or safety-critical functions that require physical testing beyond the current design stage.

9 Structures and Materials

9.1. Structural Design Scope and Requirements

The selected concept is a tail-sitter VTOL UAS that captures the suspended payload from below using an upward-launched net and then guides the coupled balloon-payload system toward a safe recovery zone. The structure must therefore support both conventional aircraft loads and the additional loads introduced by the hover, capture and tethered-descent phase.

The structural design has three main objectives. First, the airframe shall provide sufficient stiffness and strength during vertical take-off, transition, cruise, hover, descent and landing. Second, the capture load path shall transfer the loads from the net and tether into the main fuselage frame without relying on weak local skin attachments. Third, the structure shall remain inspectable and repairable after a mission, since the system is intended to be reusable rather than disposable.

The structures, materials and sustainability requirements are derived from the selected Concept A architecture and from the current sizing assumptions used in the preliminary design. The reference maximum take-off mass is m_{TO} = 51.13 kg. The final installed battery mass is 11.4 kg, while structural load introduction points are sized using explicit margins because the capture, propulsion and landing loads are concentrated rather than purely distributed. The requirements are split into structural requirements and sustainability requirements to avoid mixing strength, mass, lifecycle and

environmental constraints in one table.

Table 9.1: Structures and Materials Subsystem Requirements

ID	Requirement	Classification
REQ-STK-19-MSN-24-SYS-41-STR-01	Structural sizing shall use m_{TO} = 51.13 kg; loads shall be updated if mass changes by more than 10%.	Driving
REQ-STK-13-MSN-16-SYS-30-STR-02	The primary airframe shall have positive margins for all design load cases in Table 9.3.	Key
REQ-STK-03-MSN-04-SYS-07-STR-03	The wing and canard shall withstand the load factor of $n = -2$ to $n = 4$ applied to cruise/climb loads.	Key
REQ-STK-05-MSN-06-SYS-11-STR-04	Each motor mount and propulsion strut shall withstand at least 500 N axial thrust.	Non-driving
REQ-STK-05-MSN-06-SYS-11-STR-05	The full propulsion-support structure shall withstand at least 2.00 kN total thrust.	Driving
REQ-STK-13-MSN-16-SYS-30-STR-06	Motor struts and landing booms shall withstand combined thrust, torque, disturbance, inertia and landing loads.	Key
REQ-STK-05-MSN-06-SYS-13-STR-07	Landing supports shall withstand a $3g$ tail-sitter landing and a 20% lateral asymmetric side load.	Key
REQ-STK-05-MSN-06-SYS-11-STR-08	The tether hardpoint and reel support shall withstand a proof load of at least 1.5 kN.	Driving
REQ-STK-05-MSN-06-SYS-11-STR-09	Concentrated loads shall be introduced through reinforced fittings, ribs, spars, frames or bulkheads.	Driving
REQ-STK-19-MSN-24-SYS-41-STR-10	The primary airframe structural mass shall not exceed 20 kg, excluding non-structural subsystems.	Key
REQ-STK-06-MSN-08-SYS-17-STR-11	Net, tether, closure line and parachute hardware shall maintain at least 50 mm propeller clearance.	Driving
REQ-STK-13-MSN-17-SYS-31-STR-12	Wing structure should not be subject to propeller resonance with 15% frequency separation from the nominal shaft frequency where possible.	Non-driving
REQ-STK-17-MSN-22-SYS-38-STR-13	Primary joints shall remain inspectable after each mission and replaceable without removing large bonded sections.	Non-driving

9.1.1. Reference Coordinate System

A body-fixed coordinate system is used for structural sizing. The x-axis is positive from tail to nose, the y-axis is positive toward the right wing, and the z-axis is positive from the top of the aircraft toward the bottom in cruise orientation. In tail-sitter hover, the same body axes are retained. Since the aircraft nose points upward during hover, the propulsive thrust direction is approximately aligned with $+x$. All structural interfaces are referenced using this same body-axis convention.

With this convention, thrust acts in $+x$, cruise drag acts in $-x$, aerodynamic lift acts in $-z$, and weight acts in $+z$ during cruise-oriented load cases. The signs are used only to define the load directions. Structural sizing is based on the absolute internal load envelope.

Table 9.2: Reference Coordinate System Used for Structural Sizing

Axis	Positive direction	Structural use
x	Tail to nose	Longitudinal position of the battery, reel, tether hardpoint, wing root, canard, and propulsion mounts. Positive x is also the thrust direction in hover and cruise.
y	Toward the right wing from the centerline	Wing bending, motor lateral placement, asymmetric landing loads, and off-axis tether loading.
z	Top to bottom in cruise orientation	Vertical placement of battery, landing supports, launcher, propulsor offsets, and tether load introduction. Lift acts in $-z$, while weight acts in $+z$.

9.2. Loads Identification and Materials Selection

The selected structure consists of a CFRP main wingbox, a CFRP canard D-spar, a frame-and-longeron fuselage structure, metallic fittings at concentrated load interfaces, and aluminium motor struts with aft landing booms. The main load-path philosophy is to avoid introducing concentrated loads directly into unsupported skin panels. Concentrated forces are instead transferred through ribs, spars, bulkheads, local reinforcement plates and metallic inserts.

The present section defines the load cases, material allocation, lifting-surface sizing, fuselage sizing and structural verification logic used to obtain the integrated structural layout. The complete structural

assembly is shown later in Figure 9.16, after the subsystem-level sizing and verification steps have been introduced.

Table 9.3: Design Load Cases and Dominant Internal Resultants

Case	Load case description	Sizing input	Dominant resultant
LC1	Cruise/climb wing-borne loading, with trimmed lift, drag, matching cruise thrust, gravity and inertial force closure.	$1g$ cruise/climb trim; load factors from $n = -2$ to $n = 4$ applied for sizing.	Vertical shear V_z, bending M_y, and axial force N.
LC2	Symmetric tail-sitter hover with all propulsors active.	Nominal installed-thrust case based on 4×163 N from the PPA sizing point, with $1g$ axial gravity/inertia closure.	Mainly axial force N.
LC3	Asymmetric propulsion proof case.	Upper propulsors loaded using the local structural proof thrust of 500 N per propulsor.	Axial force N, local bending M_y, and propulsion-interface loads.
LC4a	Symmetric tail-sitter landing.	$3g$ landing reaction along the fuselage axis.	Axial compression/tension N.
LC4b	One-sided tail-sitter landing with lateral ground reaction.	$3g$ one-sided landing; side load equal to 20% of landing reaction.	Lateral shear V_y and local landing-support bending M_z.
LC5	Tether recovery with hover thrust opposed by the tether load at the centre of gravity.	Local tether proof load of 1.5 kN applied at the tether hardpoint and reel support.	Axial force N through the tether hardpoint and central fuselage.
LC6	Transition between hover and cruise at representative attitudes.	Transition attitudes of 60°, 45°, and 30°; thrust adjusted for force balance using the current PPA sizing point.	Combined axial force N, vertical shear V_z, and bending M_y.

For each load case, the applied external loads are converted into internal sectional resultants: axial force N, lateral shear V_y, vertical shear V_z, torsion M_x, and bending moments M_y and M_z. The preliminary sizing then uses the absolute envelope of these resultants. This avoids sizing the fuselage around only one nominal flight condition and makes the driving regions clear: axial loading is governed by hover and tether recovery, vertical bending by wing-borne flight, and lateral loading by asymmetric tail-sitter landing.

Normal Flight Load Path

During wing-borne cruise and climb, aerodynamic lift is generated by the main wing and canard. The distributed lift loads are carried by the skins, spar caps and webs of each lifting surface. These loads are then transferred into the wing and canard root fittings and finally into reinforced fuselage bulkheads and longerons. The main wing carries the largest aerodynamic load and is therefore treated as the primary lifting structure.

Capture and Tether Load Path

During capture and tow-down, the tether and reel loads are introduced into the fuselage through the capture hardpoint and reel support. These loads shall be transferred into a reinforced central bulkhead rather than into the fuselage skin alone. The tether load path is therefore designed to connect the reel support, local frames, longerons and surrounding bulkheads into one reinforced load-introduction region.

Landing and Ground Handling Load Path

During tail-sitter landing and ground handling, landing loads enter the aircraft through the aft booms and propulsor support structure. These loads are transferred into the main wing through the motor strut hardpoints, then into wing root and fuselage structure. The motor strut and landing boom are therefore treated as joint-dominated components, where local bearing, buckling and impact resistance

are as important as global material strength.

9.2.1. Material Selection Philosophy

A mixed-material strategy is used for the BELLONA structure because the selected tail-sitter concept combines mass-sensitive aerodynamic surfaces with concentrated load-introduction points from the propulsion, landing and capture systems. The material selection therefore follows the load path rather than assigning one material family to the complete airframe.

The material allocation for the main structural and recovery components is summarised in Table 9.4. This allocation is based on the material strategy from the Midterm Report, but updated to match the final structural architecture and the final wingbox sizing approach.

Table 9.4: Material Selection Summary for the Main Structural and Recovery Components

Component group	Selected material	Selection rationale
Wing spar caps and highly loaded longitudinal wingbox members	Unidirectional CFRP/epoxy [46]	Selected for high axial stiffness and strength in the dominant spanwise bending direction, making it suitable for carrying the main wing-root bending loads with low mass.
Fuselage skin	Sandwich composite structure consisting of GFRP [47], Nomex honeycomb core [48], and adhesive [49].	Electromagnetic-wave-transparent GFRP skin reinforced by the core structure. The skin is intended to retain the aerodynamic fuselage shape under pressure, rather than carry primary structural loads.
Wing skins, spar webs, fairing shell, local wingbox panels, and canard D-box	Quasi-isotropic CFRP/epoxy [50]	Selected for multi-directional load transfer, aerodynamic surface quality, and torsional continuity. The lower modulus compared with UD CFRP is included in the transformed-section wingbox sizing.
Fuselage longerons, hat stringers, frames, and moderate brackets	Aluminium 6061-T6	Selected for a repairable and inspectable frame-and-longeron fuselage. Aluminium is easier to bolt, drill, replace, and inspect than a fully bonded composite fuselage frame.
Motor mounts, motor struts, landing booms, and compact hardpoints	Aluminium 7075-T6	Used where high local strength, bearing resistance, and compact load introduction are required, especially around propulsion and tail-sitter landing loads.
Tether hardpoint inserts, pins, shafts, critical fasteners, and wear-sensitive fittings	AISI 4130 steel or stainless steel	Reserved for compact parts with high local bearing, wear, or proof-load demands. Steel is used only where aluminium would require excessive local thickness or would be vulnerable to bearing damage.
Battery tray, electronics tray, and avionics support plates	G10/FR4 or aluminium	G10/FR4 is used where electrical isolation is required. Aluminium is used where heat spreading, local stiffness, or direct mechanical load transfer is more important.
Net, tether, closure line, and emergency line	UHMWPE/Dyneema-type fibre	Selected for very high tensile strength-to-mass ratio in flexible recovery hardware. These parts are treated as high-wear items with explicit inspection and replacement criteria.
Local abrasion protection at tether exit, reel bay, and net-launcher opening	Aramid/epoxy or local protective plies	Used to improve abrasion, handling, and impact resistance in regions exposed to line contact, net launch loads, or repeated ground handling.
Landing pads, vibration isolation, and local contact protection	EPDM rubber	Used as a replaceable compliant layer to reduce local impact damage and simplify post-landing inspection.
Sensor housings, fairings, cable guides, and non-primary covers	PA-CF or ASA printed polymer	Used only for non-primary parts where low cost, fast replacement, and geometric flexibility are more important than structural strength.

Composite materials are used where stiffness-to-mass and aerodynamic surface quality dominate, while metallic materials are used at bolted joints, hardpoints, inserts and compact fittings. For the lifting surfaces, the CFRP material choice is split into two functional groups: Unidirectional (UD) CFRP for bending-dominated members, and Quasi-isotropic (QI) CFRP for skins. Aluminium alloys

(such as 6061-T6 and 7075-T6) are utilized for the fuselage frames, longerons, and strut supports due to their reliable bearing strengths and ease of manufacturing.
Where aluminium stiffeners are used inside composite wing or canard structures, they are treated as mechanically attached or bonded secondary stiffening elements rather than co-cured composite members. Local glass-fibre isolation plies, primer or adhesive layers shall be used between CFRP and aluminium parts to reduce galvanic-corrosion risk and avoid direct carbon-aluminium contact.
The reference properties used for the preliminary sizing of these primary CFRP and metallic materials are summarised in Table 9.5. These values are treated as preliminary sizing limits rather than certified material allowables, because the final composite properties depend heavily on layup and manufacturing, while metallic properties vary slightly by stock thickness.

Table 9.5: Reference Material Properties Used for Structural Sizing

Property	**UD CFRP** [46]	**QI CFRP** [50]	**Aluminium 6061-T6** [51]	**Aluminium 7075-T6** [51]
Compressive yield/strength [MPa]	950	570	276	503
Tensile yield-/strength [MPa]	1000	740	276	503
Tensile modulus E [GPa]	121.6	55	69	71.7
Shear modulus G [GPa]	24	4.2	26	26.9
Density [kg/m^3]	1790	1520	2700	2810

This strategy also supports the sustainability requirements by limiting CFRP to mass-sensitive primary structures, keeping highly loaded interfaces inspectable and replaceable, using recyclable metals for concentrated load paths, and treating the net, tether, pads and printed covers as controlled replacement items rather than hidden structural consumables.

9.2.2. Wing and Canard Cruise/Climb Load Distribution

The cruise and climb aerodynamic loads on the main wing and canard are modelled using preliminary half-span lift distributions. These distributions are used as structural sizing inputs for shear force and bending moment calculations. They are not intended to represent a complete trimmed aerodynamic solution at a specific angle of attack.
Using the current integrated mass estimate, the aircraft weight is approximately

$$W = mg = 51.13 \cdot 9.81 = 501.4 \text{ N}.$$

For consistency with the PPA trim solution, the baseline cruise/climb structural load split uses $L_w = 347.8$ N on the main wing and $L_c = 153.6$ N on the canard. The canard therefore carries a significant positive lift contribution because it is also the main longitudinal trim surface. In addition to this trim-consistent load split, the main wing is also checked with a conservative wing-only case in which the full aircraft weight is assigned to the main wing:

$$L_{w,\text{cons}} = W = 501.4 \text{ N}.$$

The trim-consistent split is used to describe the nominal cruise/climb load path, while the wing-only case is retained as an upper-bound check for main-wing bending.
The spanwise lift is estimated using Schrenk-type distributions. The classical Schrenk distribution is the average of a planform-based distribution and an elliptical distribution:

$$q_s(y) = \frac{1}{2}\left[q_p(y) + q_e(y)\right]. \tag{9.1}$$

To avoid a non-zero lift at the finite wing tip, a tip roll-off is applied:

$$q_{\text{raw}}(y) = q_s(y)\left[1 - \left(\frac{y}{b/2}\right)^{n_r}\right], \tag{9.2}$$

where n_r is the roll-off exponent. The final modified Schrenk distribution is then renormalised so that the integrated lift remains equal to the required surface lift:

$$q_{\mathrm{ms}}(y) = \frac{L}{2\int_0^{b/2} q_{\mathrm{raw}}(y)\,\mathrm{d}y} q_{\mathrm{raw}}(y). \tag{9.3}$$

This gives a smooth preliminary lift distribution with zero lift at the tip. It is used as a representative structural loading method rather than a high-fidelity aerodynamic prediction.

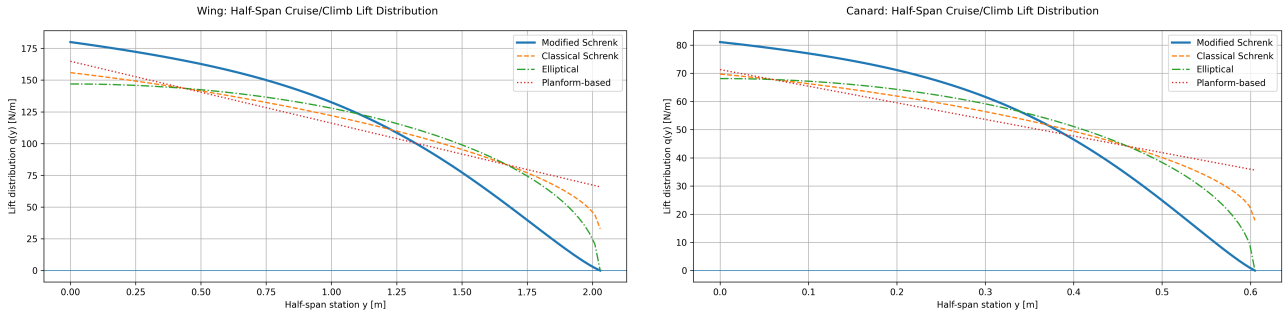

(a) Main Wing **(b)** Canard

Figure 9.1: Half-Span Cruise/Climb Lift Distributions for the Main Wing and Canard, Comparing Planform-Based, Elliptical, Classical Schrenk and Modified Schrenk Methods

Two vertical structural load diagrams are generated for the main wing. The first neglects structural weight relief and therefore gives a conservative estimate of the aerodynamic root bending moment. The second includes distributed structural weight and propulsor/mount weight, giving a more realistic cruise/climb load path. The distributed structural weight is scaled with the square of the local chord ratio:

$$q_{\mathrm{w}}(y) = q_{\mathrm{w,ref}} \left(\frac{c(y)}{\bar{c}} \right)^2 . \tag{9.4}$$

For the current design, the full-wing structural mass is 7.91 kg, corresponding to 3.955 kg per half-wing before chordwise redistribution. The distributed structural weight is scaled with the square of the local chord ratio. Each propulsion unit attached to the wing is represented by a point inertial load of 2.865 kg at the motor station, consistent with the selected propulsion-unit mass. Local mount and bracket masses are included in the structural mass margin and checked separately at the propulsion hardpoints.

The internal shear force and bending moment diagrams are obtained by integrating the distributed loads from tip to root and superimposing the point loads at their spanwise locations. Vertical loads produce a bending moment about the aircraft x-axis, M_x, while chordwise propulsor thrust produces a bending moment about the aircraft z-axis, M_z.

9.2.3. Main Wing Load Diagrams

The main wing is checked using two half-span load cases: a vertical aerodynamic bending case and a chordwise propulsion case. The vertical case is used to size the spar caps and wingbox for bending about the aircraft x-axis, while the chordwise case is used to size the propulsion load path and wingbox for bending about the aircraft z-axis.

It is important to note that the load distributions, plotted diagrams, and baseline numerical values presented in this section all represent a $1g$ steady level flight condition ($n = 1$). For the final sizing and evaluation of structural margins, these forces and moments are scaled by the required ultimate load factors, which cover a design envelope ranging from $n = -2$ to $n = 4$.

The vertical load case with relief includes the modified Schrenk lift distribution, distributed wing structural weight and propulsion-unit inertial loads. This case is used to show the realistic cruise/climb load path. The conservative no-relief case neglects structural weight relief and is retained for upper-bound wingbox bending. The numerical root shear and root bending values are taken from the regenerated load diagrams in Figure 9.2; these diagrams shall be updated whenever the aircraft mass, wing geometry, propulsion-unit mass or lift split changes.

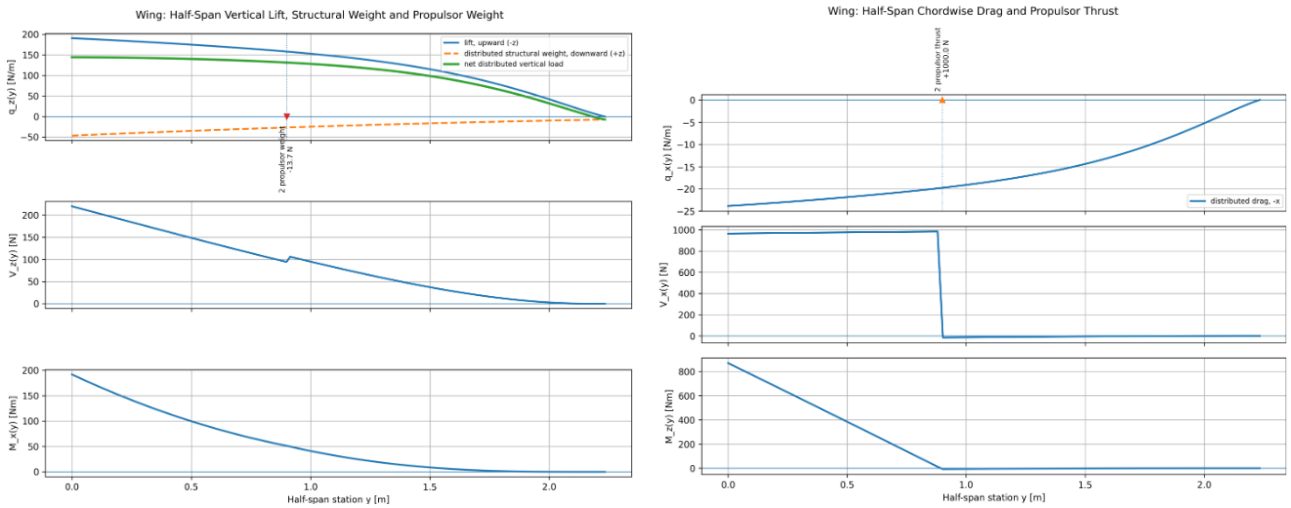

(a) Lift-Only Case, No Weight Relief **(b)** Lift with Structural and Propulsor Weight Relief

Figure 9.2: Main-Wing Half-Span x-Axis Load, Shear Force and Bending Moment Diagrams (Plotted for $n = 1$)

The chordwise case represents cruise with maximum propulsor thrust. Each half-wing carries two propulsors located at $y_p = 0.9$ m from the wing root. With 500 N of maximum thrust per propulsor, the total chordwise point load on one half-wing is $F_{x,\text{half}} = 2 \cdot 500 = 1000$ N and the maximum root bending moment about the aircraft z-axis is $M_{z,\text{root}} = F_{x,\text{half}} y_p = 1000 \cdot 0.9 = 900$ Nm.
Although the plotted cruise case in Figure 9.2 also includes aerodynamic drag, the drag is small compared with the maximum thrust and acts in the opposite direction, therefore providing chordwise load relief. For sizing, only the maximum thrust is therefore retained. A pure maximum-hover thrust case gives a similar spanwise propulsion load for the wing structure and is not plotted separately, since neglecting drag in the cruise maximum-thrust case already gives the conservative value used for sizing.

9.2.4. Main Wingbox Sizing Method

The preliminary main wing structure is modelled as a CFRP wingbox with two spar webs, skin panels, spar caps and discrete stiffeners. The front and rear spars are placed at approximately $0.3c$ and $0.7c$, respectively. The fairing portion of the airfoil is not credited as a primary load-carrying member, it is assumed to carry only local aerodynamic pressure and shape-retention loads. This is conservative for the bending and torsion checks because the fairing area is excluded from the load-bearing section properties.
The wingbox is evaluated at $n = 100$ spanwise stations across one half of the wing using the local chord and airfoil geometry. The cross-section model used in the sizing process is presented in Figure 9.3.

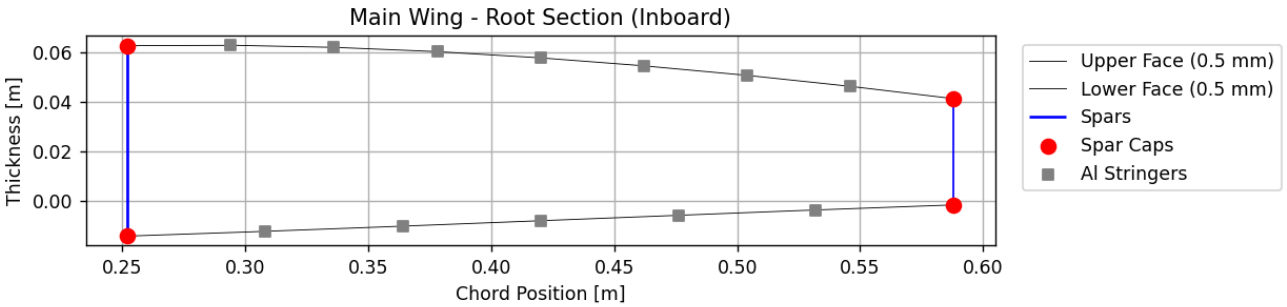

Figure 9.3: Cross-Section Model Used in the Sizing Process

Cross-section geometry

To determine the centroid positions along the span, all structural elements are treated as discrete point areas located at their respective geometric centers. The primary challenge lies in the discretization of the airfoil skin. The skin is divided into $m = 100$ equally spaced elements along the chord. A local coordinate system is established at the leading edge intersection with the chord line, where the x-axis points toward the trailing edge along the chord line, and the y-axis points upward.
Assuming the skin has a uniform thickness t, the cross-sectional area A_i of each discretized skin

element i bounded between x_a and x_b is calculated by multiplying its arc length by its thickness:

$$A_i = t \int_{x_a}^{x_b} \sqrt{1 + \left(\frac{dy}{dx}\right)^2}\, dx \tag{9.5}$$

To account for the variation in material stiffness between components, where the skin face sheets have an elastic modulus of $E_{\text{skin}} = 55$ GPa and the spar elements have $E_{\text{spar}} = 120$ GPa, a transformed section approach is implemented. A baseline reference modulus is defined as $E_0 = 120$ GPa, and a modular ratio $k_i = E_i/E_0$ is evaluated for each element. The first transformed area moments are defined inline as $Q_y = \sum_{i=1}^{m} k_i x_i A_i$ for the first moment about the y-axis and $Q_x = \sum_{i=1}^{m} k_i y_i A_i$ for the first moment about the x-axis. With the transformed centroid position available for each element, the transformed area moments of inertia (I^*_{xx}, I^*_{yy}, and I^*_{xy}) can be calculated applying the same k_i factor to all discrete elements.

Internal Stresses

To calculate the internal axial stresses, multiple loading cases are taken into account. First, asymmetric bending is evaluated due to moments created along the local x-axis (primarily from aerodynamic lift and structural weight) and the y-axis (primarily from drag and propulsion forces). Additionally, the wing must withstand landing and hover load conditions, during which bending occurs predominantly around the y-axis. These applied moments can be extracted using loading diagrams and geometric parameters.

Using the calculated transformed section properties, the normal stress $\sigma_{z,i}$ acting on a given element i located at (x_i, y_i) is directly scaled by its modular ratio k_i. The asymmetric bending stress equation is structured as follows:

$$\sigma_{z,i} = \frac{k_i}{I^*_{xx} I^*_{yy} - (I^*_{xy})^2} \left[\left(M_y I^*_{xx} - M_x I^*_{xy}\right)(x_i - \bar{x}) + \quad \left(M_x I^*_{yy} - M_y I^*_{xy}\right)(y_i - \bar{y}) \right] \tag{9.6}$$

where M_x and M_y are the internal bending moments acting about the local x and y axes, respectively. Besides that, an important contribution to the internal forces arises from Load Case 3 (LC3), where an engine failure on one wing results in asymmetric thrust, creating additional torsion along the span. This effect is estimated by considering the maximum hover thrust T generated by a single propeller acting at a spanwise lever arm y, generating a twisting moment $M_z = T \cdot y$.

To calculate the resulting shear stresses quickly and conservatively, the wingbox is approximated as a single thin-walled closed cell. Under this assumption, the torsional shear stress τ_i in a given structural component is calculated directly using Bredt's simplified formula:

$$\tau_i = \frac{M_z}{2 A t_i} \tag{9.7}$$

$$\tau_{\text{flex},i} = \frac{V_z Q_i}{I^*_{xx} t_i} \tag{9.8}$$

where A is the total enclosed area of the wingbox cross-section, and t_i is the actual load-bearing thickness of the element being evaluated.

Last shear stress considered in the analysis is the shear flow due to internal shear force. This is modeled using the classical flexural shear formula for an elastically transformed section. For a given structural element i with a load-bearing thickness t_i, the flexural shear stress $\tau_{\text{flex},i}$ induced by the vertical shear force V_z is expressed in the second relation above.

These flexural shear stresses are superimposed with the torsional shear stresses to establish the critical shear margins across the skin and spar webs.

Design Process

The evolution of the wingbox design involved a transition from an initial sandwich panel configuration, optimized during the midterm stage, to a fully converged, monolithic stiffened architecture in the final design phase.

The initial structural optimization loop was based on geometric and loading parameters from the midterm report, which utilized a larger wing area. This iteration evaluated a sandwich panel skin design featuring Rohacell foam cores bounded by thin isotropic CFRP facesheets. To prevent local buckling, the algorithm swept through multiple stringer quantities, with the objective of optimizing the overall wingbox mass.

The initial optimizer converged on a minimum structural mass of 11.40 kg utilizing a 4-stringer layout. This arrangement heavily relied on an 8.0 mm Rohacell foam core paired with ultra-thin, multi-layered facesheets (0.20 mm each, totaling 0.40 mm per skin layout) to meet stability requirements. The complete baseline parameters from this midterm loop are contrasted against the final design in Table 9.6.
Following a post-midterm design review, the structural concept was modified to eliminate the foam core entirely, transitioning to a pure monolithic stiffened panel architecture. The final converged geometric parameters derived from this updated sizing loop are detailed in Table 9.6.

Table 9.6: Comparison of Initial (Sandwich) and Final (Monolithic Stiffened) Sizing Specifications

Design Parameter	Initial Value	Final Value
Upper Skin Thickness (Inboard)	0.20 mm × 2	0.50 mm
Upper Skin Thickness (Outboard)	0.20 mm × 2	0.50 mm
Lower Skin Thickness (Inboard)	0.20 mm × 2	0.50 mm
Lower Skin Thickness (Outboard)	0.20 mm × 2	0.50 mm
Aerodynamic Fairing Thickness	0.2 mm	0.50 mm
Front Spar Web Thickness	1.56 mm	1.54 mm
Rear Spar Web Thickness	1.00 mm	1.00 mm
Individual Spar Cap Area	50.00 mm^2	50.00 mm^2
Number of Upper Stiffeners (Inboard)	4	7
Number of Lower Stiffeners (Inboard)	4	5
Number of Stiffeners (Outboard)	1 Upper, 1 Lower	1 Upper, 1 Lower
Individual Stiffener Area	10.00 mm^2	21.30 mm^2
Sandwich Core Thickness	8.00 mm	0.00 mm
Calculated Structural Mass	**11.40 kg**	**7.91 kg**

The separation of design variables into inboard and outboard regions is established to capture the severe spanwise loading gradients inherent to cantilever wings. Because the bending moment (M_x) and shear force (V_z) accumulate maximum values at the wing root, the inboard section demands significantly greater structural robustness. Additionally, the boundary between these two regions is dynamically driven by the wing-mounted engine station. The inboard structure must support both the regional aerodynamic pressures and the severe concentrated thrust and inertial loads of the propulsion system under high-G and engine-out maneuvers. Conversely, the outboard region is isolated from these engine loads, permitting a much lower structural mass distribution characterized by a drop down to a single central stiffener on both the top and bottom surfaces.
The transition to a monolithic panel layout introduced a severe penalty regarding localized stability. Without the continuous out-of-plane support provided by the foam core, the unbraced skin panels became highly sensitive to compressive buckling between the stringers. To evaluate this constraint, the optimizer calculates the critical compressive skin buckling stress using the classical plate buckling formula:

$$\sigma_{cr,\text{skin}} = k_c \frac{\pi^2 E}{12(1-\nu^2)} \left(\frac{t}{b}\right)^2$$

where k_c is the compressive buckling coefficient (dependent on panel aspect ratio and boundary conditions), E is the material elastic modulus, $\nu = 0.33$ is Poisson's ratio, t is the skin thickness, and b is the unsupported width between stiffeners. The conservative approach of setting $k = 5$ was assumed. Simultaneously, the stringers acting to break up the skin panels are subjected to column buckling checks between the structural ribs. The critical Euler buckling stress for these stiffeners is given by:

$$\sigma_{cr,\text{col}} = \frac{\pi^2 E}{(L_e/\rho)^2}$$

where L_e is the effective column length (rib spacing multiplied by an end-fixity factor) and ρ is the stiffener's radius of gyration.
To compensate for the loss of core stiffness and prevent $\sigma_{cr,\text{skin}}$ from falling below the operational compressive stresses, without drastically increasing skin thickness beyond manufacturing limitations,

the final optimizer decreased the unsupported panel width b. It achieved this by significantly increasing the inboard upper stiffener count to 7 and the lower count to 5, while doubling the individual cross-sectional area of the aluminum stringers to 21.30 mm^2 to increase their resistance to global column buckling. Only central stiffeners are left in the outboard section after the propeller mounting point as stresses in that section are relatively low and they do not cause buckling. Furthermore, the absolute minimum gauge constraint for the monolithic aerodynamic fairing CFRP skin was capped at 0.50 mm globally to maintain adequate localized safety margins.
To evaluate the behavior of the monolithic wingbox under critical design loads, the spanwise stress distributions were mapped into three-dimensional space. Figure 9.4 shows the critical load case in each scenario, which consisted of combined LC1 and LC3.

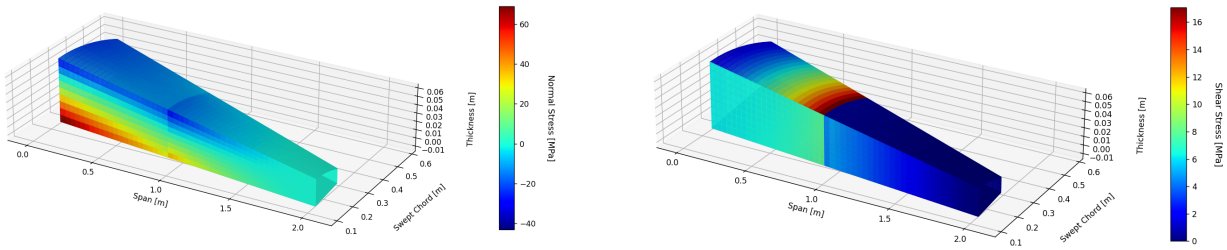

(a) Longitudinal Normal Stress (σ_z) **(b)** Superimposed Shear Stress (τ)

Figure 9.4: Internal Stress Distributions Acting on the Monolithic Wingbox Under Combined Load Cases

In the normal stress plot in Figure 9.4a, a classical cantilever bending behavior is clearly visible. The upper skin is subjected to uniform compression (indicated by the deep blue region peaking at approximately −40 MPa), while the lower skin experiences pure tension (peaking near +60 MPa). The highest stress concentrations are localized at the root and track directly along the front and rear spar webs, proving that the elastically-weighted unidirectional spar caps effectively absorb the bulk of the global bending moment before it tapers off toward the wingtip.
Conversely, the shear stress plot in Figure 9.4b exhibits a highly localized behavior driven by the Load Case 3 asymmetric engine-out condition. A prominent, high-stress band peaking at roughly 17 MPa forms on the skin panels immediately inboard of the engine station ($y = \pm 0.90$ m) . This behaviour highlights the continuous path of the torsional shear flow, which transfers the asymmetric propulsor proof load from the motor station back toward the wing root and fuselage attachment. Immediately outboard of the engine station, the shear stress drops abruptly toward zero, confirming that the outer wing section is structurally isolated from the major torsional loads of the propulsion system.

9.2.5. Canard Structural Sizing

The canard is treated as a secondary lifting surface and is sized with a simplified load model. Unlike the main wing, it does not carry propulsors or landing supports. Therefore, only the vertical aerodynamic load case and the chordwise drag case are considered.
The canard structural load case uses the trimmed canard lift of 153.6 N. This load is applied to the current canard geometry, with $S_c = 0.357$ m^2 and $b_c = 1.34$ m. The vertical load case is used for the canard root shear and bending moment, while the chordwise drag case is retained as a secondary root-fitting check.

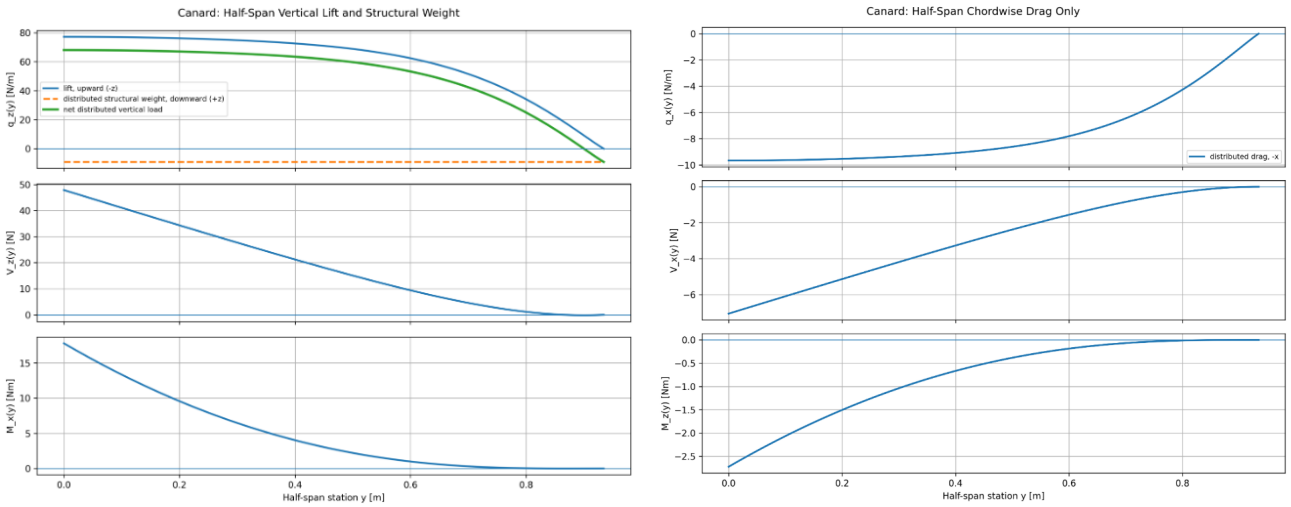

(a) Vertical Load Case **(b)** Chordwise Drag Case

Figure 9.5: Canard Half-Span Load, Shear Force and Bending Moment Diagrams

A CFRP D-shape box is selected for the canard. The concept consists of a main spar at approximately $0.25c$, connected to a closed leading-edge skin. This gives a light, torsion-resistant section without requiring a full two-spar wingbox. Since the canard loads are small compared with the main wing loads, the sizing is driven mainly by root attachment stiffness and skin buckling. The aluminum stiffeners inside act to break up the unbraced panel width, thereby preventing localized skin buckling of the canard's leading-edge composite. The remainder of the aerodynamic profile is maintained using non-structural Oracover film [52] to minimize weight aft of the spar. The D-Box layout can be analyzed in Figure 9.6.

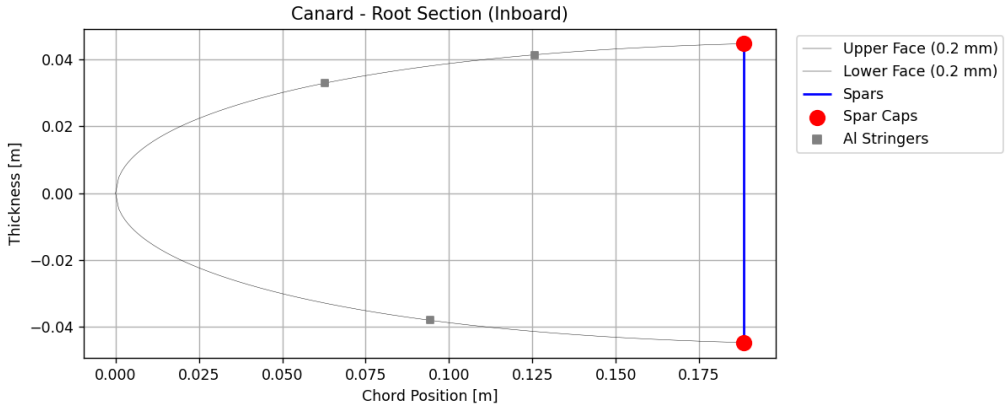

Figure 9.6: Canard Structural Layout

At the root, the D-spar and root rib are connected to a reinforced fitting on the forward fuselage frame, which includes the actuator to allow variable pitch control. The optimization software finalized the sizing based on the maximum aerodynamic flight load. As with the main wing, the stiffener count tapers across the span; the root section requires 2 upper and 1 lower stiffener to resist buckling near the attachment point, whereas the outboard half of the section tapers down to just 1 central stiffener on both the top and bottom surfaces. The dimensions used in the final design are detailed in Figure 9.6. Figure 9.7 presents the normal stress map in the canard at the critical loads.

Table 9.7: Canard Sizing Parameters

Description	Value	Unit
Spar Web Thickness	1.6	mm
Spar Caps Cross-Sectional Area	80	mm^2
Upper Skin Stiffener Count (Inboard)	2	–
Lower Skin Stiffener Count (Inboard)	1	–
Upper & Lower Stiffener Count (Outboard)	1	–
Individual Stiffener Cross-Sectional Area	15	mm^2
Aerodynamic Skin Thickness	0.25	mm

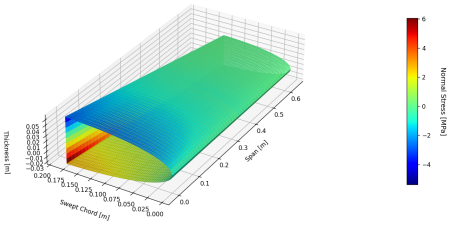

Figure 9.7: Normal Stress Map of the Canard

9.2.6. Ribs Sizing

The structural ribs serve two primary functions: they preserve the aerodynamic cross-section of the wing under pressure, and they break up the unsupported length of the longitudinal stringers to prevent Euler column buckling. To optimize the mass of the internal structure, the rib spacing is dynamically adapted based on the spanwise loading zones. In the highly loaded inboard section (from the root to the engine station at $y = 0.9$ m and $y = -0.9$ m), the spacing is constrained to a dense pitch of 0.20 m. This tight spacing minimizes the effective column length of the aluminum stringers, thereby maximizing their critical buckling stress in the region where global bending compression is most severe. Outboard of the engine station, where the compressive and shear stresses diminish significantly, the rib pitch is relaxed to 0.35 m to shed unnecessary structural weight.
The structural thickness of each individual rib is sized analytically to resist the local vertical shear flow. The optimizer calculates the minimum required thickness using the classical shear flow relation:

$$t_{req} = \frac{V_z Q}{I_{xx} \tau_{allow}}$$

The final internal arrangements of the primary aerodynamic surfaces, highlighting the positions of the structural spars and ribs, are shown below. Figure 9.8 displays the main wing framework, while Figure 9.9 outlines the smaller canard configuration.

Figure 9.8: Internal Structural Layout of the Main Wing with Spars and Ribs

Figure 9.9: Internal Structural Layout of the Canard Assembly

9.2.7. Motor Strut and Landing Boom Design

The propeller units are supported by external motor struts mounted to the main wing. In the updated preliminary model, each pylon consists of one main hollow circular support tube between the wing hardpoint and the motor node, and one aft landing boom extending rearwards from the motor node. The diagonal backstay from the earlier concept is not included in this sizing model. Therefore, the main support tube is treated as a bending-dominated cantilever rather than as part of a truss.
The struts were sized using hollow circular 7075-T6 aluminium tubes. Aluminium was selected for this preliminary design because the struts are joint-dominated and landing-loaded members, where isotropic behaviour, simple bolted or clamped joints, local bearing tolerance and inspectability are important.
The main support tube has a cantilever length of 0.70 m, equal to the required propeller clearance from the wing attachment plane. A maximum thrust of 500 N per propeller and a side load of 20% of thrust are applied at the motor node. These loads give a resultant root bending moment of

$$M_{\text{main}} = h\sqrt{T^2 + F_{\text{side}}^2} = 305.9 \text{ Nm}. \tag{9.9}$$

The 2 kg motor and propeller assembly is also checked with a $6g$ inertial load, giving 117.7 N axial load. The motor torque is taken as 25 Nm.
The aft landing boom has a length of 0.70 m. The landing case assumes a 75 kg aircraft, a $3g$ landing factor, and four landing contact points, giving a landing reaction per pylon of

$$R_{\text{land}} = \frac{n_{\text{land}} m g}{N_{\text{contacts}}} = 551.8 \text{ N}. \tag{9.10}$$

Since the boom is approximately aligned with the tail-sitter landing load path, this reaction is applied as axial compression in the aft boom. Additional bending is included from a 10° off-axis landing component and ground drag equal to 25% of the landing reaction. This gives a resultant transverse bending force of 168.0 N, corresponding to an aft-boom root bending moment of 117.6 Nm.

Table 9.8: Preliminary Motor Strut Tube Sizing Results Per Propeller Pylon

Member	Quantity	Outer diameter [mm]	Wall [mm]	Length [mm]	Mass [kg]
Main support tube	1	40.0	1	600.0	0.166
Aft landing boom	1	28.0	1	700.0	0.134
Total per pylon	**–**	**–**	**–**	**–**	**0.301**

Table 9.9: Calculated Member Loads and Stress Results for the Selected Tubes

Member	Axial [N]	Bending [Nm]	Torsion [Nm]	VM stress [MPa]	Stress margin	Buckling margin
Main support tube	117.7	305.9	25.0	325.2	0.03	51.69
Aft landing boom	551.8	117.6	0.0	268.2	0.24	1.76

The resulting structural mass is approximately 0.301 kg per propeller pylon, excluding brackets, clamps, bolts, local reinforcement and landing pad hardware. The selected tubes pass the preliminary von Mises stress, torsion and Euler buckling checks. However, the stress margin of the main support tube is small, so the selected dimensions should be treated as minimum preliminary sizes.

9.2.8. Fuselage Primary Structure Sizing

The fuselage's main function is to house the battery, avionics, tether reel and interaction mechanism, but also to transfer loads between the wing, canard, landing supports, propulsion system and capture hardpoint. The fuselage is therefore treated as a primary structural member. The sizing method used in this phase is a preliminary one-dimensional beam model, intended to define a conservative first structural layout before detailed CAD and finite-element verification.

Fuselage Loads

The fuselage coordinate system is defined with x along the fuselage from tail to nose, y laterally, and z vertically. The updated fuselage length is $L_f = 3.05$ m. The preliminary beam model uses the wing and landing-load station at $x = 0.60$ m, the centre of gravity and tether hardpoint at $x = 1.60$ m, the canard station at $x = 2.70$ m, and the nose at $x = 3.05$ m. The outer fuselage envelope is kept as a rounded rectangular section with width 0.42 m, height 0.32 m, and corner radius 0.08 m. Difference in height and width are the result of the minimum required space for the battery capsule and such configuration minimizes the wetted area. This makes the weight of the fuselage smaller.

A conservative no-skin structural assumption is used for the first fuselage sizing. The aerodynamic skin is therefore not assumed to carry axial, bending or shear loads. Instead, the fuselage is idealised as a frame-and-longeron structure with two side longerons and hat stringers on the upper and lower flat panels.

The fuselage was analysed using cruise/climb, hover, asymmetric hover, landing, tether recovery and transition load cases. For each case, the external loads were converted into internal axial force, shear force and bending moment diagrams. The absolute internal-load envelopes shown in Figure 9.10 were then used to size the number of stringers, the stringer dimensions and the side-longeron dimensions.

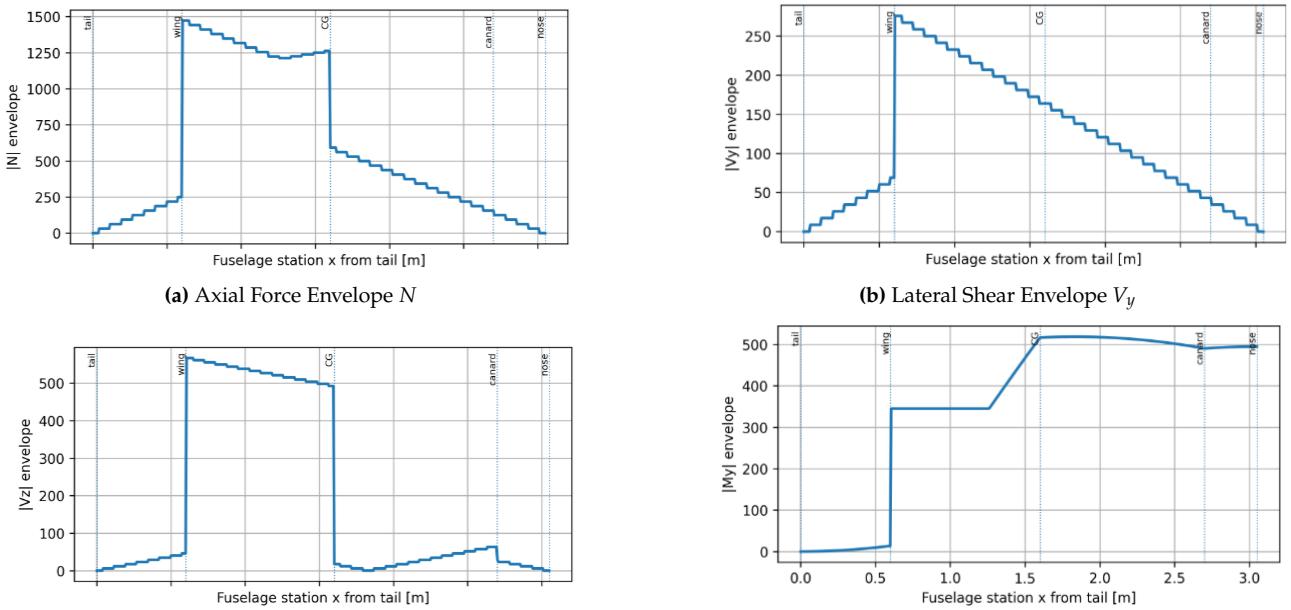

(a) Axial Force Envelope N

(b) Lateral Shear Envelope V_y

(c) Vertical Shear Envelope V_z

(d) Bending Moment Envelope M_y

Figure 9.10: Main Fuselage Internal-Load Envelopes Used for Preliminary Member Sizing. The Axial Force and Vertical Bending Define the Longitudinal-Member Stress Level, While the Shear Envelopes Are Used to Check the Stringer Webs, Longerons and Local Frame Load Paths

The asymmetric tail-sitter landing case is shown separately in Figure 9.11 because it gives the largest lateral shear. In this case, the aircraft is assumed to land tail-first, so the main landing reaction acts approximately along the body $+x$-axis. A lateral side load equal to 20% of the landing reaction is included to represent cross-drift or an imperfect touchdown. The landing reaction is applied at the actual landing-support offset from the fuselage, not at the propulsor spanwise station. Therefore, this case is mainly a local landing-support and wing-root interface driver.

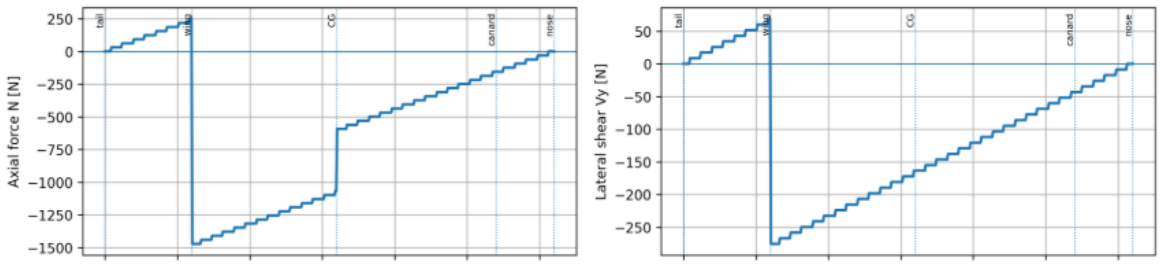

Figure 9.11: LC4b Asymmetric Tail-Sitter Landing Internal Axial and Lateral Shear Loads. The Jumps Correspond to Concentrated Loads at the Landing/Wing and Centre-of-Gravity Stations, While the Sloped Regions Are Caused by the Distributed Inertial Balancing Loads Used to Close the Beam Free-Body Diagram

The approximate envelope values used in the preliminary sizing are summarised in Table 9.10. Torsion M_x and the corrected M_z landing moment were checked separately, but they are not the main drivers of the current global no-skin fuselage member sizing.

Table 9.10: Approximate Fuselage Load Envelope Used for Preliminary Sizing

Resultant	Approximate maximum	Main sizing use
$\lvert N\rvert_{\max}$	1.45 kN	Longeron and stringer axial stress
$\lvert V_y\rvert_{\max}$	0.28 kN	Lateral shear and asymmetric landing check
$\lvert V_z\rvert_{\max}$	0.56 kN	Vertical shear through longerons and frames
$\lvert M_y\rvert_{\max}$	0.52 kNm	Upper/lower stringer bending stress
$\lvert M_x\rvert_{\max}$	Negligible	Not driving in the current beam model
$\lvert M_z\rvert_{\max}$	Local check	Landing-support and wing-root reinforcement

Longeron and Stringer Sizing

Several conventional stiffener cross-sections were considered for the fuselage longitudinal structure, as shown in Figure 9.12. Closed rectangular box sections were preferred for the side longerons because

they provide good bending stiffness and local robustness for load introduction. Hat stringers were selected for the upper and lower flat panels because they offer higher local buckling resistance than simple flat strips and can be attached efficiently to frames or skin panels.

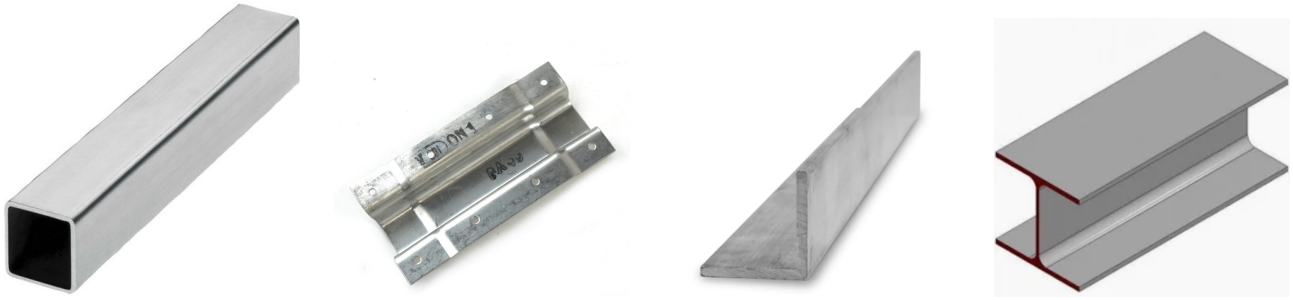

(a) Rectangular Box **(b)** Hat Stringer **(c)** L-Section **(d)** I-Section

Figure 9.12: Common Stiffener and Longeron Cross-Section Concepts Considered for the Preliminary Fuselage Structure. Closed Box Sections Provide High Bending and Torsional Stiffness, While Open Sections Such as Hat, L, and I Stiffeners Offer Simpler Manufacturing and Attachment Options

The selected preliminary section contains two hollow-box side longerons and four hat stringers, with two stringers on the upper flat panel and two on the lower flat panel. The side longerons provide the main continuous axial load path and support the vertical shear, while the upper and lower hat stringers increase bending stiffness about the y-axis. The layout is shown in Figure 9.13.

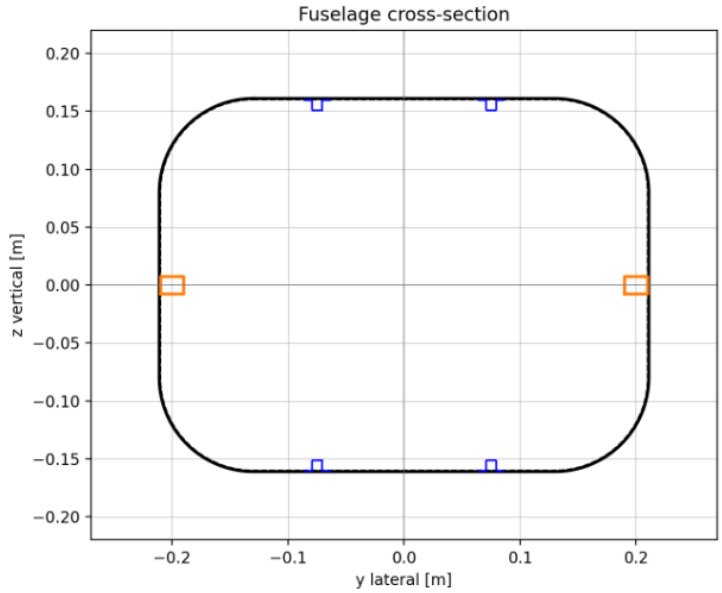

Figure 9.13: Selected Preliminary No-Skin Fuselage Cross-Section With Two Side Longerons and Upper/Lower Hat Stringers

The normal stress in each longitudinal member is evaluated by superimposing the internal axial forces and bending moments. The vertical shear is assumed to be carried strictly by the two side longerons, while lateral shear is assumed to be carried by the webs of the upper and lower hat stringers. This gives a conservative load allocation because the external skin is not used as a shear-carrying closed shell. The combined stresses are then evaluated against a standard Von Mises equivalent stress yield check. In addition to material yielding, the structure is checked against local plate buckling (for the hat-stringer webs) and global Euler column buckling (for the side longerons between frames), utilizing the same stability relationships defined previously in Subsection 9.2.2.
The lightest feasible preliminary section found by the sizing search is summarised in Table 9.11.

Table 9.11: Selected Preliminary Fuselage Longitudinal-Member Section

Parameter	Value	Unit
Side longerons	$15 \times 20 \times 1.0$	mm
Upper hat stringers	2	–
Lower hat stringers	2	–
Hat height	8.0	mm
Hat crown width	8.0	mm
Hat flange width	6.0	mm
Hat thickness	0.8	mm
Total longitudinal-member area	247.2	mm^2
I_y	2.82×10^6	mm^4
I_z	5.94×10^6	mm^4
Estimated longitudinal-member mass	1.74	kg

The governing stress result is a Von Mises stress of 76.9 MPa, compared with an allowable stress of 166.7 MPa (after applying a safety factor of 1.5 to the preliminary aluminium-equivalent yield stress). The side-longeron column buckling margin is lower than the material-yield margins and therefore drives the transverse frame pitch. The selected section is acceptable for preliminary sizing, provided that the frame spacing is not increased without rechecking column buckling.

Transverse Frames and Bulkheads

The transverse structure is required to maintain the rounded-rectangular fuselage shape, support the longitudinal members against column buckling, and introduce concentrated loads from the wing, canard, landing supports, battery rails and tether reel into the fuselage. For this reason, the transverse structure is divided into two types:

- light intermediate frames, which mainly preserve the section shape and reduce the unsupported length of the stringers and longerons;
- reinforced bulkheads, which are placed at primary load introduction stations such as the wing root, canard root, battery bay and tether reel.

Based on the column buckling constraint of the selected longeron section, the theoretical maximum allowable frame spacing (Euler limit) is 445.5 mm. However, the preliminary design does not utilize this full value. The spacing is capped at 300 mm to reduce the risk of cross-section distortion, properly support the no-skin longitudinal members, and provide regular attachment points for equipment and local reinforcements. For the finalized 3.05 m fuselage length, the actual stationing is driven primarily by the locations of the wing, battery bay, tether reel, and canard attachment. The station layout in Table 9.12 keeps the largest regular unbraced bay at 300 mm, ensuring the column-buckling assumption used in the fuselage sizing remains valid.

Table 9.12: Updated Preliminary Frame and Bulkhead Stationing

Station x [m]	Function
0.00	Tail/end bulkhead
0.30	Light intermediate frame
0.60	Reinforced wing, motor-strut and landing-load bulkhead
0.90	Light intermediate frame
1.20	Light intermediate frame / equipment support
1.40	Battery bay front support frame
1.60	Reinforced CG, tether reel and capture-load bulkhead
1.80	Battery bay rear support frame
2.10	Light intermediate frame
2.40	Light intermediate frame
2.70	Reinforced canard attachment bulkhead
2.90	Light nose support frame
3.05	Nose/end bulkhead

The frame ring is estimated using a stiffness-support criterion in which the frame bending stiffness is taken as three times the strong-axis stiffness of the hat stringer. Approximating the frame ring locally

as a flat strip:

$$I_{\text{frame}} = \frac{t_{\text{frame}} d_{\text{frame}}^3}{12}$$

where t_{frame} is the frame material thickness and d_{frame} is the radial depth of the frame. With a minimum frame thickness of 5 mm, the resulting preliminary frame radial depth is approximately 20 mm. The light frames are therefore defined as rounded-rectangular ring formers with 5 mm wall thickness and 20 mm radial depth.
The bulkheads are checked as shear webs using the maximum shear loads from the fuselage envelope. The theoretical shear thickness required is well below 1.0 mm, which is impractical for manufacturing, impact resistance, and bolted interfaces. Therefore, the recommended bulkhead thickness is governed by the minimum gauge of 5 mm, not by pure shear strength. Reinforced bulkheads at the tether reel, wing root and canard root shall include local metallic inserts or load-spreading plates to prevent local bearing failure.
The internal arrangement of the fuselage is illustrated in Figure 9.14. This shows the stiffening structure with the stringers position adjusted in one section to allow for the battery removal. The frames spacing on this visualization is only informational and not updated to the final value.

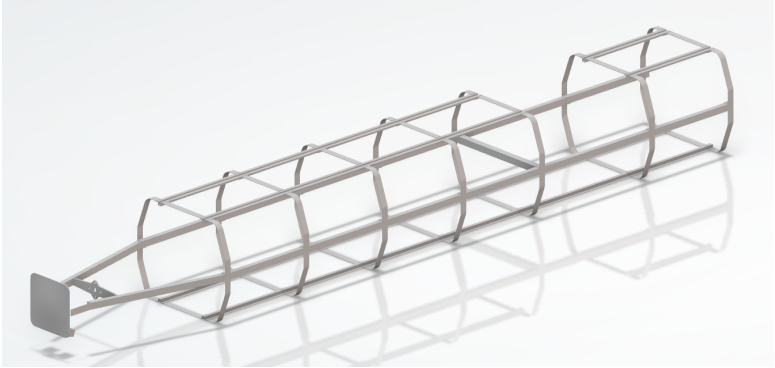

Figure 9.14: Internal Structural Layout of the Fuselage Showing Load-Bearing Bulkheads

Fuselage Skin

The load-carrying function of the fuselage skin was omitted in the initial load path. This does not mean there are no loads acting on the skin. The aerodynamic pressure will possibly deform or buckle weak structure, which makes the structural optimization more difficult. To make the structure resistant and as light as possible, the bio-inspired honeycomb sandwich structure as in Figure 9.15 was chosen. GFRP was chosen as the load carrying element, Nomex core is used to shape the structure. Components are bonded by the adhesive in between core and skin layers.

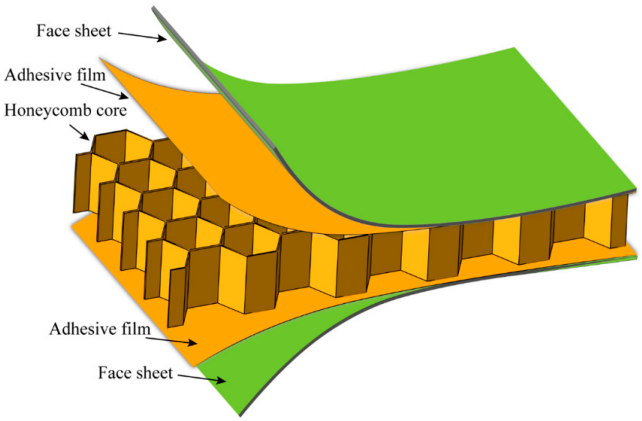

Figure 9.15: Composite Sandwich Panel [53]

To make the fuselage skin with its largest area as light as possible, the high-end lightweight products were analyzed. It is shown that 300 $\frac{\text{g}}{\text{m}^2}$ GFRP can be successfully used in sandwich composites [47]. Then, the typical manufactured Nomex plates for non-critical components are characterized by thickness of 3 mm making this layer 86 $\frac{\text{g}}{\text{m}^2}$. The lightest possible adhesive layers are rated using Pound per Square Foot (PSF) metric. Aerospace graded adhesives usually have the minimum of 0.03 PSF

resulting in the $135\frac{g}{m^2}$ [49]. The resulting weight of the sandwich is then $956\frac{g}{m^2}$ which is on the edge of existing panel densities.

9.3. Verification and Validation

Table 9.13: Structures and Materials Verification and Validation Plan

Req. ID	Verification and Validation Steps	Met
REQ-STK-19-MSN-24-SYS-41-STR-01	Mass estimation using CAD model and sizing software confirmed the initial mass margin.	✓
REQ-STK-13-MSN-16-SYS-30-STR-02	Structural verification software was developed. Margins and failure modes presented in Subsection 9.3.2	✓
REQ-STK-03-MSN-04-SYS-07-STR-03	Sizing and verification software simulated the maximum wing loading based on the maneuver envelope	✓
REQ-STK-05-MSN-06-SYS-11-STR-04	Each motor pylon shall withstand a maximum propeller thrust load of at least 500 N per propeller including a SF of 2.	✓
REQ-STK-05-MSN-06-SYS-11-STR-05	Wing sizing based on the propulsion force equal up to 2.06 kN	✓
REQ-STK-13-MSN-16-SYS-30-STR-06	Perform FEA simulations of combined thrust, torque, inertia, and landing loads through multi-axis structural testing of the motor struts and booms.	×
REQ-STK-05-MSN-06-SYS-13-STR-07	Struts and landing booms are analyzed for point loads corresponding to 3 g landing	✓
REQ-STK-05-MSN-06-SYS-11-STR-08	Conduct a proof load pull-test of at least 1.5 kN on the fully integrated tether hardpoint and reel support assembly.	×
REQ-STK-05-MSN-06-SYS-11-STR-09	Inspect final CAD models and manufactured airframe components to verify that all concentrated load paths feature reinforced structural members.	✓
REQ-STK-19-MSN-24-SYS-41-STR-10	CAD model and sizing software both estimated the primary structure to fall under the weight limit	✓
REQ-STK-06-MSN-08-SYS-17-STR-11	Perform kinematic clearance checks in CAD, followed by physical measurement on the integrated prototype, to ensure 50 mm clearance is maintained.	✓
REQ-STK-13-MSN-17-SYS-31-STR-12	FEM vibrational analysis showed that the operational limit of propulsion system is outside the first harmonic frequencies and their margins	✓
REQ-STK-17-MSN-22-SYS-38-STR-13	Perform a simulated maintenance teardown to confirm primary joints remain inspectable and demonstrate joint replacement without destructive debonding.	×

To ensure the complete airframe complies with all subsystem requirements, a comprehensive structural verification process is required. This process begins by reconciling the overall mass and cost against the initially allocated budgets. Subsequently, detailed analyses of critical load paths and potential failure modes are conducted on the integrated assembly. Finally, a vibrational analysis is performed to mitigate any risks of propeller-induced resonance. The fully integrated structural assembly is presented in Figure 9.16.

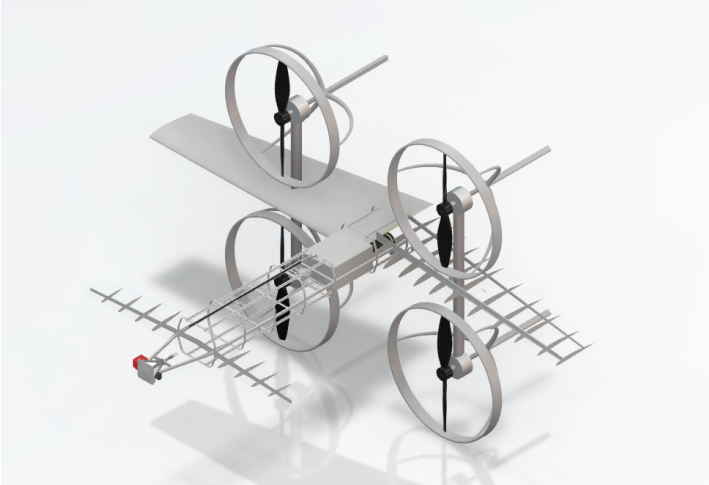

Figure 9.16: Complete Internal Structural Layout of the Fully Integrated Airframe

9.3.1. Structural Mass and Cost Budget

The highly complex and expensive nature of composite materials make it crucial to accurately assess possible mass an cost of components. This will be done by analyzing different elements separately.

The components consist of the main wing skin, ribs, and canard D-box skin made of quasi-isotropic CFRP; then the fuselage skin structure using the GFRP and Nomex composite; Aluminium 6061-T6 stiffeners, stringers, struts and landing legs are the last part. All remaining components, including joints and local supporting elements are assumed to weight around 20% of the total structural mass. The accurate wing and canard mass estimations were implemented in sizing script. Other structural parts, especially the fuselage geometry was based on the 3D model. Combined weights are presented in Table 9.14.
Most of the composites are difficult to manufacture on the medium scale, that is why the off the shelf materials are considered to estimate the cost. All composite skin components sum at around 7 m^2. The price per square meter of quasi-isotropic CFRP of 175 EUR [54] results in the total of 1244.5 EUR. The total of main spars for the wing and canard of uni-directional CFRP with the cost of 130 EUR per square meter [55] give the sum of 234 EUR. Aluminium components end up at roughly 750 EUR [56]. Finally, the most expensive part, the skin can be estimated using existing panels that cost around 559 EUR per square meter [57]. The entire structures cost, with the assumed contingency of 20% for other elements and manufacturing of specific shapes leaves the cost at 7745 EUR and is summarized in Table 9.14.

Table 9.14: Airframe Structure Side-by-Side Evaluation Matrix

Component / Assembly	Mass [kg]
Fuselage	10.30
Wing	7.91
Canard	1.27
Primary Structure Subtotal	**19.48**

Structure Component	Price [EUR]
Fuselage skin	4265.17
Canard + Wing Skin + Ribs	1244.50
Stiffeners	750.00
Spars	234.00
Others	1251.93
Total Structure Cost	**7745.60**

9.3.2. Failure Mode Analysis

To ensure continued airworthiness under ultimate flight loads, a comprehensive failure mode analysis was evaluated across the primary lifting surfaces and fuselage. This assessment isolates the critical structural boundaries, elastic instabilities, and localized material limits that define the vehicle's safe operating envelope.

Primary Wingbox

All structures were verified under the safety factor SF = 1.5. The primary load-bearing wingbox exhibits exceptional resistance to catastrophic material yield, with the carbon fiber spar webs and aluminum longitudinals maintaining massive safety buffers (> 270 MPa) under peak multi-axial stress. Interlaminar matrix shear along the spanwise transitions also remains securely within the required composite degradation limits. Consequently, the critical failure mode for the wing assembly shifts away from material fracture directly to elastic thin-shell instability.
Specifically, the dominant failure mechanism is driven by localized elastic buckling along the unstiffened lower skin panel. As outlined in Table 9.15, this panel has the smallest calculated stability margin, +0.02 MPa. This means that lower-skin panel stability, rather than ultimate material strength in the spar webs or stringers, defines the governing structural limit of the current wingbox sizing. The result should therefore be interpreted as a preliminary minimum-gauge design that requires local buckling verification before hardware release.

Table 9.15: Wingbox Structural Yield and Stability Margins (Compressive Limits, including SF and load factor)

Structural Element	Material Limit	Max Observed Load	Calculated Margin
Axial Stress Bounds			
CFRP Aerodynamic Skin	570.00 MPa	31.65 MPa	+538.35 MPa
CFRP Front/Rear Spar Web	950.00 MPa	69.06 MPa	+880.94 MPa
Aluminum 6061-T6 Stringers	276.00 MPa	36.23 MPa	+239.77 MPa
Interlaminar Shear Bounds			
Composite Matrix Shear	50.00 MPa	35.09 MPa	+14.91 MPa
Elastic Buckling Stability			
Upper Monolithic Panel	28.18 MPa	21.97 MPa	+6.21 MPa
Lower Monolithic Panel	15.85 MPa	15.83 MPa	+0.02 MPa

Canard

The canard structure experiences highly scaled aerodynamic control inputs but maintains massive, uncompromised material strength safety margins across all primary load paths. As compiled in Table 9.16, peak axial stresses in the carbon fiber skins (2.77 MPa) and spar webs (6.05 MPa) utilize less than 1% of their ultimate material capacity. Similarly, the interlaminar matrix shear remains benign at only 3.63 MPa.

Consequently, the definitive and gating failure mode for the canard assembly is thin-shell elastic panel buckling rather than material rupture. Driven by the expanded un-stiffened lower geometric span (b = 94.2 mm), the lower monolithic skin panel operates at a critically narrow buckling stability margin of just +0.01 MPa. This renders the lower canard skin the primary structural bottleneck, meaning localized surface wrinkling and skin oil-canning will immediately dictate the limits of the component's operational envelope before any actual material failure occurs.

Table 9.16: Canard Structural Yield and Stability Margins (including SF and load factor)

Structural Element	Material Limit	Max Observed Load	Calculated Margin
Axial Stress Bounds			
CFRP Aerodynamic Skin	570.00 MPa	2.77 MPa	+567.23 MPa
CFRP Front/Rear Spar Web	950.00 MPa	6.05 MPa	+943.95 MPa
Aluminum 6061-T6 Stringers	276.00 MPa	3.42 MPa	+272.58 MPa
Interlaminar Shear Bounds			
Composite Matrix Shear	50.00 MPa	3.63 MPa	+46.37 MPa
Elastic Buckling Stability			
Upper Monolithic Panel	3.15 MPa	2.61 MPa	+0.54 MPa
Lower Monolithic Panel	1.40 MPa	1.39 MPa	+0.01 MPa

Fuselage

The fuselage primary structure follows a different failure hierarchy from the main wing and canard. While the lifting surfaces are governed mainly by local monolithic skin buckling, the fuselage is modelled as a no-skin frame-and-longeron structure. The aerodynamic sandwich skin is therefore not credited as a primary axial, bending or shear-carrying member in the preliminary global sizing model. Instead, the main loads are carried by the two hollow-box side longerons, the upper and lower hat stringers, and the transverse frames and reinforced bulkheads.

As compiled in Table 9.17, material yielding is not the governing fuselage failure mode. The maximum normal stress is 72.2 MPa, and the maximum Von Mises stress is 76.9 MPa, both remaining below the aluminium-equivalent allowable stress of 166.7 MPa. The vertical and lateral shear stresses also remain well below their allowable limits. Therefore, the fuselage is not primarily limited by material strength in the current preliminary sizing.

The most critical global check is elastic column buckling of the side longerons between transverse frames. The calculated longeron buckling stress is 140.0 MPa, compared with an equivalent observed compressive stress of 71.1 MPa. This corresponds to a reserve factor of approximately 1.97, or a margin ratio of approximately 0.97 when expressed as $RF - 1$. The transverse frame pitch is therefore the main global stability driver: increasing the unsupported length between frames would reduce the longeron buckling margin before material yielding becomes critical.

A second important fuselage limitation is local hardpoint behaviour. The global beam model captures the axial, shear and bending envelopes, but it does not fully resolve local bearing, pull-through, fastener shear, insert crushing or local panel distortion at the wing root, landing-support bulkhead, tether reel and canard attachment. These regions therefore require local metallic inserts, load-spreading plates and proof-load verification in the next design phase.

Table 9.17: Fuselage Structural Yield and Stability Margins

Structural Element	Limit	Max Observed Load	Calculated Margin
Axial Stress Bounds			
Longitudinal members	166.7 MPa	72.2 MPa	+94.5 MPa
Fuselage section VM	166.7 MPa	76.9 MPa	+89.8 MPa
Shear Bounds			
Side longerons	96.7 MPa	12.1 MPa	+84.6 MPa
Hat-stringer webs	96.7 MPa	15.3 MPa	+81.4 MPa
Elastic Stability			
Hat-web panel	2584 MPa	72.2 MPa	+2511.8 MPa
Side-longeron column	140.0 MPa	71.1 MPa	+68.9 MPa

9.3.3. Vibrational Analysis

The dominant on-board dynamic excitation is the four-rotor propulsion system. Its shaft frequency varies over roughly 15–45 Hz (≈ 900–2700 rpm) during run-up and run-down, but the vehicle spends almost all of its operating life at the cruise/hover setting of about 33.3 Hz (≈ 2000 rpm). The lowest elastic wing modes are therefore assessed both against this swept range and, more importantly, against the steady operating frequency [58, 59].

The modal frequencies are estimated with a reduced one-dimensional Euler–Bernoulli cantilever-beam finite-element model of the half-wing. The bending stiffness $EI(y)$ and running mass $\bar{m}(y)$ are taken directly from the sized wing-box cross-section properties along the span, and the clamped–free eigenproblem $\mathbf{K}\phi = \omega^2\mathbf{M}\phi$ is solved with consistent mass matrices [60, 61]. Such stick-beam idealisations are the standard tool for preliminary wing dynamics, reproducing the fundamental modes to within a few per cent of full three-dimensional models, with the larger deviations confined to the higher and torsional modes [62]. To reflect this, the fundamental bending mode is assigned a ±15% confidence band and the less reliably captured higher modes a conservative ±30%. The 3D visualization of the reduced-order model over the normalized span can be seen in Figure 9.17.

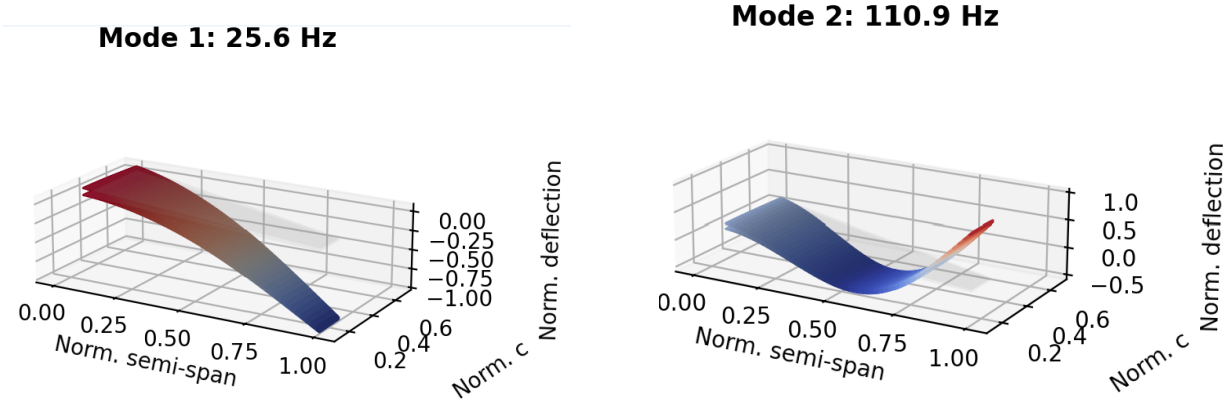

(a) Mode 1 **(b)** Mode 2

Figure 9.17: First Two Reduced-Order Wing Mode Shapes from the Modal Analysis

The first three vertical-bending frequencies are $f_1 = 25.6$ Hz, $f_2 = 110.9$ Hz and $f_3 = 282.7$ Hz, example bending deflection can be seen in Figure 9.18b. Modes 2 and 3 lie far above the swept range and are of no concern. The fundamental mode falls inside the swept range, but it sits about 30% below the steady operating frequency, so it never coincides with the sustained operating point (Fig. 9.18a). The frequencies between 15 Hz and the operating point, including f_1, are only traversed transiently each time the motor is spun up or down. Because the shaft speed is continuously changing, the dwell time in the neighbourhood of f_1 is short and the response never builds to the steady-state resonant amplitude; the peak transient response decreases further as the sweep rate increases [63]. Sustained resonance, which requires prolonged excitation at the natural frequency, therefore does not occur, and the fundamental mode is carried as a minor, transient-only residual risk.

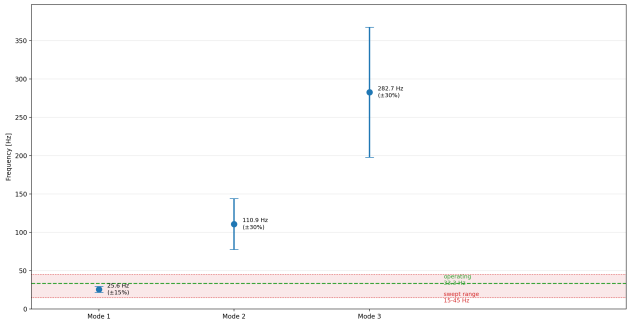

(a) Resonance Interference Diagram

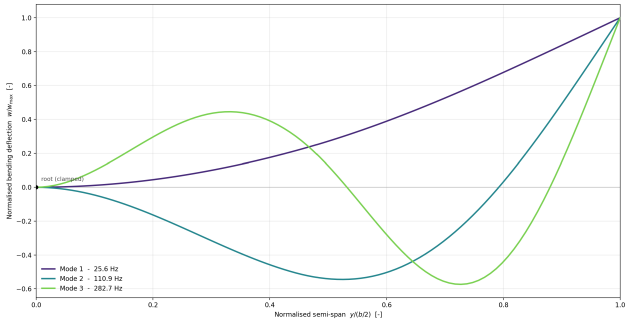

(b) Euler-Bernoulli Bending Mode Shapes

Figure 9.18: Visualization of Relevant Modes

10 Ground System

The ground system provides the ground-side infrastructure required to keep BELLONA ready, launch it safely, maintain command and telemetry links, and support recovery and restowing. It is developed as the Operations and Ground Station Subsystem (OGS), covering the deployable station, power and charging equipment, communication hardware, sensors, control electronics, and mechanical launch/recovery mechanisms.

The design is detailed to the level needed for subsystem integration and preliminary sizing. The CAD model defines the selected layout, major interfaces, and critical mechanisms, while production detailing, environmental qualification, and integrated launch-recovery testing remain future work.

10.1. Ground System Scope and Design Objective

The ground system scope is limited to the infrastructure and interfaces needed to operate the tail-sitter UAS from an airport ground station. External systems are included only where they affect charging, launch authorization, release, recovery, telemetry, or emergency control. The resulting scope boundary is given in Table 10.1.

Table 10.1: Ground System Scope Boundary

Included in ground system	Excluded from ground system
Station enclosure, base structure, and deployment mechanisms	ATC infrastructure and airport-wide procedures
Ground-side command, telemetry, operator, and ATC communication interfaces	Aircraft flight-control internals
Power input, UAS charging, and backup energy supply	Onboard propulsion design
Weather, health, fire, and safety monitoring hardware	Balloon interaction mechanism design
Launch, docking, clamping, release, and restowing hardware	Autonomous mission-planning algorithm
Maintenance access, service interfaces, and inspection provisions	Aircraft structure outside the ground-station interface

10.2. Operations and Ground Station Requirements

Table 10.2 lists the key OGS subsystem requirements. Only requirements classified as key (out the 45) are included in this condensed table.

Table 10.2: Key Operations and Ground Station Subsystem Requirements

ID	Requirement
REQ-STK-01-MSN-01-SYS-01-OGS-01	The operations and ground station subsystem shall complete the ground launch sequence in less than 5 min.
REQ-STK-03-MSN-04-SYS-06-OGS-02	The operations and ground station subsystem shall deploy the UAS from stored configuration to vertical launch configuration in less than 5 min.
REQ-STK-03-MSN-04-SYS-07-OGS-03	The operations and ground station subsystem shall perform the deployment sequence without manual physical intervention.

Table 10.2: Key Operations and Ground Station Subsystem Requirements (continued)

ID	Requirement
REQ-STK-03-MSN-04-SYS-07-OGS-05	The operations and ground station subsystem shall rotate the UAS by 90 deg from horizontal storage orientation to vertical launch orientation.
REQ-STK-03-MSN-04-SYS-07-OGS-06	The operations and ground station subsystem shall restrain a 51.13 kg UAS during pre-release motor spool-up.
REQ-STK-03-MSN-04-SYS-07-OGS-07	The operations and ground station subsystem shall release the UAS after the release command is confirmed.
REQ-STK-03-MSN-04-SYS-07-OGS-11	The operations and ground station subsystem shall confirm clamp opening before permitting UAS thrust increase above pre-release spool-up level.
REQ-STK-05-MSN-06-SYS-11-OGS-13	The operations and ground station subsystem shall support a 51.13 kg UAS with a minimum safety factor of 1.5 during storage.
REQ-STK-05-MSN-06-SYS-13-OGS-14	The operations and ground station subsystem shall capture the returning UAS within a lateral docking capture envelope of 0.10 m.
REQ-STK-07-MSN-09-SYS-46-OGS-22	The operations and ground station subsystem shall withstand sustained winds up to 13 m/s during ground operation.
REQ-STK-07-MSN-09-SYS-46-OGS-23	The operations and ground station subsystem shall withstand gusts up to 21 m/s during ground operation.
REQ-STK-12-MSN-15-SYS-27-OGS-25	The operations and ground station subsystem shall inhibit UAS launch until ATC clearance is received.
REQ-STK-12-MSN-15-SYS-27-OGS-26	The operations and ground station subsystem shall transmit live station status to ATC through a LTE cellular router.
REQ-STK-12-MSN-15-SYS-27-OGS-27	The operations and ground station subsystem shall transmit live UAS telemetry to ATC through a LTE cellular router.
REQ-STK-13-MSN-16-SYS-28-OGS-29	The operations and ground station subsystem shall provide secondary RF emergency communication during all mission stages and recovery.

10.3. Ground System Architecture

The ground system is divided into mechanical, electrical/control, and communication branches, as shown in Figure 10.1. This decomposition defines the structure used for CAD organization, load-case allocation, interface definition, and verification traceability. The mechanical branch stores, deploys, recovers, and restrains the UAS. The electrical/control branch supplies power, supervises station states, and executes safety logic. The communication branch provides the operational links between the ground station, ATC, the remote operator, and the aircraft.

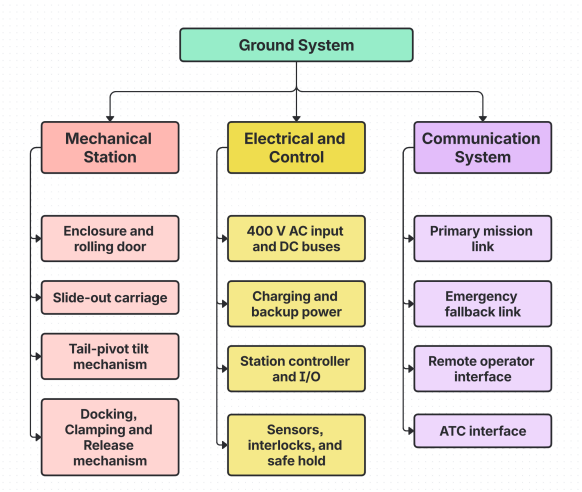

Figure 10.1: Ground System Functional Decomposition

10.3.1. Mission Role and External Interfaces

The ground system receives launch approval, confirms readiness, deploys the aircraft, maintains communication during the mission, and supports recovery and restowing after return. The main external interfaces are summarised in Table 10.3.

Table 10.3: Main OGS Interfaces

Interface	Direction	Information / load exchanged
ATC / airport operations	External to OGS	Clearance, aborts, station status, and UAS telemetry
UAS	Two-way	Charging, commands, telemetry, docking references, and release state
Remote operator	Two-way	Monitoring, overrides, aborts, and maintenance commands
Electrical supply	Into OGS	400 V three-phase mains and backup-power charging
Environment	Into OGS	Wind, rain, temperature, warnings, and external hazards
Maintenance crew	Two-way	Access, service ports, battery replacement, and logs

10.3.2. Subsystem Breakdown

The functional decomposition is translated into the lower-level assemblies listed in Table 10.4. Each assembly is assigned a subsystem ID so that requirements, CAD parts, load cases, and verification activities can be traced to the same architecture.

Table 10.4: Ground Station Subsystem Breakdown

Subsystem	Main function
Enclosure and base structure	Protects the UAS and supports station hardware
Rolling launch door	Opens the launch path and protects standby enclosure
Slide-out carriage system	Moves the UAS nose-first out before tilt-up
Tail-pivot tilt mechanism	Rotates the UAS to vertical launch position
Docking, clamping, and release system	Captures, restrains, releases, and restows the UAS
Power, charging, and backup energy	Powers station loads and charges the UAS in standby
Control, sensing, and safety I/O	Runs state logic, monitoring, interlocks, and safe hold
Communication system	Provides mission, fallback, operator, and ATC links
Safety and maintenance interfaces	Supports aborts, alarms, fire response, access, and servicing

10.3.3. Ground Station Layout and Zoning

The ground station is divided into a large UAS deployment bay and a smaller technical bay, as shown in Figure 10.2. The UAS bay contains the launch platform, fixed rails, rack-and-pinion drive, tilt mechanism, and docking cradle. The technical bay contains the battery cabinet, power electronics, control and communication hardware, and service access. The partition between the two zones reduces exposure of the stored UAS to battery and electrical hazards. The UAS outline in the updated planform is included as a scale and clearance reference only; the detailed docking and clamping geometry is defined separately at interface level.

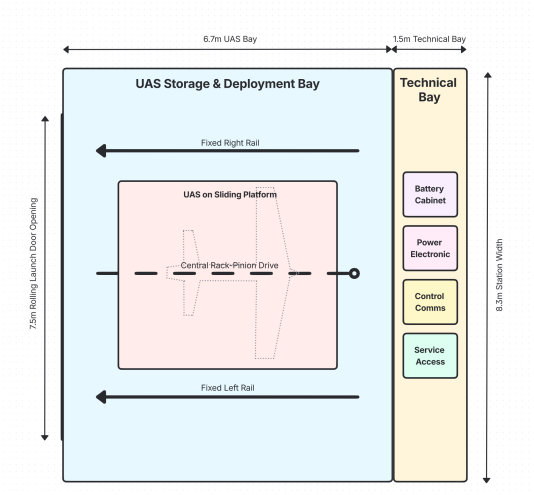

Figure 10.2: Top-View Layout and Zoning of the Ground Station, Including the UAS Outline for Scale

10.4. Operational Sequence and Functional Flow

The ground-station operation is organized as a controlled state sequence from standby to launch, recovery, and restowing. The sequence is designed so that the UAS is never released unless the station

has confirmed ATC clearance, safe environmental conditions, correct mechanism positions, and a valid release command. The simplified physical sequence is shown in Figure 10.3.

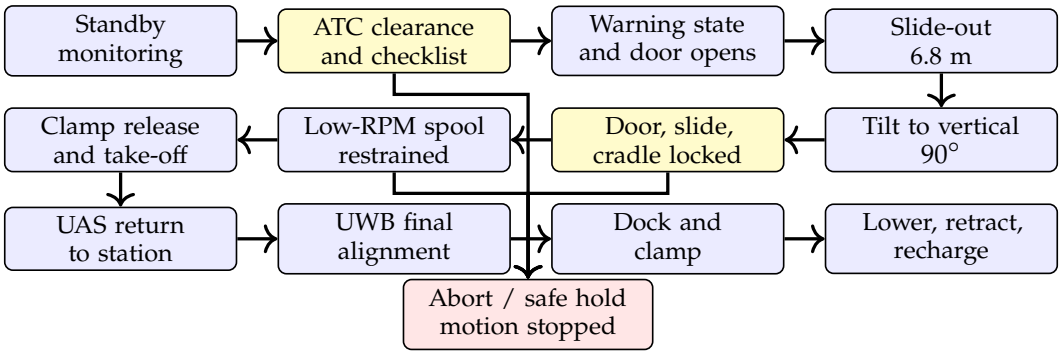

Figure 10.3: Simplified Operational Sequence of the Ground Station

10.4.1. Standby and Pre-Launch Checks

During standby, the UAS is stored fully assembled inside the enclosure. The ground station remains monitored and continuously checks the aircraft, station mechanisms, power system, communication links, and local environment. The monitored parameters are summarised in Table 10.5.

Table 10.5: Standby Monitoring and Pre-Launch Checks

Check group	Monitored parameters	Launch condition
Power availability	Airport mains availability and backup power state	Sufficient power available for launch or safe hold
Aircraft energy state	UAS battery charging state and charging-interface status	Battery charged and charging disconnected before motion
Battery safety	Battery-bay smoke, off-gas, and temperature	No battery fault or thermal warning present
Environmental limits	Wind speed, wind direction, rain, and ambient temperature	Conditions within permitted launch envelope
Mechanism positions	Door, carriage, cradle, and clamp position feedback	All mechanisms in commanded and confirmed positions
Communication and approval	Communication availability, ATC clearance state, and operator approval	Valid communication link and launch approval received

10.4.2. Launch Sequence

After approval, all deployment actions are performed automatically by the ground station to minimize human exposure. The UAS is first isolated from charging, moved clear of the enclosure, rotated into the vertical launch orientation, and released only after final position and restraint checks have been confirmed.

Table 10.6: Ground-Station Launch Sequence

Step	Phase	Action
1	Approval	Receive ATC clearance and operator approval
2	Warning state	Activate warning lights and enter the exclusion state
3	Door opening	Open the rolling launch door
4	Energy isolation	Disconnect the UAS charging interface
5	Carriage release	Release the stored-position carriage lock
6	Slide-out	Translate the UAS nose-first by at least 6.8 m
7	Carriage lock	Lock the carriage in the extended position
8	Tilt-up	Rotate the UAS by 90° using the tail-pivot tilt mechanism
9	Cradle lock	Lock the cradle in the vertical position
10	Restrained spool-up	Spool the motors at low RPM while the UAS remains restrained
11	Release	Release the clamps after final launch confirmation

10.4.3. Recovery and Restowing Sequence

The recovery sequence reverses the launch sequence where possible. Final alignment is supported by ultra-wideband (UWB) docking anchors and the recovery geometry of the cradle. After contact, the docking system confirms position and load transfer before the clamps close.

Table 10.7: Ground-Station Recovery and Restowing Sequence

Step	Phase	Action
1	Cradle contact	Detect UAS contact in the cradle
2	Docking confirmation	Confirm docking-foot contact and acceptable position
3	Securing	Closing the clamps and securing the UAS
4	Tilt-down	Lower the cradle from vertical to horizontal
5	Carriage unlock	Unlock the extended carriage
6	Retraction	Retract the carriage into the enclosure
7	Recharge	Reconnect the charging interface
8	Enclosure closure	Close the rolling door
9	Reset	Complete the post-mission self-check and maintenance flagging

10.4.4. Abort and Safe-Hold Logic

Abort logic remains active until the UAS has been released. Before release, an abort command stops all ground-station motion, keeps or returns the clamps to the closed state, and prevents thrust increase above the restrained spool-up level.

If the abort occurs during sliding or tilting, the station holds its current configuration using the slide lock, actuator braking, carriage locks, and backup-powered control electronics.

If airport mains power is lost during deployment, the backup power system keeps the control electronics, sensors, communication interface, and critical actuators available long enough to enter a safe-hold state. If automatic cradle recovery fails during return, the UAS does not force a docking attempt. Instead, it diverts to the alternate safe landing zone, while the station remains open for inspection or manual intervention.

10.5. Communication Architecture

The Ground System communication architecture is divided into two redundant pathways to ensure safe, steady, and resilient operation of the UAS. The network topology splits data handling responsibilities across a high-bandwidth primary data loop (LTE) for normal operations and an independent, direct radio frequency (RF) connection for secondary backup.

10.5.1. Uplink and Downlink Data Flows

To understand the operational dynamics of the platform, it needs to be analyzed along the datapath ways, as follows:

- **The Downlink Path:** This path handles high-density data heading down from the aircraft to the ground. In normal operations, it carries telemetry alongside an uncompressed, real-time video stream captured from the payload camera directly over the mobile network to local carrier towers, as can be seen in Figure 10.4.
- **The Uplink Path:** This path maps out control commands routing back up from the ground to the platform. Under normal conditions, automated flight paths, position corrections, and mission commands originate at the ground station and pass up through cellular infrastructure. During an emergency, the uplink instantly switches to a direct, RF modem link to transmit manual joystick steering and emergency takeover commands.

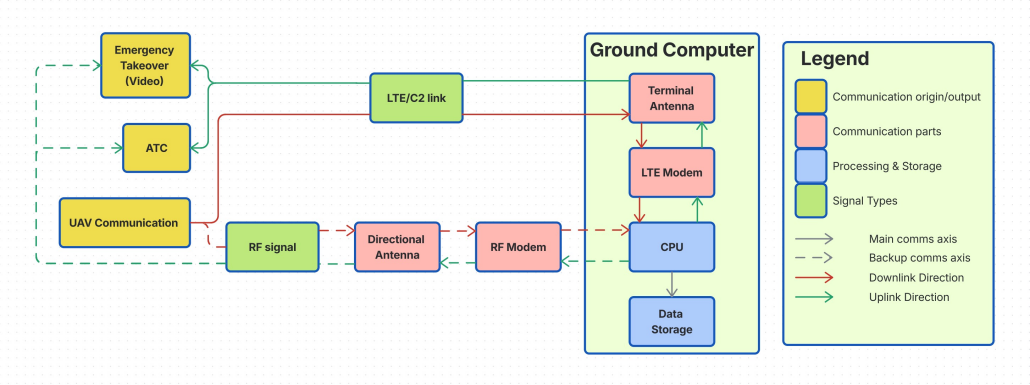

Figure 10.4: Flow Diagram of the Downlink Mission Architecture

10.5.2. Communication Components and Hardware Layout

As can be seen in Figure 10.4 the communication parts represent actual hardware used in the communications of the UAS. In the primary loop segments, connecting through a cellular network, only a single computer, seen in Figure 10.5b, is needed for the architecture. Additionally, for the backup capabilities, an omnidirectional antenna, depicted in Figure 10.5a and a modem seen in Figure 10.5c add to the final architecture.

(a) Directional Antenna

(b) Computer with integrated LTE, SSD memory, etc

(c) Modem

Figure 10.5: Additional Communication Components

Table 10.8: Consolidated Communication Subsystem Electrical Load, Mass, and Cost Budget

Component	Qty.	Mass [kg]	Power [W]	Cost [€]	Source
Onlogic k300 PC	1	-	-	3800	Onlogic k300 with additional specs [64]
5.8 Horizon MIMO Modem	1	0.57	15	2700	Horizon 5.8 (MIMO) [65]
RF omnidirectional antenna	1	0.12	-	8	ANT-433-CW-HD-SMA [66]
Chinowing T30	1	2.4	37.8	3500	T30 Controller [67]

10.5.3. Emergency Takeover and User Interface (UI)

The Emergency Takeover is the proposed contingency in case of defects or partial failure of the UAS. This allows for human intervention into the system in a safe and controlled manner. With the use of a remote control, seen in Figure 10.6, the UAS is controlled within an acceptable range to still track and intercept the Balloon payload system.

Figure 10.6: Chinowing T30

An example of the ground station interface is presented in Figure 10.7. This user interface (UI) prototype displays critical visual, telemetry, and system health metrics required for mission success. To ensure long-term sustainability, the system is designed for local operators following a brief baseline training period. Grounded in the user taxonomy established by Shneiderman et al. [68], the software architecture scales across three distinct user profiles to balance cognitive load with operational depth:

- **Inexperienced Operator:** Responsible for routine flight monitoring. Lacking a formal aviation background, this user relies on an intuitive, minimalist interface that eliminates cognitive clutter.
- **Experienced Operator:** Conducts daily operations but has achieved system mastery over time. This profile utilizes higher operational autonomy and a denser presentation of real-time telemetry datasets.
- **UAS Engineer:** Interacts with the interface primarily for system deployment, post-flight data extraction, hardware maintenance, and diagnostics. This profile requires deep access to the underlying technical architecture rather than operational shortcuts.

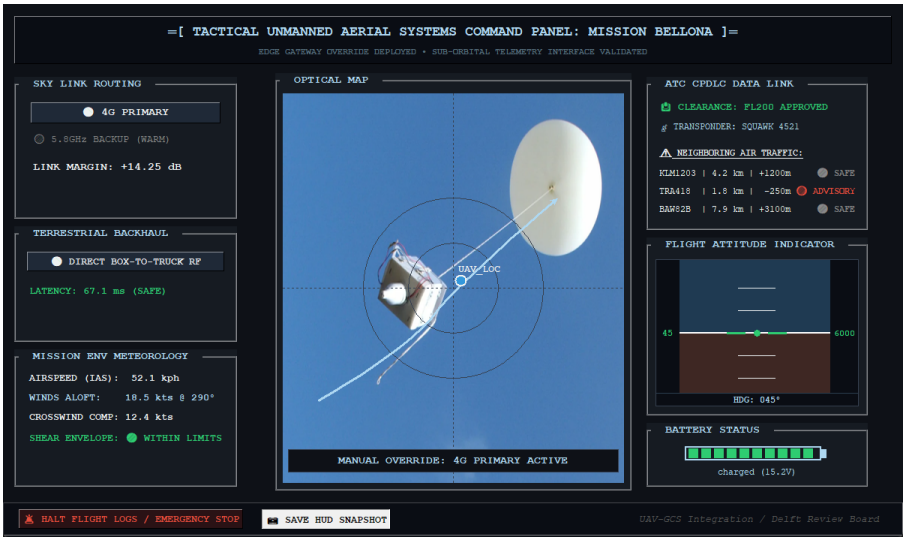

Figure 10.7: User Interface Prototype

10.5.4. Primary Network Path Analysis

To evaluate communication link viability, linear transmitter power (P_{W}) is converted to logarithmic decibel-milliwatts (P_{dBm}):

$$P_{\mathrm{dBm}} = 10 \log_{10} \left(\frac{P_{\mathrm{W}}}{10^{-3}} \right) \tag{10.1}$$

The link margin (M) is governed by the received signal strength (P_{rx}) relative to the receiver sensitivity floor (P_{sens}):

$$P_{\mathrm{rx}} = \mathrm{EIRP} + G_{\mathrm{rx}} - L_{\mathrm{p}} \tag{10.2}$$

$$M = P_{\mathrm{rx}} - P_{\mathrm{sens}} \tag{10.3}$$

Where the effective isotropic radiated power (EIRP) accounts for transmitter output and losses, while the receiver antenna gain (G_{rx}) is a specified hardware constant. Atmospheric and free-space attenuation over the operational range are captured by the generalized path loss function $L_{\mathrm{p}} = 20 \log_{10}(d) + 20 \log_{10}(f) + 32.44 + L_{\mathrm{env}}$, where L_{env} represents localized environmental and canopy degradation. Calculating all the values and then getting the margin from the values from Table 10.9 is computed as:

$$M = 25.0\,\mathrm{dB} + 3.0\,\mathrm{dB} - 118.5\,\mathrm{dB} - (-116.45\,\mathrm{dB}) = 25.95\,\mathrm{dB} \tag{10.4}$$

The detailed link budget for the primary network can be seen in Table 10.9. The link amounts to the capabilities of downlinking the video signal, position and current state of the UAS. Using the same architecture for the uplink gives a higher margin since there is less amount of data sent up to the UAS. These include authorizations, flight path instructions and emergency control manoeuver inputs, which require a lower bandwidth than the downlink.

Table 10.9: Communication Budget for Primary Network (LTE)

Component	Downlink Value (dB)	Uplink Value (dB)
Transmitter EIRP	25.0	60.0
Transmitting Antenna Gain	+2.0	+17.0
Free Space + Environmental Path Loss	-118.5	-118.5
Receiving Antenna Gain	+3.0	+2.0
Receiver Sensitivity Floor	-116.45	-109.55
Margin	**25.95**	**53.05**

10.5.5. Secondary Emergency RF Path Analysis

The secondary pipeline serves as an isolated, off-grid safety corridor using lower radio frequencies and high-gain point-to-point ground antennas to bypass public telecom infrastructure failures. Using the same approach for the linking budget as in the primary network path, the summarised values and margin can be seen in Table 10.10

Table 10.10: Communication Budget for Secondary Network (Emergency RF)

Component	Downlink Value (dB)	Uplink Value (dB)
Transmitter EIRP	27.5	20.2
Transmitting Antenna Gain	+0.7	+0.7
Free Space + Environmental Path Loss	-127.78	-103.74
Receiving Antenna Gain	+12.0	+0.7
Receiver Sensitivity Floor	-93.02	-118.0
Margin	**4.74**	**35.16**

10.6. Ground Station Electrical Architecture

The ground-station electrical architecture is shown in Figure 10.8. It distributes airport mains power, backup power, UAS charging power, actuator power, sensor power, communication power, and safety-control signals across the station. The architecture is limited to the ground station; the internal UAS electrical system is treated as an external interface through the charging connector, telemetry link, and docking/release sensors.

10.6.1. Power Input and Distribution

The station is supplied by a 400 V three-phase airport mains input, routed through the main disconnect, circuit protection, residual-current and earth-fault protection, and the main AC contactor. The protected AC rail feeds the UAS charger, backup-power branch, and low-voltage DC supplies. The DC distribution is split into 24 V, 12 V, and 5 V buses so that actuator, electronics, communication, sensor, and logic loads remain separated and individually monitored.

Table 10.11: Ground-Station Electrical Buses

Bus	Main loads	Protection / monitoring
400 V AC	Airport mains input, main AC contactor, charger input, backup-power input, and AC distribution rail	Main disconnect, circuit breaker, residual-current protection, and earth-fault monitoring
24 V DC	Rolling door control, slide-drive control, tilt linear actuators, clamp/release actuators, safety I/O, and field modules	DC fuses, voltage/current sensing, and safety contactor
12 V DC	Industrial-computer support electronics, communication hardware, UWB/RF modules, and auxiliary station devices	DC fuse branch and voltage/current sensing
5 V DC	Logic-level sensors, embedded modules, and low-power status electronics	Regulated DC supply and local branch protection

The backup-power branch uses a battery/inverter or UPS path to maintain control after mains loss. Its capacity is driven by the need to complete one launch–recovery cycle, or at minimum enter safe hold while preserving communication, sensing, and critical actuator control. Solar panels are treated only as an auxiliary charging source, not as the primary launch-power supply.

10.6.2. Stored-State Charging

During standby, the UAS remains installed in the station and is connected to the charging interface. The charging path includes the UAS battery charger, a charging socket or docking connector, a charging-port protection switch, and charging voltage, current, and temperature sensing. These measurements allow the station to confirm that the UAS battery is ready before launch.

Before the slide carriage moves, the charging interface is disconnected, and the open state is confirmed. This prevents the charging connector from carrying mechanical load during the 6.8 m slide-out motion. A failed disconnect confirmation inhibits deployment, because a trapped or live charging connector would create both a mechanical damage risk and an electrical arcing risk.

10.6.3. Control, Sensors, and Safety Interlocks

The control architecture is based on a separation between normal control and safety-critical permission logic. The industrial processing computer handles supervision, communication, logging, and operator interaction. The ground-station PLC and safety relay chain handle mechanism sequencing, launch inhibition, emergency-stop response, and safe-hold commands. The station uses sensor feedback to confirm that every launch step has reached its safe state before the next step is allowed. Weather sensors define whether launch preparation is allowed, battery-bay sensors monitor stored-state safety, mechanism sensors confirm door/slide/cradle/clamp positions, and docking sensors confirm recovery contact.

Electrical-health sensors monitor the power path so that the station can stop motion or enter safe hold during undervoltage, overcurrent, ground-fault, or mains-loss conditions.

Table 10.12: Ground-Station Sensor and Interlock Groups

Sensor group	Sensors / interlocks	Used for
Weather monitoring	Ultrasonic anemometer, rain or precipitation sensor, ambient temperature sensor	Launch permission and standby monitoring
Battery-bay safety	Smoke detector, lithium off-gas sensor, battery-bay temperature sensors, fire/heat detection	Charging permission and fire response
Mechanism position	Door limit switches, slide limit switches, cradle angle encoder, vertical/horizontal lock switches, clamp-state switches	Launch sequence interlocks
Docking and recovery	Docking-foot contact switches, UWB anchors, final recovery position references	Recovery alignment and clamp permission
Electrical health	Mains voltage/current sensors, 24 V/12 V/5 V bus voltage and current sensors, UPS state, ground-fault monitor	Fault detection and safe hold
Safety interface	Emergency-stop buttons, warning beacon state, launch-inhibit status, safety contactor feedback	Abort response and motion permission

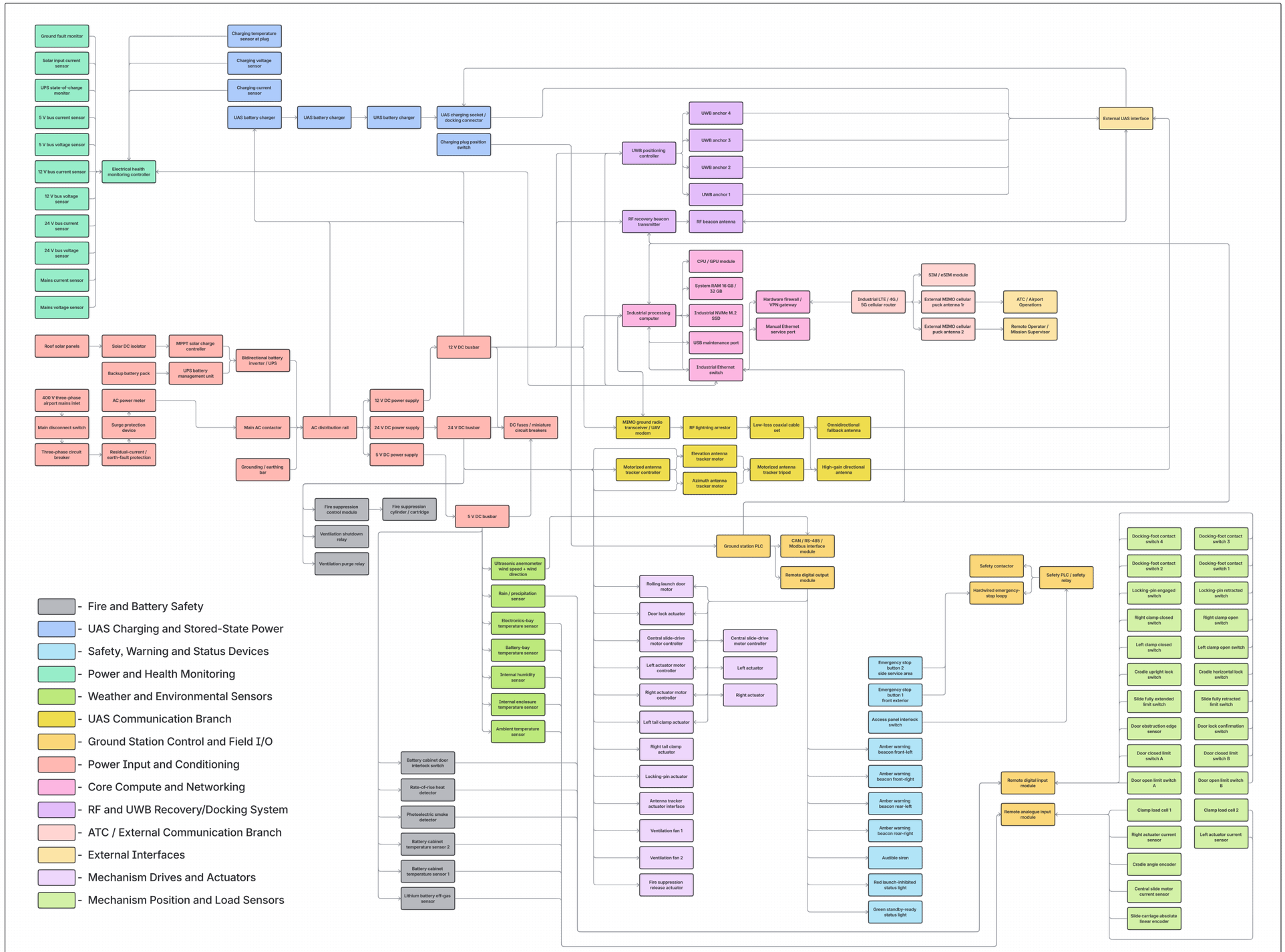

Figure 10.8: Electrical Architecture of the Ground Station

10.6.4. Actuator and Mechanism Interfaces

All powered mechanisms are commanded through the ground-station control system and are linked to position feedback. The rolling launch door must be confirmed open before slide motion is allowed. The slide carriage must be confirmed extended and locked before the tilt mechanism can rotate the UAS upright. The cradle must be confirmed vertical and locked before restrained motor spool-up is permitted.

The clamp and release actuators form the final launch interlock. During low-RPM spool-up, the clamps remain closed, and the UAS is restrained by the ground station. Final release is only permitted after the release command is confirmed and the clamp state can be verified. During recovery, the same clamp interface secures the UAS after docking contact has been detected.

Table 10.13: Actuator Interfaces and Required Feedback

Actuator group	Electrical interface	Required feedback
Rolling launch door	Motor controller or door actuator branch on the 24 V control system	Door open/closed limit switches, obstruction edge sensor, door lock confirmation
Slide-out carriage	Central rack-and-pinion drive motor controller	Stored limit, extended limit, slide lock state, motor current feedback
Tail-pivot mechanism	Left and right tilt linear actuator controllers	Cradle angle encoder, horizontal/vertical lock switches, actuator current feedback
Clamp and release system	Clamp actuators, locking-pin actuators, release actuator branch	Clamp open/closed switches, locking-pin engaged/retracted switches
Ventilation and warning devices	Fan relays, warning beacon outputs, safety relay outputs	Fan state, warning state, safety contactor feedback

The main electrical design risk is not the nominal power distribution, but the fault behaviour during motion. A single sensor fault, actuator overcurrent, loss of mains power, or emergency-stop input before release must leave the UAS restrained and the station in a safe mechanical configuration. For this reason, the actuator interfaces are not only sized for motion, but also for braking, locking, state confirmation, and safe-hold operation.

10.7. Mechanical Systems Design

The mechanical design is implemented as a container-like deployable ground station, shown in Figure 10.9a. The CAD model includes the main insulated enclosure, roof solar panels, external antennas, warning light, ventilation louvre, support feet, fixed slide rails, sliding platform, and tail-pivot tilt mechanism.

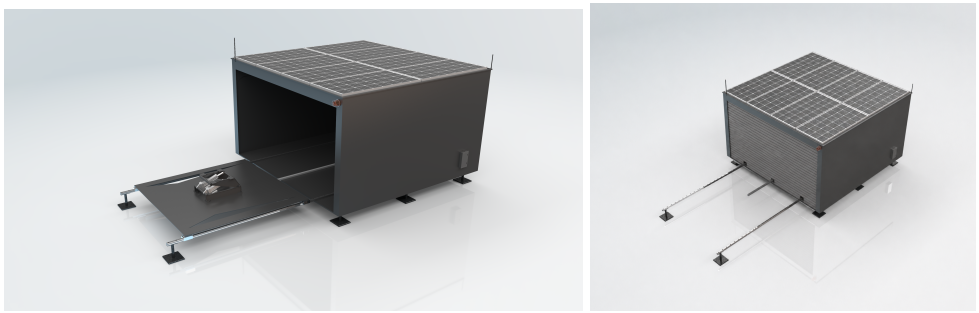

(a) Platform-extending/deployed state. **(b)** Stored State With Rolling Door Closed

Figure 10.9: CAD Renders of the Ground Station in Representative Operational States

10.7.1. Enclosure and External Features

The enclosure provides year-round outdoor protection and creates a controlled launch/recovery interface. The current representative CAD model uses an approximate external envelope of 8.2 m by 8.3 m by 4.2 m. This envelope shall be updated after the final UAS dimensions are frozen.

Table 10.14: External Ground-Station Features Included in the CAD Concept

External feature	Purpose
Rolling launch door	Opens the deployment path while avoiding collision with the extended UAS
Roof solar panels	Provide auxiliary sustainable energy input
LTE antenna	Supports the primary cellular communication interface
Backup antenna	Supports the secondary RF communication path
Warning light	Warns personnel during launch, recovery, or fault states
Ventilation louvre	Provides airflow for technical bay cooling and purge modes
Leveling feet	Level and stabilize the station during operation
Side service hatch	Provides access to technical bay components

10.7.2. Internal Zoning and Maintenance Access

The UAS bay and technical bay are physically separated. The UAS bay remains open to preserve clearance for the sliding platform and tilt mechanism, while the technical bay houses the battery cabinet, power electronics, communication equipment, safety relays, and service ports. This improves fire and battery-safety isolation, cable routing, maintenance access, and aircraft protection during standby.

10.7.3. Rolling Door and Launch Opening

A rolling garage door is selected for the final CAD concept. The main reason is geometric clearance: the door can retract above the opening while the platform extends horizontally through the front of the station. The fixed slide rails pass through small lower cut-outs in the door plane. These cut-outs shall be sealed with flexible brush seals or sliding covers in a future detailed enclosure design.

Table 10.15: Rolling Door Design Values

Parameter	Value	Status
Clear opening width	7.5 m	Requirement
Clear opening height	3.6 m	Requirement
Door type	Rolling garage door	CAD baseline
Rail cut-outs	Two lower rail passages	CAD baseline
Door detailed mechanism	Not fully modelled	Future detail

10.7.4. Slide-Out Rail and Rack-and-Pinion System

The UAS is carried on a sliding platform, not directly on the floor. Two fixed rails guide the platform on the left and right sides. These rails are always present and extend through the front opening. The central drive uses a rack-and-pinion system mounted along the slide direction. A geared motor on the moving platform drives a pinion against the rack, translating the platform nose-first.

Table 10.16: Slide System Architecture and Moving-Platform Power Interfaces

Part	Function
Fixed left/right rails	Carry and guide the sliding platform
Sliding platform	Carries UAS, docking cradle, and tilt mechanism
Central rack	Provides fixed linear drive path
Pinion and gearmotor	Converts motor torque into platform translation
Stored and extended locks	Remove holding load from drive motor in static states
Limit switches / encoder	Confirm position for interlock logic
Moving power and signal harness	Routes 24 V actuator power and command/feedback lines to the tilt actuators, clamp/release actuators, locking pins, limit switches, encoders, docking sensors, and clamp-state sensors on the moving platform
Cable chain / protected service loop	Manages the moving harness over the 6.8 m slide travel so that power and sensor lines do not snag, tension, or interfere with the rail and rack-and-pinion mechanism
Platform junction box	Provides the local interface between the fixed station wiring and the moving-platform mechanisms, allowing the tilt, clamp, docking, and slide feedback lines to be isolated and serviced

10.7.5. Tail-Pivot Tilt Mechanism

The tilt mechanism rotates the UAS from horizontal storage orientation to vertical launch orientation after the platform has translated outside the enclosure. The current design uses a tail-pivot cradle driven by two side-mounted linear actuators.

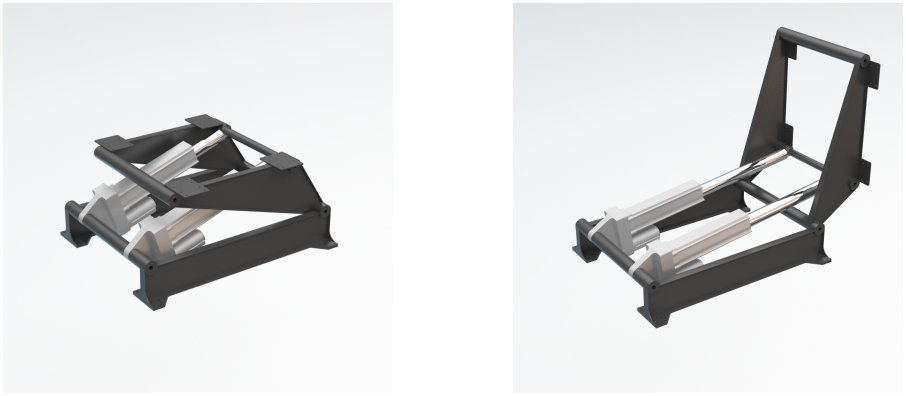

(a) Pivot Mechanism in the Lowered Position **(b)** Pivot Mechanism in the Upright Position

Figure 10.10: Ground Station Pivot Mechanism in the Lowered and Upright Positions

The tilt mechanism is built around a fixed base frame on the sliding platform and a rotating cradle frame connected to the UAS tail interface. The cradle rotates about a bearing-supported pivot shaft and is driven by two linear actuators mounted symmetrically on either side of the structure. Support plates interface with the docking mechanism, while horizontal and vertical hard stops define the motion limits. Locking features secure the cradle in the vertical launch position.

The CAD view is kept at mechanism level rather than showing a high-fidelity UAS attachment model. The UAS orientation is defined by the tail-pivot cradle: the tail interface sits in the rotating cradle, the nose points away from the station during slide-out, and the aircraft rotates to a vertical launch attitude after tilt-up. The detailed guide surfaces, clamp brackets, contact pads, and locking-pin geometry are treated as future detailed-design work in the docking and clamping interface.

The tilt mechanism is currently a representative detailed CAD model. Final actuator loads and joint loads shall be recalculated from the engineering drawing after the exact pivot-to-actuator dimensions, actuator stroke, actuator angles, and cradle side spacing are extracted.

10.7.6. Docking, Clamping, and Release System

The docking, clamping, and release system forms the mechanical interface between the returning UAS and the tail-pivot cradle. It guides the UAS into the cradle, confirms touchdown, transfers docking loads into the structure, restrains the aircraft during motor spool-up, and releases it only after the launch command and safety interlocks are confirmed. The required lateral capture envelope is 0.10 m. The detailed docking hardware is defined at interface level. As shown in Figure 10.8, the logic is supported by UWB anchors, docking-foot contact switches, clamp-state switches, locking-pin switches, clamp load cells, actuator current sensors, and cradle position feedback. Due to time constraints, the guide surfaces, contact pads, clamp brackets, locking-pin geometry, and switch mounts are not fully modelled in CAD. The current model therefore reserves the cradle volume and mounting regions, while the detailed docking geometry remains future work.

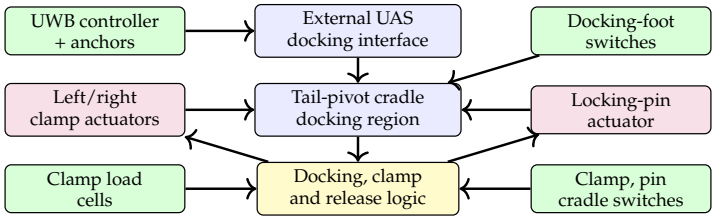

Figure 10.11: Docking, Clamping, and Release Interfaces Derived from the Ground-Station Electrical Architecture

During recovery, UWB anchors support final alignment to the cradle. Docking-foot switches confirm touchdown before clamp closure, while clamp load cells, clamp-state switches, locking-pin switches, and cradle feedback confirm that the UAS is seated, restrained, and ready for restowing.

During launch, the same interface restrains the UAS during low-RPM motor spool-up. Release is

inhibited until the carriage is extended and locked, the cradle is vertical and locked, the clamps are in the correct state, and the release command is confirmed. The locking pin then retracts and the left/right clamps open to release the UAS.

Table 10.17: Docking, Clamping, and Release Design Values

Parameter group	Value / implementation	Status
Docking accuracy and alignment	0.10 m lateral capture envelope; final alignment by UWB controller using anchors 1–4.	Req./baseline
Touchdown and load transfer	Touchdown by docking-foot contact switches 1–4; landing loads transferred through docking feet, cradle support plates, and replaceable contact pads.	Baseline/detail
Docking design load	3.0 kN off-nominal docking load.	Sizing baseline
Launch restraint and release	Left/right tail clamp actuators and locking-pin actuator; release permitted only after door-open, slide-extended, cradle-locked, clamp-state, and release-command interlocks are satisfied.	Baseline
State and health feedback	Clamp open/closed switches, locking-pin engaged/retracted switches, clamp load cells 1–2, cradle angle encoder, upright/horizontal lock switches, and left/right actuator current sensors.	Baseline
CAD maturity	Cradle mounting regions reserved; detailed docking guide geometry, pads, clamp brackets, locking-pin geometry, and switch mounts remain future detailed-design work.	Future detail

The interface summary in Table 10.17 is therefore consistent with the electrical architecture in Figure 10.8 and the functional interface shown in Figure 10.11.

10.8. Mechanical Load Cases

The mechanical load cases define what the ground station must withstand. The table uses simplified load values for readability; detailed calculations are kept in the sizing spreadsheet and mechanism sizing notes. The load application is made explicit because different cases enter the structure through different interfaces. UAS weight, docking, tilt, and launch loads enter through the cradle, clamps, docking feet, sliding platform, rail blocks, and rail supports. Door wind loads enter through the rolling door curtain, guides, and front frame. Global tipping loads are finally reacted by the container feet and the rail-support feet through the ground-support polygon.

Table 10.18: Ground Station Mechanical Load Cases

LC ID	Condition	Description	Loads / Values	Applied to / load path
LC-OGS-01	Stored UAS static support	UAS stored horizontally inside the enclosure.	UAS design weight: 0.74 kN	Cradle supports, sliding platform, rails, and station feet
LC-OGS-02	Rolling door opening	Door opens before deployment.	Opening: 7.5 m by 3.6 m; motor load from door supplier data	Door motor, drum, guides, and door frame
LC-OGS-03	Rolling door closed in gust	Door and frame resist wind when closed.	Door design wind load: 14.22 kN	Door curtain and guides into front frame, base frame, and feet
LC-OGS-04	Slide carriage extension	Platform translates nose-first outside the enclosure.	Slide travel: 6.8 m; design drive force: 2.0 kN	Rack-and-pinion interface between moving platform and fixed rail/base frame
LC-OGS-05	Slide carriage fully extended	Carriage supports UAS and tilt mechanism outside the station.	Moving mass: 395 kg; design vertical load: 5.81 kN	Sliding platform through rail blocks into rail supports and rail feet
LC-OGS-06	Tilt rotation	Cradle rotates UAS from horizontal to vertical.	Design tilt moment: 2.24 kNm; actuator force: 2.93 kN per side	Pivot shaft, actuator mounts, cradle frame, and sliding platform
LC-OGS-07	Cradle locked upright	UAS is held vertically before release.	UAS design weight: 0.74 kN; cradle lock sized with LC-OGS-08	Vertical cradle locks, pivot supports, platform, and rails
LC-OGS-08	Upright UAS in operational gust	UAS held upright in 21 m/s gust.	Wind force: 6.91 kN; overturning moment: 8.55 kNm	UAS/cradle interface into platform, rails, rail feet, and station feet
LC-OGS-09	Restrained low-RPM spool-up	Motors spool while clamps remain closed.	Pre-release thrust design load: 0.22 kN	Tail clamps and locking pins into cradle and platform

Table 10.18: Ground Station Mechanical Load Cases (continued)

LC ID	Condition	Description	Loads / Values	Applied to / load path
LC-OGS-10	Launch release transient	Clamps open and UAS transitions to free flight.	Minimum clamp rating: > 2.0 kN per clamp	Clamp jaws, release actuator, locking pins, and tail interface
LC-OGS-11	Nominal docking impact	UAS lands into cradle at nominal speed.	Nominal landing design load: 0.92 kN	Docking feet/contact pads into cradle, platform, rails, and feet
LC-OGS-12	Off-nominal docking impact	UAS contacts cradle harder than nominal.	Selected docking load: 3.0 kN	Docking feet/contact pads into cradle, platform, rails, and feet
LC-OGS-13	Lateral docking error	UAS enters cradle with lateral offset.	Capture envelope: 0.10 m	Cradle guide surfaces and lateral supports into platform and rails
LC-OGS-14	Tipping with carriage extended	Platform extended outside the enclosure.	Moving mass: 395 kg; design vertical load: 5.81 kN	Combined station and rail-support foot polygon
LC-OGS-15	Tipping in upright gust	Wind acts on upright UAS and cradle.	Overturning moment: 8.55 kNm; check against station mass and foot support polygon	UAS/cradle moment reacted by station and rail-support feet

10.9. Mechanical Sizing and Component Selection

The mechanical sizing calculations are used to convert the ground-station architecture into component-level rating targets. The calculations focus on the mechanisms that drive the design: the slide-out platform, tail-pivot tilt mechanism, rolling door, docking interface, and clamping system. A safety factor of 1.5 is applied to the main structural and mechanism loads.

10.9.1. Sizing Inputs

The current sizing is based on the UAS and mechanism dimensions shown in the CAD model and engineering drawings. The UAS mass is assumed to be 51.13 kg. The stored UAS envelope is taken as 3.2 m by 4.1 m by 2.475 m. From the top-view geometry sketch, the UAS centre of gravity is estimated at approximately 1.60 m from the nose. Since the tail-pivot interface is located near the rear of the UAS, the resulting CG lever arm about the pivot is also approximately 1.60 m.

Table 10.19: Main Mechanical Sizing Inputs

Parameter	Value	Use
UAS mass	51.13 kg	Storage, tilt, launch restraint
UAS length	3.2 m	Tilt moment arm and packaging
UAS width	4.1 m	Station width and recovery clearance
UAS height / propeller envelope	2.475 m	Door and cradle clearance
Estimated UAS CG from nose	1.60 m	Pivot moment calculation
Estimated CG lever arm about tail pivot	1.60 m	Tilt actuator sizing
Slide travel	6.8 m	Deployment timing
Rail spacing	4.920 m	Slide support stability
Rail-block longitudinal spacing	4.789 m	Rail load distribution
Number of rail blocks	4	Vertical support calculation
Pivot base plate thickness	25 mm	Local mounting design
Safety factor	1.5	Design load sizing

10.9.2. Slide System Sizing

The slide-out platform carries the UAS, cradle, tilt mechanism, and auxiliary hardware. The moving mass and corresponding design vertical load are:

$$m_{\text{moving}} = 395 \text{ kg}; \quad W_{\text{moving,design}} = m_{\text{moving}} g SF = 5.81 \text{ kN} \tag{10.5}$$

With four rail blocks, the average design vertical load per block is:

$$F_{\text{block,avg}} = \frac{W_{\text{moving,design}}}{4} = 1.45 \text{ kN} \tag{10.6}$$

The selected rail blocks should therefore have a static capacity comfortably above 1.45 kN per block. A minimum rating of 5 kN per block is selected to account for uneven load sharing, impact during recovery, rail misalignment, and dynamic motion loads. The 4.920 m rail spacing reduces roll sensitivity,

while the 4.8 m spacing between blocks on the same rail improves pitch stability when the platform is extended.
The central rack-and-pinion drive is sized using the selected slide drive force:

$$F_{\text{slide,selected}} = 2.0 \text{ kN} \tag{10.7}$$

For a pinion radius of $r_p = 0.05$ m and drive efficiency $\eta = 0.8$, the required motor torque is:

$$T_{\text{motor}} = \frac{F_{\text{slide}} r_p}{\eta} = 125 \text{ Nm} \tag{10.8}$$

The slide-drive motor should therefore provide:

$$T_{\text{motor,selected}} \geq 150 \text{ Nm} \tag{10.9}$$

The rack shown in CAD is representative; final rack-and-pinion selection is driven by the 2.0 kN tangential drive force and the required motor torque rather than by the visual CAD tooth scale. The final rack, pinion, gearbox, and brake shall be selected as a compatible set.
For a slide travel of $s_{\text{slide}} = 6.8$ m and slide speed of $v_{\text{slide}} = 0.10$ m/s, the slide time is 68 s.
This is acceptable within the 5 min ground launch requirement, leaving time for door opening, charging disconnect, tilt-up, restrained spool-up, and release.

10.9.3. Tilt Mechanism Sizing

The tilt mechanism rotates the UAS from horizontal storage orientation to vertical launch orientation using two linear actuators. From the CAD model, the retracted actuator pin-to-pin length is 1304.87 mm. The available stroke and approximate extended length are:

$$s_{\text{act}} = L_{\text{stroke,end}} - L_{\text{stroke,start}} = 614.53 \text{ mm } L_{\text{act,extended}} = L_{\text{act,retracted}} + s_{\text{act}} = 1919.40 \text{ mm} \tag{10.10}$$

The worst-case tilt load occurs close to the horizontal configuration, where the UAS weight has the largest moment arm about the tail pivot. The UAS and cradle design moments are:

$$M_{\text{UAS}} = m_{\text{UAS}} g x_{\text{CG,pivot}} SF = 1.18 \text{ kNm } M_{\text{cradle}} = m_{\text{cradle}} g x_{\text{cradle}} SF = 1.06 \text{ kNm} \tag{10.11}$$

The total design moment about the pivot is therefore$M_{\text{tilt,design}} = M_{\text{UAS}} + M_{\text{cradle}} = 2.24$ kNm. From the lowered-position drawing, the actuator line is defined by a horizontal offset of 1241.44 mm and a vertical offset of 401.87 mm. The corresponding perpendicular moment arm about the pivot is:

$$r_{\perp} = \frac{x_{\text{act}} z_{\text{act}}}{L_{\text{act,retracted}}} = 0.382 \text{ m} \tag{10.12}$$

With two actuators sharing the moment, the required actuator force per side is:

$$F_{\text{act}} = \frac{M_{\text{tilt,design}}}{2 r_{\perp}} = 2.93 \text{ kN} \tag{10.13}$$

A minimum actuator rating of 5 kN per actuator is selected. This provides margin for friction, imperfect load sharing between left and right actuators, off-axis loads, and transient loads during start/stop motion. The actuator must also include holding capability or be supported by a mechanical lock so that the UAS can remain safely held if power is lost during rotation.

10.9.4. Door and Enclosure Load Considerations

The rolling door opening area and operational-gust dynamic pressure are:

$$A_{\text{door}} = b_{\text{door}} h_{\text{door}} = 27 \text{ m}^2 \; q = \frac{1}{2} \rho V^2 = 270.1 \text{ N/m}^2 \tag{10.14}$$

Using $C_D = 1.3$ and $SF = 1.5$, the closed-door design wind load is:

$$F_{\text{door,design}} = q C_D A_{\text{door}} SF = 14.22 \text{ kN} \tag{10.15}$$

This load sizes the door guides, locking system, and front frame. It does not directly size the rolling door motor, because the motor is governed mainly by curtain mass, drum radius, friction, counterbalancing, and desired opening speed. The final door supplier must therefore provide both the motor rating and the guide/lock wind-load rating.

10.9.5. Docking and Clamp Sizing

The docking interface is sized using the selected off-nominal conservative docking load of 3 kN. This load is applied through the docking feet, replaceable contact pads, and cradle support plates.
The clamp system restrains the UAS during low-RPM motor spool-up and secures it after docking. The preliminary clamp requirement and preferred catalogue rating are:

$$F_{\text{clamp}} \geq 2.0 \text{ kN per clamp } F_{\text{clamp,preferred}} = 5.0 \text{ kN per clamp} \tag{10.16}$$

This margin is appropriate because clamp loads may include off-axis contact, release impulse, wear, and imperfect alignment during recovery. The current interface uses left and right clamp actuators together with a locking-pin actuator.

10.9.6. Off-the-Shelf Component Selection

Table 10.20 converts the sizing results into component-level rating targets. The table does not freeze supplier brands; it defines the required catalogue class and minimum rating for later detailed selection.

Table 10.20: Mechanical Off-the-Shelf Component Selection Targets

Component	Required rating	Selected rating target	Load case
Rolling door package	7.5 m by 3.6 m clear opening	Industrial rolling door package	LC-OGS-02/03
Door guides and locks	14.22 kN closed-door wind load	≥ 15 kN total	LC-OGS-03
Linear rails and blocks	5.81 kN moving design load; 1.45 kN average per block	≥ 5 kN per rail block	LC-OGS-04/05
Central rack-and-pinion	2.0 kN tangential slide-drive force	≥ 3 kN tangential rating	LC-OGS-04
Slide gearmotor	125 Nm calculated torque	≥ 150 Nm with brake	LC-OGS-04
Tilt linear actuators	2.93 kN calculated force per actuator; 614.5 mm stroke	≥ 5 kN per actuator	LC-OGS-06
Pivot shaft and bearings	2.24 kNm design tilt moment plus actuator reactions	Sized from drawing-based reaction check	LC-OGS-06/08
Tail clamps	> 2.0 kN per clamp	5.0 kN preferred	LC-OGS-09/10
Docking pads	3.0 kN off-nominal docking load	≥ 3.0 kN contact capacity	LC-OGS-11/12
Leveling feet	Station support, levelling, and overturning stability	Heavy-duty adjustable feet	LC-OGS-14/15

The most critical mechanical uncertainties are the final UAS CG location, the exact cradle mass properties, the local pivot-bracket stresses, and the detailed docking contact geometry.

10.10. CAD Implementation and Design Iteration

The CAD model was used to check whether the architecture could be physically integrated. It includes the main enclosure, external features, fixed slide rails, deployed sliding platform, and detailed tail-pivot mechanism.
The most important design iterations were:

1. **Door concept refined:** the final CAD uses a rolling garage door because it clears the deployed platform and avoids panel interference.
2. **Slide architecture fixed:** the model uses fixed left and right rails with door cut-outs, plus a central rack-and-pinion drive.
3. **Tilt actuation clarified:** the final CAD uses two linear actuators rather than screw-jack terminology.
4. **External features added:** solar panels, antennas, warning light, ventilation louvre, support feet, and service hatch were added to improve system realism.
5. **Subsystem zoning introduced:** the UAS deployment bay and technical bay are separated to improve safety and maintainability.

The CAD is not a manufacturing release model. Missing details include final door guide design, seal design around rail cut-outs, detailed cable routing, exact actuator mounting loads, detailed clamp geometry, final UAS envelope, and environmental sealing.

10.11. Ground System Verification and Validation

This section summarises the verification and validation status of the OGS subsystem requirements. A check mark indicates that the requirement is currently supported by CAD inspection, analytical sizing, architecture review, or functional-flow verification. A tilde indicates partial verification, where final dimensions, supplier data, integrated simulation, or physical testing are still required. A cross indicates that the requirement is not yet verified.

Table 10.21 summarises the verification and validation status of the key OGS subsystem requirements. Only requirements classified as key in Table 10.2 are included in this condensed table; the remaining driving and non-driving requirements are retained in the full V&V matrix and traceability database.

Table 10.21: Key Ground System Verification and Validation

Req. ID	Verification and Validation Steps	Met
REQ-STK-01-MSN-01-SYS-01-OGS-01	Partially verified through the functional flow and timing budget. Full validation requires integrated launch-sequence demonstration.	~
REQ-STK-03-MSN-04-SYS-06-OGS-02	Partially verified through slide-speed sizing and tilt-sequence architecture. Full validation requires timed deployment test.	~
REQ-STK-03-MSN-04-SYS-07-OGS-03	Partially verified by the control/electrical architecture and functional flow. Software and hardware integration testing is still required.	~
REQ-STK-03-MSN-04-SYS-07-OGS-05	Partially verified by the tail-pivot CAD model. Final actuator geometry and physical rotation testing are still required.	~
REQ-STK-03-MSN-04-SYS-07-OGS-06	Partially verified by clamp load allocation and low-RPM spool-up load case. Clamp-detail testing is still required.	~
REQ-STK-03-MSN-04-SYS-07-OGS-07	Partially verified by the launch sequence logic. Detailed release hardware and jam-free release testing are still required.	~
REQ-STK-03-MSN-04-SYS-07-OGS-08	Partially verified by door-state interlock logic in the functional flow and electrical architecture. PLC testing is still required.	~
REQ-STK-03-MSN-04-SYS-07-OGS-09	Partially verified by slide-position sensing and extended-position lock logic. Integrated sensor testing is still required.	~
REQ-STK-03-MSN-04-SYS-07-OGS-10	Partially verified by tilt-position sensing and vertical-lock logic. Final lock design and testing are still required.	~
REQ-STK-03-MSN-04-SYS-07-OGS-11	Partially verified by clamp-state logic. Hardware testing is still required before this can be fully validated.	~
REQ-STK-05-MSN-06-SYS-11-OGS-13	Partially verified by stored UAS support load case using 51.13 kg and safety factor 1.5. Final structural drawing and detailed stress checks are still required.	~
REQ-STK-05-MSN-06-SYS-13-OGS-14	Partially verified by the 0.10 m docking envelope requirement and UWB/docking architecture. Full validation requires automatic recovery tests.	~
REQ-STK-07-MSN-09-SYS-46-OGS-22	Partially verified by wind load cases for sustained wind operation. Detailed structural verification is still required.	~
REQ-STK-07-MSN-09-SYS-46-OGS-23	Partially verified by gust load cases. Full validation requires final projected area, structural analysis, and wind testing.	~
REQ-STK-12-MSN-15-SYS-27-OGS-25	Partially verified by launch-inhibit logic. ATC interface testing is still required.	~
REQ-STK-12-MSN-15-SYS-27-OGS-26	Partially verified by LTE communication architecture and station-status data path. End-to-end field test is still required.	~
REQ-STK-12-MSN-15-SYS-27-OGS-27	Partially verified by LTE communication architecture and UAS telemetry data path. End-to-end field test is still required.	~
REQ-STK-13-MSN-16-SYS-28-OGS-29	Partially verified by the secondary RF emergency communication architecture and link-budget analysis. Field validation is still required.	~

10.12. Limitations and Future Work

The current ground-station design reaches the level required for subsystem integration, CAD-level packaging, and preliminary mechanical sizing. The enclosure, rolling door, slide system, tail-pivot tilt mechanism, electrical architecture, and communication architecture have been defined to a sufficient level for the final design phase. The pivot-mechanism drawing is used in this report to close the local tilt-system checks, including actuator forces, pivot reactions, bearing loads, bracket stresses, and locking loads.

Several items still remain outside the current design maturity:

- final UAS envelope and centre-of-gravity data must be confirmed;
- the detailed docking and capture mechanism attached to the pivot cradle must be designed;

- the clamp geometry and release interface must be developed beyond the current representative CAD level;
- rolling door cut-out sealing must be designed in detail;
- backup-power capacity must be validated against a full launch-recovery cycle;
- Code Red storage survival requires detailed environmental load definition and enclosure verification;
- automatic docking must be validated with UWB positioning and physical recovery trials;
- 100-cycle durability must be verified through repeated mechanism cycling.

The most important next design step is the detailed design of the docking mechanism that attaches to the pivot cradle. This mechanism must guide the returning UAS into the cradle, absorb docking loads, confirm contact, clamp the aircraft securely, and allow release during the next launch. Its geometry must be developed together with the UAS landing/contact points so that the docking interface, clamp loads, UWB alignment tolerance, and recovery sequence can be verified as one integrated system.

11
Final Design

This chapter presents an overview of the BELLONA final design. First, the budget comparison is presented. The changes in the structure of cost and mass breakdown between subsystems are presented and explained. The integration part presents the layout and how elements are attached. It is concluded with the introduction to the certification process.

11.1. Technical Budgets

Resource allocation was driving the subsystem development along the design process. Evolution of the budgets and relocation of the cost and mass margins from one subsystem to another made it possible to achieve the goal of the converging interdepartmental estimates on the current state of the UAS. The initial values presented at the beginning of the detailed design phase are compared with the final values in this chapter to show how the mass and cost changed over time.
The analysis starts with the initial estimate of weights at the end of the preliminary phase and can be seen in Figure 11.1 together with the final values. The pie charts are sized to represent the budgets decreasing over time by respective circle sizes. The change in the miscellaneous rubric from 10.6% to only 4.8% shows how the design maturity increased the confidence in the final values. The most important changes can be summarized by the Electronics subsystem's decrease in mass due to a change in the energy density. At the same time, larger wing area and mass budget at the lower edge of the ratios used in the industry increased the allowance of the Structures subsystem. The hover authority at 6 km drastically increased the weight of the propellers.

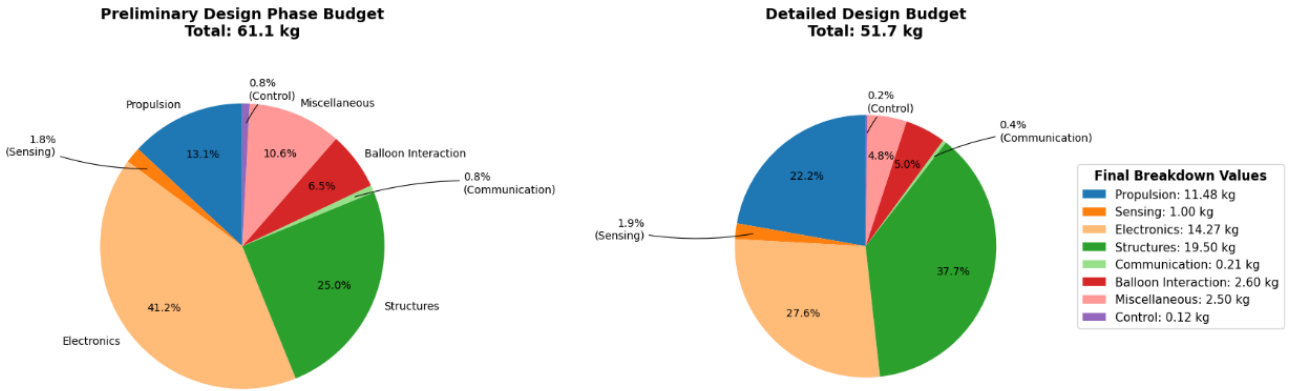

Figure 11.1: Mass Budgets Evolution

The cost budgets are presented in Figure 11.2. The contingencies based on the prices are larger than in the mass estimates. This is due to uncertainty in the suppliers and market state during the start

of the production phase. The growth in confidence is still visible in the diagrams. A large share of the composite materials in the Structures subsystem justifies the budget extension again. Cheaper components found at the existing suppliers make most of the CSE and PPA departments' subsystems take less of the budget.

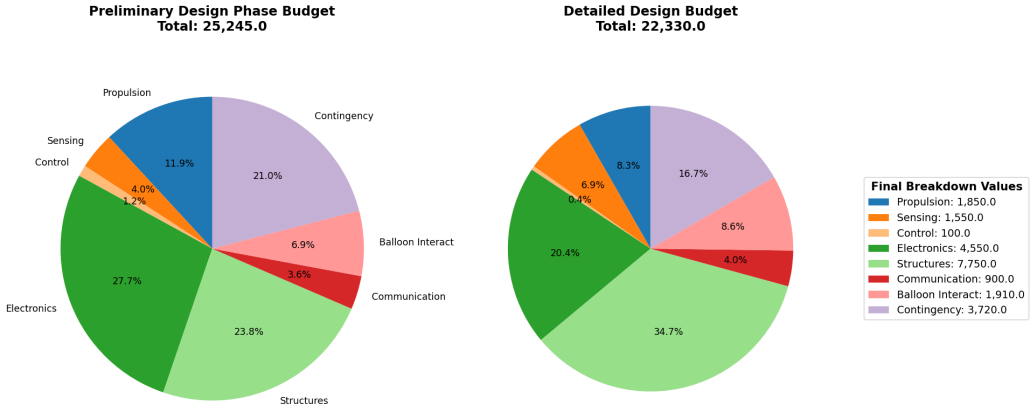

Figure 11.2: Cost Budgets Evolution

The targets set in the Preliminary Design Phase were met by both mass and cost. This means that the initial estimates were accurate enough to make the design process successful.

11.2. CAD Integration

The final BELLONA design is the result of converging all subsystem designs into a single physically and functionally compatible configuration. Integration activities focused on closing the interfaces among structures, propulsion, avionics, the balloon interaction mechanism, and the ground segment, while maintaining compliance with the final mass, power, and cost budgets.

(a) Isometric View **(b)** Top View

Figure 11.3: Final Renders Showing the Isometric and Top Views of the Aircraft

Figure 11.3a shows the final integrated aircraft configuration. This is a clean view with the fuselage skin and tether guide. Clear extrusions for the sensors at the front part and propeller struts integrated with the landing legs and wings are visible. The net cover blends with the fuselage cover, and the nose-fuselage connection ensures the aircraft does not lose its aerodynamic properties. Figure 11.3b presents the aerodynamic boat-tail. This view also helps to understand the configuration and relative placement of all components. The same can be achieved by consulting the Figure 11.4a, which shows the 15 cm clearance between the wing and the propeller. The propeller ducts are not yet sized, but are already presented in the CAD model.

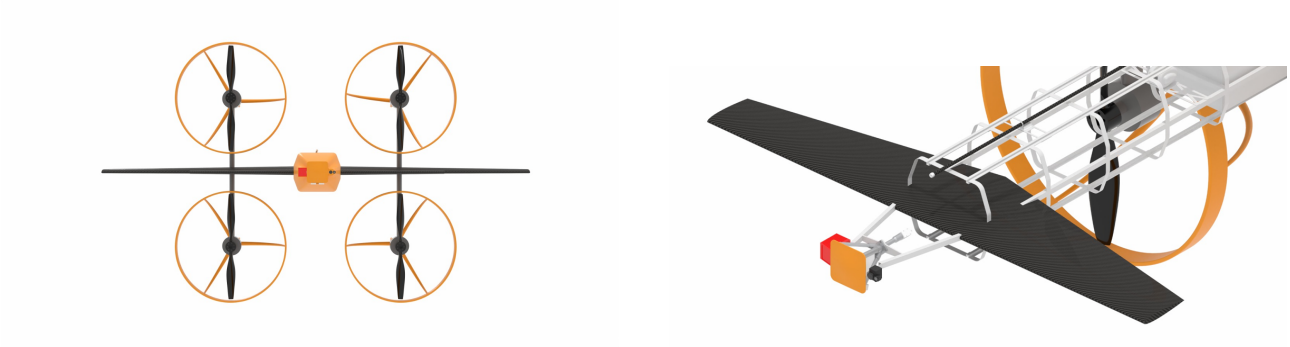

(a) Front View **(b)** Sensors Placement

Figure 11.4: Final Renders Showing the Front and Sensor Views of the Aircraft

The internal sensors layout is presented on Figure 11.4b. The field of View is not obstructed by any other element, and the net gun is also attached to the main fuselage structure by the elements that can transmit the impulse of the net shot.
The missing elements include the integration of a variable-pitch canard and an electrical harness connected to the battery box in the fuselage. The future project plan takes the evolution of the CAD model into account.
The integrated design was verified through iterative updates of the common CAD model and the system budgets. The final configuration closes all major interfaces and provides a consistent baseline for future prototype development and system-level testing.

11.3. Regulatory Compliance and Certification Strategy

Under Commission Delegated Regulation (EU) 2019/945 and Commission Implementing Regulation (EU) 2019/947 [69], UAS operations are classified as Open, Specific, or Certified. BELLONA falls within the Specific Category, requiring operational authorisation from the Dutch National Aviation Authority (ILT) supported by a Specific Operations Risk Assessment (SORA).
The SORA methodology evaluates the Ground Risk Class (GRC; risk to people on the ground) and the Air Risk Class (ARC; risk of collision with manned aircraft) to determine the Safety Assurance and Integrity Level (SAIL), which defines the required operational safety objectives (OSOs). A summary of all the steps required for certification is illustrated in Figure 11.5

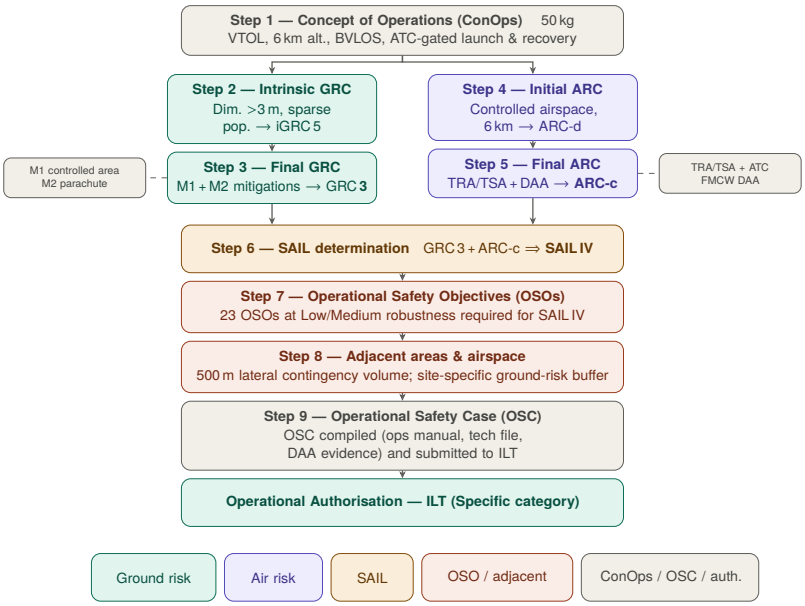

Figure 11.5: SORA Steps Required for Certification

SORA Assessment and Risk Profiles

For a characteristic dimension > 3 m, the operational environment yields an intrinsic iGRC = 5 (based on the baseline scenario of sparse population density and a controlled recovery area). Applying mitigations M1 (ground area restricted, −1) and M2 (recovery parachute, −1) with a Final GRC = 3.

Operational Env.	Controlled ground area	Sparse population	Populated area	Gathering of people
iGRC	4	5	6	7

The operation requires high-altitude intercept operations (150–6000 m AGL) within class C airspace, which leads to an unmitigated ARC of ARC-d. Mitigations include ATC coordination, flight-plan approval, Temporary Reserved/Segregated Airspace (TRA/TSA), and FMCW radar/GNSS-based Detect-and-Avoid (DAA). This bounds the air risk to a governing residual Final ARC = c.
Combining Final GRC = 3 and Final ARC = c yields SAIL IV [70], requiring medium-to-high assurance evidence across 23 OSOs grouped into six compliance domains as detailed in Table 11.1

Table 11.1: Required Evidence Domains for Compliance Assessment

Domain	Evidence Required
Operations	Approved operations manual
Personnel	Training and competency records
Maintenance	Approved maintenance programme
Command & Control	Robustness and failsafe validation
DAA Capability	Total System Performance Requirements (TSPR)-compliant demonstration
Safety & Security	Failure Modes and Effects Analysis (FMEA), software assurance, cyber assessment

Requirements imposed by certification

The SAIL IV classification fixes several design constraints that future iterations must carry forward as inputs. The DAA architecture must demonstrate quantitative TSPR-compliant performance, the airframe and capture-load path must be designed to withstand the proof-load qualification levels required for structural sign-off, and the C2 link, flight software, and ground station must each support the failsafe, FMEA, and cybersecurity evidence. These are necessarily theoretical at the current design stage: concrete thresholds, such as whether anti-collision or position lighting will be mandated as a SAIL IV condition for operating within the Vilnius TMA, cannot be confirmed until formal SORA review and pre-application consultation with the ILT have taken place.

Operational Safety Case and Certification Roadmap

The Operational Safety Case (OSC) submitted to ILT will compile the SORA assessment, operations manual, maintenance programme, technical design file, DAA performance evidence, and ground station documentation. Remaining gaps to achieve readiness are outlined below:

SORA / Ops Manual: Formal review by qualified assessor; final ATC/crew procedures.

DAA / Software: Quantitative TMPR validation; assurance and verification documentation.

Structures / Maintenance: Proof-load qualification testing; approved maintenance process.

Cyber / Airspace: Independent security assessment; Letter of Agreement with ANSP/ATC.

Ground Station: Site approval and equipment qualification.

An early pre-application consultation with the ILT is recommended to validate these SORA assumptions and lock down evidence requirements before final OSC submission.

12 Operations and Logistic Concept Description

This section defines the operational and logistic concept for deploying BELLONA as an airport-based balloon-interception system. Its purpose is to show how the complete system is operated, supported, reset, and scaled at airport level. The concept therefore links the UAS, ground stations, airport operations crew, ATC, and external authorities into one operational sequence.
The concept is based on a pre-approved airport ConOps (Concept of Operations) and airspace coordination framework, while each real launch still requires tactical ATC clearance and operator confirmation. This creates a balance between rapid response and airspace safety: the system is already installed, charged, monitored, and procedurally approved before an incident occurs, but the UAS

is only released when the current traffic, weather, mission geometry, and recovery conditions are acceptable.
Vilnius Airport is used as the reference deployment example because it is representative of the operating environment considered in the certification and market discussion. However, the Vilnius layout is only an example application of the concept. The operational principles are intended to remain applicable to other airports after site-specific station placement, airspace procedures, possible recovery-zone selection, and authority interfaces have been updated.

12.1. Airport Deployment Concept

The reference deployment consists of three relocatable BELLONA ground stations positioned within the airport perimeter. Each station contains one fully assembled UAS, local launch and recovery mechanisms, the station power system, communication equipment, local monitoring sensors, and mission-support hardware. The stations are not permanent buildings, they are containerised or semi-mobile airport assets that can be repositioned if airport layout, runway use, coverage requirements, or authority constraints change.
The primary reason for using three stations is area coverage rather than redundancy. However, the baseline three-station deployment is not intended to cover the entire CTR. Instead, it provides priority response coverage around the airport from feasible airport-side station locations. The final locations are constrained by airport land, service-road access, power availability, obstacle clearance, security control, runway operations, and safe launch orientation. Coverage overlap between stations can still provide degraded backup capability if one station is unavailable, but the baseline assumption remains one active UAS per station.
The reference airport deployment is illustrated in Figure 12.1. The figure should be read as a representative airport-level coverage concept, not as a detailed construction layout or an optimised final station-placement study. Final station positions would require a site survey, local ATC procedures, obstacle assessment, service-road access assessment, power and data connection checks, and airport security approval.

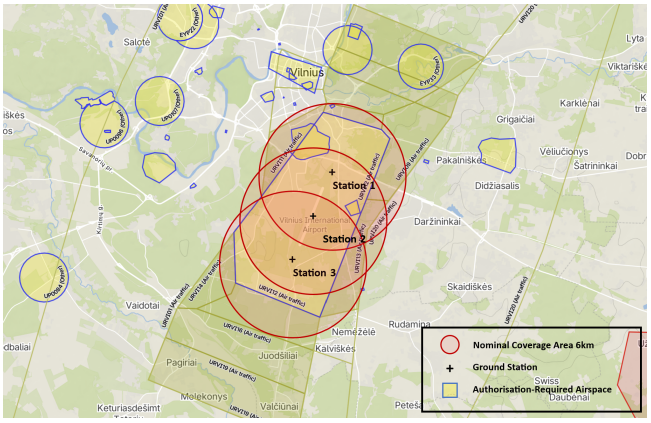

Figure 12.1: Example airport-level deployment concept for three BELLONA ground stations at Vilnius Airport. Red circles show nominal 6 km response coverage from feasible airport-side station locations and Yellow Geometry shows Authorisation-Required Airspace

Each ground station has the same nominal response capability. The coverage radius is linked to the UAS mission envelope. In the current performance model, the UAS is sized for a balloon intercept case with a 6000 m altitude and 6000 m horizontal ground range. At airport level, the nominal coverage footprint should therefore be interpreted as the region in which the UAS can be launched, climb, acquire the target, perform the capture sequence, and still retain sufficient energy margin for controlled descent and return-to-station or safe recovery. Local restrictions such as runway approach paths, obstacle fields, dense public areas, and ATC constraints may reduce the usable part of the geometric coverage region.

12.2. Airspace Coordination and Launch Approval

BELLONA operates in controlled airport airspace and therefore cannot be treated as a stand-alone UAS launch system. The operational concept assumes that the airport, ATC, regulator, airport operations crew, and relevant authority have agreed on a pre-approved ConOps before operational

deployment. This framework defines the station locations, allowed launch conditions, communication responsibilities, emergency procedures, recovery-zone criteria, and the conditions under which temporary reserved or segregated airspace may be activated.
During an actual incident, launch approval remains tactical. The airport operator first observes or receives the balloon track through airport radar or another airport surveillance source. This cue is sent to the selected BELLONA ground station, where the airport operations crew verifies mission feasibility. The UAS is not released until ATC has cleared the mission, the airport operations crew has confirmed the command, the ground station has passed its pre-launch checks, and the mission computer has confirmed that a suitable recovery concept exists. The operational approval chain is included at the start of the nominal mission flow in Figure 12.2.
ATC is responsible for airspace control and tactical clearance. The airport operations crew is responsible for operating BELLONA and confirming that the station is ready to launch. The authority is responsible for recovery and handling of the captured payload or balloon material once it is on the ground. This separation is important because ATC controls the airspace, while the authority handles the physical payload, especially when the payload may be suspicious, hazardous, or security-related.

12.3. Operational Readiness and Station Standby

Each station remains in a mission-ready standby state during the airport-defined operational period. The UAS is stored fully assembled inside the station and connected to the charging interface to maintain battery health and readiness. The station monitors relevant UAS, ground-station, and external parameters, such as battery health, communication status, or local weather.
Airport or local mains power is the primary station supply. Backup batteries are included to complete a launch-recovery cycle where feasible, or to maintain a safe hold state if mains power is interrupted. Solar power may be included as an auxiliary charging source, but it is not treated as the primary power source for immediate launch readiness.
The station-readiness concept is summarised in Table 12.1.

Table 12.1: Operational Standby Concept for One BELLONA Station

Standby element	Operational purpose	Ready condition
UAS storage	Keep the UAS protected, assembled, and mechanically restrained.	UAS secured in cradle and clamps.
Battery connection	Maintain battery health and launch charge state.	Battery within charge and temperature limits.
Station power	Support monitoring, charging, communication, and emergency safe hold.	Mains available or backup power sufficient.
Environmental monitoring	Prevent launch in unsuitable wind, rain, temperature, or visibility conditions.	Weather inside launch envelope.
Communication links	Maintain connection to airport operator, ATC interface, UAS, and station controller.	Valid command and telemetry links.
Mechanism monitoring	Confirm that door, slide, cradle, clamps, and locks are in safe positions.	All mechanisms in commanded standby state.
Launch approval state	Prevent unauthorised or unsafe release.	ATC clearance and operator confirmation required.

Once a valid mission command is received, the station executes the automatic physical deployment sequence. The UAS charging interface is disconnected before motion, the rolling door opens, the slide carriage translates the UAS clear of the enclosure, the cradle rotates the UAS into vertical launch orientation, the motors spool while the UAS remains restrained, and the clamps release only after final launch confirmation. Human presence near the UAS is therefore not required during the physical launch sequence.

12.4. Nominal Mission Flow

The nominal mission begins when a balloon track is detected by airport surveillance and ends when the UAS has returned to its originating ground station and the station has been reset for a new mission.

The mission flow is shown in Figure 12.2. The diagram combines the airport-level operational chain with the UAS mission profile and ground-station state sequence.

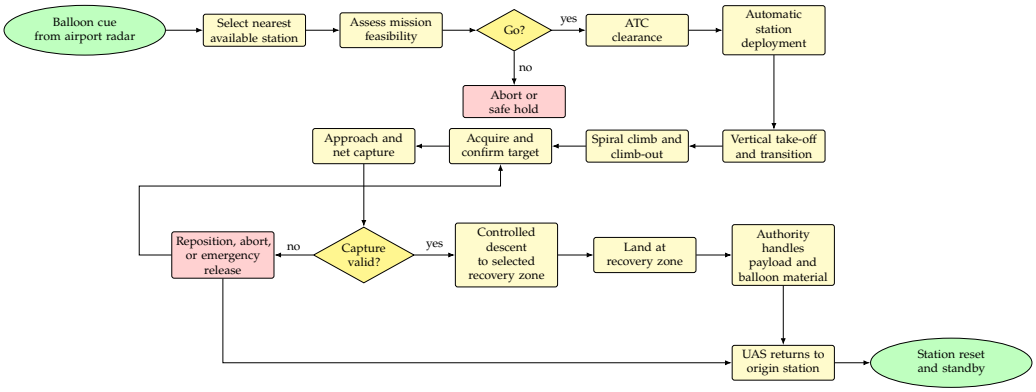

Figure 12.2: Nominal Airport-Level Mission Flow for One BELLONA Sortie, Including the Main Abort Paths

The loop from the off-nominal interaction block back to target acquisition represents repositioning before net deployment, for example when target confirmation or approach geometry is insufficient. It does not imply that the capture mechanism can be fired repeatedly after one net deployment. Once the net has been deployed or the capture state is invalid, the UAS either transitions to the recovery sequence, aborts the interaction, performs emergency release if required, or returns to the origin station when this remains safe and cleared.

The selected UAS trajectory is consistent with the performance model. After station release, the UAS performs a vertical take-off and transitions to wing-borne flight. To avoid overshooting the 6000 m horizontal range before reaching the required altitude, the trajectory uses an initial spiral climb around the launch region before climbing out to the target. The outbound sequence remains inside the 600 s mission budget, while the post-capture phase is governed by target drift, remaining energy, wind, and recovery-zone availability.

12.5. Operational Roles and Interfaces

The operational concept separates responsibilities between airspace control, system operation, and payload handling. This separation avoids ambiguity during high-pressure events and ensures that suspicious payloads are not handled by personnel who are not trained or authorized for that task.

Table 12.2: Operational Roles in the BELLONA Airport ConOps

Role	Responsibility
ATC	Controls the airspace, grants or denies tactical launch clearance, coordinates traffic separation, and manages any temporary reserved or segregated airspace procedures.
Airport operator	Detects or receives the balloon cue from airport surveillance and initiates the BELLONA response chain.
Airport operations crew	Operates the BELLONA station, confirms readiness, monitors mission state, performs post-mission reset, and returns the station to standby.
Ground station controller	Executes automatic station deployment, launch interlocks, charging isolation, mechanical sequencing, docking, restowing, and local health monitoring.
UAS autonomy system	Executes navigation, target acquisition, terminal approach, capture, descent guidance, landing, and return-to-station within approved limits.
Authority	Handles the recovered balloon, payload, suspicious cargo, evidence, disposal, or handover after landing. This may be police, border authority, airport security, or another designated body.
Maintenance personnel	Perform scheduled inspections, repair, component replacement, software updates, and deeper maintenance beyond normal turnaround checks.

The interface logic is shown in Figure 12.3. The airport operations crew does not replace ATC authority over the airspace, and ATC does not handle the recovered payload. The UAS and ground station are controlled through the approved operating procedure and are inhibited from launching unless all required clearances and readiness checks are valid.

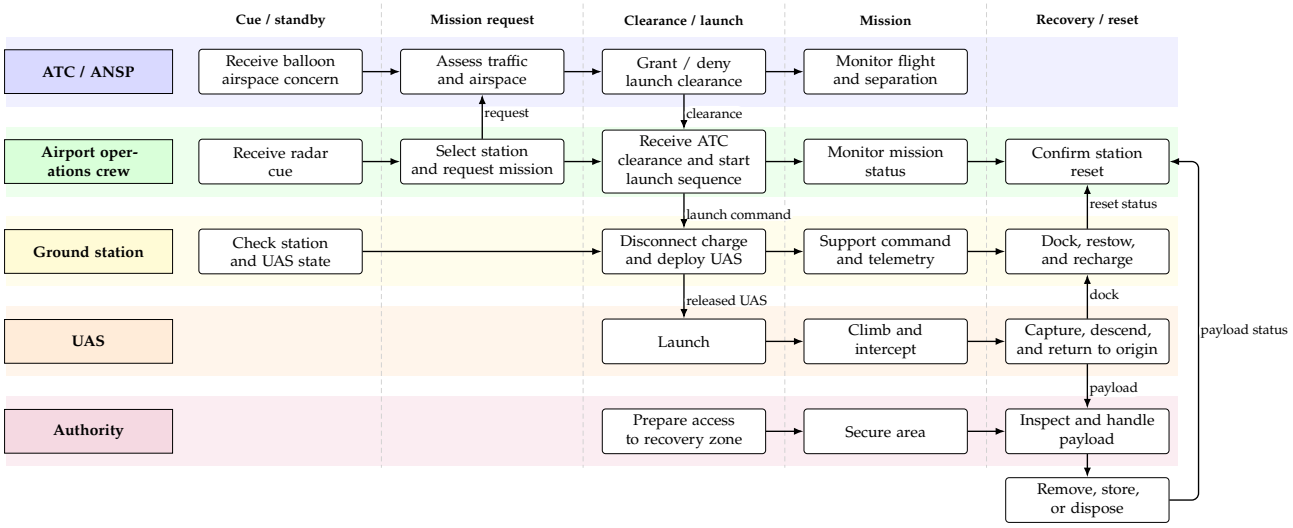

Figure 12.3: Operational Interface Flow Between ATC, Airport Operations Crew, Ground Station, UAS, and Authority

12.6. Dynamic Recovery-Zone Selection

The recovery zone is not fixed before launch. It is selected dynamically because the coupled UAS–balloon payload system is affected by wind drift, balloon residual lift, payload mass, descent duration, remaining energy, and local ground risk. Each station may have preferred local recovery areas, but the actual recovery point can be inside or outside the airport perimeter depending on the target track and wind conditions.

A candidate recovery zone is considered suitable when it satisfies the criteria in Table 12.3. If several candidate zones satisfy these suitability criteria, the selected zone is the one with the lowest combined ground, airside, obstacle, and operational risk. If multiple zones have comparable risk, preference is given to the zone that minimises flight time, simplifies authority access, and preserves the largest remaining energy margin.

Table 12.3: Recovery-Zone Suitability Criteria

Criterion	Selection requirement
Reachability	The zone must be reachable with the remaining battery energy, including wind effects, controlled descent, reserve margin, and return-to-station where applicable.
Ground safety	The zone should avoid passenger areas, public roads, dense occupancy, and areas with frequent vehicle or pedestrian movement.
Airside compatibility	The zone must not conflict with active runway, taxiway, apron, or protected approach/departure operations unless specifically coordinated and cleared.
Obstacle clearance	The zone should provide enough open space to land the UAS and captured system with separation from buildings, masts, fences, parked vehicles, antennas, and lighting systems.
Authority access	The zone must be accessible to the responsible authority through airport service roads, perimeter gates, or coordinated external access routes.
Hazard separation	The zone should avoid fuel storage, power infrastructure, critical airport systems, and other sensitive or hazardous locations.
Operational awareness	The mission must remain monitorable through adequate communication, telemetry, and situational awareness.

When the UAS reaches the selected recovery zone, the priority is to place the captured payload and balloon material into a controlled ground state. After landing, the UAS remains safe and restrained until the authority has secured or removed the payload and balloon material. The nominal concept then allows the UAS to return to its originating station, provided that the UAS state, energy margin, weather, link quality, and ATC clearance remain acceptable. If return-to-station is not possible, the UAS remains at the recovery location for manual retrieval by the airport operations crew or designated

maintenance personnel.

12.7. Off-Nominal and Abort Concept

The system must be able to abort before launch, during climb, terminal approach, capture, and recovery. Abort decisions depend on UAS state, target state, airspace state, and predicted recovery outcome. The UAS is not committed to physical interaction unless the target is confirmed, energy margin remains sufficient, a suitable recovery zone exists, and abort options are still available. The main off-nominal cases are summarised in Table 12.4.

Table 12.4: Operational Abort and Contingency Cases

Mission phase	Trigger	Operational response
Pre-launch	Failed station check, no ATC clearance, poor weather, insufficient battery, or invalid operator approval.	Launch is inhibited and the station remains in safe hold.
Launch deployment	Door, slide, cradle, clamp, charging disconnect, or lock confirmation fails.	Motion stops, the UAS remains restrained, and the station enters safe hold until inspected.
Climb and intercept	Loss of communication, excessive wind, insufficient energy margin, or airspace conflict.	The UAS returns to station, enters holding, or lands at a predefined safe location according to ATC instruction.
Terminal approach	Target is not confirmed, tracking quality is poor, or interaction geometry is unsafe.	The UAS repositions, reattempts the approach, or aborts before net launch.
Capture	Net fails to deploy, partial capture occurs, excessive tether load is detected, or payload swing becomes unacceptable.	If no net has been deployed, the UAS may reposition for a new approach. After deployment or partial capture, it aborts, releases if required, or activates emergency payload-protection logic.
Recovery descent	Predicted landing zone becomes unsuitable or energy margin becomes insufficient.	The recovery zone is reselected, or the UAS proceeds to the safest reachable zone.
Post-landing	Payload is suspicious, hazardous, or security-related.	Airport operations crew keeps clear; the responsible authority secures, inspects, removes, or disposes of the payload.
Return-to-station	The UAS cannot safely depart the recovery zone or lacks energy margin.	The UAS remains secured at the recovery location and is retrieved manually.

12.8. Payload Handover and Authority Recovery

Payload recovery is separated from UAS operation. After landing in the selected recovery zone, the authority is responsible for payload approach, inspection, removal, storage, evidence handling, or disposal. This role may be fulfilled by police, border authority, airport security, or another designated body depending on the incident. For normal meteorological or scientific payloads, the authority may recover the payload and balloon material for disposal or return to the owner. For suspicious, smuggling-related, or unknown payloads, the airport operations crew should not handle the payload unless local procedure explicitly assigns that role. Their responsibility is to maintain UAS safety, coordinate with ATC and station systems, and support the authority with location and mission data.

BELLONA lands → UAS safed → authority secures payload → payload removed → UAS cleared to return.

This prevents the UAS operator role from becoming a law-enforcement or hazardous-material handling role, while ensuring that the captured balloon system is not left uncontrolled after landing.

12.9. Post-Mission Logistic Reset

After payload handover, the nominal procedure is for the UAS to return to the same ground station from which it launched. Returning to the origin station simplifies inventory control, battery tracking,

maintenance records, mission-kit replacement, and responsibility assignment. Cross-station recovery may be possible in future operational versions, but is not part of the baseline logistics concept. The post-mission reset flow in Figure 12.4 combines automatic station actions with mandatory human turnaround inspection.

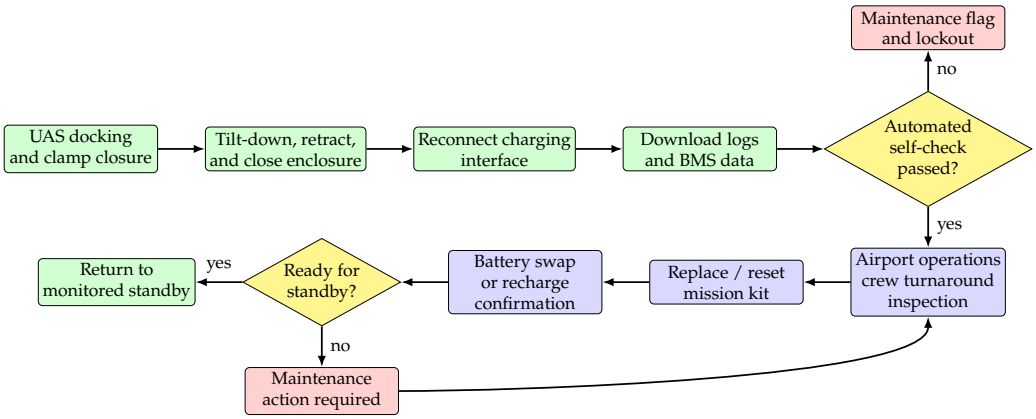

Figure 12.4: Post-Mission Logistic Reset Flow for One BELLONA Ground Station

The reset process is based on modular mission kits, containing items directly affected by the interaction and requiring replacement, repacking, or detailed inspection after use: net, tether, launcher consumables, reel interface, closure line, and emergency parachute pack where applicable. Instead of repacking all items under time pressure inside the station, the used kit is removed and replaced with a pre-packed serviceable kit, then inspected, cleaned, repaired, repacked, or discarded offline according to maintenance rules.

Table 12.5: Mandatory Post-Mission Turnaround

UAS, battery, and mission data	Mission-kit and station inspection
Safing: isolate and safe the UAS after docking.	Structure: inspect propellers, motor mounts, landing supports, and visible structure.
Data: download flight logs, mission data, battery data, and station logs.	Capture hardware: inspect the tether hardpoint, reel bracket, tether, net, closure line, and launcher area.
Battery: check battery state, battery temperature history, and charge acceptance.	Consumables: replace fired cartridges or launcher consumables where applicable.
Emergency systems: check the emergency release and parachute system if it was armed, triggered, or exposed to abnormal loads.	Sensors and references: clean or check sensors, docking references, UWB anchors, cameras, and communication hardware.
Readiness: sign off the station as mission-ready or place it into maintenance lockout.	Station systems: confirm that the station door, slide, cradle, clamps, locks, charging interface, and warning systems are functional.

12.10. Maintenance and Availability Concept

The availability concept is based on one UAS per station, supported by rapid post-mission turnaround and scheduled maintenance. Since the three-station layout is primarily for coverage, losing one station reduces covered area or response quality rather than simply removing a redundant spare. Maintenance planning should therefore avoid taking multiple stations offline at the same time. The maintenance basis is 20 missions per year over a 5-year service life, giving 100 missions before major overhaul or replacement of life-limited elements. This basis is used for the operational logistics concept and should be updated if the business model or reliability analysis adopts a different mission rate.

Table 12.6: Maintenance Levels for the BELLONA Operational Concept

Level	Interval	Purpose and scope
Level 1: Turnaround	After every mission	Airport operations crew performs station reset, mission-kit replacement, visual inspection, battery check, log download, safing confirmation, and standby release.
Level 2: Scheduled maintenance	Periodic, based on mission count or calendar interval	Maintenance personnel inspect wear items, docking accuracy, rails, clamps, launcher condition, battery health, calibration, backup power, communication equipment, and software logs.
Level 3: Major overhaul	After 100 missions or 5 years, unless earlier triggered	Deep inspection or replacement of life-limited components, structural hardpoint checks, launcher and reel refurbishment, battery replacement decision, software update, and complete station qualification check.
Condition-based maintenance	Any time abnormal loads, failed checks, hard landing, emergency release, or thermal warning occurs	Station enters lockout until the affected subsystem is inspected and released by maintenance personnel.

This layered concept avoids unnecessary major maintenance after every flight while still requiring a human safety check after each mission. The UAS is therefore not treated as a fully unattended system after recovery. Automatic docking and self-checks reduce workload, but the final return-to-standby decision remains dependent on a documented post-mission inspection.

12.11. Operational Design Implications

The operations and logistics concept creates system-level design constraints for the final BELLONA system, linking airport deployment to the UAS, ground station, communications, maintenance, and certification strategy. These implications are summarised in Table 12.7.

Table 12.7: Design Implications from the Operations and Logistics Concept

Area	Implication
Station placement	Stations must provide priority airport-centred response coverage while maintaining service-road access, power availability, obstacle clearance, security control, and safe launch orientation.
Airspace integration	The system requires pre-approved procedures, tactical ATC clearance, operator confirmation, abort logic, and compatibility with temporary reserved or segregated airspace.
Mission planning	Station selection must account for target track, wind, energy margin, recovery-zone availability, airspace state, and station readiness.
Recovery planning	Recovery zones must be selected dynamically using safety, reachability, obstacle, authority-access, and airside-compatibility criteria.
Payload handling	Suspicious or security-related payloads are handled by the authority, not the airport operations crew, unless local procedures state otherwise.
Ground-station design	The station must support automatic launch and recovery, safe charging, backup power, environmental monitoring, warning states, interlocks, and maintenance lockout.
UAS design	The UAS must launch from a restrained vertical state, climb within the mission budget, acquire the target, descend under control, land at a dynamic recovery zone, and return to the origin station where feasible.
Logistics	Mission-kit elements such as nets, tethers, launcher consumables, closure lines, and emergency packs should be modular for quick exchange and offline inspection.
Availability	Since three stations mainly provide coverage, maintenance must avoid simultaneous downtime of multiple stations.
Lifecycle	The baseline maintenance assumption is 20 missions per year over 5 years, with 100 missions before major overhaul or replacement of life-limited elements.

Overall, this concept turns BELLONA from a single UAS into an airport response capability. The three-station layout provides priority response coverage around the airport, while pre-approved ConOps and tactical ATC clearance keep launches compatible with controlled airspace. Dynamic recovery-zone logic ensures capture is only attempted when the post-capture state can be managed safely. The reset and maintenance concept then returns the system to standby without treating the UAS as disposable or assuming unrealistic fully unattended recovery.

13 Reliability, Availability, Maintainability, and Safety Characteristics

The Reliability, Availability, Maintainability and Safety (RAMS) characteristics describe the basis for safe and reliable operation of BELLONA. Based on the operational sequence described in Chapter 12, this chapter translates the operational concept into reliability, availability, maintainability, and safety characteristics that all subsystems must satisfy.
The RAMS objective is to ensure that BELLONA can complete a balloon-interception mission without introducing unacceptable risk to aircraft, airport users, ground personnel, infrastructure, or the recovered payload-handling process.

13.1. RAMS Boundary and Assumptions

The RAMS assessment covers all BELLONA subsytems, meaning external airport procedures, ATC decision-making, and authority payload handling are treated as operational interfaces rather than RAMS design items.
The main assumptions used for the RAMS baseline are:

- the UAS is stored fully assembled and restrained in the ground station before launch;
- launch is inhibited unless station checks, UAS checks, tactical clearance, and the authorised launch command are valid;
- the mission profile includes vertical launch, transition, climb, target acquisition, capture, controlled descent, and recovery;
- the system is designed for repeated operational use rather than single-use interception;
- abnormal loads, hard landings, emergency releases, thermal warnings, or failed self-checks trigger maintenance lockout.

13.2. Safety-Critical Functions and Characteristics

The safety-critical functions are the functions whose failure could lead to loss of control, unsafe release, collision risk, uncontrolled descent, or unsafe payload handling. To avoid repetition, these technical functions, their failure triggers, and their exact fail-safe behaviors are detailed in Table 12.4 within the operational concept (Section 12.7).
The RAMS layer establishes the mandatory safety constraints (what the system must prevent), which relate directly to the operational layer via the automated states, software blocks, and recovery pathways mapped in Figure 12.2.

13.2.1. Reliability Characteristics

Reliability is defined as the ability of the UAS and ground station to perform the commanded mission without failure of a safety-critical function. For BELLONA, reliability is most important during launch, transition, target acquisition, capture, recovery descent, and docking or safe landing. The design should therefore minimise single points of failure in functions that directly affect controllability, release inhibition, capture safety, and emergency recovery.
The main reliability characteristics are detailed in Table 13.1:

Table 13.1: Reliability Characteristics Definition

Characteristic	RAMS Requirements and Design Logic
Fault tolerance in flight control	The flight control architecture shall remain stable after credible single-sensor or single-actuator faults, or shall transition to a controlled abort mode.
Reliable launch interlocking	Mechanical release shall require positive confirmation of station state, UAS state, charging isolation, clearance state, and authorised launch command.
Robust sensing	Target acquisition and relative navigation shall use sensor consistency checks to prevent capture attempts based on uncertain or degraded measurements.
Reliable capture decision logic	The net-launch command shall be inhibited unless target confirmation, geometry, closure rate, tether state, and recovery feasibility are valid.
Graceful degradation	Failures shall lead to safe hold, retry, abort, return, or controlled landing rather than immediate mission loss.
Logged fault evidence	All safety-relevant failures shall be recorded so that repeated faults can be identified before the next mission.

13.2.2. Availability Characteristics

Availability is defined as the probability that the BELLONA system is ready to perform a mission when requested. In the RAMS context, availability is not the same as the airport deployment layout. The operational chapter defines how multiple stations are positioned and used. RAMS instead defines the characteristics that allow each station to remain serviceable and prevent unsafe availability claims. The availability characteristics are detailed in Table 13.2:

Table 13.2: Availability Characteristics Definition

Characteristic	RAMS Requirements and Design Logic
Readiness monitoring	Each station shall continuously report whether the UAS, battery, communication links, launch mechanisms, and safety interlocks are available for mission use.
Automatic fault isolation	The system shall identify whether an unavailable state is caused by the UAS, ground station, battery, launch mechanism, communication system, or software state.
No false-ready state	A station shall not be reported as mission-ready if any safety-critical check is failed, bypassed, stale, or unknown.
Degraded availability reporting	If one subsystem is unavailable, the system shall distinguish between complete station unavailability and reduced mission capability.
Maintenance lockout integration	Any abnormal event shall automatically remove the affected UAS or station from available status until inspection release.

13.2.3. Maintainability Characteristics

Maintainability is the ability to inspect, repair, reset, and release the system for further use with limited downtime and without hidden damage. The detailed turnaround procedure is part of the Operations and Logistics concept. In RAMS, maintainability is limited to the design characteristics that make that procedure safe and repeatable.
The maintainability characteristics are detailed in Table 13.3

Table 13.3: Maintainability Characteristics Definition

Characteristic	RAMS Requirements and Design Logic
Modular replacement	Mission-affected items such as nets, tethers, launcher consumables, reel interfaces, and emergency packs should be replaceable as modules rather than repaired under time pressure.
Accessible inspection points	Safety-critical structures, hardpoints, propulsion units, clamps, rails, charging interfaces, and tether-load paths shall be inspectable without major disassembly.
Built-in test capability	The UAS and ground station shall support automatic checks of sensors, actuators, interlocks, battery state, communication links, and stored fault states.
Clear release criteria	The system shall define objective conditions for returning to standby, including successful self-checks, no active lockouts, valid battery state, and inspection sign-off.

Table 13.3: Maintainability Characteristics Definition (continued)

Characteristic	RAMS Requirements and Design Logic
Traceable maintenance records	Mission count, fault history, battery history, emergency events, and replaced modules shall be recorded for each UAS and station.

13.2.4. Safety Characteristics

Safety is defined as the ability of BELLONA to prevent unacceptable risk to air traffic, people, infrastructure, and payload-handling personnel. The safety concept is based on prevention first, followed by controlled abort, controlled recovery, and maintenance lockout.
The main safety barriers are detailed in Table 13.4:

Table 13.4: Safety Barriers Definition

Barrier Type	RAMS Requirements and Design Logic
Pre-launch barriers	Launch inhibition, station readiness checks, UAS readiness checks, weather checks, clearance-state verification, and authorised launch-command validation.
In-flight barriers	Geofencing, trajectory monitoring, target-confirmation logic, energy-margin monitoring, lost-link logic, and abort modes.
Capture barriers	Net-launch inhibition unless target certainty, approach geometry, tether state, and recovery feasibility are acceptable.
Recovery barriers	Controlled descent, dynamic recovery-zone validation, emergency release where required, and emergency parachute recovery for catastrophic cases.
Post-event barriers	After abnormal loads, hard landing, emergency release, thermal warning, failed self-check, or structural concern, the system automatically locks out.

13.3. RAMS Verification Approach

RAMS compliance shall be demonstrated using a combination of analysis, simulation, inspection, ground testing, flight testing, and operational evidence. The verification approach is summarised in Table 13.5.

Table 13.5: RAMS Verification Approach

RAMS area	Verification method	Evidence produced
Reliability	Failure-mode analysis, subsystem tests, endurance tests, and mission simulation.	Failure logs, reliability estimates, fault-response results, and endurance-test records.
Availability	Readiness-state testing, lockout testing, and station health-monitoring tests.	Availability status logic, no-false-ready checks, and degraded-state reports.
Maintainability	Inspection trials, module replacement trials, access checks, and maintenance-record review.	Replacement times, inspection checklists, maintenance logs, and release records.
Safety	Hazard analysis, abort-mode testing, lost-link testing, emergency recovery testing, and operational simulation.	Hazard mitigation matrix, abort validation, emergency-mode results, and safety-case evidence.

14
Production Plan

The plan focuses on the manufacturing, assembly and integration sequence. Its purpose is to identify the main build steps, integration gates and acceptance checks for building the system.
The production approach is modular. Major subsystems are manufactured separately, and integrated only after their interfaces have been checked. Modularity supports inspection and replacement after a mission, reducing lifecycle cost and avoiding unnecessary replacement of the primary airframe.

14.1. Production Scope and Assumptions

The plan assumes a low-rate small-series production. Commercial off-the-shelf components are used where possible, while custom manufacturing is reserved for the composite airframe, metallic

load-introduction fittings, battery support structure, balloon-interaction mounts, ground-station interfaces and integration brackets or fairings.
Production starts only after the main configuration items have been frozen. This frozen build baseline corresponds to the start block of the MAI flow in Figure 14.1.

14.2. Production Streams

The first production phase consists of parallel manufacturing and procurement streams. Long-lead commercial components are ordered first, while custom structural, electrical and balloon-interaction parts are manufactured in parallel. The main streams are summarised in Table 14.1.

Table 14.1: Main BELLONA Production Streams Before Final Integration

Stream	Main items	Release condition before integration
Airframe structure	Wing, canard, fuselage frame, motor and landing supports, battery tray and hardpoints.	Laminate quality, dimensions, hole alignment and hardpoint access accepted by the structural check.
Propulsion module	Motors, ESCs, propellers, local wiring and propulsion mounting hardware.	Propulsion module assembled and accepted by the propulsion functional check.
Electrical and avionics	Battery, BMS, contactors, fuses, DC/DC converter, controller, sensors, radios and harnesses.	Power and signal wiring, labels, polarity, continuity, insulation and data links accepted by the electrical and data check.
Balloon-interaction module	Launcher, net package, tether, reel, guide, closure line and parachute container.	Launcher safe state, tether deployment, routing and reset behaviour accepted by the mechanism dry-run gate.
Ground station	Bay, rails, pivot, charging interface, antennas, interlocks and control electronics.	Mechanical fit, command link, charging access and emergency removal accepted by the ground-station check.

14.3. Assembly and Integration Flow

The complete assembly sequence is shown in Figure 14.1. The flow is organised as a swimlane diagram. Each lane represents one production stream, while the flow direction represents the progression from the frozen build baseline, through module production and checks, toward aircraft integration, ground-station coupling and release to testing.

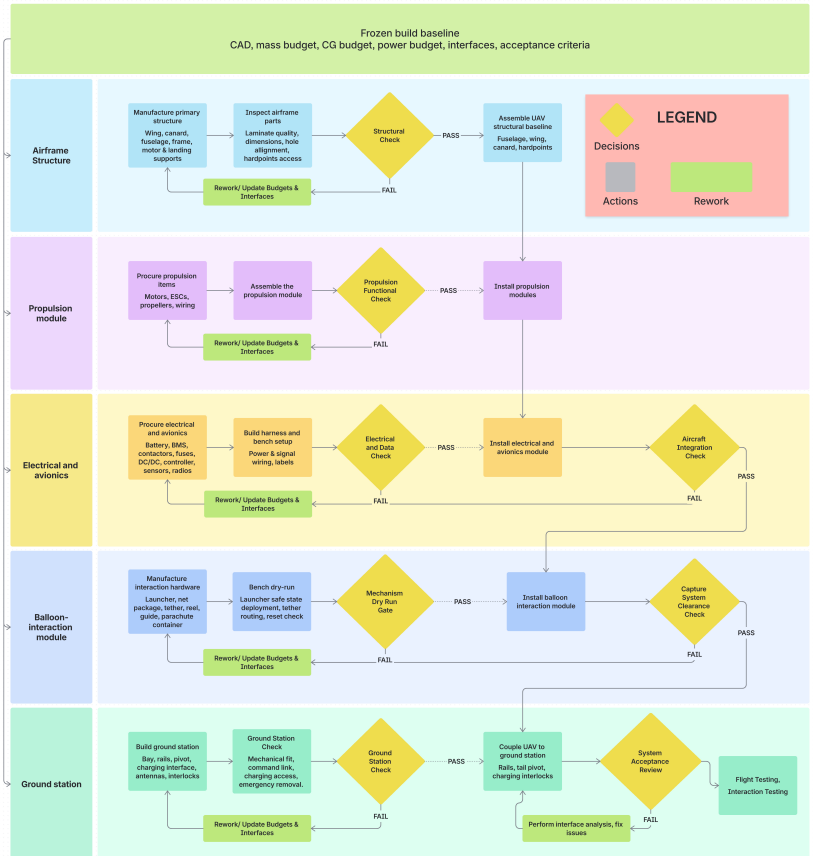

Figure 14.1: Manufacturing, Assembly and Integration Flow for the BELLONA System. Subsystems Are Produced and Checked in Parallel Before Staged Aircraft-Level and Ground-Station Integration

The flow starts from the frozen build baseline, which fixes the CAD layout, mass budget, centre-of-gravity budget, power budget, interfaces and acceptance criteria. The airframe, propulsion, electrical and avionics, balloon-interaction and ground-station streams are then developed in parallel. Failed checks do not proceed directly into integration. Instead, they return to rework, where the affected drawings, budgets and interfaces are updated before the module is released again.

Aircraft assembly starts with the airframe structure. The wing, canard, fuselage frame, motor supports, battery tray and hardpoints are manufactured, inspected and released through the structural check. The propulsion module is installed after the propulsion functional check, followed by the electrical and avionics module after the electrical and data check.

The aircraft integration check is performed after the structural, propulsion, electrical and avionics modules have been installed. This check confirms that the installed aircraft remains consistent with the released configuration and that the basic mass, centre-of-gravity, power, data and emergency-shutdown paths are acceptable.

The balloon-interaction module is integrated only after the aircraft integration check. The launcher, net, tether, reel, guide and parachute container are fitted to the reinforced mounting locations. The capture-system clearance check then verifies the tether path, reel motion, launcher clearance, parachute-container access and absence of interference with the aircraft structure or propeller clearance zones.

The ground station is produced and checked in parallel with the UAS. It is coupled to the aircraft only after the ground-station check has confirmed the mechanical fit, command link, charging access and emergency-removal path. Remaining interface issues are corrected before the system acceptance review and release to flight and interaction testing.

14.4. Integration Gates

The production process is controlled using integration gates. Each gate produces a clear output that must be inspected, demonstrated or tested before the next integration step begins. The main gates are

summarised in Table 14.2.

Table 14.2: Main Production and Integration Gates for the BELLONA System

Gate	Purpose	Acceptance output
Structural check	Confirm that the primary structure and hardpoints match the released CAD and load-path assumptions.	Laminate quality, dimensions, hole alignment and hardpoint access accepted.
Propulsion functional check	Confirm that each propulsion module is ready for aircraft installation.	ESC communication, motor direction, mounting condition and low-power motor operation accepted.
Electrical and data check	Confirm that the power, signal and data paths can be energised and monitored safely.	Continuity, polarity, insulation, connector labelling, sensor data and telemetry links accepted.
Mechanism dry-run gate	Confirm that the balloon-interaction hardware moves through its intended states without interference.	Launcher safe state, tether deployment, tether routing, reel motion and reset behaviour accepted.
Ground-station check	Confirm that the standalone ground station is ready to interface with the aircraft.	Mechanical fit, command link, charging access, interlocks and emergency removal accepted.
Aircraft integration check	Confirm that the airframe, propulsion, electrical and avionics modules form a coherent aircraft configuration.	Updated mass and centre-of-gravity record, power-on result, data-link result and emergency-shutdown check accepted.
Capture-system clearance check	Confirm that the balloon-interaction subsystem can be installed and operated without local interference.	Tether path, reel motion, launcher clearance, parachute-container access and propeller-clearance zones accepted.
System acceptance review	Confirm that the aircraft, ground station and interaction subsystem are ready for controlled testing.	Open-issue list reviewed, safety-critical interfaces accepted and release to flight and interaction testing approved.

These gates connect the production plan to the distributed verification and validation evidence presented in the relevant subsystem chapters. In the production plan, inspection is used for geometry, material, access and installation checks, while demonstration is used for arming, shutdown, interlocks, reel motion and parachute-door actuation. Quantitative tests such as propulsion loading, communication performance, tether strength and launcher repeatability are not defined as production gates themselves. Instead, they are handed over to the corresponding subsystem V&V sections, where the detailed procedures, acceptance limits and remaining open verification items are defined.

14.5. Release to Flight and Interaction Testing

After final integration, the system is released to flight and interaction testing through the system acceptance review. This review confirms that the aircraft mass and centre of gravity are recorded, all module-level checks are closed, safety-critical interfaces are inspected, and unresolved issues are listed before controlled testing begins.

The verification and validation evidence is distributed across the relevant subsystem sections. The production plan therefore only defines the release conditions for testing: module-level checks must be closed, safety-critical interfaces must be accepted, and unresolved issues must be recorded before controlled testing begins. Detailed compliance evidence remains in the respective subsystem V&V tables and verification discussions.

14.6. Post-Mission Reset and Reuse

Post-mission reset is included in the production logic because BELLONA is intended to be reusable rather than rebuilt after each sortie. After landing, the aircraft is powered down, the high-voltage system is isolated, the launcher is safed, and mission telemetry, interaction logs and BMS data are downloaded before hardware inspection.

The reset inspection focuses on components most likely to experience wear or local damage: propellers, motor mounts, landing supports, battery restraint, tether hardpoint, reel bracket, tether, net, launcher, guide, parachute container and electrical connectors. Worn soft goods, propellers, pads or fastening elements are replaced as field-level items. A new mission is authorised only after the reset checklist confirms structural serviceability, acceptable battery health, correct net and tether packing, smooth

reel operation, sensor calibration, communication availability and ground-station clearance.

14.7. Production Limitations and Future Work

The present plan is suitable for preliminary design and prototype planning. A manufacturing release would require additional production detail before hardware fabrication, including released engineering drawings, tolerances, laminate schedules, bonding procedures, fastener specifications, harness drawings, battery-pack assembly procedures, tooling definitions, ground-support equipment drawings, supplier quality requirements and final acceptance-test limits.

The next design phase should convert the current CAD model and subsystem budgets into an interface-controlled manufacturing package. The most critical drawings are the tether hardpoint, reel support, launcher mount, battery tray, motor mounts, tail-pivot mechanism and deployment-platform interface, since these parts govern the main concentrated loads, safety-critical motion paths and maintenance access points of the BELLONA system.

15
Risk Assessment

Risk management is used to identify, assess, and control the driving uncertainties affecting the development and operation of the BELLONA system. Since the mission involves the detection, interception, interaction, and recovery of an uncooperative free-floating balloon, several technical and operational risks must be considered. They are of critical importance because failures during interaction or recovery could jeopardize the reusability of the system, regulatory compliance, the mission, and public safety.

15.1. Methodology Overview

The analysis considers both department-specific risks and system-level risks that arise from subsystem interaction, such as mechanical interfaces, data exchange, power budgets, and mission-phase dependencies. The first step is risk planning, where responsibilities are assigned and the structure of the risk register is defined. Each risk is linked to a responsible department or team member to ensure that mitigation actions can be followed up during the project [71]. In addition, each risk is assigned a unique identifier to maintain clear traceability and organization within the risk register. The second step is risk identification. In this stage, possible adverse outcomes are identified based on the mission phases, functional flow diagram, subsystem responsibilities, and system-level interfaces. This includes both technical risks within individual departments and general integration risks between subsystems [71].

After identification, each risk is assessed using two parameters: probability and impact. Probability describes how likely the risk is to occur, while impact describes the severity of its consequences if it occurs. Both are rated on a scale from 1 to 5, as described in Table 15.1. The combination of these two values gives an indication of the initial risk level and allows the most critical risks to be prioritized. The risk analysis step then considers which prevention and contingency measures are appropriate. Prevention measures aim to reduce the probability of occurrence, while contingency measures reduce the impact if the risk still occurs [71].

For each risk, an initial risk score is obtained by multiplying the probability and impact ratings:

$$R = P \cdot I, \qquad R_r = P_r \cdot I_r \tag{15.1}$$

where P_r and I_r are the residual probability and impact after prevention and contingency measures have been considered. These scores are not used as absolute measures of risk, but as a consistent way to compare and prioritize risks within the project.

The probability score was assigned based on the likelihood of the failure occurring, considering design maturity, environmental uncertainty, subsystem complexity, number of interfaces, and availability of verification data. The impact score was assigned based on the severity of the consequence for mission success, public safety, regulatory compliance, cost, and schedule if the risk were to occur. As such, the probability and impact values are prone to change as the design advances into more complex stages.

Finally, the risks are handled by assigning mitigation actions and estimating the residual probability and impact after mitigation. These residual values are used to evaluate whether the risk has been reduced to an acceptable level or whether further design changes are needed [71]. As such, the complete risk register is presented in Table 15.2. The risk register must be continuously updated throughout the project, as the probability, impact, and relevance of each risk may change as the design matures, subsystem interfaces are defined, and additional analyses are completed. The addition or removal of risks is documented in Section 15.3.

Table 15.1: Risk Assessment Scales: Probability and Impact [71]

Probability Scale

Level	Rating	Range (Prob.)
Very High	5	$\geq 70\%$
High	4	$25\% \leq PR < 70\%$
Moderate	3	$10\% \leq PR < 25\%$
Low	2	$1\% \leq PR < 10\%$
Very Low	1	$< 1\%$

Impact/Consequence Scale

Level	Rating	Description
Catastrophic	5	Prevents completion of the mission or causes complete loss of the required technical capability.
Critical	4	Severely degrades system performance, making mission success uncertain or only achievable with major limitations.
Moderate	3	Noticeably reduces system performance, but the primary mission remains achievable with reduced efficiency, capability, or safety margin.
Marginal	2	Causes minor degradation of performance or affects secondary mission objectives without preventing primary mission success.
Negligible	1	Causes only inconvenience or minor non-operational effects, with no meaningful impact on technical performance.

Table 15.2: Technical Risk Register with Prevention, Contingency, Residual Risk Ratings, and Responsible Member

ID	Description	P	I	Prevention	Contingency	P_r	I_r	Resp.
RSK-BIG-01	Balloon becomes uncontrollable or unrecoverable after interaction.	2	5	Use gradual interaction and verify that nominal contact does not tear or destabilize the balloon.	Stop interaction, disengage, re-track the balloon, then retry or abort.	1	4	MK
RSK-BIG-03	Recovered material, tether, or payload cannot be handled safely after landing.	1	2	Use clear release points, low stored energy, simple handling steps, and remote shutdown.	Power down, isolate the area, and detach the material using manual recovery procedures.	1	1	MK
RSK-BIG-04	Net launch or deployment fails during upward firing from below the payload.	3	4	Define allowable launch distance, hover stability, and relative-speed limits before firing; ground-test launcher packing, trigger timing, and net opening repeatability.	Abort the capture attempt, recover or clear the net if possible, and reattempt only if energy and tracking margins remain sufficient.	2	2	DB
RSK-BIG-05	Net closure or clearance fails after deployment, causing partial capture or contact between the net, tether, corner weights, and UAS.	3	5	Use cinch/tension confirmation, propeller clearance zones, tether routing constraints, and ground tests with representative payload shapes and net deployment geometries.	Release or loosen the net if safe; otherwise enter controlled descent or trigger the emergency separation sequence if aircraft safety is threatened.	2	4	DB

ID	Description	P	I	Prevention	Contingency	P_r	I_r	Resp.
RSK-SMS-01	Launch, vibration, or transit loads damage mounts or structural supports.	2	4	Check load paths and vibration for all mission phases; apply safety factors and avoid single-point failures.	Abort or land safely, then inspect the platform before relaunch.	2	3	JW
RSK-SMS-04	Post-flight inspection misses damage or degraded components.	2	3	Use a checklist with clear no-go criteria for structure, tethers, batteries, and mechanisms.	Ground the system until the affected component is inspected, repaired, or replaced.	1	2	AM
RSK-SMS-06	Tether, net rim, cinch line, or attachment point fails under gust, payload swing, or towing loads.	3	5	Size soft-goods and attachment points for combined payload, drag, gust, and dynamic swing loads with appropriate safety factors.	Release the tether or captured bundle only if the backup descent state is controlled; otherwise reduce speed and descend with limited manoeuvring.	2	4	JW
RSK-SMS-07	Tether reel jams or fails to regulate tension during transition or descent.	2	4	Use a torque limiter, controlled payout mode, reel position sensing, and dynamic load testing before flight.	Reduce manoeuvre aggressiveness, or release the tether if tension threatens aircraft control.	1	3	AM
RSK-SCE-01	Software errors cause unsafe commands or loss of mission functions.	4	3	Use modular software, code reviews, simulation testing, and a dedicated software V&V plan.	Switch to manual mode, terminate the mission early, or use remote shutdown.	2	2	AT
RSK-SCE-02	Detection, identification, or tracking fails due to environment or sensor limits.	3	2	Select sensors for expected range, contrast, FOV, lighting, and clutter; use filtering and multi-frame confirmation.	Request updated target data or abort if detection exceeds the time/energy margin.	2	2	FR
RSK-SCE-03	Battery degradation is underestimated, causing energy or power issues.	2	3	Include ageing, temperature, discharge rate, and cycle life in the energy budget and check battery health pre-flight.	Abort before interaction and return or land while reserve remains. Replace degraded packs.	1	2	AT
RSK-SCE-05	Navigation or communication degrades during launch or transit.	2	2	Use redundant navigation sources and verify the communication link budget.	Enter degraded-navigation or lost-link mode: hold, return-to-home, or land safely.	1	2	FR
RSK-SCE-06	Tether tension, reel position, or capture-confirmation sensing gives incorrect feedback.	3	4	Use sensor calibration, plausibility checks between reel state and load measurements, and conservative confirmation thresholds before towing.	Treat the capture state as uncertain, reduce towing speed, hold position if possible, or release/abort if the measured loads become unsafe.	1	3	AT
RSK-SCE-07	Propulsion, battery, ESC, or avionics thermal limits are exceeded during climb or terminal hover.	3	4	Check component thermal limits using the climb, hover, and terminal loiter power cases; include cooling provisions where required.	Reduce power demand, disable non-critical electrical loads, abort capture, or land before thermal limits are exceeded.	2	3	AT
RSK-SCE-08	High-voltage propulsion switching causes electromagnetic interference with sensors, communication, or flight-controller signals.	3	4	Separate high-power and signal wiring, use shielding and grounding rules, and perform EMI checks during integration.	Switch to degraded sensing or manual-supervised mode, increase separation from the target, or abort if control or tracking signals become unreliable.	2	3	FR

ID	Description	P	I	Prevention	Contingency	P_r	I_r	Resp.
RSK-OGS-01	Launch or landing area is unsuitable.	2	3	Define site criteria and inspect multiple launch/landing areas beforehand.	Move to an alternate site, abort before take-off, or divert to a safe landing area.	2	2	GZ
RSK-OGS-02	Incomplete go/no-go assessment allows unsafe mission authorization.	2	3	Use a checklist for weather, airspace, public exposure, battery, communication, and system readiness.	Cancel or delay launch and repeat the checklist after resolving the issue.	2	2	GZ
RSK-OGS-03	Recovery or descent path crosses people, infrastructure, or restricted areas.	4	2	Predict the recovery area before interaction and include it in mission decision logic.	Suspend interaction, reposition, or abort if the predicted path is unsafe.	2	2	PB
RSK-OGS-04	Recovery zone becomes unsuitable during towing descent.	3	4	Continuously update the predicted recovery zone using wind, descent rate, tether angle, and remaining energy before and after capture.	Redirect to an alternate recovery zone, reduce descent aggressiveness, or abort/release only if the backup descent state remains safe.	1	3	PB
RSK-PPA-01	Battery reserve is consumed before return and landing.	3	5	Budget energy for all mission phases and enforce reserve and retry limits.	Stop search/interaction and return or land at an alternate site before reserve depletion.	2	3	AD
RSK-PPA-02	UAS lacks thrust or stability during climb or transit.	3	3	Size propulsion with thrust margin and check stability with the interaction mechanism installed.	Reduce the mission envelope, return to launch, or land safely.	2	3	AP
RSK-PPA-03	Post-contact forces exceed UAS control capability.	2	5	Model post-contact drag, lift, payload mass, tether tension, and coupled dynamics.	If post-contact loads exceed the limit, release the tether/net, retreat to safe standoff, re-stabilize, and retry once only if control and battery margins remain sufficient, otherwise abort.	2	3	AP
RSK-PPA-04	Payload pendulum motion grows during towing descent and destabilizes the UAS.	4	4	Include suspended-load dynamics in the control model and limit descent acceleration, turn rate, and tether speed.	Reduce speed, increase damping through reel control, widen the recovery path, or release the tether if aircraft stability is threatened.	2	3	AP
RSK-PPA-05	Balloon drag or residual lift exceeds available towing or descent authority.	3	5	Check towing force against worst-case balloon diameter, gust load, tether angle, payload mass, and energy margin before interaction.	Abort before capture if the authority margin is insufficient, or release/disengage if safe recovery cannot be maintained after contact.	2	4	AD
RSK-PPA-06	Aircraft exceeds the allowable angle of attack or stalls during hover-to-cruise or back transition.	4	5	Verify the transition corridor with dynamic simulation and include angle of attack and stall speed margins in the transition control law.	Abort the transition, return to hover or climb mode if controllable, recover airspeed and retry only inside the verified transition envelope.	2	4	AP

15.2. Risk Maps

In order to better visualize the risks in terms of probability and impact/consequence, the events are plotted in a risk map in Figure 15.1. By doing so, the relative severity of each risk can be assessed at a glance, allowing the team to identify which risks require the most urgent attention. Risks positioned in

the upper-right region of the map combine high probability with high impact and therefore represent the most critical threats to the project. Conversely, risks located in the lower-left region have limited probability and/or limited impact, and can therefore be accepted more easily or monitored with less priority.
The risk map also supports comparison between the situation before and after prevention and contingency measures are applied. In this way, the effectiveness of the proposed mitigation strategy can be evaluated by observing whether risks move toward lower-probability and lower-impact regions of the map.
The comparison between the initial and residual maps shows the expected effect of the prevention and contingency measures listed in Table 15.2. Most risks move toward lower-severity regions after mitigation. The remaining key residual risks for Concept A are related to net launch and closure, tether and reel loads, payload pendulum motion, towing authority in wind, and subsystem budget or interface growth. These risks will therefore remain the main monitoring points during the next design phase.

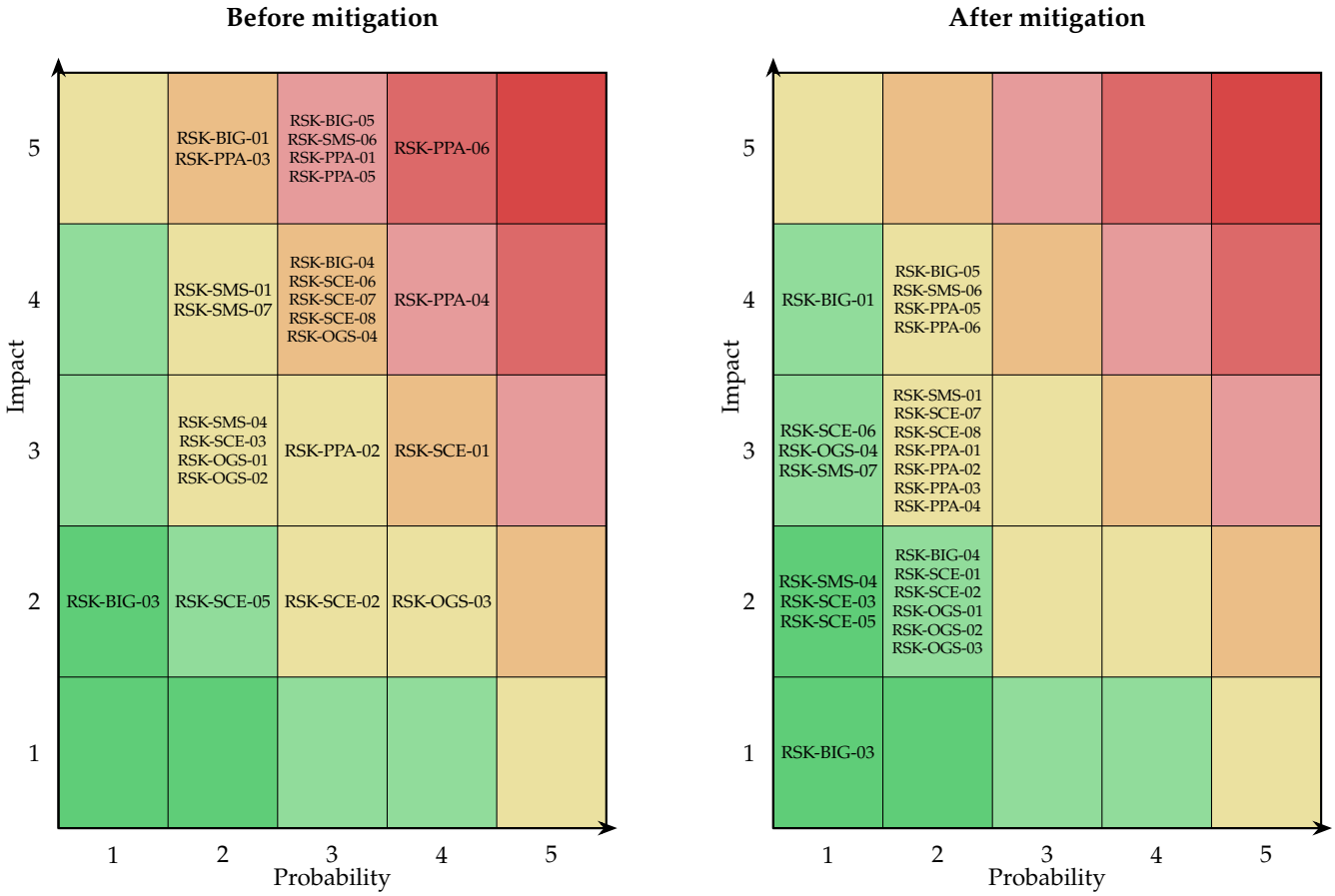

Figure 15.1: Technical Risk Maps Before and After Prevention and Contingency Measures

15.3. Changelog

Last updated: 16/06/2026

The risk register was updated from the Midterm Report to reflect the progression from concept-level design to final subsystem definition.

1. **Removed risks: RSK-GEN-01**, **RSK-GEN-02**, **RSK-GEN-03**, **RSK-GEN-04**, **RSK-SMS-02**, **RSK-SMS-03**, and **RSK-SMS-05** were removed because several general system-level and early structural-material uncertainties have been reduced through subsystem definition, interface development, final budget consolidation, and structural design maturation.
2. **Added risks: RSK-PPA-06**, **RSK-SCE-07**, and **RSK-SCE-08** were added to cover final-design risks related to transition angle-of-attack and stall margin, electrical peak-current and thermal loading, and sensor-to-control alignment. **RSK-PPA-06** was added because the tail-sitter transition remains a critical design driver and the aircraft must remain within its allowable angle-of-attack

and stall-speed limits during hover-to-cruise and back transition. **RSK-SCE-07** was added because the final electrical architecture must support high propulsion power during climb and hover, making peak current draw, voltage sag, and thermal loading important verification points. **RSK-SCE-08** was added because terminal approach and net launch depend on accurate relative-state estimation, requiring consistent sensor alignment, timing, and coordinate-frame definitions.

Update: 18/05/2026

1. **Removed risks: RSK-BIG-02** was removed because selected concept captures the suspended payload from below and does not rely on direct balloon-envelope capture. **RSK-SCE-04** was removed because the wiring-detail risk was too broad for this concept-specific update and is already covered by electrical integration and interface risks.
2. **Added risks: RSK-BIG-04**, **RSK-BIG-05**, **RSK-SMS-06**, **RSK-SMS-07**, **RSK-SCE-06**, **RSK-OGS-04**, **RSK-PPA-04**, and **RSK-PPA-05** were added to cover Concept A risks related to net deployment, net closure, tether-load management, reel behaviour, capture-state feedback, recovery-zone prediction, payload swing, and towing authority.

16 Return on Investment, Cost Breakdown and Operational Profit

This chapter evaluates whether the final BELLONA concept can become financially viable after the Design Synthesis Exercise (DSE). The return on investment (ROI) analysis and the Cost Break-down Structure (CBS) are combined in one chapter because both are derived from the same post-DSE financial model. The CBS identifies the cost elements required to mature, produce, deploy and support the system, while the ROI analysis evaluates whether these costs can be recovered through product sales and recurring service revenue.
The financial model is based on the latest BELLONA spreadsheet plan. It includes unit production cost, recurring service cost, staff and non-staff operating expenses (OPEX), long-term asset investment, capital expenditure (CAPEX), customer acquisition cost (CAC), external funding, taxation and cash-flow development. Unless stated otherwise, yearly monetary values are expressed in EUR thousands.

16.1. Financial Model Scope and Key Assumptions

BELLONA is assumed to follow a direct product-sale business model with additional annual maintenance and service revenue. One unit is defined as one self-sufficient deployable BELLONA system: one unmanned aircraft system (UAS), one ground station, the balloon-interaction hardware, commissioning and customer handover. This definition is used because the ground station is not only a control box, but the infrastructure that stores, charges, deploys, recovers and resets the UAS.
The unit definition is deliberately kept at the individual-system level. Although an airport-equivalent deployment is assumed to require three units on average, this is a deployment-sizing assumption rather than a new accounting unit. Keeping one unit equal to one self-sufficient system preserves the modularity of the concept, allows customers to scale coverage gradually, and keeps production cost, service revenue and maintenance cost traceable per delivered system. If customer tenders later consistently require three systems, the commercial offer could be packaged as a three-unit deployment bundle without redefining the underlying financial-model unit.

Table 16.1: Key Financial Assumptions Used in the Updated BELLONA Model

Parameter	Value used	Model interpretation
Business model	Product sale + annual service	Hardware revenue is generated at delivery; service revenue scales with the active installed base.

Parameter	Value used	Model interpretation
Unit definition	1 UAS + 1 ground station	Includes aircraft, ground station, interaction hardware, commissioning and handover.
Airport-equivalent deployment	3 units	Allows operational coverage and availability during charging, inspection and maintenance.
New-unit sales price	EUR 121,000 / unit	Updated price after including the ground station in the unit definition.
Airborne UAS and interaction hardware	EUR 23,222 / new unit	Sub-EUR 25k airborne part of the complete unit cost; the remaining production cost is dominated by the ground station.
One-time cost of goods sold (COGS)	EUR 99,622 / new unit	Bottom-up production estimate including UAS, ground station, manufacturing and installation.
Annual service revenue	EUR 11,999 / active unit / year	Maintenance, support, software/device management and readiness package.
Recurring service COGS	EUR 2,400 / active unit / year	Maintenance parts, device management, quality-assurance (QA) allowance and technician support.
Direct operator mission cost	EUR 150 / mission	Energy, reset, consumables, inspection and minor wear; kept outside the company profit-and-loss statement.
Total external funding	EUR 3.15M	Equity and grants required before sustained profitability.
Target year	Year 6	First year with positive net profit in the updated model.

16.1.1. Financial Model Structure and Derivation

To make the financial plan traceable, the spreadsheet separates assumptions, projections and derived results. Assumptions are fixed model inputs, such as the unit definition, sales price, one-time COGS, annual service revenue, recurring service COGS, OPEX, CAPEX, taxation and external funding. Projections are year-by-year scenario inputs, most importantly the new-unit sales ramp and resulting active installed base. Derived results are then calculated from these inputs: revenue, COGS, gross profit, operating profit, net profit, operating cash flow, closing cash and ROI.

Revenue is calculated from new-unit sales revenue plus annual service revenue from all active units. One-time COGS scales with new units delivered, while recurring service COGS scales with the active installed base. The active installed base is cumulative because each delivered unit is assumed to remain in service throughout the modelled period. The direct operator mission cost is kept outside the company profit-and-loss statement (P&L), because it is treated as an airport operating cost rather than a BELLONA company cost.

The sales ramp is a baseline adoption scenario rather than a measured market-share result. It assumes no commercial sales in Year 1, five controlled customer or pilot deliveries in Year 2, and faster adoption after initial references, airport acceptance and production capacity improve. Airport-equivalent deployments are shown only to connect the unit-level model to the deployment concept; they are calculated by dividing the active installed base by three and do not redefine the commercial unit.

Table 16.2: Baseline Sales-Ramp Projection Used To Derive the Sales and Installed-Base Figures

Year	New units sold	Active units	Airport-equivalent deployments
Year 1	0	0	0.0
Year 2	5	5	1.7
Year 3	12	17	5.7
Year 4	22	39	13.0
Year 5	49	88	29.3
Year 6	71	159	53.0

This structure means that the results are internally consistent with the stated assumptions, but it does not remove market uncertainty. The most sensitive assumptions are expected to be the sales ramp, development and certification duration, service-margin retention and the availability of staged external funding.

16.2. Cost Break-down Structure

The Cost Break-down Structure (CBS) identifies the post-DSE costs required to develop the BELLONA preliminary design into a deployable commercial system. It is structured as an AND tree, so every branch contributes to the total programme cost. This includes not only the physical product, but also development, testing, certification preparation, production setup, commercial scale-up and recurring support.

The CBS links the technical development logic to the financial model. Development and certification are captured mainly as research and development (R&D) staff and non-staff OPEX, unit production as one-time COGS, maintenance and support as recurring COGS per active unit, and commercialisation through customer acquisition, general and administrative (G&A) scale-up, funding needs, working capital and cash-flow projections.

Each CBS branch is divided into core and supporting cost elements. Core elements cover the direct technical, production or operational costs, while supporting elements cover the activities needed to mature, deploy, manage or scale the branch. The split is not chronological.

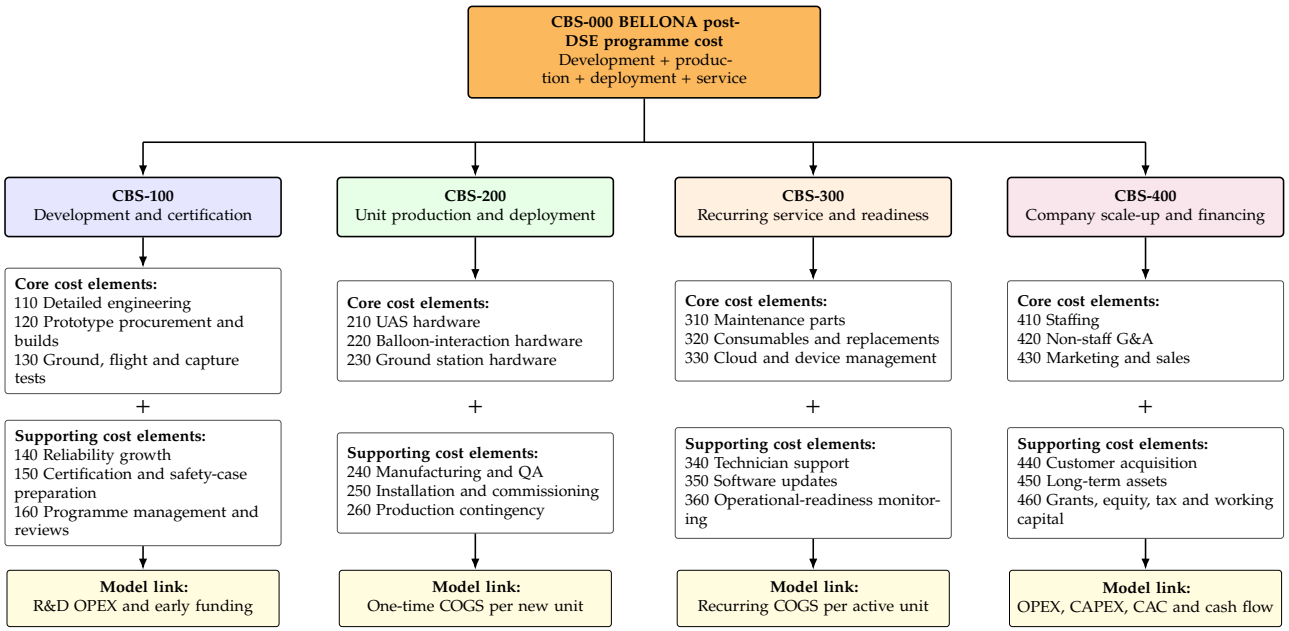

Figure 16.1: Cost Break-Down Structure for the Post-DSE BELLONA Programme. The Plus Signs Indicate that Core and Supporting Elements Are Added Within Each Branch, While the Yellow Boxes Show How Each Branch Maps Into the Financial Model

Table 16.3: CBS Mapping to the Updated Financial Model

CBS code	Cost layer	Main contents	Financial model link
CBS-100	Development and certification	Detailed engineering, prototype builds, ground and flight tests, interaction validation, reliability growth, certification preparation and programme management.	Mainly R&D OPEX and early funding requirement.
CBS-200	Unit production and deployment	UAS hardware, balloon-interaction system, ground station, manufacturing, QA, installation, commissioning and production contingency.	One-time COGS of EUR 99,622 per new unit.
CBS-300	Recurring service and readiness	Maintenance parts, consumables, replacements, device management, technician support, software updates and operational-readiness monitoring.	Recurring COGS of EUR 2,400 per active unit per year.
CBS-400	Company scale-up and financing	Staffing, non-staff G&A, sales, customer acquisition, long-term assets, working capital, grants, equity and tax effects.	Year 6 OPEX of EUR 1.968M, total external funding of EUR 3.15M and CAC of EUR 4.1k per new unit.

The CBS separates costs by how they enter the model. CBS-100 and CBS-400 are mainly programme-level costs and therefore affect OPEX, funding needs and cash flow. CBS-200 is incurred each time a new BELLONA unit is produced and delivered. CBS-300 scales with the active installed base and therefore becomes more important as more units enter service. This separation avoids mixing

development cost, production cost and recurring support cost into a single number.

Table 16.4: One-Time COGS Break-Down Per New BELLONA Unit

Cost element	Included items	Cost per unit [EUR]
Airborne UAS and interaction hardware	Propulsion, sensing, control, electronics, structures, communication, balloon-interaction hardware and subsystem contingency.	23,222
Ground station hardware	Enclosure, slide-out carriage, tilt mechanism, clamps, charging equipment, backup power, station sensing, safety interlocks and communication hardware.	68,400
Miscellaneous integration hardware	Additional fittings, brackets, wiring, connectors, fasteners, labels and mounting hardware.	1,000
Manufacturing, integration and QA	Assembly, subsystem integration, quality assurance, acceptance testing and production checks.	3,000
Installation and customer handover	Delivery setup, station calibration, commissioning, documentation and customer handover.	4,000
Total one-time COGS	**Cost incurred when one new BELLONA unit is produced and delivered.**	**99,622**

The one-time COGS table is deliberately grouped rather than expanded into every individual component. Detailed subsystem budgets are handled in the technical budget and subsystem chapters. The airborne UAS and interaction hardware remain below EUR 25k per unit, at EUR 23,222. However, the complete commercial unit also includes the deployable ground station, which raises total one-time COGS to EUR 99,622 and makes the ground station the largest production-cost contributor. Annual profitability is therefore not driven by hardware margin alone, but also by recurring service revenue from the active installed base.

16.3. Unit Economics

The updated model gives a positive but limited hardware margin, because the unit now includes the ground station. The service margin is much higher and therefore becomes increasingly important as the installed base grows.

Table 16.5: Updated BELLONA Unit Economics

Revenue stream	Revenue [EUR]	COGS [EUR]	Gross profit [EUR]	Gross margin
New unit sale	121,000	99,622	21,378	17.7%
Annual service per active unit	11,999	2,400	9,599	80.0%

The hardware sale covers the one-time production cost and generates a moderate margin. However, the business case is not driven by hardware alone. New-unit sales create the installed base, while the annual maintenance and service package improves long-term profitability.

16.4. Sales Ramp, Revenue and Profitability

In the baseline scenario, commercial entry starts in Year 2 with the first five controlled customer or pilot units sold. This is an optimistic assumption for a post-DSE aerospace system and should be interpreted as early commercial deployment after parallel technical maturation, not as fully mature market-wide operation. If development, certification preparation or airport acceptance takes longer, the ramp and payback would shift later, while the per-unit economics would remain unchanged.
By Year 6, the installed base reaches 159 active units, equivalent to approximately 53 airport-equivalent deployments. The active installed base is important because it drives recurring service revenue and stabilises the business beyond new hardware deliveries.

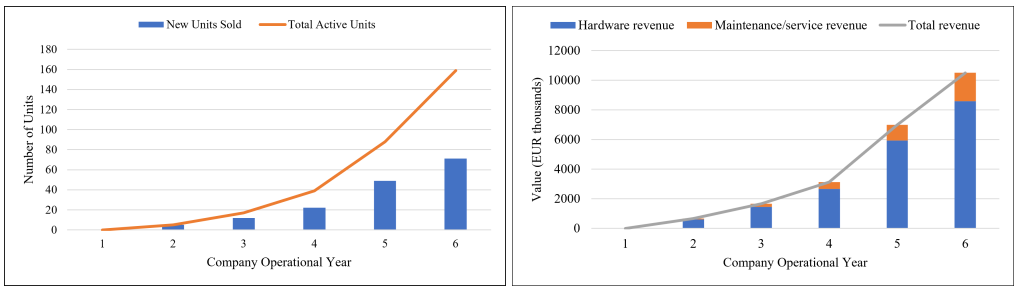

(a) Baseline Projected Sales Ramp and Active Installed Base From Table 16.2 **(b)** Hardware and Maintenance/Service Revenue Split

Figure 16.2: Sales and Revenue Development from Year 1 to Year 6

The financial ramp is shown in Figure 16.3. Revenue grows strongly from Year 2 onward, but COGS and OPEX also increase as production, staffing, certification support and field operations scale up. The company therefore remains loss-making during the early years, approaches break-even in Year 5, and reaches positive net profit in Year 6.

Operating cash flow follows the same trend: it is negative during the development and ramp-up phase, but improves as sales volume and recurring service revenue increase. By Year 6, operating cash flow becomes positive, showing that the business can support its day-to-day operations from its own activity. Closing cash remains positive throughout the period due to the staged funding injections, and increases again by Year 6 as profitability and cash generation improve.

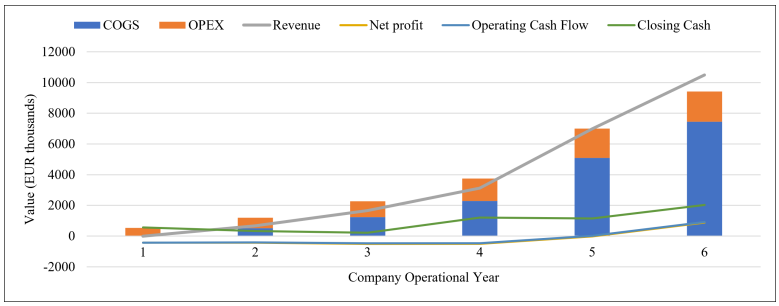

Figure 16.3: Profit-and-Loss Development From Year 1 to Year 6

16.5. Operating Expenses, Staffing and Assets

The model includes the main operating cost categories rather than treating OPEX as a single unexplained value. This is important because the post-DSE programme requires engineering staff, certification work, manufacturing preparation, field support, sales activity and customer deployment. Staff costs are separated from non-staff OPEX, while long-term assets are captured through capital expenditure and depreciation.

Table 16.6: Target-Year OPEX Structure: Values Expressed in EUR Thousands

OPEX category	Staff cost	Non-staff OPEX	Total
General and administrative	169.0	227.0	396.0
Marketing and sales	162.5	130.0	292.5
Research and development	1,137.5	100.0	1,237.5
Depreciation and amortisation	–	–	42.1
Total operating expenses	**1,469.0**	**457.0**	**1,968.1**

By Year 6, the company employs 25 full-time-equivalent (FTE) staff including founders, management, engineering, certification, manufacturing, supply-chain, sales and field-support roles. The large R&D staffing component is consistent with the technical maturity still required after DSE: flight testing, control refinement, certification preparation, ground-station integration and reliability improvement.

Table 16.7: Target-Year Supporting Financial Metrics

Metric	Year 6 value	Interpretation
Employees including founders	25 FTE	Supports engineering, certification, manufacturing, sales and field support.
Customer acquisition cost	EUR 4.1k / new unit	Marketing and sales cost divided by new units sold in the target year.
Customer acquisition cost per deployment	EUR 12.4k / 3-unit deployment	Approximate commercial cost to acquire one airport-equivalent deployment.
Operating leverage	0.58	Revenue growth increasingly exceeds OPEX growth as the installed base scales.
Long-term asset investment	EUR 40k	Test equipment, fabrication tools, IT hardware, production jigs, field equipment and intangible assets.
Depreciation and amortisation	EUR 42.1k	Annual accounting charge from the fixed-asset base.

16.6. Funding Plan and ROI Interpretation

The funding plan is staged to cover development and commercial scale-up before net profitability. The model assumes EUR 1.0M of equity funding and EUR 50k of grant funding in Year 1, followed by EUR 200k and EUR 400k of grants in Years 2 and 3. A larger EUR 1.5M equity round is included in Year 4 to fund scale-up, field support, staffing and production expansion. Total external financing before the target year is therefore EUR 3.15M.

These funding values are benchmarked against European high-risk innovation funding ranges rather than treated as secured commitments. For reference, the European Innovation Council (EIC) Accelerator supports start-ups and small and medium-sized enterprises with grants below EUR 2.5M and investments between EUR 0.5M and EUR 10M, while ESA Business Incubation Centres (ESA BICs) provide EUR 50k equity-free funding for product and intellectual-property development [72]. The assumed EUR 3.15M external financing should therefore be interpreted as a plausible staged funding requirement for a hardware-intensive aerospace start-up, not as a confirmed financing plan.

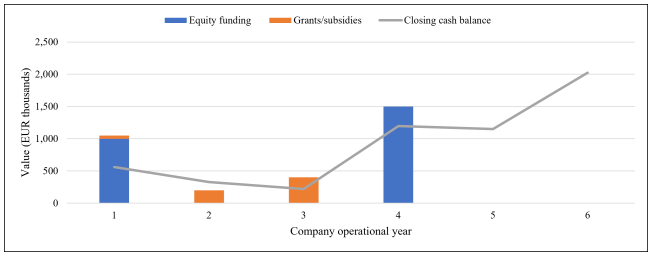

Figure 16.4: Funding Sources and Closing Cash Balance Across Six Operational Years

Using the DSE target-year ROI definition, ROI is calculated from the Year 6 net profit and the implied total cost of generating the Year 6 revenue:

$$ROI_{Y6} = \frac{871.55}{10498.84 - 871.55} = 0.0905 \approx 9.1\% \tag{16.1}$$

The target-year ROI is positive because the model reaches sufficient annual revenue to offset production cost, operating expenses and taxation in Year 6. Including the ground station in the unit definition increases COGS and reduces the hardware margin, but it also makes each delivered unit a complete self-sufficient operational system. Year 6 should therefore be interpreted as the first profitable commercial year rather than a mature steady-state year.

Cumulative net profit over Years 1-6 remains negative at approximately EUR 1.02M, so full payback still requires continued growth beyond the modelled horizon. This is acceptable for a post-DSE commercialisation case because BELLONA requires substantial early investment in testing, certification preparation, staffing, field support and customer acquisition before the installed base becomes large enough to generate recurring service income.

Overall, the updated model indicates a plausible baseline path to operational profitability under the stated assumptions. The path is plausible in the sense that the revenues, costs, staffing, funding and cash-flow results are linked through explicit model drivers. It should not be read as a validated market forecast or as the result of a full sensitivity analysis. The main uncertainties remain the sales ramp, development and certification duration, service-margin retention and external funding availability.

BELLONA is not justified by hardware sales alone: the hardware margin is positive but limited because each complete unit includes a deployable ground station. The financial case depends on building a sufficiently large installed base and maintaining high-margin annual service revenue. By Year 6, the model reaches 159 active units, EUR 10.50M in annual revenue, EUR 872k in net profit, positive operating cash flow, EUR 2.02M closing cash and a target-year ROI of approximately 9.1%.

17 Sustainability Assessment

This chapter presents a screening-level sustainability assessment of the final BELLONA design. The objective is to identify the main environmental drivers per successful recovery mission. The assessment focuses on electric operation, reusable hardware, recoverability, replacement items, operational noise, and end-of-life handling.
Before detailing the methodology and life-cycle inventory, Table 17.1 establishes the baseline sustainability, environmental, and operational constraints that must be satisfied by the UAS architecture.

Table 17.1: Sustainability and Lifecycle Requirements for the BELLONA System

ID	Requirement	Classification
REQ-STK-12-MSN-15-SYS-27-SUS-01	The BELLONA UAS shall use electric energy storage for flight propulsion.	Driving
REQ-STK-06-MSN-08-SYS-17-SUS-02	Nominal operation shall not intentionally fragment the balloon, release the payload, or create debris above 50 g.	Driving
REQ-STK-06-MSN-08-SYS-17-SUS-03	All deployed hardware above 50 g shall remain attached or be recoverable after nominal operation.	Driving
REQ-STK-06-MSN-08-SYS-17-SUS-04	The capture and descent system shall aim to avoid cutting, uncontrolled rupture, and uncontrolled descent of the balloon-payload system.	Driving
REQ-STK-11-MSN-13-SYS-25-SUS-05	Major airframe, propulsion-support, ground-station and recovery hardware shall be reusable after post-flight inspection.	Key
REQ-STK-11-MSN-13-SYS-25-SUS-06	High-wear components shall have documented inspection and replacement criteria.	Key
REQ-STK-11-MSN-13-SYS-25-SUS-07	Wing, canard, battery tray, motor struts, landing booms, tether hardpoint and mission-kit interfaces shall be modular and replaceable.	Key
REQ-STK-12-MSN-15-SYS-27-SUS-08	Each major material group shall have a defined reuse, repair, recycling or disposal route.	Key
REQ-STK-12-MSN-15-SYS-27-SUS-09	Nominal operational noise shall target 65 dB(A) at 100 m as a preliminary design KPI.	Non-driving
REQ-STK-12-MSN-15-SYS-27-SUS-10	Charging emissions shall be reported per sortie for the selected mission energy and electricity mix.	Non-driving
REQ-STK-12-MSN-15-SYS-27-SUS-11	The lifecycle assessment shall use one BELLONA UAS over 100 successful recovery missions as the baseline functional unit.	Non-driving
REQ-STK-11-MSN-13-SYS-25-SUS-12	Single-use or unrecovered components shall be avoided, or justified by mass, cost, material and safety need.	Key

17.1. Goal, Scope and Boundary

The assessment is a screening-level life-cycle assessment (LCA) of BELLONA. It is not a certified LCA. Its purpose is to estimate the order of magnitude of the climate impact and to identify which design choices dominate the sustainability of the project.
The main functional unit is one successful BELLONA recovery mission, including launch, interception, capture, controlled descent, landing, recovery of deployed hardware where feasible, post-flight inspection, reset, and battery recharge. This unit is used because the useful service is controlled recovery of a hazardous balloon-payload system, not flight time or vehicle mass.
Reusable hardware is allocated over an assumed service life of:

$$N_{\text{life}} = 100 \text{ missions},$$

supporting the 20 missions per year over a 5 year service period. Lifetime and replacement rate strongly affect the per-mission result. A controlled sustainable design deviation is retained for the

net launcher. The aircraft propulsion remains fully electric, but the selected launcher uses a blank rifle cartridge as a compact impulse source. The cartridge is therefore treated as a small operational consumable and as a safety, storage, handling, and regulatory compliance driver.
In this section, all impact terms I represent climate-change impact expressed in kg CO_2-eq. The quantitative mission-normalised impact is calculated as:

$$I_{\text{mission}} = \frac{I_{\text{reusable}} + I_{\text{EOL}}}{N_{\text{life}}} + I_{\text{operation}}, \tag{17.1}$$

where I_{reusable} is the manufacturing impact of reusable hardware, I_{EOL} is the end-of-life impact or recycling credit, and $I_{\text{operation}}$ is the electricity impact per sortie. Replacement items are retained as a qualitative screening item in this assessment, because their final replacement intervals, damage rates, recovery rates and supplier-specific emission factors are not fixed at this stage. They are therefore discussed as maintenance and design-control drivers rather than added to the numerical baseline. Transport is excluded because deployment distance and operator logistics are not fixed.

17.2. Inventory and Emission Factors

A cradle-to-grave boundary is used at screening level. It includes material production, component manufacturing, assembly, operation, maintenance, replacement items, and end-of-life handling. Factory infrastructure, development prototypes, human labour, supplier transport chains, staff commuting, and avoided damage from successful balloon recovery are excluded from the quantitative result.

Table 17.2: System Boundary for the BELLONA Screening Sustainability Assessment

Stage	Included	Excluded or simplified
Materials and manufacturing	Airframe, propulsion hardware, battery pack, electronics, recovery hardware, net, tether, pads, and fittings.	Supplier-specific production routes and workshop infrastructure.
Operation	Mission electricity, charging efficiency, and battery recharge.	Operator energy use and external airport infrastructure.
Maintenance	Inspection-driven replacement of net, tether, pads, propellers, and launcher consumables.	Major crash repair in the baseline case.
End-of-life	Metal recycling, battery recycling, electronics waste, composite disposal, and polymer waste.	Quantified credit for pre-vented balloon damage.

The inventory is grouped into reusable hardware, high-wear items, and direct mission inputs. Reusable hardware is allocated over N_{life}, while high-wear items are treated as qualitative inspection-driven replacement items.

Table 17.3: BELLONA Life-Cycle Inventory Used for the Screening Calculation

Inventory group	Item	Quantity	Unit
System reference	Complete UAS mass	51.13	kg
	Battery pack mass	11.40	kg
	Installed battery energy	4.74	kWh
	Mission energy before contingency	3.019	kWh/mission
Reusable hardware	Airframe structure	19.48	kg
	Propulsion hardware	11.46	kg
	Onboard electronics and actuation	3.074	kg
	Capture hardware, reel and parachute group	3.60	kg
	Wiring and harness	0.43	kg
High-wear items	Net assembly	0.565	kg
	Tether	0.090	kg
	EPDM landing pads	0.200	kg
Direct inputs	Blank launcher cartridge	1	cartridge/mission
	Recharge electricity	calculated	kWh/mission

The emission factors in Table 17.4 are assumptions based on real data. Supplier environmental product declarations or database values should replace them in a certified LCA. The sensors and electronics emission factor varies the most because it varies wildly depending on the final PCB, sensors, optics, radar, chips, casing, and supplier.

Table 17.4: Emission Factors Used for the Screening-Level Sustainability Assessment

Item	Baseline EF	Range	Source or rationale
CFRP/epoxy composite	50 $kgCO_2eq/kg$	25-80	Screening value for CFRP parts [73, 74].
Aluminium structure	6.6 $kgCO_2eq/kg$	0.5-14.8	European primary aluminium baseline.[75].
Steel fittings	2.2 $kgCO_2eq/kg$	0.7-2.3	Based on worldsteel global GHG intensity [76].
Li-ion battery pack	70 $kgCO_2eq/kWh$	55-100	Capacity-based battery production factor [77].
Electronics and sensors	25 $kgCO_2eq/kg$	10-100	Specific parts dependent.
UHMWPE net and tether	2.5 $kgCO_2eq/kg$	2.5-6	HDPE/UHMWPE proxy [78].
EPDM pads	5.0 $kgCO_2eq/kg$	2.5-6.1	Synthetic-rubber screening range [79, 80].
Dutch grey electricity	0.497 $kgCO_2eq/kWh$	0.25-0.50	Dutch grey-electricity factor [81].

For material and component groups, production impact is estimated as:

$$I_i = m_i EF_i, \tag{17.2}$$

where m_i is mass and EF_i is the emission factor. For the battery, the capacity-based estimate is:

$$I_{\text{battery}} = E_{\text{battery}} EF_{\text{battery,kWh}}. \tag{17.3}$$

Furthermore,the replacement impact is calculated as such:

$$I_{\text{replacement}} = \sum_j \frac{m_j EF_j}{N_{\text{replace},j}} + I_{\text{cartridge}} \tag{17.4}$$

The blank launcher cartridge is not assigned a numerical emission factor in the baseline calculation. Its direct climate contribution is expected to be small compared with the rest of the hardware, and it is therefore retained as a qualitative operational consumable and replacement driver.

17.3. Operational Energy

BELLONA is fully electric during flight, so no direct exhaust emissions are produced during operation. The operational climate impact is caused by the electricity required to recharge the battery:

$$E_{\text{grid}} = \frac{E_{\text{mission}}}{\eta_{\text{charge}}}, \qquad I_{\text{operation}} = E_{\text{grid}} EF_{\text{electricity}}. \tag{17.5}$$

A charging efficiency of $\eta_{\text{charge}} = 0.90$ is assumed.
The final electrical-system sizing gives a mission energy of 3.019 kWh before contingency and an installed battery energy of 4.74 kWh. With the Dutch grey-electricity factor of 0.497 $kgCO_2eq/kWh$, the operational impact is estimated in Table 17.5.

Table 17.5: Operational Electricity Impact for One BELLONA Mission

Case	Energy used [kWh]	Grid energy [kWh]	Impact [$kgCO_2eq$]
Modelled mission energy	3.019	3.35	1.67
Mission energy with 15% contingency	3.472	3.86	1.92
Full installed battery recharge	4.74	5.27	2.62

17.4. Noise

Noise is included as a sustainability and social-acceptance KPI because BELLONA may operate near airports and airport-adjacent communities. For the present concept, the nominal operational noise requirement is defined as a preliminary design KPI of 65 dB(A) at 100 m. This distance is considered more representative for the scale of the current vehicle and for the expected operational stand-off from nearby observers. The KPI is treated as a preliminary design target rather than a certification claim. This distinction is important because European environmental-noise assessment commonly uses long-term indicators such as L_{den} and L_{night}, which represent averaged day-evening-night or night-time exposure [82]. These indicators are therefore not directly equivalent to a short, intermittent,

safety-driven recovery sortie. Similarly, Directive 2003/10/EC defines occupational exposure action values of 80 and 85 dB(A), and an exposure limit value of 87 dB(A), based on daily or weekly worker exposure [83]. These values are useful for context, but they are not used as direct compliance criteria for the BELLONA outdoor mission.
A first-order noise estimate will use the empirical formula on the sound pressure level 1 meter from the propeller at Equation 17.6 [84]

$$\mathrm{SPL}_{1,\max} = 83.4 + 15.3 \log P_{br} - 20 \log D + 38.5 M_t - 3(B-2) + 10 \log N_p \approx 109\,\mathrm{dB} \tag{17.6}$$

where P_{br} is the power used by propeller, D is the propeller diameter, M_t is blade tip mach number, B is blades number and N_p is the number of propellers. Free-space propagation at 100 m gives:

$$SPL_{100,\max} = \mathrm{SPL}_{1,\max} - 20 \log \frac{100}{1} \approx 69\ \mathrm{dB}. \tag{17.7}$$

This value represents a conservative first-order maximum SPL estimate for the present propeller configuration. The most prominent noise components are blade passage frequencies, shown as peaks on the spectrogram in Figure 17.1. Their noise level can be up to 10 dB stronger than the broadband noise. Synchronizing blades in 90° phase can decrease the tonal components by 19 dB [85]. If the dominant tonal components are reduced by this amount, the far-field noise level could decrease toward approximately 60 dB at 100 m. This indicates that the 65 dB(A) KPI at 100 m is considered achievable for the concept, provided that tonal-noise mitigation is incorporated in the final rotor-operating strategy.
The result should be interpreted as a concept-level indication of expected acoustic performance, not as a verified compliance result. Further development would require actual outdoor testing and assessing the sound using a human-centered Perceived Annoyance metric.

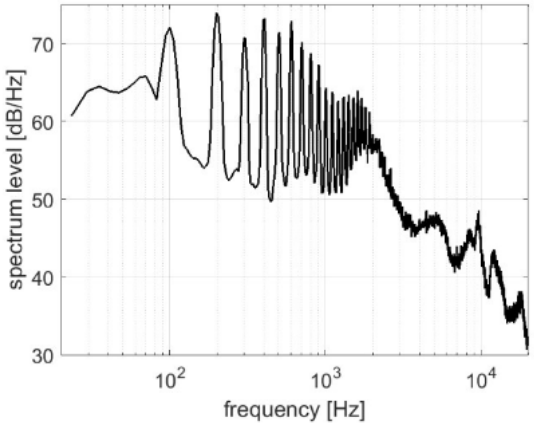

Figure 17.1: Example of Aerial Vehicle Noise Spectrogram

17.5. Manufacturing, Maintenance and Reuse

Reusable hardware is allocated over the expected system lifetime:

$$I_{\text{reusable,mission}} = \frac{\sum_i m_i EF_i}{N_{\text{life}}}. \tag{17.8}$$

The baseline case uses $N_{\text{life}} = 100$ missions, consistent with the operational assumption of 20 missions per year over 5 years before major overhaul.
The same operational philosophy from the production and operations is interpreted here from a sustainability perspective: large assemblies are reused, high-wear mission-kit items are inspected or replaced, and retired components are separated by material group for repair, recycling, or controlled disposal.
The battery production impact is estimated from the installed capacity:

$$I_{\text{battery}} = 4.74 \cdot 70 = 332\ \mathrm{kgCO_2eq}. \tag{17.9}$$

Allocated over 100 missions, this gives:

$$I_{\text{battery,mission}} = \frac{332}{100} = 3.32 \text{ kgCO}_2\text{eq/mission}. \tag{17.10}$$

The known onboard electronics and actuation mass is:

$$m_{\text{electronics}} = 0.992 + 0.575 + 0.360 + 0.217 + 0.930 = 3.074 \text{ kg}. \tag{17.11}$$

Using 25 $\text{kgCO}_2\text{eq/kg}$, this gives:

$$I_{\text{electronics}} = 3.074 \cdot 25 = 76.9 \text{ kgCO}_2\text{eq}, \qquad I_{\text{electronics,mission}} = \frac{76.9}{100} = 0.77 \text{ kgCO}_2\text{eq/mission}. \tag{17.12}$$

High-wear items are treated as inspection driven replacement items. The mission kit includes the net, tether, launcher consumables, closure line, reel interface and emergency parachute pack. After a sortie, the used kit can be removed and replaced by a serviceable kit, while the used kit is inspected, cleaned, repaired, repacked or discarded. Because the final replacement intervals and damage rates are still uncertain, these items are treated qualitatively in the baseline screening result.

Table 17.6: Maintenance Actions Supporting Reuse and Replacement Control

Action	Scope
After every mission	Inspect structure, propellers, landing pads, net, tether, launcher, battery, parachute and exposed wiring. Download logs and BMS data. Replace damaged or worn parts.
Every 20 missions	Inspect joints, hardpoints, motor mounts, fasteners, connectors, battery health and structural interfaces in more detail.
Major overhaul gate	After 100 missions or 5 years, decide on refurbishment, replacement of life-limited elements, or retirement.

The main sustainability benefit of this approach is that high-wear components are separated from reusable aircraft hardware. This reduces the risk that local damage to the net, tether, landing pads or launcher items causes premature retirement of larger assemblies.

17.6. Off-Nominal Environmental Effects

The quantitative assessment above represents the environmental impact of a successful recovery mission. However, the main environmental concern for BELLONA is likely associated with failed or off-nominal missions. A failed mission could result in uncontrolled balloon descent, payload release, balloon fragmentation, unrecovered net or tether material, aircraft crash damage, battery damage. In such cases, the environmental burden would no longer be dominated only by recharge electricity or allocated manufacturing impact, but also by lost hardware, damaged materials, possible hazardous payload contents, and clean-up effort.

These effects are not quantified in the baseline LCA because their impact depends strongly on failure probability, impact location, payload type, aircraft damage severity, and the fraction of material recovered after the event. They are therefore treated as qualitative environmental risk drivers. From a sustainability perspective, reducing the probability and consequences of a failed mission is therefore at least as important as reducing the nominal per-sortie energy use.

17.7. KPIs and Design Recommendations

The sustainability KPIs in Table 17.7 are design-control values, not certified performance claims.

Table 17.7: Sustainability KPIs for the BELLONA Baseline Design

Indicator	Baseline value or target	Use
Functional unit	One successful recovery mission	Defines the delivered service.
Baseline service life	100 missions	Allocates reusable hardware impact.
Mission energy	3.019 kWh before contingency	Used for operational electricity impact.

Table 17.7: Sustainability KPIs for the BELLONA Baseline Design (continued)

Indicator	Baseline value or target	Use
Operational GWP	1.67–1.92 $kgCO_2eq$/mission	Grid-electricity estimate for modelled and contingency cases.
Battery production impact	332 $kgCO_2eq$	One of the main quantified manufacturing contributors.
Debris prevention	No uncontrolled debris above 50 g	Sustainability and safety driver.
Acoustic footprint	Target: 65 dB(A) at 100 m, with mitigation potential toward 60 dB at increased stand-off distance	Open verification item requiring testing.
End-of-life routing	Defined for metals, batteries, electronics, composites and polymers	Prevents unmanaged disposal.

Aluminum and steel parts are considered recyclable if the final design allows disassembly. The Li-ion battery pack requires controlled recycling or specialist disposal. Electronics are treated as e-waste. CFRP/epoxy parts require controlled disposal or specialist composite recycling where available. No recycling credit is applied in the baseline calculation.
The preliminary assessment indicates that operational electricity is not expected to dominate the sustainability burden. Larger contributors are expected to be production of the battery, electronics, composite structure, propulsion hardware and any hardware that is frequently replaced or not recovered after failed capture.
The design should therefore prioritise system lifetime, inspection access, modular mission-kit replacement, recovery of deployed hardware, battery health tracking, and verified noise reduction. CFRP should be used only where the mass saving is justified at system level, while aluminium or steel are preferred for inspectable fittings, hardpoints and repairable load-transfer parts where possible.

18 Compliance and Sensitivity

With the design finalized and sufficiently analyzed, the compliance with the user requirements from the beginning of the design stage must be checked. In addition, the final design must be checked for robustness to the most important parameters changing and the subsequent effect on the compliance.

18.1. Compliance Matrix

The compliance with the most essential user requirements is given in Table 18.1.

Table 18.1: System-Level Requirement Compliance and Verification Matrix

Req. ID	Verification and Validation Steps	Met
REQ-STK-01	Validated by implementing a dedicated Balloon Interaction System, which is independently verified and validated.	✓
REQ-STK-02	Validated through simulations using empirical data from the onboard sensor suite to confirm onboard detection and terminal tracking. Combined with ground cueing, this validates the requirement up to 6000 m AGL.	✓
REQ-STK-03	Validated via trajectory modeling and simulation to ensure sufficient power is available for interception within 10 min.	✓
REQ-STK-10.2	Verified via a Bill of Materials (BOM) cost audit and procurement accounting, confirming a total aerial system acquisition cost below €25000 (excluding ground station), adjusted for inflation as of 01.01.2026.	✓
REQ-STK-11	Verified via operational logistics modeling and post-flight analysis of maintenance, refurbishment, and consumables costs, confirming a per-mission cost below €500 (inflation-adjusted).	✓

While the most important user requirements are validated, it should be noted that all of the above require further validation due to the project's current theoretical stage.

18.2. Final Design Sensitivity Analysis

The PPA sensitivity study in Section 6.11.1 identified the transition stall cap and battery specific energy as the two dominant MTOW drivers, together responsible for mass swings of up to ±14% and ±12% respectively under ±10% parameter perturbations. Intercept altitude and forward-flight efficiency ranked next. This section traces those top-ranked parameters through to requirement compliance for every subsystem, demonstrating that the final design remains feasible under realistic variations.

Parameter Propagation

Transition stall cap (±10%). A tighter cap forces a larger wing to stay inside the back-transition corridor, raising MTOW by ≈ 14% (to ≈ 58 kg). The resulting mass increase flows into:

- **PPA / Structures:** Wing area grows to maintain stall compliance; structural mass scales accordingly. The design retains positive stall margin in all cases, so REQ-STK-01 (balloon removal capability) is not violated.
- **BIG / Reel & Tether:** A heavier aircraft raises the peak tether tension during capture. The +14% MTOW case was checked against the tether load budget; the safety factor remains above the required minimum.
- **Cost (REQ-STK-10.2 / REQ-STK-11):** A larger wing adds material cost. A 14% MTOW increase propagated through the BOM cost model yields an acquisition cost increase of ≈€1 200, keeping the system below the €25 000 ceiling.

Battery specific energy (−10%). Reducing pack-level specific energy raises MTOW by ≈ 12% through heavier batteries and increased hover/climb power demand.

- **PPA endurance:** The energy budget is rerun for the degraded pack. Even at −10% specific energy the aircraft closes on the 10-minute interception window (REQ-STK-03), with ≈ 45 s of margin remaining.
- **Structures:** Structural mass scales with MTOW; the +12% case stays within the design load envelope.
- **Cost:** A heavier battery pack adds ≈€600 to acquisition cost, remaining below the €25 000 cap.

Intercept altitude (±10%). Higher intercept altitude increases climb energy and time. At +10% altitude the mission time reaches ≈ 9.7 min, still within the 10-minute window of REQ-STK-03. Detection range (REQ-STK-02) is unaffected because the sensing subsystem budget was sized to 6 000 m AGL independently of intercept altitude.

Summary

Table 18.2 summarises requirement compliance across the identified worst-case parameter perturbations.

Table 18.2: Requirement Compliance Under Worst-Case Parameter Perturbations

Req. ID	Description	Nominal	Stall cap +10%	Sp. energy −10%	Alt. +10%
REQ-STK-01	Balloon removal	✓	✓	✓	✓
REQ-STK-02	Detection to 6 000 m AGL	✓	✓	✓	✓
REQ-STK-03	Intercept within 10 min	✓	✓	✓	✓
REQ-STK-10.2	Acquisition cost < €25 000	✓	✓	✓	✓
REQ-STK-11	Mission cost < €500	✓	✓	✓	✓

All five key requirements remain satisfied under the worst-case individual perturbations of the most critical sizing parameters. The design is therefore considered robust to realistic uncertainties in battery technology, aerodynamic modelling assumptions, and operational altitude variation.

19 Future Developments

19.1. Project Design and Development Logic

The BELLONA design is now a theoretical concept. The post-DSE development logic outlines the technical trajectory to mature this design into a verified prototype.

Transitioning to hardware focuses on mitigating risk across heavily coupled subsystems with high uncertainty: propulsion margins, net deployment, tether-load control, structural load transfer, and sensor fusion. This begins with Phase VII: Design Optimization for Production and Phase VIII: Prototyping & Component Integration.

To manage dependencies, lower-level components require verification before high-risk operational trials (e.g., capture require prior ground verification of the net launcher). This leads into Phase IX: Certification to satisfy regulatory and safety requirements.

Post-certification, the system moves through Phase X: Low-rate initial production into Phase XI: Full-scale commercial scaling. Operational deployment requires Phase XII: Operation support & Fleet management, concluding with Phase XIII: End-of-life recycling & Disposal (First Drone produced).

19.2. Critical Development Dependency

The primary post-DSE development dependency is the capture-load chain. The net, tether, reel, guide, hardpoint, fuselage frame, and flight control logic form a tightly coupled system. Development must validate net deployment, capture confirmation, tether tension regulation, propeller clearance, aircraft stability, and emergency breakaway before representative capture trials are justified.

Other activities such as: propulsion refinement, transition simulation, sensor validation, and ground station procedures can proceed in parallel, provided their interfaces remain controlled. These activities are mapped to the development gates and Figure 19.1. The program is structured around sequential maturity gates (Table 19.1), where progression depends on verifying explicit exit conditions for safety-critical subsystems.

Table 19.1: Proposed Post-DSE Development Gates for BELLONA

Name	Exit Condition
Preliminary baseline freeze	DSE configuration, budgets, interfaces, and risks under configuration control.
Critical-technology proof	Subsystem concepts (net deployment, reel, breakaway, transition model, sensor fusion) verified via breadboard or simulation.
Detailed design freeze	Released CAD, manufacturing drawings, harness layouts, and inspection criteria available for fabrication.
Prototype integration complete	Physical integration and interface verification of aircraft, ground station, sensing, propulsion, and capture mechanism.
Ground-test readiness	Completion of static proof-loading, launcher safety, reel load, EMI, and software-in-the-loop (SIL) testing.
Flight envelope expansion	Flight demonstration of VTOL, hover, transition, cruise, and automated failsafes without firing the capture system.
Interaction validation	Demonstration of dummy-payload capture, tethered descent, swing management, and emergency breakaway under controlled conditions.
Pre-production release	Implementation of test-derived modifications; updated BOM, cost models, maintenance, and training documentation.

These gates are governed by the capture system. Before representative trials, this must be verified as an integrated system. Other tasks can proceed in parallel.

19.3. Relation to Schedule and Cost Breakdown

The development logic defines the technical sequence, which is translated into a schedule by the Gantt chart in Figure 19.1 and allocated resources via the Cost Breakdown Structure.

Early development prioritizes reducing risks, subsystem testing, transition verification, capture mechanics, structural proof loading, and regulatory preparation before committing to representative flight trials. Later phases shift from feasibility to repeatability, including production drawing release, quality control, operator training, and maintenance planning.

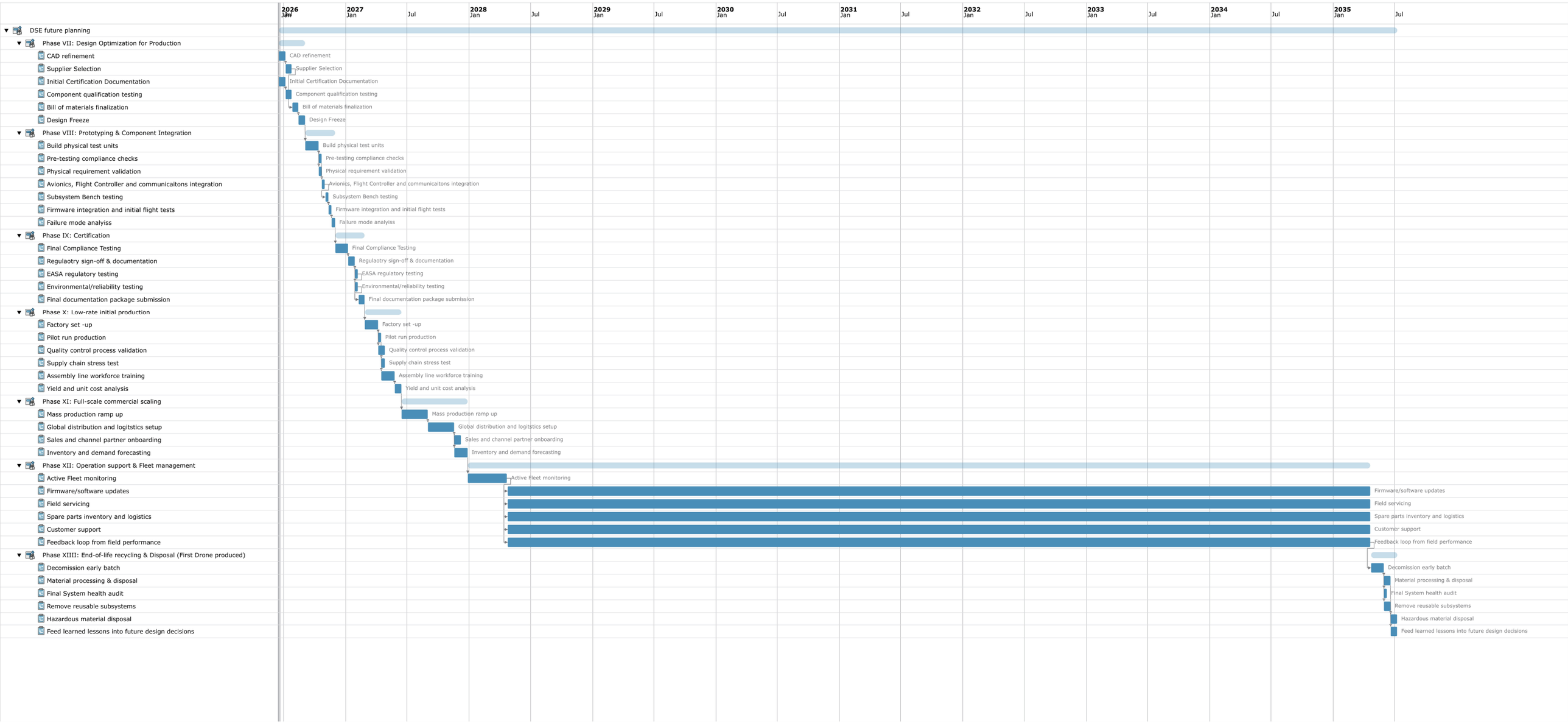

Figure 19.1: Future Developments Gantt Chart

20
Conclusion and Recommendations

The BELLONA UAS addresses the operational damage created by uncooperative, free-floating balloons. This project successfully delivers a design that bridges the gap between high-cost military interception systems and passive monitoring. The resulting architecture fulfills the three strategic pillars set out at the start of the project through directly traceable, sized technical implementations.

Safety-First Interception: To eliminate ground-debris risk, the UAS captures targets from below using a fine-meshed net rather than a kinetic or destructive method. Flight safety is underpinned by a failure-tolerant navigation and control framework that fuses multiple sensing modalities, while net closure itself is doubly assured through both corner weights and a drawstring mechanism.

Economic Accessibility: To lower the entry barrier for civil operators, unit production cost is kept at €99,622 (€23,222 for the UAS and €66,400 for the ground station), with most recurring revenue instead generated through the accompanying ground station. This was achieved through a modular, reusable architecture built from off-the-shelf components. Minimal reliance on operational consumables keeps the cost per sortie under €500.

Engineering Rigour and Synthesis: The multidisciplinary design closes its mass-iteration loop at an MTOW of 51.13 kg. Driven by the high-altitude trajectory requirement, the 4.74 kWh pouch-cell battery provides sufficient energy to climb to the 6,000 m ceiling within 454.1 s, while preserving adequate margin against the mission energy budget.

Additionally, the detailed design presented in this report has converged to a self-consistent, theoretically sound baseline, advancing the project from a paper design towards a flight-tested prototype requires further verification, validation, and, in several areas, additional design maturation. This is especially important for two specific aspects.

Capture-System: Prioritise de-risking the net, and breakaway chain, since this is BELLONA's core differentiating subsystem and the one with the least physical verification to date. This path favours building a ground-based or tethered-hover capture rig to test net deployment, closure, and emergency separation against a representative dummy payload.

Certification-First: Prioritise early engagement with the Dutch ILT and a formal SORA review before committing further to hardware iteration. The SAIL IV classification and its associated Operational Safety Objectives rest on assumptions that are still provisional at this stage of the design, including detect-and-avoid performance, structural proof-load levels, and whether anti-collision lighting might ultimately be required for operation within the Vilnius TMA, so this path treats early regulatory feedback as the most schedule-critical activity, reducing the risk of late redesign driven by certification findings.

Beyond BELLONA itself, the development process also surfaced lessons worth carrying into future design syntheses. Centralising shared budgets, within a single concurrent-engineering loop, rather than letting each subsystem converge independently, proved essential to reaching a consistent baseline.

Likewise, designing high-load interfaces to remain inspectable and replaceable, rather than permanently bonded, materially supports reusability and is a principle that generalises well beyond this specific airframe. Finally, treating regulatory and certification constraints as design drivers from the earliest concept phase, rather than as a downstream compliance check, is necessary for such a certification-driven drone.

References

[1] World Meteorological Organization. *Guide to Meteorological Instruments and Methods of Observation (CIMO Guide)*. Tech. rep. No.8. WMO, 2018.

[2] Air Help. *Cost of disrupted flights to the economy*. Accessed June 2026. May 2024. URL: https://downloads.regulations.gov/DOT-OST-2024-0062-0001/attachment_7.pdf.

[3] Air Help. *2023 Air Travel and Disruption: A Global Overview*. Accessed June 2026. 2024. URL: https://downloads.regulations.gov/DOT-OST-2024-0062-0001/attachment_9.pdf.

[4] Al Jazeera. *Lithuania declares state of emergency over smuggler balloons from Belarus*. Accessed June 2026. Dec. 2025. URL: https://www.aljazeera.com/news/2025/12/9/lithuania-declares-state-of-emergency-over-smuggler-balloons-from-belarus.

[5] BBC News. *Balloon incursions: Lithuania revenue losses and airport closures*. Accessed June 2026. Dec. 2025. URL: https://www.bbc.com/news/articles/c39pr3d10wlo.

[6] Euromaidan Press. *Poland flooded with 59 Belarusian GPS-tagged balloons by Christmas Eve*. Accessed June 2026. Dec. 2025. URL: https://euromaidanpress.com/2025/12/29/poland-flooded-with-59-belarusian-gps-tagged-balloons-by-christmas-eve/.

[7] UAV Defence. *New Counter-Drone Tech Trends 2024–2025: Lasers & Microwaves*. Accessed June 2026. 2025. URL: https://uav-defence.com/new-emerging-counter-drone-tech-lasers-high-power-microwaves-net-drones-2024-2025-trends/.

[8] Airsight Security. *Air to Air Drones and Net Guns: Kinetic Counter-Drone Technology*. Accessed June 2026. 2024. URL: https://www.airsight.com/knowledge-hub/counter-drone-technology/air-to-air.

[9] Future Data Stats. *Counter-Drone Systems Market Research Report 2024*. Accessed June 2026. 2024. URL: https://www.futuredatastats.com/counter-drone-systems-market.

[10] Grand View Research. *Anti-Drone Market Size, Share & Trends Analysis Report, 2026–2033*. Accessed June 2026. 2025. URL: https://www.grandviewresearch.com/industry-analysis/anti-drone-market.

[11] Mordor Intelligence. *Anti-Drone Market Size & Share Analysis — Growth Trends & Forecasts (2026–2031)*. Accessed June 2026. 2025. URL: https://www.mordorintelligence.com/industry-reports/anti-drone-market.

[12] RFE/RL Belarus Service. *Up In The Air: Are Balloons From Belarus A Smuggling Operation? A Hybrid Attack? Or Both?* Accessed June 2026. Nov. 2025. URL: https://www.rferl.org/a/balloons-belarus-smuggling-hybrid-attack-lithuania-cigarettes/33586992.html.

[13] European Commission. *Action Plan on Drone and Counter Drone Security*. Accessed: 2026-06-22. 2026. URL: https://digital-strategy.ec.europa.eu/en/policies/drone-security.

[14] European Union Aviation Safety Agency. *Drone Incident Management at Aerodromes*. Accessed: 2026-06-22. 2021. URL: https://www.easa.europa.eu/en/drone-incident-management-aerodromes-part-1.

[15] Tiede, B., Chapman, J., Schnulo, S. L., and Nitzsche, M. P. *Battery Key Performance Projections Based on Historical Trends and Chemistries*. Tech. rep. NASA/TM-20220005588. Accessed 17 June 2026. NASA Glenn Research Center, 2022. URL: https://ntrs.nasa.gov/citations/20220005588.

[16] Atomfair LLC. *High-Energy Anode-Free Pouch Cell 460 Wh/kg 22–52 Ah*. Supplier product data, accessed 17 June 2026. 2026. URL: https://atomfair.com/product/high-energy-anode-free-pouch-cell-460whkg/.

[17] Doo, J. T. et al. *NASA Electric Vertical Takeoff and Landing Aircraft Technology for Public Services: A White Paper*. Tech. rep. NASA/TM-20210016168. Accessed 17 June 2026. NASA, 2021. URL: https://ntrs.nasa.gov/citations/20205000636.

[18] Stone, R. H. and Clarke, G. "Optimization of Transition Manoeuvres for a Tail-Sitter Unmanned Air Vehicle". In: *Australian Aerospace International Congress*. Establishes the $T/W \geq 1.15$ tail-sitter transition bound. Canberra, Australia, 2001.

[19] Leishman, J. G. *Principles of Helicopter Aerodynamics*. 2nd ed. Cambridge Aerospace Series. Ch. 2 momentum theory in hover, derivation of $P_i = T\sqrt{T/(2\rho A)}$; Ch. 3 blade-element-momentum theory and figure of merit. Cambridge, UK: Cambridge University Press, 2006. ISBN: 978-0521858601.

[20] Thomas, G. L. "Power System Redundancy Design Trends for All-Electric Urban Air Mobility Aircraft". In: *AIAA SciTech Forum*. Accessed 17 June 2026. 2023. URL: https://ntrs.nasa.gov/citations/20220018016.

[21] Gur, O. and Rosen, A. "Optimizing Electric Propulsion Systems for Unmanned Aerial Vehicles". In: *Journal of Aircraft* 46.4 (2009), pp. 1340–1353. DOI: 10.2514/1.40293.

[22] Sch"omann, J. and Hornung, M. "Design of Hybrid-Electric Propulsion Systems for Small Unmanned Aircraft". In: *4th CEAS Air and Space Conference*. Accessed 17 June 2026. Link"oping, Sweden, 2013. URL: https://mediatum.ub.tum.de/doc/1183222/document.pdf.

[23] Oliviero, F. *Fundamentals on Wing Aerodynamics*. AE2111-II Aerospace Design and Systems Engineering Elements II lecture slides, Delft University of Technology. Aircraft Design 1, 2024–2025 course material. 2024.

[24] Oliviero, F. *Weight Estimation and Iterations in Aircraft Design*. AE2111-II Aerospace Design and Systems Engineering Elements II lecture slides, Delft University of Technology. Aircraft Design 5, 2024–2025 course material. 2024.

[25] Finck, R. D. *USAF Stability and Control DATCOM*. Tech. rep. AFWAL-TR-83-3048. Section 4.1.3.2 gives the lift-curve-slope formula attributed to Polhamus. Wright-Patterson AFB, OH: Air Force Wright Aeronautical Laboratories, 1978.

[26] Selig, M. S., Donovan, J. F., and Fraser, D. B. *Airfoils at Low Speeds*. Soartech 8. Volume 1 of the UIUC Low-Speed Airfoil Tests; tabulated polars for SD7037, SD7032, SD7062 and related Selig–Donovan sections. Virginia Beach, VA: SoarTech Publications, 1989.

[27] Roskam, J. *Airplane Design Part VI: Preliminary Calculation of Aerodynamic, Thrust and Power Characteristics*. Lawrence, KS: DARcorporation, 1985. ISBN: 978-1884885525.
[28] Gudmundsson, S. *General Aviation Aircraft Design: Applied Methods and Procedures*. Ch. 15 on drag analysis lists CD0 reference values for light aircraft. Oxford, UK: Butterworth-Heinemann / Elsevier, 2014. ISBN: 978-0123973085.
[29] Raymer, D. P. *Aircraft Design: A Conceptual Approach*. 6th ed. AIAA Education Series. Ch. 5 (wing loading and thrust-to-weight), Ch. 12 (aerodynamics), Ch. 17 (performance and flight mechanics), Ch. 21 (vertical flight). Reston, VA: American Institute of Aeronautics and Astronautics, 2018. ISBN: 978-1624104909.
[30] Stahl, P. and Rixen, D. "Sizing of Multicopter Air Taxis—Weight, Endurance, and Range". In: *Aerospace* 11.3 (2024), p. 200. DOI: 10.3390/aerospace11030200.
[31] Ruijgrok, G. J. J. *Elements of Airplane Performance*. 2nd ed. Delft, The Netherlands: Delft Academic Press / VSSD, 978-94-6518-164-6.
[32] Si, J., Niu, Y., and Wang, B. *A Review of Nonlinear Filtering Algorithms in Integrated Navigation Systems*. Oct. 2025. DOI: 10.3390/s25206462.
[33] Urrea, C. and Agramonte, R. "Kalman Filter: Historical Overview and Review of Its Use in Robotics 60 Years after Its Creation". In: *Journal of Sensors* 2021 (2021). ISSN: 16877268. DOI: 10.1155/2021/9674015.
[34] Hornung, A., Wurm, K. M., Bennewitz, M., Stachniss, C., and Burgard, W. "OctoMap: An efficient probabilistic 3D mapping framework based on octrees". In: *Autonomous Robots* 34.3 (Apr. 2013), pp. 189–206. ISSN: 09295593. DOI: 10.1007/s10514-012-9321-0.
[35] Garda, C. E., Preti't, D. M., and Morari
, M. *Model Predictive Control: Theory and Practice a Survey**. Tech. rep. 3. 1989, pp. 335–338.
[36] Uhlenbeck, G. E. and Ornstein, L. S. "On the Theory of the Brownian Motion". In: *Phys. Rev.* 36 (Sept. 1930), pp. 823–841. DOI: 10.1103/PhysRev.36.823.
[37] Veld, R. C. van't, Van Kampen, E., and Chu, Q. P. "Stability and robustness analysis and improvements for incremental nonlinear dynamic inversion control". In: *AIAA Guidance, Navigation, and Control Conference, 2018*. American Institute of Aeronautics and Astronautics Inc, AIAA, Jan. 2018. ISBN: 9781624105265. DOI: 10.2514/6.2018-1127.
[38] Atmaca, D., Visser, C. de, and Kampen, E.-J. van. "Active Incremental Nonlinear Dynamic Inversion for Sensor and Actuator Fault-Tolerant Control". In: *Journal of Guidance, Control, and Dynamics* (Mar. 2026), pp. 1–11. ISSN: 0731-5090. DOI: 10.2514/1.G009705. URL: https://arc.aiaa.org/doi/10.2514/1.G009705.
[39] Liu, Y., Zhang, L., Jiang, J., Wei, S., Liu, S., and Zhang, W. "A Data-Driven Learning-Based Continuous-Time Estimation and Simulation Method for Energy Efficiency and Coulombic Efficiency of Lithium Ion Batteries". In: *Energies* 10.5 (2017), p. 597. DOI: 10.3390/en10050597.
[40] NET Systems. *Ultra Cross Knotless Knitting*. Tech. rep. 2011. URL: https://www.net-sys.com/wp-content/uploads/2025/04/UC-Netting-Details-2014-1.pdf.
[41] Zwicker, M. and Sinclair, R. J. "Pack Density Limitations of Hybrid Parachutes". In: *AIAA Aerodynamic Decelerator Systems (ADS) Conference*. Reston, Virginia: American Institute of Aeronautics and Astronautics, Mar. 2013. ISBN: 978-1-62410-202-8. DOI: 10.2514/6.2013-1395.
[42] Shin, H., Leeghim, H., Joo, T., Jang, S., and Park, G. "Design and Dynamic Analysis of a Tethered-Net-Based Space Debris Capture System with Winch-Driven Closure Mechanism". In: *Applied Sciences* 16.12 (June 2026), p. 5759. ISSN: 2076-3417. DOI: 10.3390/app16125759.
[43] Zhai Jinpeng and jeff31415. *Phoenix-s-Interior-Ballistic-Solver-PIBS*. Nov. 2015. URL: https://github.com/Prethea-Phoenixia/Phoenix-s-Interior-Ballistic-Solver-PIBS.
[44] *Daiwa 21 Seaborg 300J*. Accessed June 2026. URL: https://daiwa.my/product/21-seaborg-300j/.
[45] Parachutes, R. *Rocketman High Performance CD 2.2 Parachute*. Accessed June 2026. URL: https://www.the-rocketman.com/products/rocketman-high-performance-cd-2-2-parachutes?variant=42195940048990.
[46] Tomblin, J., Sherraden, J., Seneviratne, L., and Raju, K. S. *Advanced General Aviation Transport Experiments: A-Basis and B-Basis Design Allowables for Epoxy-Based Prepreg TORAY T700GC-12K-31E/#2510 Unidirectional Tape [SI Units]*. Technical Report AGATE-WP3.3-033051-135. Wichita, KS: National Institute for Aviation Research (NIAR), Wichita State University, 2002.
[47] CEL Components S.r.l. *Alustep 300 LIGHT - Fiberglass Skin / Aluminum Honeycomb Core Technical Data Sheet*. Accessed: 2026-06-16. CEL Components S.r.l. Bologna, Italy, 2024. URL: https://www.honeycombpanels.eu/.
[48] Easy Composites Ltd. *3.2mm Cell 29kg Nomex Aerospace Honeycomb Core Material Specification*. Accessed: 2026-06-16. Easy Composites Ltd. Stoke-on-Trent, United Kingdom, 2026. URL: https://www.easycomposites.co.uk/.
[49] MAKO Advanced Materials. *Film Adhesives For Advanced Bonding Applications*. Accessed: 2026-06-16. MAKO Advanced Materials. 2026. URL: https://www.makobond.com/film-adhesives/.
[50] Tomblin, J., Sherraden, J., Seneviratne, L., and Raju, K. S. *Advanced General Aviation Transport Experiments: A-Basis and B-Basis Design Allowables for Epoxy-Based Prepreg TORAY T700SC-12K-50C/#2510 Plain Weave Fabric [US Units]*. Technical Report AGATE-WP3.3-033051-131 Rev A. Wichita, KS: National Institute for Aviation Research (NIAR), Wichita State University, Feb. 2010.
[51] *Metallic Materials Properties Development and Standardization (MMPDS-17)*. Handbook. Supersedes MIL-HDBK-5. Battelle Memorial Institute. Columbus, OH, July 2022.
[52] Lanitz Aviation. *Lanitz Aviation Products for General Aviation: ORATEX Aircraft Covering and Decal Systems Catalogue*. Accessed: 2026-06-16. Lanitz Aviation. Leipzig, Germany, 2026. URL: https://www.lanitz-aviation.com/.
[53] Han, X., Cai, H., Sun, J., Wei, Z., Huang, Y., and Wang, A. "Numerical Studies on Failure Mechanisms of All-Composite Sandwich Structure with Honeycomb Core under Compression and Impact Loading

Conditions". In: *Polymers* 14.19 (Oct. 2022). DOI: 10.3390/polym14194047. URL: https://doi.org/10.3390/polym14194047.
[54] Easy Composites. *XC130 150g Unidirectional Prepreg Carbon Fibre*. URL: https://www.easycomposites.eu/xc130-150g-unidirectional-prepreg-carbon-fibre (visited on 06/22/2026).
[55] Composite Shop. *Carbon UD 130g/m² Epoxy Prepreg*. URL: https://www.compositeshop.de/xoshop/lng/en/fibers/carbon-fiber/carbon-ud-130gm-epoxy-prepreg.html?language=en (visited on 06/22/2026).
[56] Online Metals. *Buy Aluminum Online*. URL: https://www.onlinemetals.com/en/buy/aluminum (visited on 06/22/2026).
[57] Rock West Composites. *Nomex Core Sandwich Panels*. URL: https://www.rockwestcomposites.com/nomex-core-sandwich-panels?srule=materials_asc (visited on 06/22/2026).
[58] Rao, S. S. *Mechanical Vibrations*. 6th ed. Hoboken, NJ: Pearson, 2017. ISBN: 978-0-13-436130-7.
[59] Wright, J. R. and Cooper, J. E. *Introduction to Aircraft Aeroelasticity and Loads*. 2nd ed. Aerospace Series. Chichester, UK: John Wiley & Sons, 2015. ISBN: 978-1-118-48801-0.
[60] Cook, R. D., Malkus, D. S., Plesha, M. E., and Witt, R. J. *Concepts and Applications of Finite Element Analysis*. 4th ed. New York, NY: John Wiley & Sons, 2002. ISBN: 978-0-471-35605-9.
[61] Megson, T. H. G. *Aircraft Structures for Engineering Students*. 6th ed. Oxford, UK: Butterworth-Heinemann, 2017. ISBN: 978-0-08-100914-7.
[62] Beretta, J., Cardozo, A., Paletta, N., Chiariello, A., and Belardo, M. "On the Fine-Tuning of the Stick-Beam Wing Dynamic Model of a Tiltrotor: A Case Study". In: *Aerospace* 11.2 (2024), p. 116. DOI: 10.3390/aerospace11020116.
[63] Markert, R. and Seidler, M. "Analytically Based Estimation of the Maximum Amplitude During Passage Through Resonance". In: *International Journal of Solids and Structures* 38.10–13 (2001), pp. 1975–1992. DOI: 10.1016/S0020-7683(00)00147-5.
[64] *Onlogic k300*. URL: https://www.onlogic.com/store/k300/.
[65] *5.8 Horizon MIMO Modem*. URL: https://esteem.com/horizon-5-8-ghz-radio/.
[66] *ANT-433-CW-HD-SMA*. URL: https://www.te.com/en/product-ANT-433-CW-HD-SMA.html.
[67] "T30 Controller". In: (). URL: https://www.chinowing.com/tcn/212/.
[68] Ben Shneiderman. *DESIGNING THE USER INTERFACE ..,., o*. Tech. rep. URL: http://www.aw-bc.com/dtui.c1icking.
[69] European Commission. *Commission Implementing Regulation (EU) 2019/947 of 24 May 2019 on the rules and procedures for the operation of unmanned aircraft*. Tech. rep. Official Journal of the European Union, 2019. URL: http://data.europa.eu/eli/reg_impl/2019/947/oj.
[70] European Commission. *Commission Delegated Regulation (EU) 2019/945 of 12 March 2019 on unmanned aircraft systems and on third-country operators of unmanned aircraft systems*. Tech. rep. Official Journal of the European Union, 2019. URL: http://data.europa.eu/eli/reg_del/2019/945/oj.
[71] Hamann, R. J. and Tooren, M. J. L. van. *Systems Engineering & Technical Management Techniques, Part I*. Delft, Netherlands, 2006.
[72] *EIC 2026 work programme - European Innovation Council*. URL: https://eic.ec.europa.eu/eic-funding-opportunities/eic-2026-work-programme_en?.
[73] Bianchi, I. et al. "Development and Life Cycle Analyses of Carbon Fiber Reinforced Polymer Components". In: *Journal of Materials Engineering and Performance* (2025).
[74] Fitzgerald, A. M. *Life Cycle Assessment for Carbon Fibre Manufacture*. Tech. rep. University of Surrey, 2023.
[75] European Aluminium. *A low carbon footprint*. https://european-aluminium.eu/projets/a-low-carbon-footprint/. Accessed June 2026. 2025.
[76] World Steel Association. *Sustainability Indicators Report 2025*. https://worldsteel.org/wider-sustainability/sustainability-indicators/. Accessed June 2026. 2025.
[77] Peiseler, L. et al. "Carbon footprint distributions of lithium-ion batteries and their materials". In: *Nature Communications* (2024). Reported median carbon footprints of approximately 69–77 kgCO2e/kWh for Europe and China.
[78] PlasticsEurope. *Eco-profiles and Environmental Product Declarations for Plastics*. https://plasticseurope.org/sustainability/circularity/life-cycle-thinking/eco-profiles-set/. Accessed June 2026. 2021.
[79] Flannery, B. P. et al. *Greenhouse Gas Index for Products in 39 Industrial Sectors: Synthetic Rubber*. Tech. rep. Resources for the Future, 2022.
[80] Climatiq. *Synthetic rubber emission factor.* https://www.climatiq.io/. Accessed June 2026. 2025.
[81] CO2emissiefactoren.nl. *Elektriciteit – Grijze Stroom*. https://co2emissiefactoren.nl/factoren/2025/11/51/elektriciteit-grijze-stroom/. Accessed June 2026. 2025.
[82] European Commission. *Environmental Noise Directive*. https://environment.ec.europa.eu/topics/noise/environmental-noise-directive_en. Accessed June 2026. 2026.
[83] European Environment Agency. *Exposure of Europe's population to environmental noise*. https://www.eea.europa.eu/en/analysis/indicators/exposure-of-europe-population-to-noise. Accessed June 2026. 2025.
[84] Simons, D. and Snellen, M. *Course AE4431-23 Aircraft Noise*. Lecture Notes, Delft University of Technology. Delft, Netherlands, Aug. 2024.
[85] Turhan, B., Rezgui, D., and Azarpeyvand, M. "Phase Synchronisation for Tonal Noise Reduction in a Multi-Rotor UAV". In: *Drones* 9.8 (Aug. 2025). DOI: 10.3390/drones9080544. URL: https://doi.org/10.3390/drones9080544.